Ground motion intensity measures for seismic probabilistic risk analysis

Marco de Biasio

UNIVERSITÉ DE GRENOBLE

THÈSE

Pour obtenir le grade de

DOCTEUR DE L'UNIVERSITÉ DE GRENOBLE

Spécialité : **Matériaux, Mécanique, Génie Civil**

Arrêté ministériel : 7 août 2006

Présentée par

Marco DE BIASIO

Thèse dirigée par **Fréderic DUFOUR**

préparée au sein du **Laboratoire 3SR (Sols, Solides, Structures, Risques)**
dans **l'École Doctorale IMEP-2 (Matériaux, Mécanique, Energétique, Environnent, Procèdes, Production)**

Ground Motion Intensity Measures for Seismic Probabilistic Risk Analysis

Thèse soutenue publiquement le **17 Octobre 2014,**
devant le jury composé de :

Mr. Ezio FACCIOLI
Professeur, Politecnico di Milano (Italy), Rapporteur
Mr. Panagiotis KOTRONIS
Professeur, EC Nantes (France), Rapporteur
Mr. Pierre LABBE
Expert en Génie Parasismique, EDF (France), Examinateur
Mr. Jacky MAZARS
Professeur Emérite, INP Grenoble (France), Examinateur
Mr. Fréderic DUFOUR
Professeur, INP Grenoble (France), Directeur de thèse
Mr. Stéphane GRANGE
Maître de Conférences, UJF (France), Co-encadrant de thèse
Mr. Ilie PETRE-LAZAR
Expert en Génie Parasismique, EDF (France), invité
Mr. Fréderic ALLAIN
Ingénieur en Parasismique, EDF (France), invité

Université Joseph Fourier / Université Pierre Mendès France / Université Stendhal / Université de Savoie / Grenoble INP

Credits

This Ph.D. Thesis has been realized in the period October 2011-October 2014 at the 3SR (Soils, Solids, Structures, Risks) laboratory of University Grenoble Alpes/CNRS, and with the co-direction of the "Service Etudes and Projects Thermiques et Nucléaires" (SEPTEN) of Electricité de France (EDF).

Likewise, this study has been performed as part of the work-package 5 (i.e., Improve the characterization and the exploitation of seismic ground motions) of the international, 2011-2015, SIGMA (**Se**l**I**smic **G**round **M**otion **A**ssessment) research and development project (www.projet-sigma.com) founded and leaded by EDF, AREVA, ENEL and CEA.

Acknowledgements

I want to start the acknowledgements from far in the time, saying thanks to Prof. Cino Viggiani, who four years ago encouraged me to apply to the International Master in Geomechanics, Civil Engineering and Risk. During this last, two providential events happen: I had my first contact with Earthquake Engineering, and I met Prof. Frederic Dufour and Ass. Prof. Stéphane Grange, who are respectively the director and the main co-supervisor of this Ph. D. thesis. To work with Frederic and Stéphane has been a privilege: their scientific competence, human qualities, friendly manner and good mood made the achievement of this study happy and enjoyable. I would like to thank both of them for the confidence and the autonomy they have accorded me during my PhD' years.

Likewise, I would like to thank the co-supervisors of the industrial partner (EDF): first of all thanks to Dr. Ilie Petre-Lazar, who hired me in order to do this Ph.D. thesis, and who gave me all the means to do a good job. His advices have been very precious and had an important role in the promotion of this work. Thanks to Dr. Frederic Allain and Dr. Nicolas Humbert, who followed this study and contributed with important suggestions. Also, thanks to Irmela, Thie Lin, Pauline, Damien, Salim, Sebastien and Nicolas for having welcomed me in my many passages at the EDF's offices.

In the framework of the SIGMA project, I would like to thank Dr. Philippe Renault, Dr. Jean Savy and Dr. Aybars Gurpinar for their useful comments/suggestions in early reviews of this work.

Thank to Pr. Ezio Faccioli, Pr. Jacky Mazars, Dr. Pierre Labbe, and Pr. Panagiotis Kotronis for constructive comments and suggestions, which helped improve the quality of this manuscript.

Thanks to all the good people I met during my stay in Grenoble, and who have contributed to make me smile for the most of these years of studies: Andrea, Giusy, Anna, Anggi, Maxime, Benjamin, Steven, Nouha, Sophie, Ranime, Pietro; a particular mention for

Alessandro and Tymos (and also Eddy, who gave his car) for the spectacular "rescuing operation", that time I was stuck abroad cause I lost my wallet…

Special thanks to two very good friends I met at the 3SR lab, Donia and Eleni "la blonde" (yes, I believe in friendship between man and woman!): during these years we have laughed a lot together, and, most important, they have always been present when I needed help.

The last thanks are said to be the most important, and actually they are: I want to deeply thank my parents, Michele and Rosina for having always believed in and encouraged me, and finally, I want to truly, madly and deeply say thanks to *Caroline* for being part of my life.

Table of Contents

Frequently used symbols and acronyms

ASA_R	Relative Average Spectral Acceleration
ASI	Acceleration Spectrum Intensity
β	Logarithmic Standard Deviation
CAV	Cumulative Absolute Velocity
CDF	Cumulative Distribution Function
D_m	Maximum Softening
DM	Damage Measure
DV	Decision Variable
$E\text{-}ASA_R$	Equipment Relative Average Spectral Acceleration
EDP	Engineering Demand Parameter
EPRI	Effective Peak Acceleration
ERC	Electric Power Research Institute
f_1	Equivalent Reinforced Concrete
FEMA	Fundamental frequency
FFM	Free Field Motion
FIM	Foundation Input Motion
FRS	Floor Response Spectra
GMPE	Ground Motion Prediction Equation
IM	Intensity Measure
LM	Large Magnitude
LR	Long Distance
LS	Limit State

M	Magnitude
MAF	Mean Annual Frequency
MIDR	Maximum Inter-story Drift Ratio
μ_{max}	Maximum ductility demand
NSC	Non Structural Component
PDF	Probabilistic Density Function
PBEE	Performance Based Earthquake Engineering
PEER	Pacific Earthquake Engineering Research
PGA	Peak Ground Acceleration
PSHA	Probabilistic Seismic Hazard Analysis
R	Distance
R_{hyp}	Hypocentral Distance
ρ	Correlation coefficient
SE	Standard Error
SM	Small Magnitude
SPRA	Seismic Probabilistic Risk Analysis
SR	Short Distance
SSI	Soil Structure Interaction
T_1	Fundamental Period
TC3	Test Case 3
V_{S30}	Shear waves velocity in the upper 30 meters soil layer

Introduction

Scientific context

Traditional earthquake design philosophy is based on preventing structural and non-structural elements of buildings from any damage in low-intensity earthquakes, limiting the damage in these elements to repairable levels in medium-intensity earthquakes, and preventing the overall or partial collapse of buildings in high-intensity earthquakes. After 1994 Northridge and 1995 Kobe earthquakes, the structural engineering community realized that the amount of damage, the economic loss due to downtime, and repair cost of structures were unacceptably high, even though those structures complied with available seismic codes based on traditional design philosophy (Lee and Mosalam, 2006). The concept of Performance-Based Earthquake Engineering (PBEE) has its roots from this realization.

The U.S. Vision 2000 report (SEAOC, 1995) is one of the early documents of the first generation PBEE. In such report, Performance-Based Earthquake Design (PBED) is defined as a design framework which results in the desired system performances at various intensity levels of seismic hazard. The system performance levels are classified as fully operational, operational, life safety, and near collapse, while hazard levels are classified as frequent, occasional, rare, and very rare events. The designer and owner consult to select the desired combination of performance and hazard levels to use as design criteria objective. The intended performance levels corresponding to different hazard levels are either determined based on the public resiliency requirements, e.g. hospital buildings, or by the private property owners, e.g. residential or commercial buildings. Subsequent documents of the first generation PBEE (FEMA, 2000) express the design objectives using a similar framework, with slightly different performance descriptions and hazard levels. The element deformation and force acceptability criteria corresponding to the performance are specified for different structural and non-structural elements for linear, nonlinear, static, and/or dynamic analyses. At that time, these criteria do not possess any probability distribution, i.e. element performance evaluation is deterministic. The defined relationships between engineering demands and component performance criteria are based somewhat inconsistently on relationships measured in laboratory tests, calculated by analytical models, or assumed on the

basis of engineering judgment (Moehle, 2003), and in addition, element performance evaluation is not tied to a global system performance.

Considering the shortcomings of the first-generation procedures, a more robust PBEE methodology has been developed (Porter, 2003; Krawinkler, 2005; Haselton *et al*., 2008; Gunay and Mosalam, 2012) at the Pacific Earthquake Engineering Research (PEER) Center. Unlike earlier PBEE methodologies, element forces and deformations are not anymore directly used for performance evaluation. Indeed, one of the main features of the PEER-PBEE methodology is the explicit calculation of system performance measures, such as monetary losses, downtime (duration corresponding to loss of function), and casualties, which are expressed in terms of the direct interest of various stakeholders.

Most important, the key feature of the PEER-PBEE methodology is the rigorous consideration of uncertainties in the calculation of performance through the use of the sciences of *Probability* and *Statistics*, which are specifically established in order to make scientific judgments in the face of uncertainties and variations. Accordingly, uncertainties in earthquake intensity, ground motion characteristics, structural response, physical damage, and economic and human losses are explicitly considered in the method. This makes a fundamental difference with respect to *deterministic* seismic risk assessment methods, which "by-pass" the explicit consideration of uncertainties through the consideration of "worst scenario events" and the introduction of high safety factors, thus resulting in over dimensioned designs and/or redundant retrofitting-actions with consequent unnecessary increment of costs.

However it must be said that up to now, due to the probabilistic nature of the methodology and the various analysis stages it consists of, applications of Seismic Probabilistic Risk Analysis methodology (outside the Nuclear energy field) have been conducted mostly by academics with little attention by practicing engineers. However, an increasing trend to use probabilistic PBEE as a design method is boosted by the consequences of recent earthquakes, which have shown that traditional earthquake design philosophy has fallen short of meeting the requirements of sustainability and resiliency (Cimellaro *et al*., 2010; Moehle and Frost, 2012). Indeed, it is an accepted fact that the probabilistic PBEE methods are gaining popularity (e.g., FEMA, 2012) and they are expected to be proposed for standard design codes in the near future (e.g., Pinto, 2014).

Aim and tasks of the study

The study presented in this manuscript is inserted in the framework of the reduction of uncertainty in probabilistic PBEE methodologies. Specifically, this contribution aims to reduce the uncertainty coming from the engineering characterization of seismic ground motions. Such an uncertainty, which has been shown (Porter, 2003) to have significant weight, affects the effectiveness of the Seismic Hazard Analysis phase and in turns the efficiency of the Structural Demand Analysis phase of the PBEE process.

From the engineering point of view, ground motions are characterized by Intensity Measures (IMs). An IM is (mostly) a scalar property of a ground motion record that can be found simply and cheaply, and its aim is to quantify the "intensity" of the ground motion. Familiar examples of IMs include *PGA* and spectral acceleration $S_{pa}(f_1)$.

Hence, the three main tasks of the study are:

- To evaluate the performance of the IMs currently used in engineering practice as well as the performance of other IMs proposed in literature.
- To understand which are the characteristics that make earthquake excitations damaging for building structures and non-structural components.
- To develop higher performance IMs.

Organization of the report

The thesis is logically subdivided into four chapters:

1. The first chapter introduces the PBEE methodology and sets the present study in its framework. An explanation of the role and the importance of the Intensity Measures in Seismic Probabilistic Risk Analysis is given, as well as an overview of the current state-of-the-art about such parameters. The methodology used to conduct the quantitative evaluation/comparison of the IMs 'performance is also presented.

2. The second chapter is dedicated to the Intensity Measures aiming at predicting structural demand. The derivation of a new structure-specific Intensity Measure, namely ASA_R (Relative Average-Spectral-Acceleration), is proposed and the comparison with the current IMs is performed, based on: a) a large dataset of

recorded earthquake ground motions; b) numerical analyses conducted with state-of-the-art FE models representing actual load-bearing walls and frame structures, and validated against experimental test; and c) systematic statistical analyses of the results. Lastly, the limits of the examined IMs are highlighted.

3. The third chapter is focused on the Intensity Measures aiming to predict Non-Structural Components demand. Following the same approach of chapter 2, a new structure-specific Intensity Measure, namely $E\text{-}ASA_R$ (Equipment-Relative Average-Spectral-Acceleration), is proposed and the comparison with the current IMs is performed.

4. Finally, in the fourth and conclusive chapter, the study and its findings are summarized and perspectives for future work/development are suggested.

1 Seismic Probabilistic Risk Analysis

1.1 PERFORMANCE BASED EARTHQUAKE ENGINEERING (PBEE)

The Seismic Probabilistic Risk Analysis (SPRA) methodology (Kennedy *et al*., 1980); Wakefield *et al*., 2003) is, since decades, the most commonly used approach for evaluating the seismic safety of nuclear engineering structures. In recent years, this methodology has also become popular for characterizing seismic behavior of other civil structures (Hamburger *et al*., 2003; FEMA, 2012), essentially, with the name of Performance-Based Earthquake Engineering (PBEE).

In the form developed by the Pacific Earthquake Engineering Research (PEER) Center, which has been adopted herein as a reference, the PBEE methodology can be broken down into four processes (Figure 1.1): hazard analysis, structural analysis, damage analysis, and loss analysis.

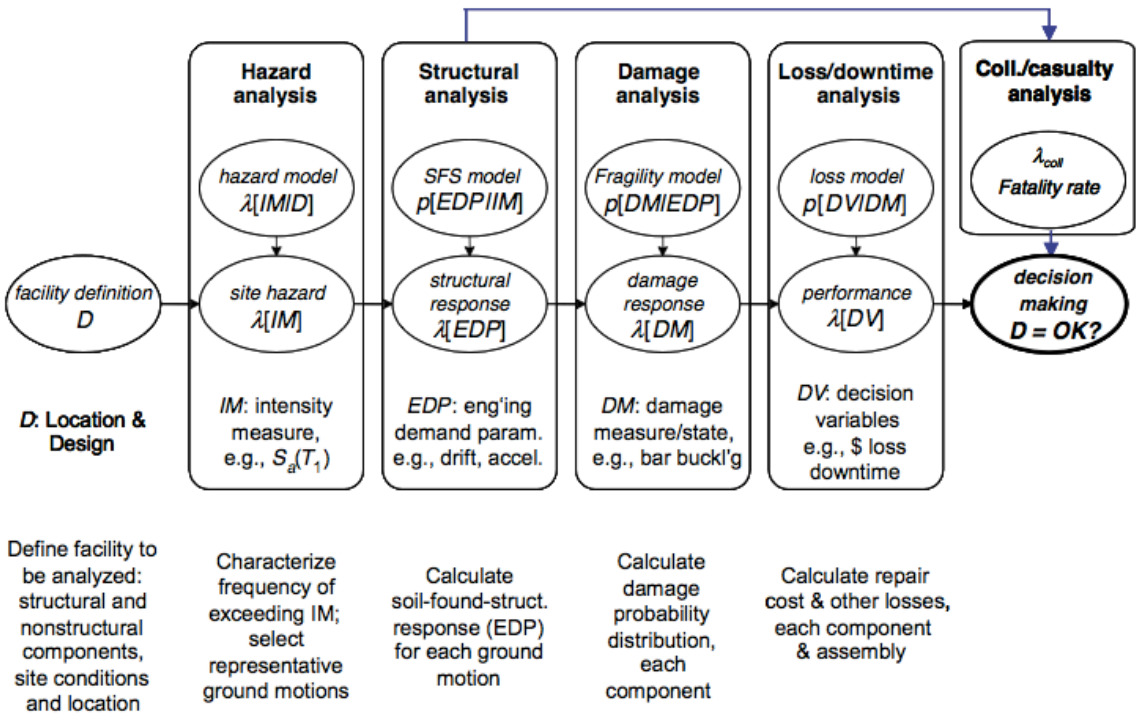

Figure 1.1 *Overview of PEER-PBEE methodology. Reproduced from Krawinkler (2005).*

During the hazard analysis, the seismic hazard is evaluated for the facility site and ground-motion time histories, whose Intensity Measures (IMs) correspond to the various

hazard levels, are produced. During the structural analysis phase, nonlinear time-history analyses are performed in order to calculate the facility's response to ground motions of a given IM in terms of drift, roof displacement, floor response spectrum features or other Engineering Demand Parameters (EDPs). During the damage analysis phase, these EDPs are used along with component fragility functions to determine Damage Measures (DMs) specific to facility components. Lastly, given these DMs, a set of variables including operability, repair costs/duration and potential for casualties can be evaluated. Such performance measures are referred to as decision variables (DVs) since they serve to inform stakeholder decisions regarding future performance.

Each relationship in this four-phase process, from location and design to IMs, IMs to EDPs, EDPs to DMs and DMs to DVs, involves uncertainties and is treated probabilistically. Indeed, the probabilistic expressions of the PBEE methodology components can be integrated by the total probability theorem (Benjamin and Cornell, 1970) and expressed as:

$$\lambda(DV) = \int_{DM}\int_{EDP}\int_{IM} p\left[DV|DM\right] p\left[DM|EDP\right] p\left[EDP|IM\right] \lambda\left(IM\right) dIM\ dEDP\ dDM \qquad (1.1)$$

where

$p[\ ]$ = Probability Density Function (PDF) of the quantity inside the brackets

$\lambda\ (IM)$ = Mean Annual Frequency (MAF) of events with intensity IM

$\lambda\ (DV)$ = MAF of events with value DV of the decision variable

Each function represents one element of the analysis methodology: $\lambda[IM]$ reflects the results of the hazard analysis; $p[EDP|IM]$ reveals the structural analysis; $p[DM|EDP]$ represents the damage analysis; and $p[DV|DM]$ returns the loss analysis.

The inspection of equation (1.1) reveals that it "de-constructs" the assessment problem into the four basic elements of hazard analysis, structural analysis, damage analysis, and loss estimation, by introduction of the three "intermediate variables," IM, EDP, and DM. Then it "re-couples" the elements via integration over all levels of the selected intermediate variables. This integration implies that in principle one must assess the conditional probabilities $p[EDM|IM]$, $p[DM|EDP]$ and $p[DV|DM]$ parametrically over a suitable range of DM, EDP, and IM levels. The assumption is that appropriate variables (IMs, EDPs and DMs) are chosen such the conditioning information do not need to be "carried forward" (e.g., given EDPs, the DMs are conditionally independent of IM; otherwise IM should appear after the EDPs in the first factor.) So, for example, the EDPs should be selected so that the DMs

(and DVs) do not also vary with intensity, once the EDP is specified. Similarly one should choose the Intensity Measure (IM) so that, once it is given, the dynamic response (EDP) is not also further influenced by, say, magnitude or distance to the source, which have already been integrated into the determination of $\lambda(IM)$ (Krawinkler and Miranda, 2004).

The present work, in the framework of the SPRA/PBEE methodologies, focuses on the interface between Hazard Analysis and Structural Analysis and aims at reducing the uncertainty in the engineering characterization of the seismic ground motions.

1.1.1 Hazard Analysis

The goal of PBEE analyses is to ensure that a structure can withstand a given level of ground shaking while maintaining a desired level of performance. Due to the great deal of uncertainty about the location, size, and resulting shaking intensity of future earthquakes, the question that arises is: what level of ground shaking should be used to perform this analysis? Probabilistic Seismic Hazard Analysis (PSHA) (Cornell, 1968; Kramer, 1996; Baker, 2008) aims to quantify these uncertainties, and combines them to produce an explicit description of the distribution of future shaking that may occur at a site.

To perform PSHA analysis leads to describe the earthquake hazard in a probabilistic manner, considering nearby faults, their magnitude-recurrence rates, fault mechanism, source-to-site distance, site conditions, etc., and employing attenuation relationships, such as Ground Motion Prediction Equations (GMPEs). The end result of hazard analysis is Hazard Curve (e.g., Figure 1.2), which describes the variation of the selected IM versus its Mean Annual Frequency (MAF) of exceedance (Bommer and Abrahamson, 2006).

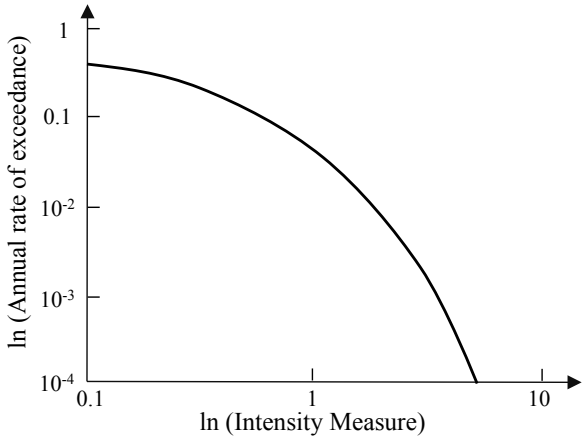

Figure 1.2 *Example of a Hazard curve, i.e. λ(IM).*

Furthermore, in order to perform time-history structural analysis, Hazard Analysis also involves the selection of a number of ground-motion time histories "compatible" with the hazard curve. For example, if *PGA* is utilized as IM, for each *PGA* value in the hazard curve, an adequate number of ground motions should be selected which possess that value of *PGA* (i.e., adequate number refers to the number of ground motions which would be adequate to provide meaningful statistical data in the structural analysis phase (see paragraph 1.2.1)). Additionally, based on the current approach (Bommer and Acevedo, 2004; Katsanos *et al*., 2010) and in order to be consistent with the probabilistic seismic hazard analysis, selected ground motions should be in principle compatible with the magnitude and distance combination which dominates the hazard for a particular value of IM (Sommerville and Porter, 2005).

Thus, the foregoing highlights the capital role of IMs in modern Probabilistic Seismic Risk Analysis methods: to quantify the seismic hazard at the facility site.

1.1.2 Structural Analysis

In PBEE, Structural Analysis is conducted to determine the response of a structure to various levels and characteristics of earthquake hazard in a probabilistic manner. For this purpose, a computational model of the structure should be developed. Uncertainties in parameters defining the structural model (e.g. mass, damping, stiffness, and strength) can be considered by varying the relevant properties in the model. Nevertheless, it is worth mentioning that Lee and Mosalam (2006), based on analyses conducted for one of the testbeds of PEER-PBEE methodology, have shown that ground motion variability is more significant than the uncertainty in structural parameters in affecting the EDPs. For such a reason, deterministic structural analyses have been conducted in this work.

For each intensity level of earthquake hazard, nonlinear time history analyses are conducted to estimate the structural responses in terms of selected Engineering Demand Parameters (EDPs), using the ground motions selected for that intensity level. EDPs may include local parameters such as element forces or deformations, or global parameters such as floor acceleration and global displacement. The PBEE formulation requires a single value for EDP. Therefore, peak values of the above EDPs are generally employed. It is possible to use different EDPs for different damageable components of a structure: for example, inter-story drift can be used for the structural system of a building (Krawinkler, 2005), while using floor acceleration for office or laboratory equipment (Comerio, 2005) of the same building. The

products of the structural analysis phase are conditional probabilities, p[EDP|IM], which can then be integrated with the λ(IM) to calculate Mean Annual Frequency of exceeding each EDP.

It is likely to observe global collapse at higher intensity levels (in a simulation, global collapse corresponds to infinite increase of response for infinitesimal increases in input intensity, i.e. global dynamic instability). Global collapse is treated separately (Figure 1.1) in PEER-PBEE methodology since its probability does not change from a damageable component to the other.

1.1.3 Damage and Loss Analyses

After the determination of probabilities of EDPs in the structural analysis phase, these probabilities should be used to determine the Probability of Exceedence of DVs. This is achieved through the damage analysis and the loss analysis stages.

The purpose of the damage analysis is to estimate the probabilities of physical damage at the component or system levels as a function of the structural response. Indeed, the response predicted by analytical demand models does not necessarily correlate to physical descriptions of damage, failure, and collapse. Therefore, observed, experimental, or analytical estimates of damage are often incorporated into the PBEE formulation by determining damage induced at different levels of structural response. The tool used to determine the above probabilities is the "*fragility function*," (detailed in paragraph 1.2.1). In the context of the PBEE damage analysis, a fragility function represents the Probability of Exceedence of a Damage Measure (DM) for different values of an EDP. Examples of Damage Measures for reinforced concrete structural elements include cracking, spalling, transverse reinforcement fracture, longitudinal reinforcement buckling, and failure. Also, Damage Measures may be defined in terms of damage levels corresponding to the repair measures that must be considered to restore the components of a facility to the original conditions (Porter, 2003). For example, Mitrani-Reiser *et al*. (2006) defined DMs of structural elements as light, moderate, and severe corresponding to repair with epoxy injections, repair with jacketing, and element replacement, respectively.

Note that damage level of a damageable component shows variance, even for the same value of EDP. This is mainly due to the differences in the pattern and history of the structural response. In fact, EDPs are generally represented as peak quantities, however differences in

the path of achieving the same peak value introduces differences in the observed damage and these differences set the variance of the DM corresponding to an EDP (for instance, the same max inter-story drift value can be "transitory" or "permanent", corresponding to different damage states, paragraph 2.3.1).

Loss analysis is the last stage of PEER-PBEE methodology, and its goal is to estimate the frequency with which various levels of performance are exceeded. In this phase, damage information obtained from the damage analysis is converted to the final decision variables (DVs). DVs are defined at the system level, such as total repair cost, number of casualties, or repair duration.

Finally, these Decision Variables can be used directly by a structural engineer in the design or re-evaluation process with the inclusion of stakeholders for decision-making about the design or retrofit.

1.2 FRAGILITY (LIMIT STATE) METHOD

It is worth to note that the formulation (Eq. 1.1) of the PEER-PBEE method contains as special case one of the most common limit-state estimation scheme. This is that using "*fragility curves*" (Kennedy *et al*., 1980), which typically represent the probability of some binary *Limit State* (LS) as a function of a ground motion parameter (IM). Such a special case is obtained from Eq. 1.1 taking as decision variable the Limit State (i.e. DV=LS) and "collapsing" the second and the third integrals, by leaving:

$$\lambda(LS) = \int_{IM} p\left[LS \middle| IM\right] \cdot \lambda\left(IM\right) dIM \tag{1.2}$$

in which p[LS|IM] is the fragility curve.

The "Fragility method" constitutes the core of the first Seismic Probabilistic Risk Assessment (SPRA) studies, which have been carried out for nuclear power plants in the U.S. in the late seventies and are now used worldwide in order to assess seismic safety of existing or projected nuclear power plants. Besides, nowadays collapse fragility functions obtained from structural analysis results are increasingly popular in structural assessment procedures (e.g., FEMA, 2012).

The key elements of this methodology, which allows for the proper evaluation of failure probability due to all possible earthquake events, are seismic hazard analysis (paragraph 1.1.1), seismic fragility evaluation for each component and substructure, and system analysis

and construction of logical fault tree model. This latter is not detailed in this report, however the reader can found details about it in EPRI (1994) or EPRI (2002).

Fragility Analysis Fragility Analysis involves the estimation of the conditional probabilities of some structural (or non-structural) Limit-State (LS) for a given ground motion "capacity" A, which is defined as the threshold seismic load before the limit-state occurs.

The current approach (Kennedy *et al*., 1980) consists in modeling ground motion capacity A as a random variable having lognormal distribution, that is:

$$A = A_m \ \varepsilon \tag{1.3}$$

where A_m is the best estimate of the ground motion median capacity (i.e. the A level with 50% probability of reaching the limit state) and ε is a log-normally distributed random variable with unit median and logarithmic standard deviation β.

A component or structure attains the limit state if its seismic capacity is less or equal to given ground motion intensity, therefore the fragility curve represents the probability to reach the limit state for a given seismic ground motion intensity a. In formal terms, the probability that a ground motion with IM=a will cause the limit state event LS is given by the Cumulative Distribution Function (CDF) of ground motion capacity A (1.3), which yields:

$$p\left[LS \middle| IM = a\right] = \Phi\left(\frac{\ln\left(\frac{a}{A_m}\right)}{\beta_R}\right) \tag{1.4}$$

where Φ (.) is the standard normal Cumulative Distribution Function. Thus by using the lognormal model a fragility curve is entirely defined by two parameters, which are the median capacity A_m and the logarithmic standard deviation β.

This fragility model can be further detailed by distinguishing *aleatory uncertainties* and *epistemic uncertainties*. The first kind of uncertainty is associated to inherent random phenomena (such as earthquakes), whereas the latter uncertainty could be reduced by having a better model and/or collecting new data. Epistemic uncertainty is considered by modeling the median capacity in Eq. (1.3) by a lognormal random variable:

$$\tilde{A}_m = A_m \ \varepsilon_U \tag{1.5}$$

whilst aleatory uncertainty is associated to variability with respect to the median. Considering uncertainty of median capacity yields:

$$A = \left(A_m \ \varepsilon_U\right) \ \varepsilon_R \tag{1.6}$$

In the above expression, both ε_R and ε_U are lognormal distributed random variables with unitary median values and respective log-standard deviations β_R and β_U. More precisely, β_U characterizes uncertainty in the knowledge of the median value whereas β_R refers to inherent randomness.

Then by virtue of (1.4) and (1.6), conditional probability of failure (i.e. fragility) becomes a random variable, expressed as:

$$p'\left[LS \middle| IM = a\right] = \Phi\left(\frac{\ln\left(\frac{a}{A_m}\right) + \beta_u \Phi^{-1}(Q)}{\beta_R}\right) \tag{1.7}$$

with $Q = p[p<p' \mid IM=x]$ the level of confidence than the conditional probability of failure p is less than p' for a ground motion of IM=a. Therefore, Equation (1.7) defines a family of curves corresponding each to a confidence level Q (Figure 1.3).

Note that the more sophisticated model (1.7) and the simple model (1.4) are linked by the relation:

$$\beta = \beta_C = \sqrt{\beta_R^2 + \beta_U^2} \tag{1.8}$$

With $\beta = \beta_C$ the fragility curve described by (1.4) is called *composite fragility*, this does not require a separated estimation of the uncertainty and can be considered as a ”best estimate” fragility curve. It can be shown (Kennedy *et al*., 1980) that the composite curve corresponds to the mean fragility curve, while expression (1.7) yields the median curve for $Q = 0.5$ or in the case only random uncertainty (i.e. $\beta_U = 0$) is considered (example in Figure 1.3).

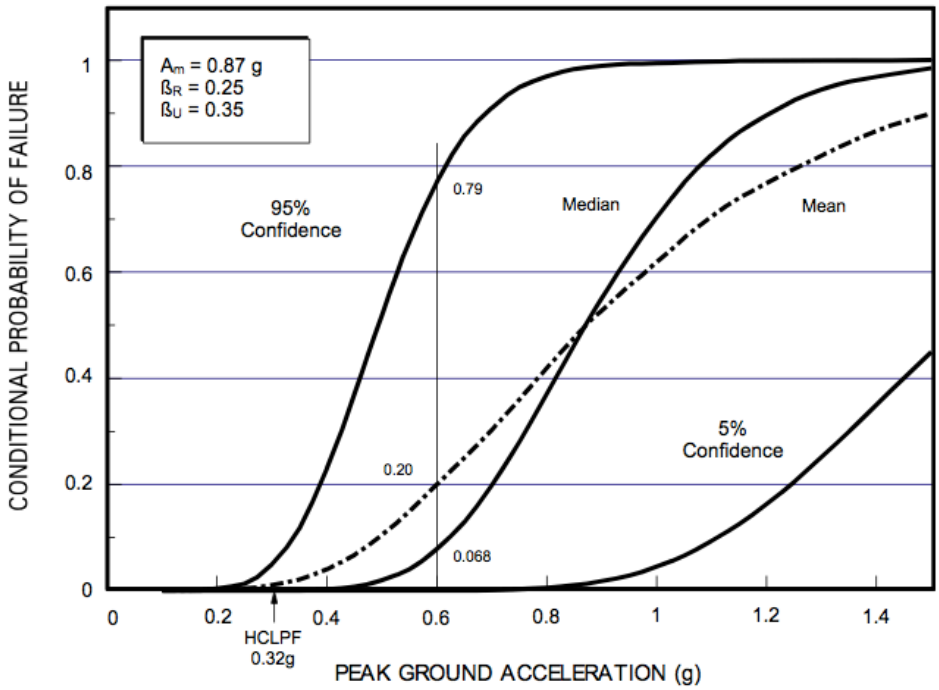

Figure 1.3 *Mean, Median, 5% Non-Exceedance, and 95% Non-Exceedance Fragility Curves for a component. Reproduced from EPRI (2009).*

1.3 INTENSITY MEASURES (IMs)

The Hazard Analysis begins with definition of one (or more) ground motion Intensity Measure (IM) that should capture the important characteristics of earthquake ground motion affecting the response of the structural framing and nonstructural components. The IM, which may be a ground motion parameter such as peak ground acceleration or spectral response quantity, is expressed typically as a function λ(IM) of Mean Annual Frequency of exceedance (Figure 1.2), which is specific to the location of the building and often to its dynamic characteristics (e.g., fundamental natural frequency).

1.3.1 Advantages of the use of Efficient and Sufficient IMs

In this paragraph, the aim is to illustrate the advantages derived by the use of efficient and sufficient IMs.

For the purpose of explication, it is assumed here that the PBEE procedure requires the engineer to confirm that the Mean Annual Frequency of an important limit state (e.g. global structural collapse), herein denoted *LS,* is less than a recommended value.

Therefore, given the PBEE objective of estimating λ_{LS} (i.e., MAF of the event *LS*), the problem subdivides in characterizing the seismicity surrounding the facility's site and

assessing the behavior of the structure given a particular earthquake event occurs. This means, in formal terms, to find λ(X) and P[LS|X]: λ(X) is the MAF of earthquake events in the region characterized by the vector X of parameters (e.g. magnitude, source-to-site distance, fault-type, etc.); P[LS|X] is the conditional probability of *LS* given an event of characteristics X. With this information the total probability theorem states that:

$$\lambda_{LS} = \int P\left[LS|X\right]\left|d\lambda(X)\right| \tag{1.9}$$

where the differential $|d\lambda(X)|$ is the "MAF density" (or absolute value of the partial derivative of λ(X)) times the product of all the components of X (i.e. dx1dx2…).

Assuming, for simplicity, that X = [M, R] (i.e. the magnitude and the source-to-site distance of the earthquake), three ways are available in order to estimate P[LS|X] (Cornell, 2004):

Method 1: Direct estimation A direct way of estimating P[LS|X] is to prepare a random sample of equally likely *n'* ground motion records, then to analyze the structure for each of the *n'* records, and count the number of observations *r* of the event *LS*. Then, the estimation of P[LS|X] is simply *r/n'*. This process must be repeated for *m* well selected sets of the parameters X_i (i = 1, ...*m)* for a total of *n = n'm* records. Then, the estimate of λ_{LS} is:

$$\lambda_{LS} \approx \sum P\left[LS|X_i\right]\Delta\lambda(X_i) \tag{1.10}$$

in which $\Delta\lambda(X_i)$ is approximately the MAF of events with characteristics X_i.

This procedure implies that the engineer must have a sample size (*n'*) large enough to estimate each of the *m* P[LS|X] adequately. Supposing, for example, that this condition of adequacy can be satisfied by estimating the mean Maximum Inter-story Drift Ratio (MIDR) with a standard error of 10% and considering, for example, that the standard deviation of the MIDR of a typical frame in near failure regime is at least 0.8 (Cornell, 2004):

A basic result in statistic (Benjamin and Cornell, 1970) tell us that:

$$SE = \frac{\sigma}{\sqrt{n}} \tag{1.11}$$

where *SE* is the Standard Error of the estimate of the mean of a random sample *n* characterized by a Standard Deviation *σ*.

Therefore, the necessary sample size is about $(0.8/0.1)^2$ (i.e. order 50). Assuming that m = 10 to 20 (in order to cover adequately the range of X = [M, R]), the total required sample size is of order 1000.

Method 2: use of an "efficient" IM With the objective of reducing the number of nonlinear analyses, it is helpful to introduce the use of an IM. With the introduction of this variable and the total probability theorem, it can be written:

$$\lambda_{LS} = \iint P\left[LS \middle| IM, X\right] f\left(IM \middle| X\right) \left| d\lambda(X) \right| \tag{1.12}$$

in which f(IM|X) is the conditional probability density function of the IM given X, which is ordinarily available as a Ground Motion Prediction Equation. The estimation of P[LS|IM, X] would proceed as in method 1 except that the records selected in each X_i "bin" (e.g., each M-R pair) should also have a specified IM level, usually obtained by simply scaling the record to that level. Then, for each of several levels of IM the set of records is analyzed and the probability for that IM level and X bin P[LS|IM, X] is estimated as in method 1 as the ratio *r/n'*. Upon repetition over the set of X_i bins, it can be written:

$$\lambda_{LS} \approx \sum\sum P\left[LS \middle| IM_j, X_i\right] \Delta f\left(IM_j \middle| X_i\right) \Delta\lambda(X_i) \tag{1.13}$$

The advantage of introducing an *efficient* IM is that the dispersion (defined here as the standard deviation of the natural log) of the MIDR given IM and X is only about 0.3 to 0.4 for a nonlinear MDOF frame at large ductility levels. This implies (Eq. 1.11) that only $(0.35/0.1)^2$ (i.e. order 10) records are necessary for each first factor in the summation. However, assuming 4 to 6 IM levels and 10 to 20 X_i bins, the total required sample size is still in the range of 500.

However, if the IM is well chosen experience shows (Shome *et al*., 1998; Cornell, 2004; Luco and Cornell, 2007) that all the variables in X may be found to be statistically insignificant, or at least practically so, i.e., the response given IM is no longer importantly sensitive to M and R. The reader must note that this is not totally unexpected: in the limit case of IM equal S_{pa} at frequency f_1, the maximum response of a simple linear SDOF oscillator with natural frequency f_1 is totally insensitive to the couple Magnitude-source-to-site-distance once the IM is known.

Method 3: Use of an "efficient" and "sufficient" IM An IM is said *sufficient* if P[LS|IM, X] = P[LS|IM], that is if the probability of the event *LS* given IM and X does not depend on X at all. In this case equation (1.12) can be simplified as:

$$\lambda_{LS} = \iint P\left[LS|IM,X\right] f\left(IM|X\right) \left| d\lambda(X) \right| = \int P\left[LS|IM\right] \left| d\lambda_{IM}(IM) \right| \tag{1.14}$$

in which λ_{IM} is simply the "hazard curve" of the IM, i.e., $\lambda_{IM}(u)$ is the mean annual frequency that the IM exceeds a specific value *u*. This can be obtained by conventional PSHA provided the engineer has specified which IM is appropriate for his particular structure. Then, the estimation of λ_{LS} reduces to selecting a set of records, scaling them to each of a set of IM levels, estimating as above the probability P[LS|IM] and then summing:

$$\lambda_{LS} \approx \sum P\left[LS|IM\right] \Delta_{IM}(IM) \tag{1.15}$$

Assuming that the dispersion of for example MIDR given a value of IM is about 0.3 to 0.4, each level will take order 10 samples and there need to be 4 to 6 levels then the total number of runs is only about 50.

Summing up,

the two main characteristics defining IMs are *efficiency* and *sufficiency*. An IM is defined efficient if it allows, for a given value, to obtain a reduced variability in the structural response; a sufficient IM, on the other hand, is defined as the one that, for a given value, renders the structural response conditionally independent of earthquake magnitude and source-to-site distance (Luco and Cornell, 2007). The choice of IM has a deep impact on the simplifying assumptions and methods that can be used to evaluate accurately and efficiently the risk integral, which aggregates the results of the sub-tasks of the PBEE process (Conte *et al*., 2003). An improved IM (i.e. able to better capture the damaging features of a record and the site hazard), besides reducing the record-to-record variability, makes criteria for selecting input ground motions for inelastic time-history analyses become less strict.

1.3.2 Effect of IMs efficiency on Fragility formulation

Figure 1.4 shows an example of fragility curves computed through the Eq. (1.7) and assuming the absence of epistemic uncertainty (i,e. $\beta_U = 0$): all the curves represented have the same median capacity A_m but different logarithmic standard deviation β_R.

The absence of epistemic uncertainty means that median capacity A_m is affected only by aleatory uncertainty β_R, which is essentially due (EPRI, 2009) to the randomness of the earthquake characteristics given the same IM value (i.e. record to record variability). Besides, as it will be clarified in paragraph 1.4.3, β_R is the *efficiency* of the Intensity Measure.

Accordingly, if the chosen ground motion Intensity Measure is not well correlated to the considered limit-state (for instance, failure), then the β_R value (i.e., IM efficiency) reflects this 'uncertainty'. Consequently (Figure 1.4), the poorer the correlation between ground motion IM and limit-state, the larger the value of β_R, and the more spread out (i.e., flat) the fragility curve becomes indicating a wider range of ground motion intensities (IM=a) over which there is probability than the limit-state will be reached (i.e. larger uncertainty).

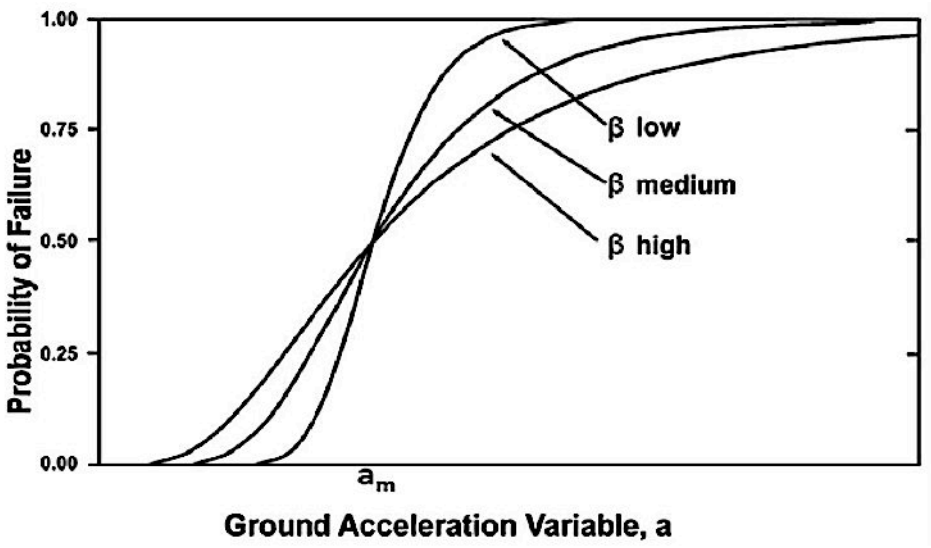

Figure 1.4 *Fragility curves based on the lognormal distribution with same median capacity a_m and different logarithmic standard deviation $\beta = \beta_R$. Reproduced from EPRI (2009).*

1.3.3 State of the Art

Intensity Measures can be usefully classified in three main groups:

- *Peak based IMs*: measures of maximum absolute values of ground motion's time history characteristics.
- *Duration based IMs*: integration of a ground motion time histories' characteristic over the duration of the signal.
- *Frequency-response based IMs*: based on the response of elastic oscillators to the ground motion time history.

An author's selection of the most recognized IMs from each of these classes (Table 1.1) is compared in this study. The Intensity Measures selected are examples of the best-known measures that have been proposed to quantify the damage potential of seismic events. Although, such list of IMs is not exhaustive as the literature is full of different variations of the given parameters.

The possibility of using IMs is a critical aspect within the framework of Probabilistic Seismic Hazard Analysis (PSHA). Highly efficient IMs, which due to their complex formulation render seismic hazard computations impossible, tend not to be employed in engineering practice despite their high performance. For instance, the IM of Luco and Cornell (2007) requires for its definition (Eq. 1.16) the values of the first two natural period (T_1, T_2), the first two modal participation factors (PF_1, PF_2) and the yield displacement (d_y) of the structure:

$$IM_{Luco\&Cornell} = \frac{S_d^I\left(T_1,\xi_1,d_y\right)}{S_d\left(T_1,\xi_1\right)} \cdot \sqrt{[PF_1^2 \cdot S_d\left(T_1,\xi_1\right)]^2 + [PF2_1^2 \cdot S_d\left(T_2,\xi_2\right)]^2} \tag{1.16}$$

Therefore, IMs requiring more substantial structural information than fundamental natural frequency are not considered in this comparative study. Furthermore, such advanced, complex and even elaborate IMs often show slight improvements in performance with respect to simpler ones (Fontara *et al.*, 2012).

***Table 1.1** IMs, from literature, compared in the study*

TYPE	IM	NOTES
Frequency Response Based	$S_{pa}(T_1)$	S_{pa} = pseudo-spectral acceleration at fundamental period
	$I_H = \int_{0.1}^{2.5} S_v(T,\xi)\ dT$	S_v = spectral velocity ξ = damping ratio
	$EPA = \frac{1}{2.5}\int_{0.1}^{2.5} S_{pa}(T,\xi)\ dT$	S_{pa} = pseudo-spectral acceleration ξ = damping ratio
	$ASI = \int_{0.1}^{0.5} S_{pa}(T,\xi)\ dT$	S_{pa} = pseudo-spectral acceleration ξ = damping ratio
	$S* = S_{pa}(T_1)\left(\frac{S_{pa}(T_2)}{S_{pa}(T_1)}\right)^{0.5}$	S_{pa} = pseudo-spectral acceleration T_1 = fundamental period $T_2 = 2 * T_1$
	$I_{NP} = S_{pa}(T_1)\left(\frac{S_{paAV}(T_1,...,T_2)}{S_{pa}(T_1)}\right)^{0.4}$	S_{paAV} = Averaged pseudo-spectral acceleration between T_1 and T_2 T_1 = fundamental period $T_2 = 2 * T_1$
Peak Based	$PGA = \max\lvert a(t)\rvert$	a(t) = acceleration time history
	$PGV = \max\lvert v(t)\rvert$	v(t) = velocity time history
Duration Based	$I_A = \frac{\pi}{2g}\int_0^{t_f} a(t)^2\ dt$	a(t) = acceleration time history t(f) = total duration of the record
	$CAV = \int_0^{t_f} \lvert a(t)\rvert dt$	a(t) = acceleration time history t(f) = total duration of the record
	$SCAV = CAV_i + \int_{i-1}^{t_i} \lvert a(t)\rvert dt$	a(t) = acceleration values in one-second interval where at least one value exceeds 0.025 g; i =1,…,n with n equal to the record length in seconds
	$a_{RMS} = \sqrt{\frac{1}{T_d}[a(t)]^2\ dt}$	a(t) = acceleration time history T_d = the time elapsed between the first and last excursions of the acceleration above 0.05g.
	$I_c = a_{RMS}^{1.5} T_d^{0.5}$	T_d = the time elapsed between the first and last excursions of the acceleration above 0.05g.

1.3.3.1 Peak-based IMs

Peak Ground Acceleration and Peak Ground Velocity The peak parameters *PGA* and *PGV* are largely used in order to classify the degree of severity of ground motions. They represent, respectively, the peak of the ground motion acceleration and velocity time series. Horizontal *PGA* has commonly been used to describe ground motions because of its natural relationship to inertial forces: indeed, the largest dynamic forces induced in certain types of structures (i.e. very stiff structures) are closely related to the *PGA*. Nevertheless, ground motions with high *PGA* are not necessarily more destructive than motions with lower *PGA*. Very high peak accelerations that last for only a very short period of time (i.e. high-frequency cycles) may cause little damage to many types of structures (Housner, 1975; Newmark, 1975; Blume, 1979; Kennedy, 1980). Indeed, it has been noted, particularly in connection with near-source motions due to low-to-moderate magnitude earthquakes, that structures have performed much better during earthquakes than would be predicted considering the instrumental *PGA* to which the structures were subjected. As reported by Kennedy (1984), examples of this behavior may be seen from the 1966 Parkfield earthquake, the 1971 Pacoma dam earthquake, the 1972 Ancona earthquake and the 1972 Melendy Ranch Barn earthquake record (Figure 1.5a): these earthquake records had instrumental *PGA* lying between 0.5 and 1.2 *g* and yet, only minor damage occurred in the vicinity of the recording sites.

With respect to *PGA*, *PGV* is less sensitive to the higher frequency content of the ground motion (Kramer, 1996), therefore it is suggested as providing a more accurate indication of the damage potential for structures which are sensitive to loading in an intermediate frequency range. Peak Ground Displacement (*PGD*) is instead associated with the low frequency components of ground motion (Kramer, 1996), therefore it could be appropriate for low fundamental frequency building (e.g., tall buildings). However, because this study does not consider such particular kind of buildings, *PGD* has not been herein investigated.

Figure 1.5 *Time and acceleration scales are identical for the two records (i.e. very similar PGA): a) Melendy Ranch 1972 earthquake (M=4.6);b) Konya 1967 earthquake (M=6.7). From Kramer (1996).*

1.3.3.2 Duration-based IMs

Cumulative Absolute Velocity The Cumulative Absolute Velocity (*CAV*) was created as a conservative predictor of earthquake damage threshold for purpose of Nuclear Power Plants safe-shut-down. It is defined as the integral of the absolute value of the acceleration time series, and, in its original formulation, it is computed by equation (EPRI, 1988):

$$CAV = \int_0^{t_f} |a(t)| dt \tag{1.17}$$

where t is the time and $a(t)$ is the acceleration time series of total duration t_f. The name Cumulative Absolute Velocity is explained by the fact that this IM can be considered as the summation of the velocity amplitudes during the time.

It is evident from the definition of *CAV* that its value increases with time until it reaches its maximum value at t_f. Therefore, *CAV* includes the cumulative effect of ground motion duration.

A physical interpretation of *CAV*, formalized by the relationship (1.18) has been proposed by (IAEA, 2013):

$$CAV = T\sqrt{\frac{1}{\pi^2}\omega_c \frac{2S_0\Delta\omega}{\omega_c}} = \sqrt{\frac{2}{\pi}}\sqrt{T}\sqrt{N}\sqrt{\frac{2S_0\Delta\omega}{\omega_c}} \tag{1.18}$$

where T is the duration of the strong motion, N is the number of load cycles, $\Delta\omega$ is the bandwidth, ω_c is the median frequency and S_0 is the power spectrum density function (Kramer, 1996). This equation shows that *CAV* is related to the duration of seismic motions, the frequency of loading over the duration and the seismic response energy. This suggests that *CAV* is a parameter which is deeply linked to cumulative, "fatigue-type", damage.

Standardized Cumulative Absolute Velocity However, it must be highlighted that the calculation of *CAV* can be biased in case of long duration records containing very low (non-damaging) acceleration cycles. For such a reason the original formulation of *CAV* was modified (EPRI, 1991) in order to standardize its calculation accounting for the record length. The recommended method of standardization consists to window the *CAV* computation to a second-by-second basis for a given time history: if the absolute acceleration exceeds 0.025 *g* at any time during each one-second interval, *CAV*, for that second, is calculated and summed (Figure 1.6).

Mathematically, the Standardized *CAV (S-CAV)* is expressed as:

$$SCAV = CAV_i + \int_{i-1}^{t_i} |a(t)| dt \tag{1.19}$$

where

a(t) = acceleration values in one-second interval where at least one value exceeds 0.025 g;

i =1,…,n with n equal to the record length in seconds

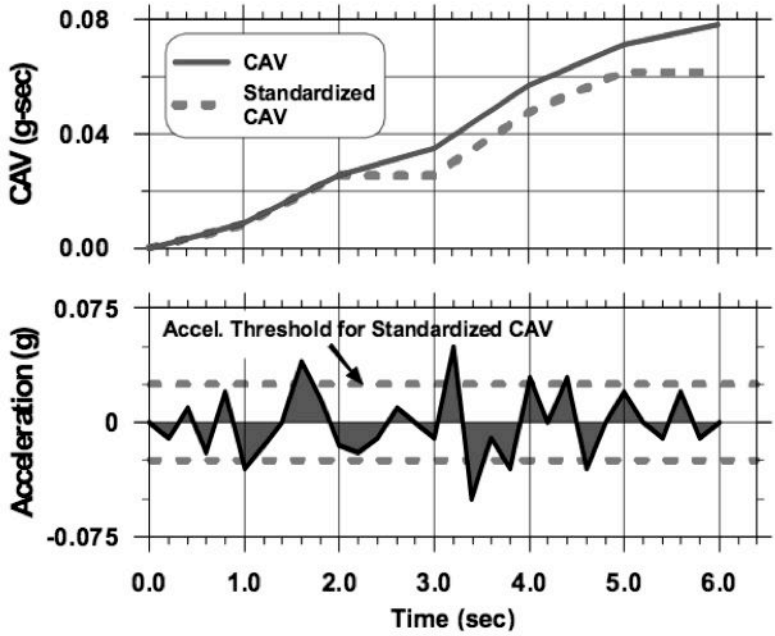

Figure 1.6 *CAV vs. S-CAV. Reproduced from Campbell and Bozorgnia (2010).*

Arias Intensity Arias (1970) suggested that the parameter E_T, given by the relation (1.20), can serve as a measure of the total energy of a signal which total duration is t_f.

$$E_T = \int_0^{t_f} a(t)^2 \, dt \tag{1.20}$$

Then, the (E_T proportional) Arias Intensity takes the form:

$$I_A = \frac{\pi}{2g} E_T \tag{1.21}$$

Successively, Housner and Jennings (1977) demonstrated that $\pi/2 * E_T$ is a measure of the capacity of the ground motion to do work on an idealized uniform population of structures of all natural frequencies; in other words, one might thus consider the Arias Intensity to be a measure of the damage potential of a ground motion record for a uniform population of structures over all the frequencies.

Root-Mean-Square Acceleration Considering the equation (1.20) the average rate of energy input (earthquake power) is given by:

$$P = \frac{E_T}{T_d} \tag{1.22}$$

where T_d is the strong motion duration of the time series.

Then, Mortgat (1979) and McCann and Shah (1979) have suggested, as IM, the Root-Mean-Square Acceleration, which is given by:

$$a_{RMS} = \sqrt{P} = \sqrt{\frac{1}{T_d}\int_0^{T_d} [a(t)]^2 \, dt} \tag{1.23}$$

Characteristic Intensity Successively (Ang, 1990) proposed the Characteristic Intensity, expressed as:

$$I_c = a_{RMS}^{1.5} T_d^{0.5} \tag{1.24}$$

Note that, differently from the I_A and the CAV that are computed on the whole duration of the record, the a_{RMS} and the I_c can be sensitive to the method used to define the *strong motion duration*. In the present work, the strong motion duration as been identified as the *bracketed duration* (Bolt, 1969), i.e. the time elapsed between the first and last excursions of the acceleration above 0.05g.

1.3.3.3 Frequency-response based IMs

Spectral acceleration at fundamental period For more than 40 years, design procedures have used low damped spectral acceleration at the fundamental period of the structure, $S_{pa}(T_1)$, as the basic intensity measures, and acceleration response spectra ordinates form the basis for both present national seismic hazard maps and building code procedures.

With respect to the *PGA*, the elastic response spectrum values have the advantage to be primarily influenced by the energy contained within a number of cycles of ground motion and to be little influenced by a few spikes of very high acceleration (Newmark and Hall, 1982). Indeed, Blume (1979) has shown that clipping the highest 30 % off the measured acceleration time history (i.e. using only the 70 % of the record, in an absolute sense, closest to the zero line) produced only about a 5 % reduction in the elastic response spectrum ordinates.

The S_{pa} (T_1) is widely used because it is the perfectly efficient (and sufficient) IM for elastic SDOF systems and Ground Motion Prediction Equations in its terms are very common. However, with respect to real structures, this IM has two major shortcomings: it ignores both the contributions of higher modes to the overall dynamic response and the elongation of the fundamental period associated with accumulation of damage.

Furthermore, the effect of duration of strong motion (or number of cycles of strong inelastic response) is not incorporated into the elastic response spectrum. Thus, a given elastic spectral response ordinate is expected to correspond to greater damage capability for a long duration earthquake than for a short duration earthquake.

Spectral Intensity The Spectral Intensity as been defined by Housner (1959) as:

$$I_H = \int_{0.1}^{2.5} S_v(T,\xi)\ dT \tag{1.25}$$

This quantity is related to the kinetic energy stored in the structure during the earthquake: for a SDOF system such energy is equal to the half of the mass times the square of the pseudo-velocity. Practically, the spectral intensity represents the area under the pseudo-velocity spectrum, the interval of integration (0.1-2.5 s) being chosen as representative of civil engineering structures.

Effective Peak Acceleration The U.S. Applied Technology Council (ATC, 1978) proposed the Effective Peak Acceleration, defined as:

$$EPA = \frac{1}{2.5}\int_{0.1}^{2.5} S_{pa}(T,\xi)\ dT \tag{1.26}$$

which range of integration of the period is the same, broadly covering civil engineering structures, of the I_H.

Acceleration Spectral Intensity Similarly, the Acceleration Spectral Intensity (1.27) has been proposed by Von Thun *et al*. (1998) in order to select ground motions for the analysis of reinforced concrete dams, which typical period is in the range 0.1-0.5 s.

$$ASI = \int_{0.1}^{0.5} S_{pa}(T,\xi)\ dT \tag{1.27}$$

Spectral Shape IMs The S^* (1.28) (Cordova *et al*., 2001) and the I_{NP} (1.29) (Bojorquez *et al*., 2011) are IMs aiming to take into account the non-linear structural

behavior. Their formulations combine to the $S_{pa}(T_1)$ factors aiming to describe the spectral shape in the period lengthening zone of the response spectrum.

$$S^* = S_{pa}(T_1) \cdot a_1^{0.5} \qquad \text{with} \qquad a_1 = \left(\frac{S_{pa}(T_2)}{S_{pa}(T_1)} \right) \tag{1.28}$$

$$I_{NP} = S_{pa}(T_1) \cdot a_2^{0.4} \qquad \text{with} \qquad a_2 = \left(\frac{S_{paAV}(T_1,...,T_2)}{S_{pa}(T_1)} \right) \tag{1.29}$$

Indeed, with $T_2 = 2T_1$, both the factors a_1 (1.28) and a_2 (1.29) constitute meters of the ascending/descending character of "smooth" response spectra (Figure 1.7). However, considering the irregular character (peaks and valleys) of low-damped response spectra derived from real ground motions time histories (e.g., Figure 1.8), the factors a_1 and a_2 are likely to introduce bias in the evaluation of the spectral shape.

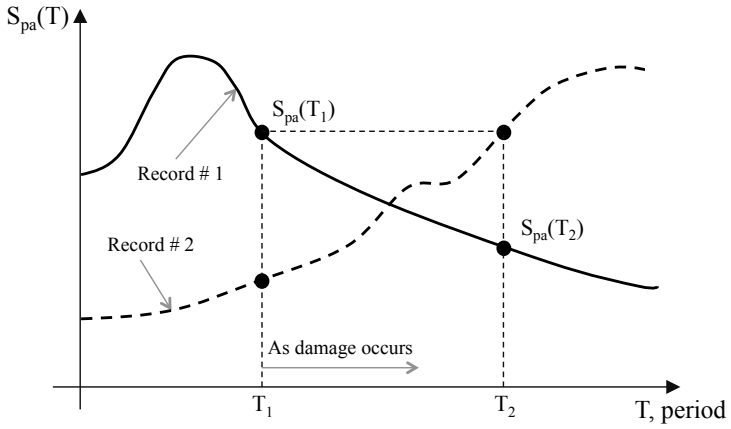

Figure 1.7 *Considering the period lengthening zone (T_1 to T_2): the record 1 decreases its "intensity" (a_1 and a_2 both < 1); the record 2 increases its "intensity" (a_1 and a_2 both > 1). Adapted from Cordova et al. (2001).*

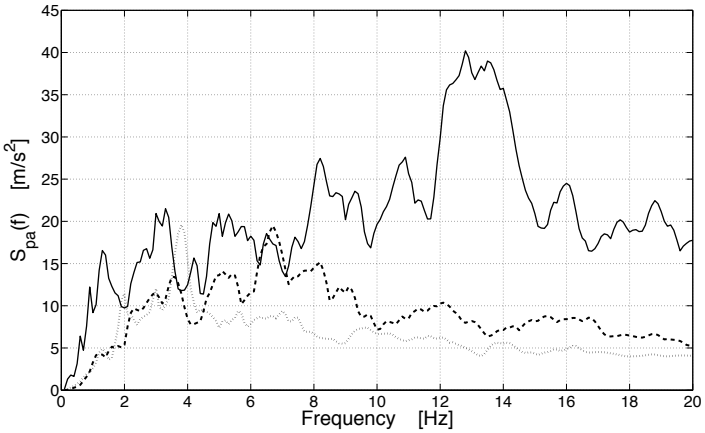

Figure 1.8 *Example: response spectra (2 % damping) for three ground motion records.*

1.4 HOW TO EVALUATE IMs PERFORMANCE

The quantitative evaluation/comparison of IMs performance is performed by following three main steps, as illustrated in Figure 1.9: a) computer analyses of accelerograms derived from the ground motion dataset to provide values of the selected IMs; b) dynamic analyses to generate the structural response of the chosen test-cases structures, for given seismic excitations; and c) statistical analyses of outputs from the two aforementioned steps to determine the efficiency and sufficiency grade for the IMs being examined.

The structural numerical analyses have been conducted with the FE code *Cast3m*®, developed by the French Atomic Energy Agency (www-cast3m.cea.fr), whilst the derivation of IMs as well the statistical analyses have been performed with numerical routines developed by the author in ambient *MATLAB*®.

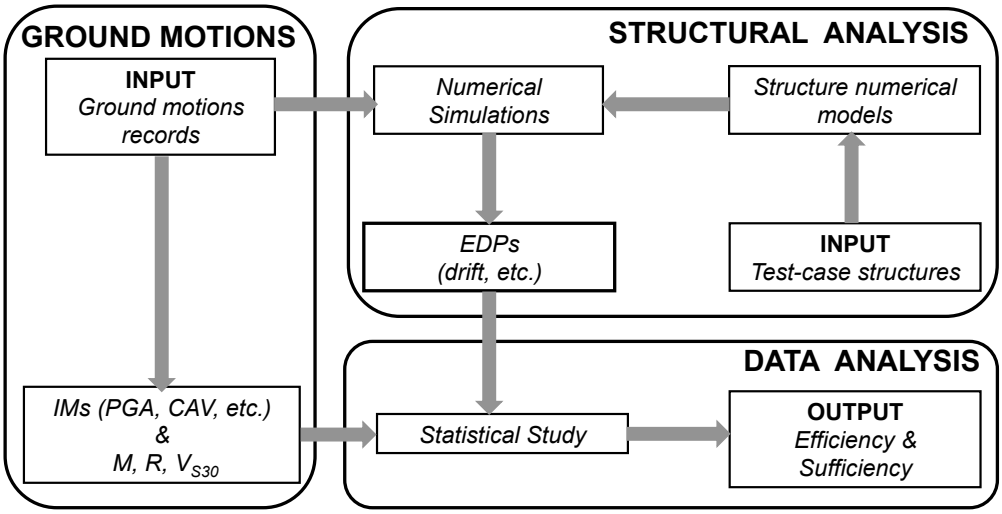

Figure 1.9 *Overview of the IMs' performance evaluation/comparison method.*

1.4.1 Structural Analysis

The study starts with the selection of the test-case buildings: the choice is gone (mostly) towards experimentally tested structures. Indeed, these serve as a validation tool for the numerical models and, provided a sufficiently precise agreement between numerical simulation output and experimental test results, give credence to the results extracted from the numerical models. Furthermore, the selected test cases feature different design characteristics (hence different dynamic properties) allowing to evaluate, in addition to the efficiency and sufficiency, also the *robustness* (Mehanny, 2009) of the IMs. The robustness describes the efficiency trends of an IM-EDP pair across different structures (i.e. different

fundamental frequency) ranges: a robust IM is one whose efficiency is stable with respect to the fundamental frequency of buildings.

To ensure adequacy for this study, the numerical models need to possess three fundamental characteristics: 1) accurate representation of the linear structural dynamic behavior (De Biasio *et al*., 2012); 2) accurate representation of the nonlinear structural behavior in order to replicate the key damage mechanisms under seismic loading; 3) low computational cost to allow, within a reasonable time frame, extending the analysis to a large number of seismic signals, thus adding statistical value to the study.

Lastly, it is important to note that in this study the numerical models serve as comparative tool, and therefore they are not created for the finest quantitative reproduction of the reality but rather for a qualitative and efficient indication of the structural response.

Once the numerical models have been created and validated against experimental tests (when available), dynamic analyses have been conducted for each test case structure making use of the whole, selected, ground-motions dataset.

1.4.1.1 Materials constitutive behavior

A fundamental aspect that arises in the framework of the “structural-demand part" (i.e., Chapter 2) of this study is the selection of the constitutive laws of the materials, concrete and steel (perfect bond is assumed between them), forming the test-case buildings. Indeed, such material behavior laws allow the numerical models to experience (or not) damage, which then is “measured” and associated to the IMs values with the purpose to perform the statistical comparative study of the IMs performance. Consequently, the choice is gone towards performing, robust and broadly-validated material constitutive laws, which are able to reproduce the behavior of both concrete and steel of structures exposed to cyclic loading.

La Borderie model for concrete The damage-based constitutive law chosen to represent concrete behavior (La Borderie *et al.*, 1994) can take into account the decrease in stiffness due to cracking, as well as the stiffness recovery that occurs at crack closure and the inelastic strains concomitant with damage (Figure 1.10). Several benchmarks against results issued from shaking table tests (i.e., Kotronis *et al*., 2005; Nguyen, 2006; Grange, 2008; Grange *et al*., 2012) have corroborated the excellent performance of the La Borderie’s constitutive law with respect to the simulation of reinforced concrete structures under seismic excitation.

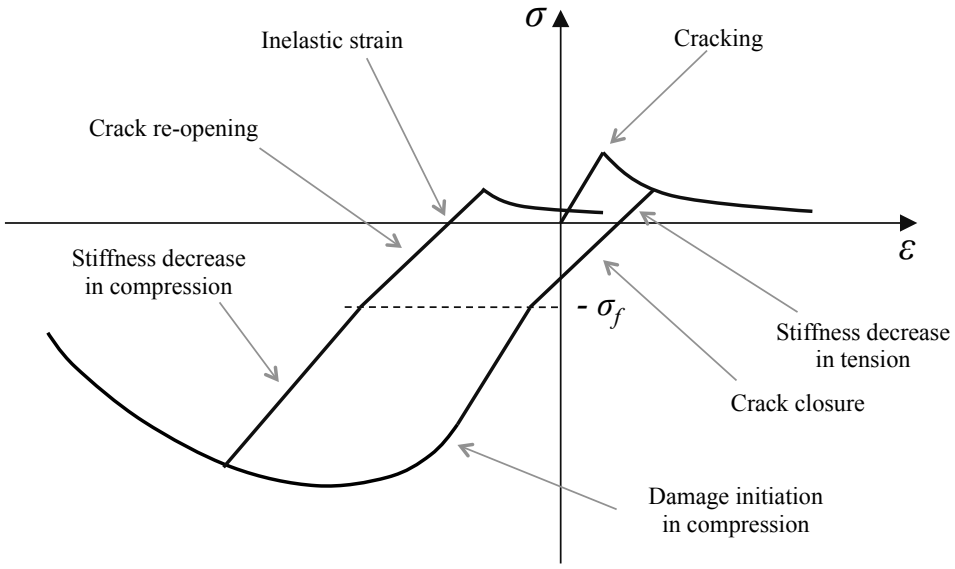

Figure 1.10 *La Borderie's constitutive law for concrete.*

The law is generally expressed in three-dimensional space, though due to the kinematic of the finite elements used in this study only uniaxial formulation is required:

$$\varepsilon = \varepsilon_e + \varepsilon_i \tag{1.30}$$

$$\varepsilon_e = \frac{\sigma^+}{E(1-D_1)} + \frac{\sigma^-}{E(1-D_2)} \tag{1.31}$$

$$\varepsilon_i = \frac{\beta_1 \cdot D_1}{E(1-D_1)} F'(\sigma) + \frac{\beta_2 \cdot D_2}{E(1-D_2)} \tag{1.32}$$

$$\sigma^+ = \sigma \quad and \quad \sigma^- = 0 \qquad if \quad \sigma > 0 \tag{1.33}$$

$$\sigma^+ = 0 \quad and \quad \sigma^- = \sigma \qquad if \quad \sigma < 0 \tag{1.34}$$

The total deformations ε (Eq. 1.30) are defined as the sums of the elastic ε_e (Eq. 1.31) and the inelastic ε_i (Eq. 1.32) deformations; σ^+ (Eq. 1.33) is the tension stress and σ^- (Eq. 1.34) is the compression stress; E is the Young modulus; β_1 and β_2 are material constants driving the inelastic deformations, respectively in tension and in compression; $F'(\sigma)$ (Eq. 1.35 and Eq. 1.36-1.38) is a function that describes the crack closure process and $-\sigma_f$ is the crack closure stress.

$$F'(\sigma) = \frac{\delta F}{\delta \sigma} \tag{1.35}$$

$$if \ \sigma \geq 0 \ then \quad F(\sigma) = \sigma \quad \Rightarrow \quad F'(\sigma) = 1 \tag{1.36}$$

$$f\ -\sigma_f \le \sigma < 0\ \ then \quad F(\sigma) = \sigma\left(1 + \frac{\sigma}{2\sigma_f}\right) \quad \Rightarrow \quad F'(\sigma) = 1 + \frac{\sigma}{\sigma_f} \tag{1.37}$$

$$f\ \sigma < \text{-}\sigma_f \ \ then \quad F(\sigma) = \frac{-\sigma_f}{2} \quad \Rightarrow \quad F'(\sigma) = 0 \tag{1.38}$$

D_1 and D_2 (in Eq. 1.31-1.32) are the variables that quantify the damage, respectively in tension and in compression: they evolve from 0 (sound material) to 1 (totally damaged material), respectfully of the irreversible thermodynamics process (i.e. their values can not decrease). The damage variables (Eq. 1.39) are driven respectively by the energetic variables Y_1 and Y_2 (Eq. 1.40-1.41), Y_{0i} are the thresholds of damage initiation and A_i are material constants.

$$D_i = 1 - \frac{1}{1 + \left[A_i\left(Y_i - Y_{0i}\right)\right]^{B_i}} \qquad i = 1,2 \tag{1.39}$$

$$Y_1 = \frac{(\sigma^+)^2}{2E\left(1 - D_1\right)^2} + \frac{\beta_1 \cdot F(\sigma)}{E\left(1 - D_1\right)^2} \tag{1.40}$$

$$Y_2 = \frac{(\sigma^-)^2}{2E\left(1 - D_2\right)^2} + \frac{\beta_2 \cdot \sigma}{E\left(1 - D_2\right)^2} \tag{1.41}$$

Menegotto & Pinto model for Steel In order to model the behavior of the steel reinforcement bars, a very well known constitutive relation (Menegotto and Pinto, 1973), which includes kinematic hardening, has been selected for the present study.

In this law, three successive zones (Figure 1.11) describe the loading curve under monotonic tension: linear elastic, perfect plastic and hardening.

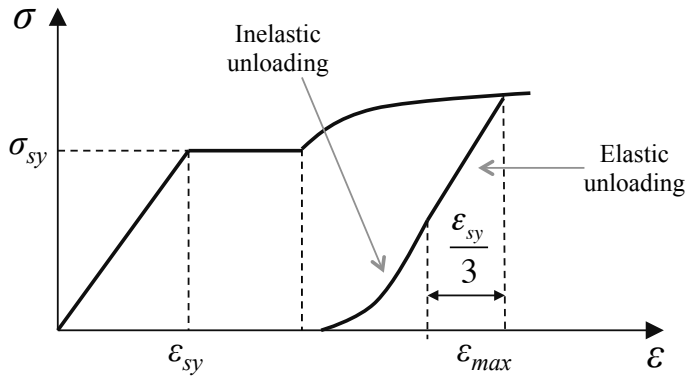

Figure 1.11 *Menegotto & Pinto's law for steel bars: activation of the Giuffre's curve.*

The response of the steel experiencing an unloading depends on the point of unloading: if the point is in the elastic zone, the response is linear; instead, if the unloading point is in the inelastic zone the response is firstly linear, and it successively becomes non-linear when the following relation is verified:

$$\left|\varepsilon_{\max} - \varepsilon\right| > \frac{\left|\varepsilon_{sy}\right|}{3} \tag{1.42}$$

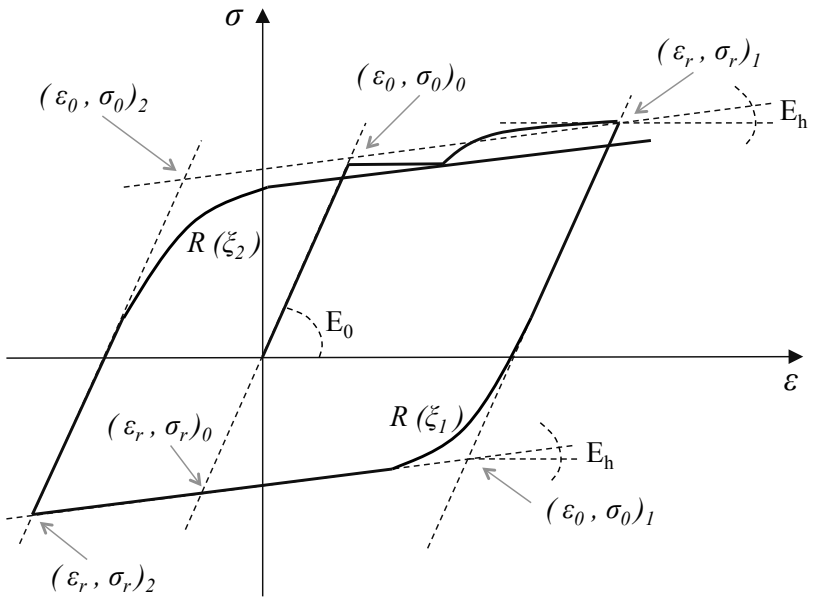

Figure 1.12 *Menegotto & Pinto's law for steel bars. Adapted from Guedes et al. (1994)*

During the loading/unloading cycles (Figure 1.12), the path between two inversion points (half-cycle) is described by:

$$\sigma^* = b \cdot \varepsilon^* + \left[\frac{(1-b)}{\left(1+(\varepsilon^*)^R\right)^{1/R}}\right] \cdot \varepsilon^* \tag{1.43}$$

where:

$$\sigma^* = \frac{\sigma_s - \sigma_r}{\sigma_0 - \sigma_r} \tag{1.44}$$

$$\varepsilon^* = \frac{\varepsilon_s - \varepsilon_r}{\varepsilon_0 - \varepsilon_r} \tag{1.45}$$

$$b = \frac{E_0}{E_h} \qquad with \qquad E_h = \frac{\sigma_{su} - \sigma_{sy}}{\varepsilon_{su} - \varepsilon_{sy}} \tag{1.46}$$

$$R = R_0 - \left(\frac{a_1 \cdot \xi}{a_2 + \xi} \right) \qquad with \qquad \xi = \frac{(\varepsilon_{\max} - \varepsilon_0)}{(\varepsilon_0 - \varepsilon_r)} \tag{1.47}$$

Eq. 1.43 defines a family of curves lying between two asymptotes of slopes E_0 and E_h having the common point (σ_0 , ε_0). The point (σ_r , ε_r) corresponds to the last point of loading inversion, the point (σ_s , ε_s) is the current point. The factor b (Eq. 1.46) represents the ratio between the hardening slope and the elastic slope. The parameter R (Eq. 1.47) describes the shape of the transition path reproducing the Bauschinger effect. The parameters R_0, a_1 and a_2 are material constants.

1.4.2 Ground motions dataset

The ground motion dataset used as input for the FE simulations has been extracted from the 2013 version of the RESORCE database (Akkar *et al.*, 2013), which compiles ground motions recorded in Europe and nearby countries during the past several decades and related to events with moment magnitude (M_w) lying between 2 and 8.

The records with moment magnitudes smaller than 4.5 and a hypocentral distance (R_{hyp}) greater than 100 km have been excluded in order to focus on earthquake excitations of engineering significance. Selecting records with respect to soil type has not been considered an essential step (Singh, 1985; Boore, 2004; Bommer and Acevedo, 2004). Accordingly (Luco and Cornell, 2007), the conditional independence (i.e. *sufficiency*) of IMs with respect to the V_{S30} (i.e. shear wave velocity in the upper 30 m) of records is analyzed.

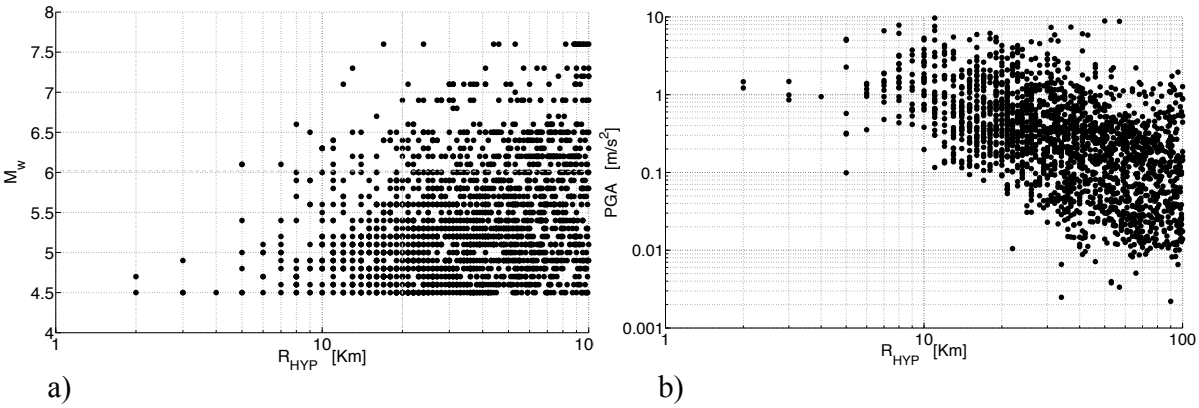

Figure 1.13 *Ground motions used in this study: a) moment magnitude vs. hypocentral distance; b) PGA (geometric mean of the horizontal components) vs. hypocentral distance*

The records (Figure 1.13) have been then clustered for specific moment magnitude and hypocentral distance intervals. In theory, magnitude-dependent clustering implies a more realistic consideration of frequency content and the strong-motion duration of ground motions (Bommer and Acevedo, 2004; Stewart *et al.*, 2002). Two magnitude groups are described in order to account for the above facts: small magnitude (SM, $4.5 \leq M_w \leq 6.0$), and large magnitude (LM, $6.0 < M_w \leq 7.6$). Records in the dataset are thus classified into two R_{hyp} bins: short distance (SR, 0 km $< R_{hyp} \leq$ 20 km), and large distance (LR, 20 km $< R_{hyp} \leq$ 100 km). No screening has been carried out to isolate "pulse-like" records; finally, the 2,045 records composing the dataset are divided into four bins, each with different magnitude and source-to-site distance intervals (Table 1.2).

Table 1.2 *Number of records in each M_w and R_{Hyp} interval pair*

	SR 0 km $< R_{hyp} \leq$ 20 km	LR 20 km $< R_{hyp} \leq$ 100 km
SM $4.5 \leq M_w \leq 6.0$	403	1,286
LM $6.0 < M_w \leq 7.6$	34	322

Regarding the computation of IMs: for the 1D-loaded test-case structures, the first horizontal component of the aforementioned dataset has been input into the FE simulations (the choice of the first component is arbitrary); hence, the IMs have been computed on such a single component. For the 3D-loaded test-case structures on the other hand, the IMs have been computed as the geometric mean of the two horizontal IM component values (Baker and Cornell, 2006a).

1.4.3 Statistical data Analysis

For each test case building, n couples of IMs and EDPs are obtained as output from the n (i.e. 2,045 selected ground-motion records) dynamic analyses.

To evaluate IM *efficiency*, the relationship between EDPs and IMs (whose values have been normalized) is written using a logarithmic transformation as expressed in (1.48), where a_1 and a_2 are constant coefficients and e_i is a random variable representing the randomness in the relationship (Cornell *et al.*, 2002):

$$\ln(EDP_i) = a_1 + a_2 \ln(IM_i) + e_i \tag{1.48}$$

Then, a Linear Least Square (LLS) regression (Figure 1.14) has been used to estimate regression coefficients a_1 and a_2 in Eq. (1.48), whose term e_i (called "residual") represents the error between the computed and estimated values of EDP_i. The validity of the LLS method requires satisfying the normal distribution condition with a constant variance of the residual e_i. Such a study data condition has been examined via residual vs. fit plots and quantile-normal plots of the residuals, both of which were found to be sound.

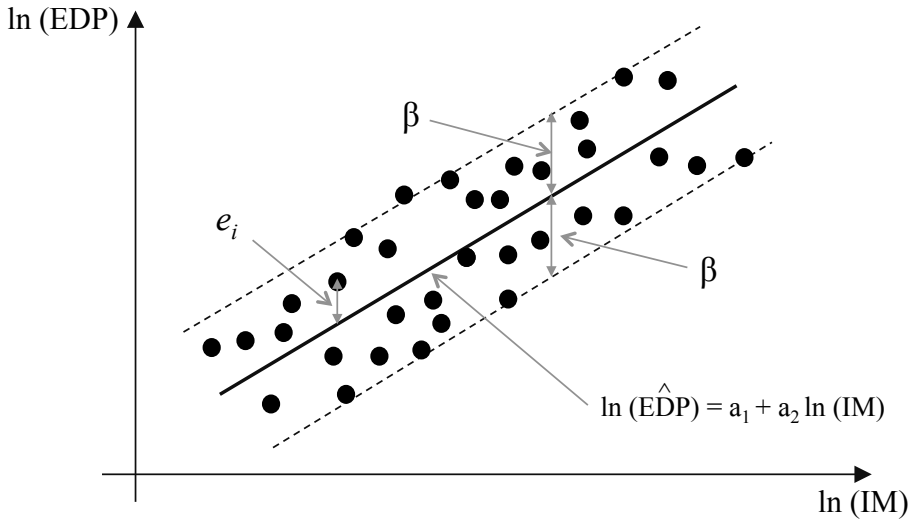

Figure 1.14 *IMs efficiency evaluation: data regression and standard deviation of the residuals.*

Consequently, IM efficiency can be evaluated (Baker and Cornell, 2004) by computing the logarithmic standard deviation (Eq. 1.49) of residual e_i between the computed and estimated values of EDP_i (Figure 1.14): the lower the standard deviation, the higher the IM efficiency.

$$\beta = \sqrt{\frac{1}{n-1}\sum_{i=1}^{n}\left[\ln(EDP_i) - \ln(\hat{EDP}_i)\right]^2} \tag{1.49}$$

In addition, IM *sufficiency* can be evaluated (Cornell, 2004) by verifying whether residuals obtained from the regression carried out using the above statistical procedure show any dependence on other ground motion parameters (i.e. magnitude, source-to-site distance and V_{S30}). In the absence of dependence, then it is possible to assume that these parameters do not affect the structural response for a given IM value. In other words, this finding implies

that with respect to the EDP considered, the selected IM provides a sufficient description of the ground motion features affecting the structural response.

Consequently, in order to assess IM sufficiency, the rank correlation coefficient according to Spearman (1925) has been calculated between regression residuals EDPs-IMs and M_w, R_{hyp} and V_{S30}. The Spearman *rank correlation coefficient* between two variables X and Y is given by the relation:

$$\rho_{Spearman} = 1 - \frac{6\sum_{i=1}^{N} D^2}{N(N^2-1)} \tag{1.50}$$

where D denotes the differences between the ranks of corresponding values of X_i and Y_i, and N is the number of pairs of values (X,Y) in the dataset. Such a coefficient measures how well the data agree with the monotonic (whether linear or nonlinear) ranking. In the case of a perfect positive correlation, the coefficient assumes a "1" value; whereas if the correlation is perfect negative, a "-1" value is assumed. Lastly, when the correlation is not perfect, it lies within the [-1, 1] interval; hence, the closest the absolute value of the correlation coefficient to zero, the more sufficient the IM.

Such efficiency-evaluation-method has been preferred to the p-value (F-test) analysis approach (Luco, 2002) cause this last provides only a “binary” evaluation of the IM (i.e. sufficient or insufficient) without to offer any indication concerning the “degree of insufficiency” (i.e., its engineering significance) when this is detected.

Finally, note that the degree of sufficiency is related the slope of the regression line in the aforementioned scatter plot: the smaller the slope, the higher the sufficiency, and the lower the absolute value of the ranking correlation coefficient (Figure 1.15).

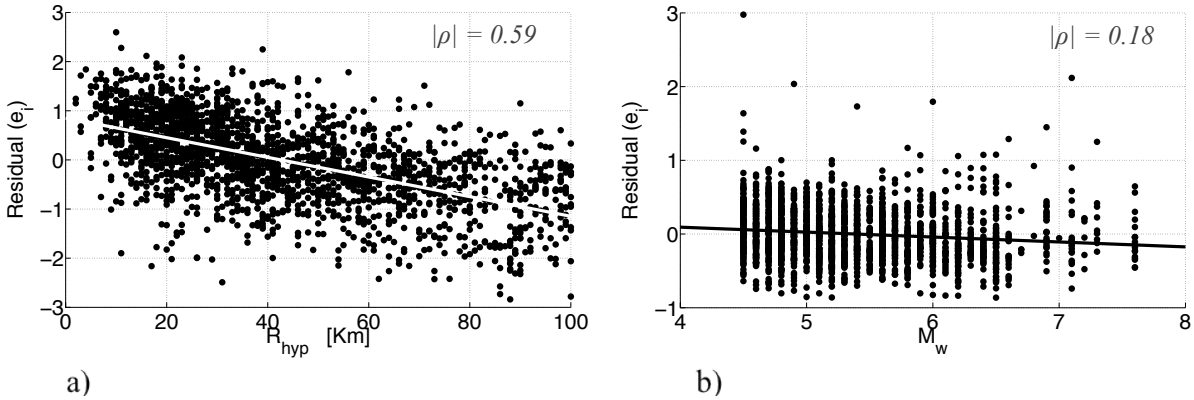

Figure 1.15 *IMs sufficiency evaluation, the sufficiency can be appreciated observing the slope of the regression line (lower the slope, higher the sufficiency): a) example of a non-sufficient IM); b) example of a sufficient IM.*

2 IMs for Structural demand

NOTE: An adaptation of this chapter has been published as: De Biasio M., Grange S., Dufour F., Allain F., Petre-Lazar I., (2014). A simple and efficient Intensity Measure to account for Non-linear Structural behavior. Earthquake Spectra, Volume 30, No. 4, pages 1–24, November 2014. DOI: http://dx.doi.org/10.1193/010614EQS006M

2.1 GROUND MOTIONS' STRUCTURAL-DAMAGING FEATURES

One of the aims of the present work is to propose a new (and more performing) Intensity Measure for structural demand prediction. In order to rationally achieve this goal, the first step is to understand which are the "physical" characteristics of earthquake records making them damaging to structures. For this scope, a non-linear numerical model of a simple test-case structure (CAMUS1, described in paragraph 2.3.1.1) has been herein the object of a study based on the use of elementary sinusoidal excitations. The use of sinusoidal signals allows in a straightforward way to create/isolate features of ground motion records supposed to be relevant in the structural damage process, and therefore to investigate on their genuine effect on the structural behavior.

2.1.1 The importance of frequency content

In order to highlight and to quantify the importance of the seismic excitation's frequency content on the structural response, two series of "preliminary" analyses have been herein performed.

2.1.1.1 Frequency and Amplitude effect

Firstly, single-sinus excitations (Fig. 2.1) with frequency ranging from 1 Hz to 10 Hz and with same amplitude (0.4 g) have been applied to the CAMUS1 structure. Both the induced max inter-story drift ratio and fundamental frequency drop have been recorded, and the $S_{pa}(f_1)$ of the sinusoidal excitations has been computed.

Results presented in Table 2.1 show that independently from the amplitude, due to the *resonance* effect the most damaging excitations are the ones whit frequency closer to the structure's fundamental frequency. This suggests that IMs that do not explicitly consider the fundamental frequency of the structure are less efficient than the ones that do it. Indeed (Table 2.1), the $S_{pa}(f_1)$ has a stronger correlation with structural damage than the *PGA*.

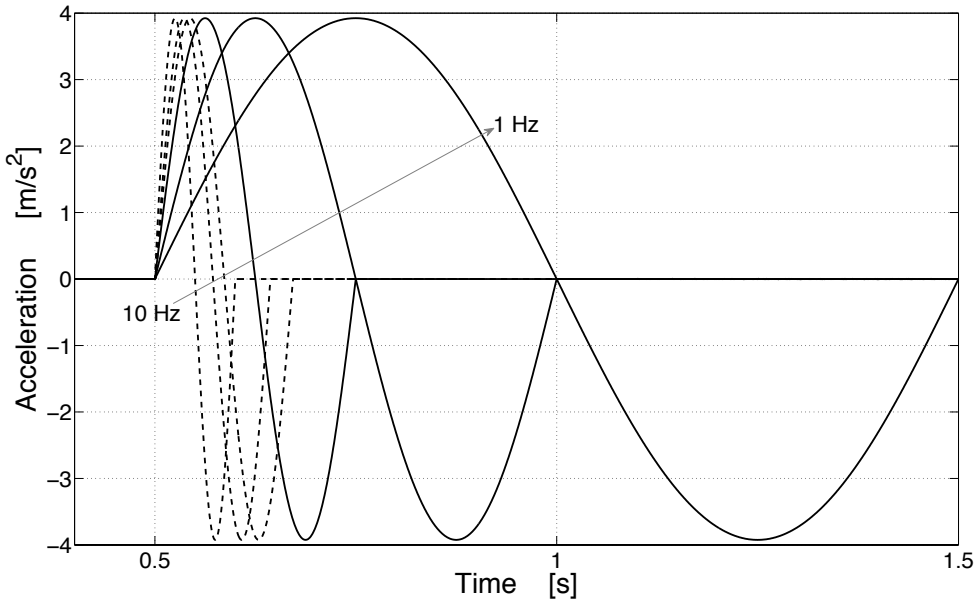

Figure 2.1 *Single-sinus signals with PGA=0.4 g.*

However, it is worth to note (Table 2.1) that the most damaging signal is not the one at the fundamental frequency of the structure (5.85 Hz) but the one at a slightly lower frequency (4 Hz). This can be interpreted considering that both the 4 Hz and the 5.85 Hz signals have the potential to damage the structure, but the 4 Hz signal is more severe once the structure is already weakened by damage (i.e., its frequency has reduced) and therefore it is able to produce further damage. This aspect will be investigated in detail in paragraph 2.4.

Finally, it is important to note (Fig. 2.1 and Table 2.1) that (at least) in the case of equal number of oscillation cycles, the *duration* of the excitation is not correlated to the structural damage. This suggests that IMs considering ground motion duration have not reasons to be more efficient with respect to IMs that instead do not take it into account.

Table 2.1 *CAMUS1: response to single-sinus signals, and signals characteristics*

Sinus Frequency [Hz]	Max drift	Frequency drop [%]	$S_{pa}(f_1)$ [m/s^2]	PGA [g]
1	1.7E-4	0	4.44	0.4
2	2.8E-4	14.5	5.82	0.4
4	5.9E-4	43.7	10.8	0.4
5.85	4.9E-4	36.9	11.6	0.4
7	4.4E-4	31.0	10.1	0.4
10	2.3E-4	14.5	6.32	0.4

2.1.1.2 Sequence effect

In order to highlight the limit of $S_{pa}(f_1)$ in case of non-linear structural behavior, a second series of analyses has been then conducted. In this, the CAMUS1 structure has been loaded with two sinusoidal excitations (Fig. 2.2), which are characterized by the same amplitude (0.4 g) and the same value of spectral acceleration (13.4 m/s^2) at the fundamental frequency of the structure (5.85 Hz). Both the signals are constituted by the sequence of two sinuses: in the first sequence, a sinus at frequency 1 Hz follows a sinus of frequency 5.85 Hz; in the second sequence, a sinus at frequency 10 Hz follows a sinus of frequency 5.85 Hz.

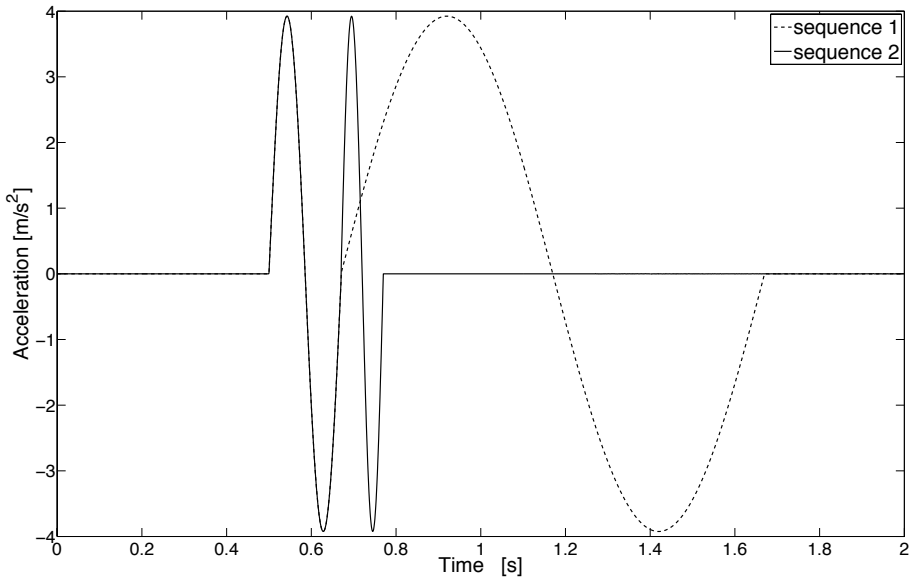

a)

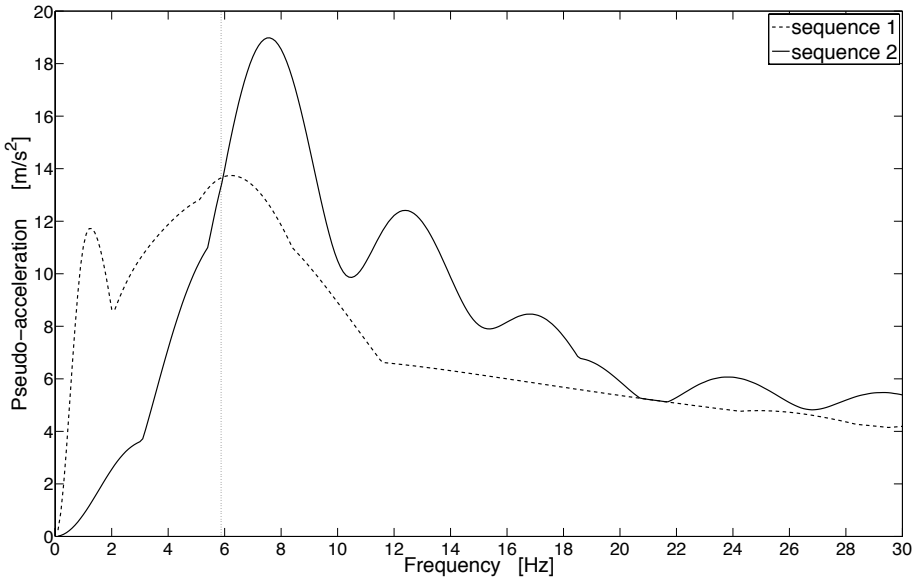

b)

Figure 2.2 *Double-sinus sequences with same PGA and same $S_{pa}(f_1)$: a) accelerograms; b) 5 % damped response spectra (the vertical line corresponds to the CAMUS1's fundamental frequency).*

The results presented in Table 2.2 evidence that despite the two excitation sequences have exactly the same *PGA* and the same $S_{pa}(f_1)$, their structural responses exhibit a difference of about 30%.

Table 2.2 *CAMUS1: response to "sequence" excitation and sequences characteristics*

Signal	Max drift	Frequency drop [%]	$S_{pa}(f_1)$ [m/s^2]	PGA [g]
Sequence 1	6.9E-4	47.2	13.4	0.4
Sequence 2	4.9E-4	31.8	13.4	0.4

Thus, it is evident that when used with respect to inelastic behaving structures, on top of *PGA* also $S_{pa}(f_1)$ can introduce bias in the "classification" of ground motions destructiveness. Indeed, an inelastic behaving structure is not characterized by a "single-value" fundamental frequency: when the elastic limit is reached irreversible damage processes (concrete cracking, joint failure, etc.) enable a progressive loss of stiffness with consequent frequency drop. In such case the $S_{pa}(f_1)$ can become ineffective because it is computed at the initial value of frequency (f_1), and therefore it carries zero information about the "intensity" of the ground motion record at the "up-to-date" (decreased) frequency of the structure.

2.2 ACCOUNTING FOR NON-LINEAR STRUCTURAL BEHAVIOR IN IMs

Based on the foregoing, in the definition of an efficient IM taking nonlinear structural behavior into account, it seems reasonable to enrich the information given by $S_{pa}(f_1)$ by considering additional spectral pseudo-acceleration values computed over frequencies (periods) other than the fundamental one. This procedure has been adopted in various IMs, for instance *EPA*, *ASI*, *S** and I_{NP} (see paragraph 1.2.2), among which the structure-specific *S** and I_{NP} combine with the $S_{pa}(T_1)$ factors so as to account for the spectral shape within the period lengthening zone. Such factors are computed based on one or more spectral pseudo-acceleration values over a period longer than T_1. Put otherwise, without considering damage phenomena and subsequent period lengthening, *EPA* and *ASI* are defined as general (as opposed to structure-specific) IMs. For both of them, the pseudo-acceleration response spectrum is integrated over a period range assumed typical of civil engineering structures (0.1-2.5 sec in *EPA*) and reinforced concrete dams (0.1-0.5 sec in *ASI*).

2.2.1 A new IM: the ASA_R

Based on the above discussion, the objective is to create an efficient IM for nonlinear behaving structures. Frequency is used instead of the more common period to describe the IM. The reason of this modification will be clarified in the following, and the equivalent definition in terms of period will ultimately be given.

The intention here is to define a structure-specific IM; the key idea consists of considering the structure's relative frequency drop (i.e. period elongation) interval as the "core" of this IM. The frequency range to be taken into account has an upper bound at the fundamental frequency and a lower bound at the maximum expected "softened" frequency, which is evaluated as a percentage of the fundamental value. A new IM is thus being proposed (De Biasio *et al*., 2014a): called *Relative Average Spectral Acceleration* (ASA_R), it is defined (Eq. 2.1) as the average spectral pseudo-acceleration over the fundamental frequency f_1 evolution interval. The term "relative" indicates the dependence of ASA_R on the structure, i.e. its fundamental frequency of vibration.

$$ASA_R(f_1) = \frac{1}{f_1(1-X_f)} \int_{X_f \cdot f_1}^{f_1} S_{pa}(f,\xi)\ df \tag{2.1}$$

where:

f_1 is the fundamental frequency of the structure,

$X_f = 1-(R/100)$ is a factor that accounts for the drop in fundamental frequency f_1,

R indicates the amount of drop (expressed as a percentage) in fundamental frequency f_1,

S_{pa} is the spectral pseudo-acceleration,

ξ is the damping value.

The exact value of R depends on the non-linearity experienced by the structure, which in turn depends on both ground motion "intensity" and structural design properties. A general optimal R value, derived from numerical sensitivity analyses, is suggested in the last part of this chapter.

The formulation (2.1) of ASA_R therefore captures, in the simplest manner, the presence of significant spectral acceleration ordinates over the range of fundamental frequency evolution: this constitutes a key characteristic required of a seismic signal in order to be destructive (NUREG, 1986; Kennedy *et al.*, 1988).

At this point, the reason behind the choice of the frequency as integration variable can be enlighten. The integration over the frequency has been considered more adapted to the definition of the proposed IM cause the integration over the period gives higher weight to lower frequency spectral ordinates (De Biasio *et al*., 2013):

$$\int_{T_1}^{T_2} S_{pa}(T,\xi)\,dT = \int_{\frac{1}{T_2}}^{\frac{1}{T_1}} \frac{S_{pa}(f,\xi)}{f^2}\,df \neq \int_{\frac{1}{T_2}}^{\frac{1}{T_1}} S_{pa}(f,\xi)\,df \tag{2.2}$$

Therefore, in the framework of the definition of the proposed IM, to integrate over the period would mean to give lower weight to the spectral ordinates closer to the "better-known" fundamental frequency and higher weight to the spectral ordinates closer to the "less-known" softened fundamental frequency. Contrarily, to integrate over the frequency means to give more weight to the spectral ordinates closer to the "well- known" fundamental period. Consequently, in order to reduce the uncertainty, it has been chosen to put more "integration weight" on the well-known fundamental frequency and thus to prefer the average of spectral pseudo-accelerations over the frequency interval.

Nevertheless once aware of the role of the integration variable, the formulation of the ASA_R can be given with respect to the period by taking $T_1=1/f_1$ and by considering the mathematical integrals' change of variable rule:

$$ASA_R(T_1) = \frac{T_1}{\left(1-X_f\right)} \int_{T_1}^{\frac{T_1}{X_f}} \frac{S_{pa}(T,\xi)}{T^2}\,dT \tag{2.3}$$

Finally, it is of capital importance noting that the simple formulation in (Eq. 2.1) or (Eq. 2.3) of ASA_R, as based exclusively on spectral pseudo-acceleration values, can lead to performing PSHA with respect to ASA_R using widespread ground motion prediction models available for $S_{pa}(T_1)$ (Bazzurro and Cornell, 2002; Stewart *et al.*, 2002; Baker and Cornell, 2006b; Inoue and Cornell, 1990; Koufoudi *et al*., 2014).

2.3 COMPARATIVE ANALYSIS

In order to evaluate the IMs efficiency and sufficiency, comparative analyses are performed following the method illustrated in paragraph 1.3. The comparison is based on three test-case structural systems.

The CAMUS1 offers a simple, well-known and representative model of a high frequency, load bearing wall structure. In order to check whether the performance of the IMs are affected

by the characteristics of the soil at the facility's site, a very simple numerical model of Soil-Structure-Interaction has also been used with the CAMUS1 structure (i.e., CAMUS1-SSI). Furthermore, with the aim to test the robustness (Mehanny *et al.*, 2009) of the IMs with respect to the dynamic characteristics of the buildings, a low-frequency moment resisting frame structure (i.e., EC8-FRAME) has been used as third test case.

2.3.1 Test-case structure: CAMUS1

2.3.1.1 Structure presentation

CAMUS1 (CEA, 1998a) is a ⅓ scale model tested in 1998 on the shaking table of the French Atomic Energy Agency, as well as in an international blind design contest. The mock-up (Fig. 10a) is composed of two parallel Reinforced Concrete (RC) walls without openings linked by five slabs. The mock-up (Fig. 2.3a) is unidirectionally loaded along the wall planes in preventing any orthogonal displacements. The total height of the structure is 5.10 m, and the total mass is approximately 36 tons (for more details, see Appendix A1). Despite being a reduced-scale model, the mock-up has been designed and tested in accordance with precise similitude criteria (Table 6) to ensure its behavior is representative of a full-scale structure.

2.3.1.2 Numerical model & multifiber beam element

The CAMUS1 numerical model (Fig. 2.3b) is constituted of a single *multifiber beam*, the cross-section of which represents the two RC structural walls.

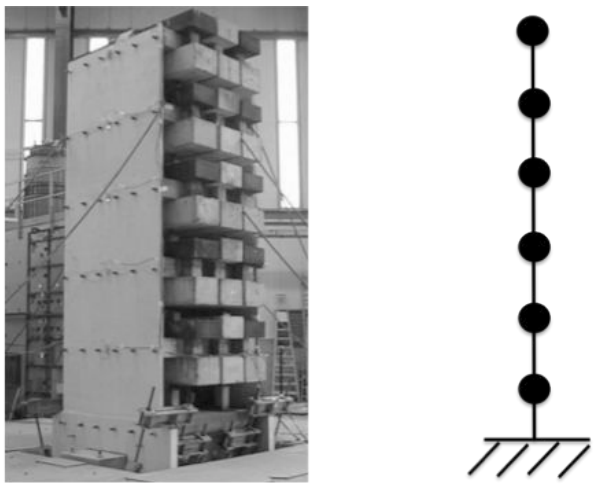

a) b)

Figure 2.3 *CAMUS 1: a) Mock-up on the shaking table; b) lumped mass multifiber numerical model.*

The multifiber modeling method allows to use comprehensive uniaxial material behavior laws in the framework of a simplified kinematic associated to beam elements. This translates in accurate, fast and easy-to-converge non-linear dynamic simulations. In a multifiber element (Figure 2.4), the displacements at the nodes allow determining the generalized deformations at the level of the beam axis. Then, the beam theory following the hyphotheses of Bernoulli (no shear deformations) or Timoshenko (with shear deformations but no warping) allows obtaining the local deformations at the level of the fibers. Successively, these deformations are used to compute the stresses, which integrated over the cross-section of the beam conduce to the generalized forces.

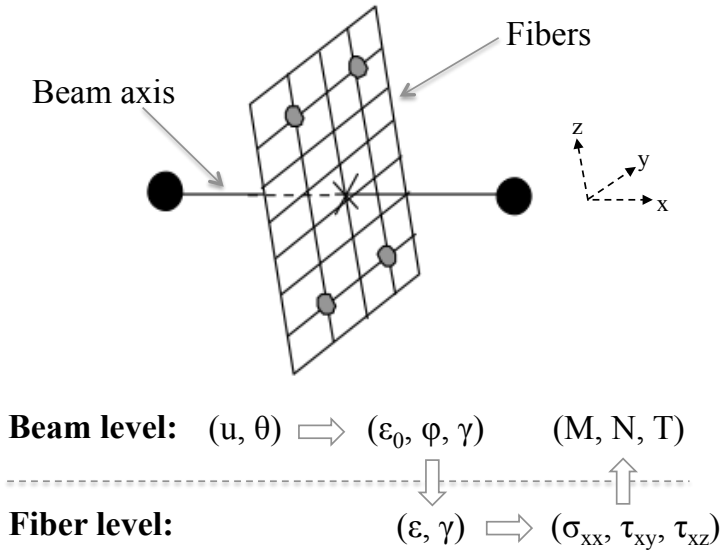

Figure 2.4 *Multifiber beam element. Adapted from Combescure (2001).*

Despite the fact such a modeling was naturally born to simulate beam-type members, the effectiveness of the multifiber element for the simplified modeling of slender structural-walls has been largely shown (Kotronis *et al*., 2005; Grange, 2008; Powell, 2010; Beyer *et al*., 2011).

Regarding the CAMUS1 mesh size, three multifiber Timoshenko beams elements (Guedes *et al*., 1994) have been arranged in the height of each story. For the cross-section discretization, six fibers along the width of the walls and one in their thickness have been considered to represent the concrete, and each longitudinal reinforcement steel bar is represented by a single fiber. The transversal reinforcement has not been represented. This mesh size has been considered a priori adequate in order to reproduce the deformation of the structure, and mesh-size parametric tests have confirmed this hypothesis.

The damage-based constitutive law chosen (for details, see paragraph 1.3.1) to represent the concrete behavior (La Borderie *et al*., 1994) is able to take into account the decrease in stiffness due to cracking, the stiffness recovery that occurs at crack closure and the inelastic strains concomitant to damage. For the steel reinforcement bars a constitutive relation including kinematic hardening (Menegotto and Pinto, 1973) has been selected (for details, see paragraph 1.3.1). The parameters of the material laws have been calibrated against elementary tests on both the concrete and the steel of the two test-case structures (see Appendix A1). Moreover, a sensitivity study during the phase of validation of the model has been performed with respect to the strength of the concrete and its tension post-peak behavior, and a significant robustness of the numerical model has been found.

Lumped mass distribution at the level of the stories has been used and Rayleigh numerical damping has been introduced in the model with a value of 2 % on the first and the second natural frequencies (i.e., which gather the most of the effective modal mass).

2.3.1.3 Model validation

The predictive capabilities of the CAMUS1 numerical model have been checked with results stemming from the experimental campaign of the structure. Being the available experimental data referred to the mock-up placed on the shaking-table (CEA, 1998a), the numerical modeling of this device has been necessary in order to correctly compare numerical and experimental results. Such a modeling has been implemented based on the simplified approach of Reynouard and Fardis (2001). In this, the stiffness and the mass of the shaking-table are modeled through rigid beams as illustrated in Figure 2.5 and (only) the value of the parameter K_{ST}, representing the stiffness of the shaking-table supports, is tuned in order to reproduce the experimentally measured natural frequencies/modes.

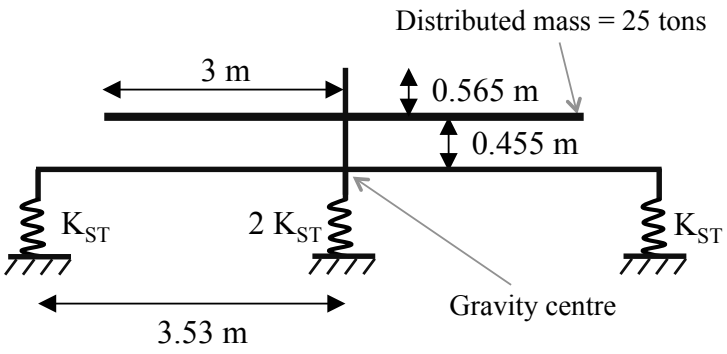

Figure 2.5 *CAMUS 1 numerical model, shaking-table model. Adapted from Reynouard and Fardis (2001).*

Then, the CAMUS1 numerical model has been checked with the experimental results of time-history simulations, which have been executed with respect to the synthetic "Nice S1 PS92" accelerogram (Fig. 2.6). The comparison is performed in terms of natural frequencies (Table 2.3), roof displacement time-history (Fig. 2.7), maximum inter-story drift ratio (Table 2.4), and damage pattern in the concrete (Fig. 2.8).

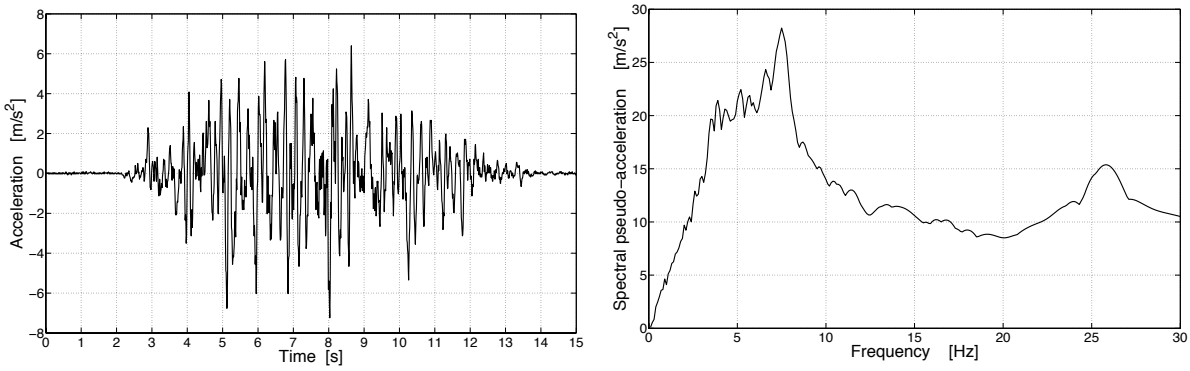

Figure 2.6 *Nice S1/PS92 synthetic accelerogram (0.72 g): a) time-history; b) Response spectrum (5% damping).*

Table 2.3 CAMUS1: Natural frequencies

Mode	Mode Type	Frequency [Hz]		
		Numerical (fixed base)	Numerical (on shaking table)	Experimental (on shaking table)
1st	Bending	9.28	7.24	7.24
2nd	Vertical	43.81	20.01	20.0
3rd	Bending	44.21	38.93	N.A.

Table 2.4 CAMUS1: Max inter-story drift

Story	RUN			
	0.2 g Experimental	0.2 g Numerical	0.72 g Experimental	0.72 g Numerical
5th	0.002	0.002	0.013	0.009
4th	0.002	0.002	0.013	0.009
3rd	0.002	0.002	0.011	0.008
2nd	0.002	0.002	N.A.	0.005
1st	N.A.	0.001	N.A.	0.002

The likeness (numerical vs. experimental) of both natural frequencies and max inter-story drifts (after low intensity solicitation, i.e. 0.2 *g*,) evidence the ability of the numerical model to reproduce the structure linear behavior.

The ability of the numerical model in reproducing the structure non-linear behavior is corroborated by the comparison of the top displacement time-histories and the max inter-story drifts (after high intensity solicitation, i.e. 0.72 *g*), as well by the comparison of the observed and the predicted damage pattern (Figure 2.8). The slight underestimation of damage by the numerical model can be explained by: a) the non-reproduction, in the numerical model, of the construction joints; b) the "accidental" damage of the mock-up (cracks in the upper part) during the construction phase (CAMUS1 benchmark organization committee, personal communication).

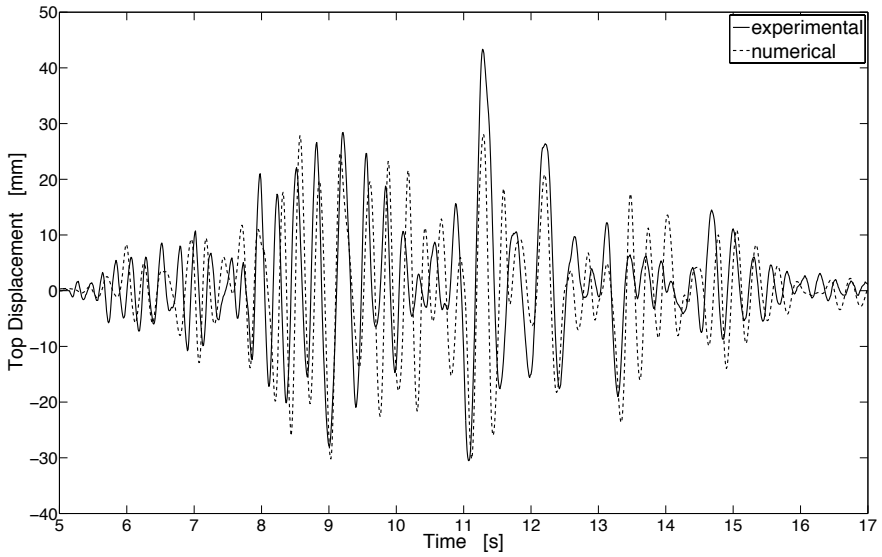

Figure 2.7 *Numerical model validation, roof displacement time-history.*

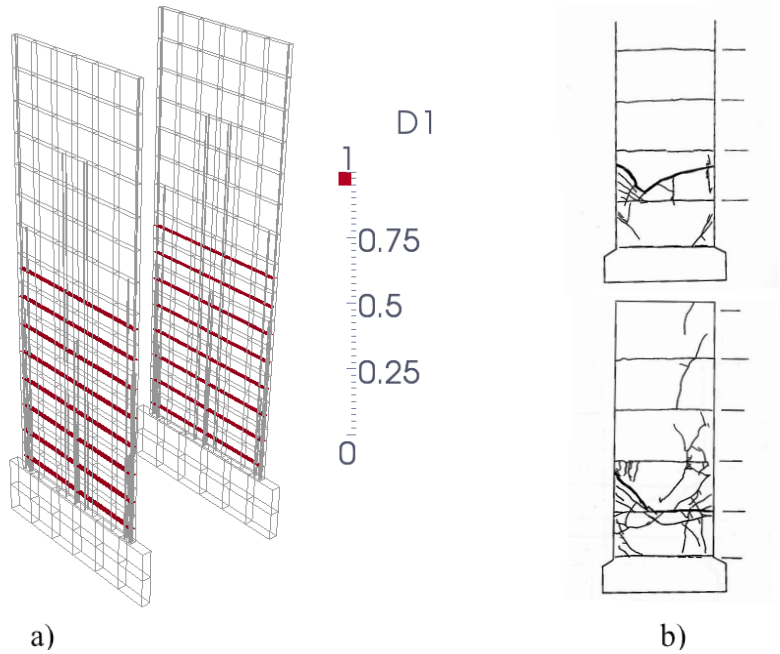

Figure 2.8 *Observed damage pattern: a) numerical, tension damage in the concrete fibers (D_1 >0.99 suggests that cracks opened); b) experimental, visible cracks in the walls (CEA, 1998b).*

It is important to note that the CAMUS1 numerical model has been validated with respect to the ⅓ scale mock-up. Nevertheless, once validated, such a model has been rescaled (Table 2.5) to full-scale: this step allows performing comparative analyses without needing to scale the seismic excitations. Finally, once the model has been created and validated, the shaking table has been eliminated from the numerical model that then has been clamped at the base (Table 2.6) to perform the comparative analyses.

Table 2.5 *Similitude factors for shaking table tests, k<1 is the scale factor (Carvalho, 1998)*

	Full-scale	Mock-up
Length	l	kl
Mass	m	k^2m
Time	t	$k^{0.5}t$
Frequency	f	$[1/k^{0.5}]f$
Acceleration	a	a
Young modulus	E	E
Force	F	$k^2 F$
Moment	M	$k^3 M$
Stress	σ	σ

Table 2.6 *Full-scale CAMUS1 structure clamped at the base, natural frequencies*

Modes	Mode Type	Frequency [Hz]
1st	Bending	5.85
2nd	Vertical	25.30
3rd	Bending	25.52

2.3.2 Test-case structure: CAMUS1-SSI

2.3.2.1 Some note about Soil-Structure Interaction

In conventional structural analysis, the assumption of fixed-base is generally used. For seismic analysis, this means that ground motions are applied directly to the bottom of the structure. In reality Soil-Structure Interaction (SSI) affects the ground motion and the response of the foundation-building system in a way that is not captured by fixed-base analyses (Haselton *et al*., 2008). Two mechanisms contribute to SSI: *inertial SSI* and *kinematic SSI*. The *kinematic SSI* characterizes the variation between the Free Field and Foundation Input Motions (FFM and FIM, respectively). Free-Field Motion refers to a

recorded ground motion at the ground surface away from any structure. The Foundation Input Motion is the theoretical motion at the base of the structure if the foundation and structure had no mass. At the building location, if free-field motions were recorded at various locations within the footprint of the building, there would be differences in the records due to the incoherence of ground motions as they reach the surface. The presence of the stiff foundation impedes this and what is observed is an averaged ground motion. This base-slab averaging combined with embedment effects lead to an effective foundation input motion different from the FFM. The *inertial SSI* relates to the structure's and foundation's mass, stiffness and damping. When a structure is subjected to ground motions, inertia from the masses above the foundation lead to development of base shear and moments at the foundation level. The foundation reacts to these forces by displacement and rotation, which in turn affect the building's motion. The motion of the foundation on the soil also allows dissipation of energy through *radiation damping* (the foundation motion acts as a source of waves that are moving away from the structure) and *hysteretic damping* from the near-field soil nonlinear dynamic response. The readers looking for more details on the subject can refer to Wolf (1985), Seco-e-Pinto (1997), and Gazetas (1991).

2.3.2.2 SSI simplified model

Therefore, in order to test the robustness of the IMs with respect to a modified structural response due to Soil-Structure-Interaction, two different boundary conditions have been simulated using the CAMUS1 test case. In the first condition, the structure is projected onto a stiff rock site (i.e., V_{S30} = 900 m/s) and then the model is simply clamped at the base (CAMUS1 model); while in the second condition, the structure is projected on a soft soil site (i.e., V_{S30} = 270 m/s) and then SSI is taken into consideration (CAMUS1-SSI model).

The SSI has been included in the CAMUS1-SSI model by means of an experimentally validated discrete *linear* model (Wolf, 1988). This simple, approximate, engineering-type model, which in the framework of a substructure-type analysis (i.e. the structure and the soil are modeled independently) can be straightforwardly incorporated in standard dynamic time domain numerical simulations, has been considered adequate for the comparative scope of the present study.

The rheological (spring-dashpots-masses) "monkey-tail" model (Figure 2.10) is able to approximately reproduce the *inertial Soil-Structure-Interaction* (i.e. where superstructure masses and foundation transmit the inertial force to the soil, thus causing further soil

deformation) as well as the *radiation damping* (i.e. wave radiation from the foundation to infinity). These two SSI effects reflect the possibility of displacement at the foundation level, natural frequency change and the capability of dissipating energy.

In order to briefly describe how the adopted SSI model work, it is useful to introduce the notion of *dynamic stiffness coefficient*, which concept can be illustrated examining a single degree of freedom system (Figure 2.9) consisting of a spring (*K*), a dashpot with viscous damping (*C*), and a mass (*M*).

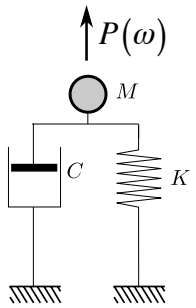

Figure 2.9 *Single Degree Of Freedom system*

Considering an harmonic excitation of frequency ω, the applied load with amplitude $P(\omega)$ will cause a displacement of amplitude $u(\omega)$: these are related, in the frequency domain, by the *dynamic stiffness coefficient* $S(\omega)$:

$$P(\omega) = S(\omega)u(\omega) \tag{2.4}$$

with

$$S(\omega) = K - \omega^2 M + i\omega c \tag{2.5}$$

The undamped natural frequency ω_1 and the damping ratio ξ are equal to:

$$\omega_1 = \sqrt{\frac{K}{M}} \tag{2.6}$$

$$\xi = \frac{C}{2\sqrt{KM}} \tag{2.7}$$

Standardizing $S(\omega)$ with its static value (i.e. $S(\omega=0) = K$) leads to:

$$S(\omega) = K\left[k(\omega) + i\omega C(\omega)\right] \tag{2.8}$$

where the dimensionless spring coefficient $k(\omega)$ and the damping coefficient $c(\omega)$ are expressed as:

$$k(\omega) = 1 - \omega^2 \frac{M}{K} = 1 - \frac{\omega^2}{\omega_1^2} \tag{2.9}$$

$$c(\omega) = \frac{C}{K} = 2\frac{\xi}{\omega_1} \tag{2.10}$$

The model of Figure 2.9 can be used to simple represent linear SSI: in this case, in Eq. (2.8) the real part of *S(ω),* characterized by *k(ω),* mainly represents the stiffness and inertia of the soil, and the imaginary component c(ω) reflects the radiation of waves propagating away from the foundation, and the material damping.

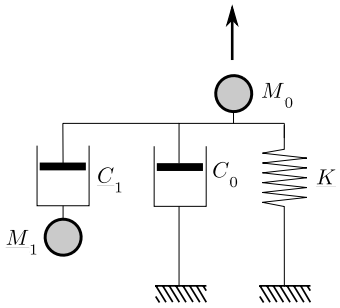

Figure 2.10 *Monkey-tail SSI discrete model (Wolf, 1988)*

Coming back to the herein adopted "monkey-tail" model (Figure 2.10), it consists of two dynamic degrees of freedom for each component of the basement motion (i.e. for CAMUS1 these are the horizontal and vertical translations, and the rocking). With respect to the SDOF system of Figure 2.9, the presence of the additional (and fictitious) degree of freedom allows to better reproduce the true (i.e. experimental) dynamic stiffness value. Indeed, after enforcing the static stiffness *K*, the parameters of both the masses and the dampers are selected to achieve an optimum fit (in the low and medium frequency range) between the dynamic stiffness coefficient of the discrete-model and the corresponding exact value.

Accordingly, the parameters of the adopted SSI model have been obtained from Wolf (1988) once defined the characteristics of the site of reference (i.e., soil density ρ and wave speed in the upper 30 meters V_{S30}) and the dimensions of the embedded prismatic foundation (for details, see Appendix A2).

Finally, note that the fundamental frequency of the full-scale CAMUS1 model, which is equal to 5.85 Hz when the model is clamped at the base (paragraph 2.3.1), *reduces to 3.80 Hz* in the configuration incorporating the aforementioned SSI model.

2.3.3 Test-case structure: EC8-FRAME

2.3.3.1 Structure presentation

EC8-FRAME (JRC, 1994) is a full-scale, four-story, high-ductility RC frame designed according to the European seismic code EC8 (EC8, 1988) and tested in 1994 on the reaction wall of the European Joint Research Center. The structure (Fig. 2.11a) is symmetrical in one direction with two equal 5-m spans, while slightly irregular in the other direction due to the different span lengths (for more details, see Appendix A3).

2.3.3.2 Numerical model

The multifiber beam modeling method (paragraph 2.1.1) has been used to model the frame structure (beams and columns) of the EC8-FRAME test case, where the slabs have been instead modeled by linear elastic shell elements (Fig. 2.11b).

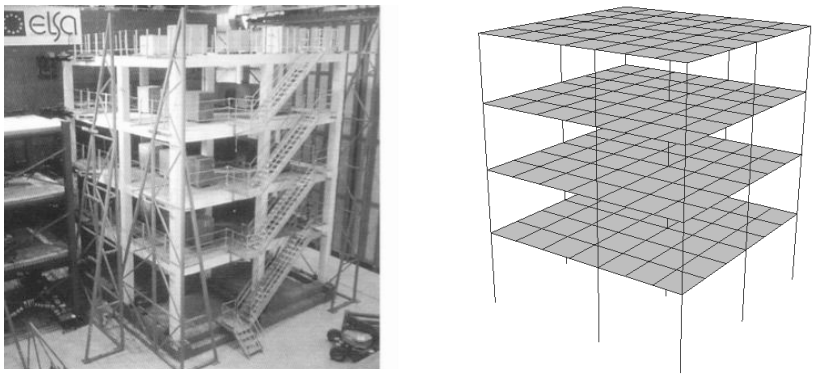

a) b)

Figure 2.11 *EC8 FRAME: a) building; b) numerical model*

Regarding the mesh size, three to four multifiber Timoshenko beam elements (Guedes *et al*., 1994) have been arranged in the length of each beam/column element. Each beam cross-section has been discretized with four concrete fibers, whereas the longitudinal reinforcement steel bars are represented one-by-one by a fiber. The transversal reinforcement has not been represented. Sensibility tests have confirmed the robustness of the mesh-size, which has been considered adequate for the *comparative aim* of the numerical model.

The damage-based constitutive law of La Borderie *et al*. (1994) has been used to model the concrete behavior whereas the Menegotto and Pinto (1973) law has been used for the modeling of the reinforcement-bar steel behavior (for details about the adopted behavior laws, see paragraph 1.3.1). The parameters of the material models have been calibrated

against elementary tests on both the concrete and the steel of the test-case structure (Appendix A3).

The masses are distributed on the elements (beams, columns and slabs) and Rayleigh numerical damping has been introduced in the model with a value of 2 % on the first and the third natural frequencies (i.e., so as to cover the vibration modes which gather the most of the effective modal mass).

2.3.3.3 Model validation

The predictive capabilities of the EC8-FRAME numerical model have been checked with the results stemming from the (reaction-wall) pseudo-dynamic tests (Takanashy, 1975), which have been performed with respect to the scaled, 6.5 surface Magnitude, 1976 Friuli earthquake record (Figure 2.12), in terms of roof displacement time history, floor response spectra and damage pattern in the concrete.

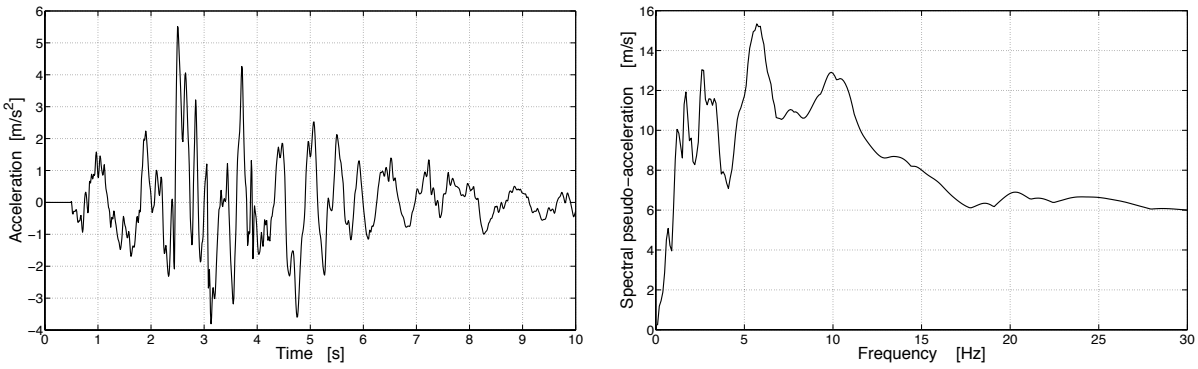

Figure 2.12 *1976 Friuli earthquake (0.56 g): a) time-history; b) Response spectrum (5% damping).*

Table 2.7 EC8-FRAME, natural frequencies

Mode	Mode Type	Numerical Frequency [Hz]	Experimental Frequency [Hz]
1st	Bending X	1.57	1.72
2nd	Bending Y	1.59	N.A.
3rd	Torsion	2.07	N.A.
4th	Bending X	5.47	5.12
5th	Bending Y	5.53	N.A.

The linear behavior of the model is validated through dynamic time history analysis performed with low input intensity loading (Fig 2.13a). Indeed, the difference among the experimental and numerical modal-analysis frequencies values (Table 2.7) does not translate in an out-of-phase behavior of the experimental and numerical displacement time-histories

(Fig. 2.13a). It is opinion of the author that this phenomenon originates from the several snap-back tests the experimental structure endured before the dynamic tests (JRC, 1994). The snap-back tests induced a minor damage state in the structure with ensuing decrease in stiffness at the time of the dynamic tests.

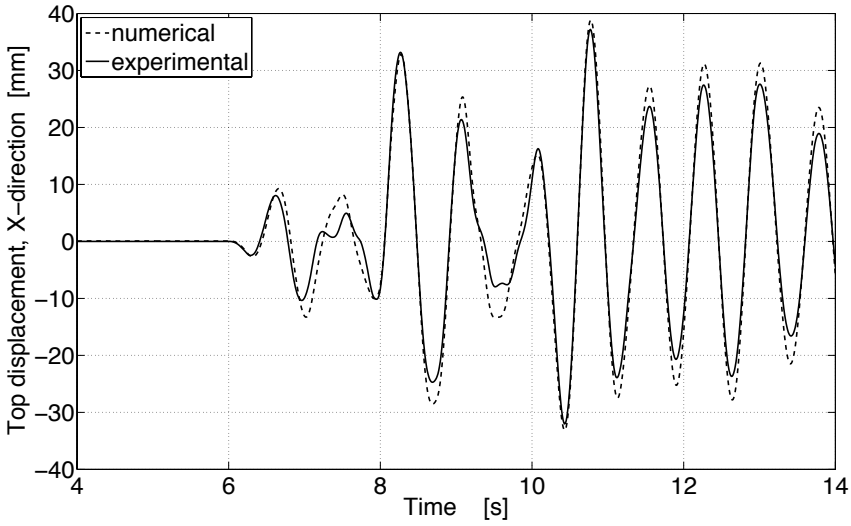

a)

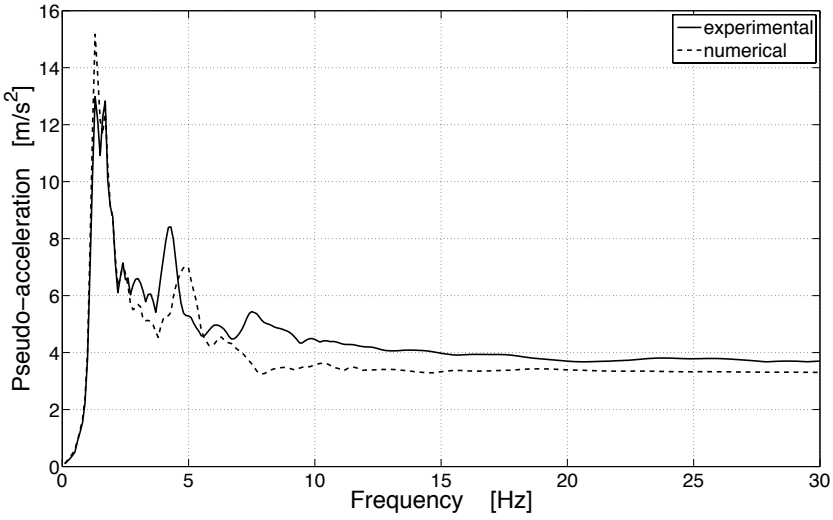

b)

Figure 2.13 *EC8-FRAME, model validation with low intensity (0.15 g) loading: a) roof displacement time history; b) roof floor response spectrum (5% damping)*

Regarding the non-liner behavior, with respect to the experimental results the numerical model slightly underestimates the structural response (Fig. 2.14). In simulating the same structure subjected to the same load, Abbasi *et al.* (2003) found similar results and conclude that such behavior is due to the assigned numerical damping, which results excessive at high level of loading (i.e., when energy dissipation related to inelastic materials behaviors takes place). This argument is (indirectly) supported by the observations of (Elnashai *et al*., 1990;

Shing *et al*., 1996; Souid *et al*., 2009), who emphasize that the introduction of viscous damping is a critical aspect of pseudo-dynamic tests. Nevertheless, from the qualitative point of view the numerical model has shown its ability to reproduce the experimentally observed damage locations (Fig. 2.15), which are positioned at the beam-to-column interfaces of the first three stories (JRC, 1994).

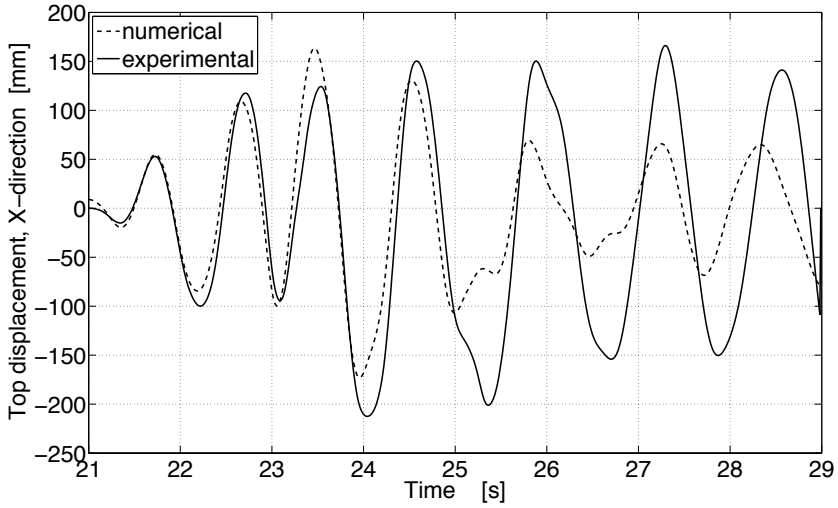

Figure 2.14 *EC8-FRAME, model validation with high intensity (0.56 g) loading: roof displacement time-history.*

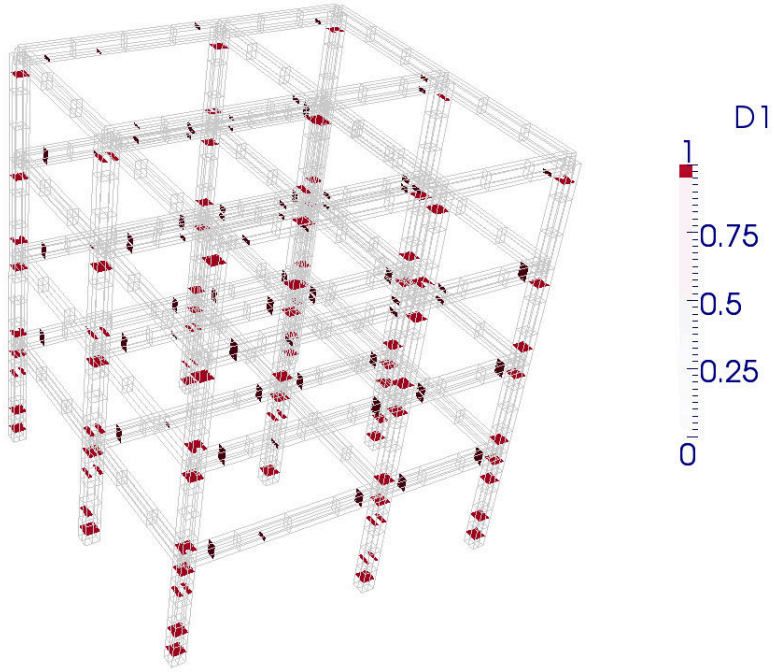

Figure 2.15 *EC8-FRAME, model validation with high intensity (0.56 g) loading: tension damage in the concrete fibers (D_1 >0.99 suggests that cracks opened).*

Therefore, based on the foregoing comparisons of numerical and experimental results, the EC8-FRAME numerical model is considered able to "qualitatively" predict with good agreement the structure' linear behavior as well as its non-linear behavior.

2.3.4 Selected Engineering Demand Parameters

Having defined the Intensity Measures (paragraph 1.2.2), the ground motion dataset (1.3.2), the statistical analysis procedure (paragraph 1.3.3) and the test-case structures (paragraphs 2.3.1, 2.3.2 and 2.3.3), in order to perform the IMs performance comparative analysis it remains to define the parameters allowing quantifying the response of the test case structures.

Such parameters are identified as Engineering Demand Parameters (EDPs) and refer to the quantities issued from structural analysis, which describe the response of the structural framing and the nonstructural components to earthquake shaking.

Among the several metrics that can be used for their classification, EDPs can be categorized as:

- *Direct or Processed*: direct EDPs are those EDPs, as member forces or inter-story drift, calculated directly by analysis or simulation; processed EDPs, as damage indices, are derived from values of direct EDPs and data on component or system capacities (Processed EDPs can be considered either EDPs or Damage Measures (DMs) and as such they can contribute to Equation (1.1) directly through the term $p[DM|EDP]$).
- *Local or Global*: local EDPs describe the damage due to seismic loading in a member or at a joint; global EDPs define the overall damage state of a structure.
- *Cumulative or Non-cumulative*: the non-cumulative EDPs are not able to take into account the cumulative effect of repeated cycles of deformation. Differently, the Cumulative EDPs have this possibility.

An author's selection of some widespread EDPs (Table 2.8) is briefly presented. The reader looking for more information can refer to Williams and Sexsmith (1995).

Table 2.8 *Some EDPs: classification.*

	Direct	Processed	Local	Global	Cumulative
Ductility ratio	X		X		
Inter-story Drift	X		X		
Park & Ang index		X	X		X
Softening		X		X	X

2.3.4.1 Local EDPs

Traditional direct and local EDPs are component forces and displacements. These basic EDPs form the basis for design provisions contained in all earlier (and many contemporary) building codes: component forces were the key product of linear-elastic simulations that used spectral acceleration at the fundamental period of the building, reduced by a response modification factor that was intended to account for the ductility and reserve strength in the framing system.

The two earliest, simplest and still widely used EDPs are the ductility ratio and the inter-story drift.

Ductility Ratio The ductility ratio (Chopra, 2007) can be defined in terms of rotation/curvature/displacement. The displacement ductility ratio (Eq. 2.11, Figure 2.16) is defined as the ratio of the maximum displacement at the end of a member u_m to the yield value u_y:

$$\mu_\delta = \frac{u_m}{u_y} \tag{2.11}$$

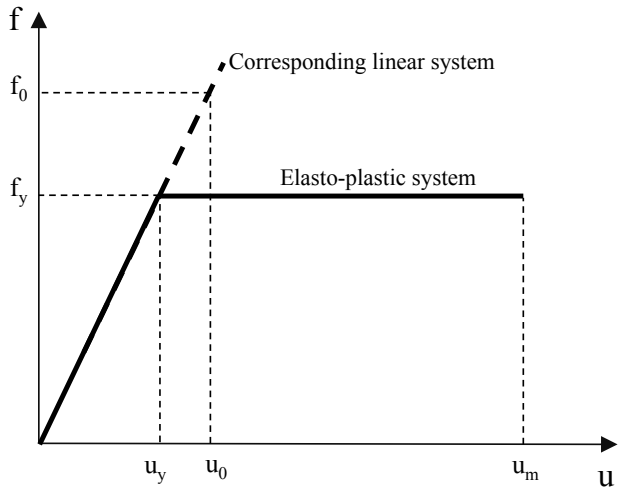

Figure 2.16 *Ductility ratio. Adapted from Chopra (2007).*

Despite its limitations with respect to cycling loading, ductility ratio is still widely used in structural assessment.

Inter-Story Drift Perhaps, the single most important response parameter to characterize the seismic behavior of a story (or of a whole building under the assumption that the failure of a single story is equivalent to the overall failure of the building) is the Maximum Inter-Story Drift Ratio (MIDR), defined as:

$$MIDR = \underset{i}{MAX} \frac{\delta_{i+1} - \delta_i}{h_i} \tag{2.12}$$

where δ_i and δ_{i+1} denote the horizontal displacements of two adjacent floors and h_i is the corresponding story height (Figure 2.17).

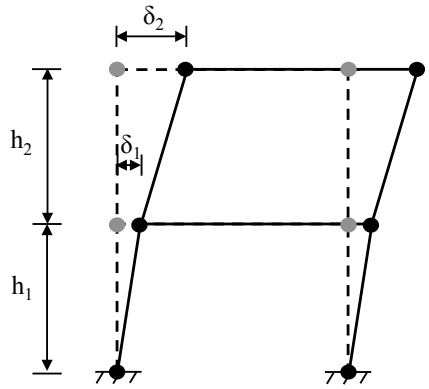

Figure 2.17 *Inter-story drift*

The MIDR is easy to measure in tests or in actual buildings struck by earthquakes, and can be correlated with available data on damage. The State-of-the-Art FEMA (2012) states: ” The demand parameter assigned to a fragility group is the one that best predicts the occurrence of the potential damage states with the least amount of uncertainty. For most structural systems (e.g., shear walls, braced frames, steel and concrete moment frames), and for many nonstructural components, story drift ratio has been selected as the best indicator of potential damageability”.

Nevertheless, the MIDR (as well as the ductility ratio) is a non-cumulative EDP. The implication of the use of non-cumulative EDPs can be explained with an example: two different ground motions may each produce the same 2 % MIDR in a structure. However, one of these ground motions may cycle the structure to this drift level one time, then restore the structure to small oscillations about its original position; while the second ground motion may cycle the structure to this drift level several times and leave the structure displaced nearly to this level. Clearly the second motion will be more damaging to the structure than the first motion, though the value of the demand, in terms of MIDR is the same.

Park & Ang Index The best-known and most widely used cumulative damage index is that of Park and Ang (1985). This consists of a linear combination of normalized deformation and energy absorption:

$$D_{P\&A} = \frac{\delta_m}{\delta_u} + \beta_e \frac{E_H}{F_y \delta_u} \tag{2.13}$$

where δ_m is the maximum displacement response of the component for a given earthquake history, δ_u the ultimate displacement capacity of the component under monotonic loading, E_H is the total hysteretic energy dissipated by the component during the ground motion, F_y the yield strength of the component and β_e a parameter accounting for strength deterioration. The first (kinematic) term of (2.13) is a simple pseudo-static displacement measure, the second (energy) term account for cumulative damage. This model has been calibrated against a significant amount of observed seismic damage, and has been used in a number of seismic vulnerability studies and probabilistic models (Ang, 1987; Barenberg and Foutch, 1988; Ciampoli *et al*., 1989; Seidel *et al*., 1989; Stone and Taylor, 1993). Nevertheless a strong drawback of the parameter $D_{P\&A}$, as well of the many other similar EDPs, is that it requires the difficult and uncertain calibration/derivation of several parameters, which are mostly dependent on the structural configuration.

2.3.4.2 Global EDPs

The overall damage state of a structure depends on both the distribution and severity of the localized damage. It is therefore possible to formulate a global damage index either by combining local indices across the structure, or by considering some overall structural characteristics.

From Local to Global Indices Global damage indices derived from local indices generally use one of two weighting systems both of which are based on subjective assessment of the influence of localized damage on the overall serviceability of the structure. The most widely used approach is to take an average of the local indices, weighted by the local energy absorptions (Park *et al*., 1985). The damage index for a single story of a structure is thus:

$$D_{story} = \frac{\sum D_i E_i}{\sum E_i} \tag{2.14}$$

where D_i is the local damage index at location i, and E_i is the energy absorbed at location i. The structure damage index can be then calculated from the stories indices in the same way. Since the locations having high damage indices will also be the ones which absorb large amounts of energy, this method puts a higher weight on the more heavily damaged elements.

A more generalized definition of the story damage index (2.14) is given by Bracci *et al*. (1989):

$$D_{story} = \frac{\sum w_i D_i^{(b+1)}}{\sum w_i D_i^b} \tag{2.15}$$

With formulation (2.15), a higher value of the exponent b results in a greater emphasis on the most severely damaged elements, while the introduction of the weights w_i allows dependence on some other parameter to be introduced. Bracci *et al*. (1989) suggested to use as w_i the gravity load supported by the element i divided for the total weight of the structure. In such a way, larger weight is given to the damage incurred at the base of the structure, with respect to upper stories, since it has a greater chance of causing structural collapse.

Softening Indices Softening indices are used to relate changes in the first few natural frequencies of a structure to the level of damage it has incurred. The original aim of this approach was to enable the assessment of structural damage very quickly after an earthquake on the basis of a single strong motion record at the structure level. However the method can also be applied in conjunction with a non-linear time-history analysis or in-situ vibration measurements (Mikael *et al.,* 2013).

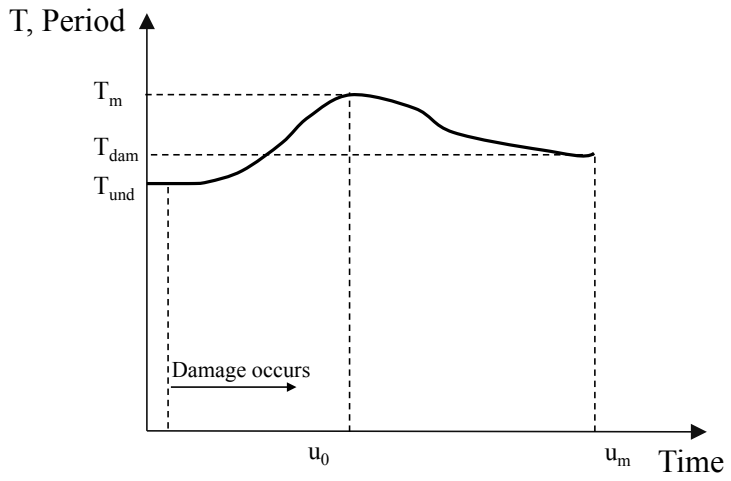

Figure 2.18 *Typical variation of the fundamental period of a structure during an earthquake. Adapted from William and Sexsmith (1995).*

It is well known (Rayleigh, 1945; Dowell, 1979) that damage causes a change in the dynamic characteristics of a structure: such change appears as a decrease in frequency (lengthening of period) caused principally by stiffness degradation, and an increase in damping (energy dissipation). Therefore, several softening indices, which are formulated as functions of the change in fundamental frequency/period of the structure during an earthquake (Figure 2.18), have been proposed.

Assuming that, given a response history, the damage affects the fundamental period but changes in the corresponding mode shapes are negligible, DiPasquale and Cakmak (1987) formulated three different softening indices:

$$D_m = 1 - \frac{T_{und}}{T_m} \tag{2.16}$$

$$D_{pl} = 1 - \frac{T_{dam}^2}{T_m^2} \tag{2.17}$$

$$D_F = 1 - \frac{T_{und}^2}{T_{dam}^2} \tag{2.18}$$

where (Figure 2.18) T_{und} (i.e., undamaged) is the initial period, T_m (i.e., maximum) is the maximum period reached during the earthquake loading, and T_{dam} (i.e., damaged) is the final structural period, which is reached once the loading finishes and part of the cracks close.

Using a damage mechanics approach DiPasquale and Cakmak (1989) showed that: D_F (i.e. final softening) is approximately equal to the average reduction in stiffness of the structure; D_{pl} (i.e. plastic softening) is essentially a measure of the plastic deformation and soil-structure interaction occurring during the earthquake; D_m (i.e. the maximum softening) is a combination of both the stiffness degradation and the plasticity effects.

Between these indices, D_m is considered the best indicator of the global damage state. Miyamura *et al.* (1989) and Cakmak *et al*. (1991) have shown that it provides a reliable estimate of whether or not yielding has occurred within the structure. However, D_F and D_{pl} can be used to provide more detailed information about the structural response since each relates to a specific form of damage.

Finally, in this comparative study the structural demand is measured in terms of Maximum Inter-Story Drift Ratio (MIDR), maximum global ductility demand (μ_{max}) and maximum softening (D_m).

Indeed, the selection of several EDPs avoids the dependency of the results on a single-type demand parameter, thus extending the validity of the findings of the study. So, the MIDR measures the *local demand* (at the level of the story), the μ_{max} measures the *global demand*, and the D_m measures the *global cumulative demand* of the structures.

The maximum global ductility demand is computed with respect to the first yielding point on the capacity curve (Fig. 2.19b) obtained by means of a pushover analysis (arbitrarily executed along the X-direction for the EC8-FRAME) of the test case structures.

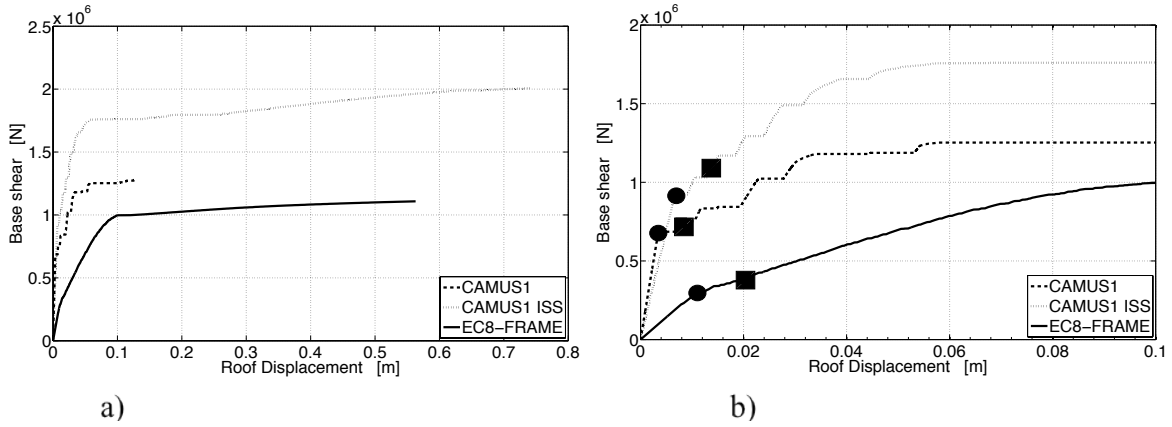

Figure 2.19 *(a) Capacity curves for the test case structures; b) close-up on both the first yielding points (circles) and the points with ductility demand μ=2 (squares).*

The maximum softening D_m (Eq. 2.16), which is indicated in the following of the report mostly as "*frequency drop*", is computed by:

$$D_m = 1 - \frac{T_{und}}{T_{\mathrm{m}}} = 1 - \frac{f_{\min}}{f_{und}} \quad [\%] \tag{2.19}$$

The value of f_{min} is evaluated by means of Fast Fourier Transform analysis of the structure's post-earthquake response under a *white noise signal*. In other words, following the earthquake record, the structure is excited by a white noise signal; then, the "softened" frequency (f_{min}) is extracted by means of a frequency-domain analysis of the structural response to the applied white noise (for a detailed explanation of the method, see for instance Brincker *et al.*, 2001 and Michel *et al.*, 2010).

2.3.5 Results

2.3.5.1 IMs Efficiency comparison

The results of the comparative statistical analysis on IM efficiency will first be presented (Tables 2.9-2.11) with respect to the four selected ground motion bins (i.e., Table 1.2, paragraph 1.4.2).

With special attention on the performance of IMs in the case of nonlinear structural behavior, results will be presented (Table 2.12 and Fig. 2.20) with respect to the selected ground motions (among the four bins) capable of producing damage in the structure. These selections have been identified as those able to generate a maximum global ductility demand, as computed relative to the first yielding point (Fig. 2.19), at least equal to 2. Such a set of ground motions will hereinafter be referred to as "damaging records". The number of these damaging records for each of the designated bins is also given in Tables 2.9-2.11.

For a comparison with the other IMs, ASA_R has been computed with two R values, respectively 20% and 40% (i.e. ASA_{20} and ASA_{40}). Choosing an "optimal R value" will be addressed in paragraph 2.3.6. The frequency response based IMs have been computed on 2 % damped response spectra (Appendix C).

Table 2.9 *CAMUS1: Logarithmic Standard deviation (β) of the residual*

		Large magnitude						*Small magnitude*					
		Short distance			*Long distance*			*Short distance*			*Long distance*		
Damaging records		*23 of 34*			*30 of 322*			*39 of 403*			*14 of 1,286*		
IM type	IM	D_m	μ_{max}	*MIDR*	D_m	μ_{max}	*MIDR*	D_m	μ_{max}	*MIDR*	D_m	μ_{max}	*MIDR*
Frequency response-based	**ASA_{20}**	**0.6**	**0.28**	**0.25**	**0.64**	**0.29**	**0.28**	**0.62**	**0.23**	**0.24**	**0.29**	**0.28**	**0.27**
	ASA_{40}	**0.63**	**0.25**	**0.25**	**0.64**	**0.34**	**0.33**	**0.64**	**0.32**	**0.32**	**0.29**	**0.34**	**0.33**
	$S_{pa}(T_1)$	0.66	0.39	0.34	0.63	0.26	0.24	0.62	0.16	0.17	0.29	0.22	0.22
	S^*	0.58	0.31	0.24	0.64	0.37	0.35	0.65	0.36	0.36	0.29	0.39	0.38
	I_{NP}	0.61	0.31	0.26	0.63	0.28	0.26	0.62	0.19	0.2	0.29	0.25	0.24
	EPA	1	0.83	0.7	0.67	0.75	0.73	0.71	0.62	0.62	0.29	0.67	0.66
	ASI	0.62	0.37	0.28	0.64	0.44	0.42	0.66	0.4	0.41	0.29	0.43	0.42
	I_H	1.19	0.99	0.87	0.71	0.92	0.91	0.74	0.76	0.77	0.29	0.84	0.83
Amplitude-based	**PGA**	0.69	0.5	0.39	0.64	0.48	0.46	0.65	0.44	0.45	0.29	0.4	0.39
	PGV	1.11	0.93	0.81	0.71	0.84	0.82	0.71	0.63	0.64	0.29	0.68	0.66
Duration-based	**I_A**	0.79	0.58	0.48	0.64	0.66	0.64	0.67	0.49	0.5	0.29	0.53	0.51
	CAV	1.08	0.88	0.78	0.7	0.93	0.92	0.71	0.66	0.68	0.29	0.75	0.74
	SCAV	0.94	0.75	0.64	0.78	0.81	0.8	0.78	0.66	0.69	0.29	0.77	0.77
	a_{RMS}	1.13	0.92	0.84	0.75	0.84	0.83	0.77	0.68	0.71	0.28	0.99	0.99
	I_C	0.81	0.59	0.49	0.73	0.79	0.78	0.75	0.64	0.66	0.28	0.99	0.99

Table 2.10 *CAMUS1-SSI: Logarithmic Standard deviation (β) of the residual*

		Large magnitude						*Small magnitude*					
		Short distance			*Long distance*			*Short distance*			*Long distance*		
Damaging records		*26 of 34*			*43 of 322*			*34 of 403*			*16 of 1,286*		
IM type	IM	D_m	μ_{max}	*MIDR*	D_m	μ_{max}	*MIDR*	D_m	μ_{max}	*MIDR*	D_m	μ_{max}	*MIDR*
Frequency response-based	**ASA_{20}**	**1.45**	**0.24**	**0.32**	**1.35**	**0.22**	**0.27**	**1.35**	**0.22**	**0.26**	**0.77**	**0.26**	**0.28**
	ASA_{40}	**1.52**	**0.25**	**0.32**	**1.37**	**0.27**	**0.32**	**1.36**	**0.29**	**0.33**	**0.77**	**0.34**	**0.35**
	$S_{pa}(T_1)$	1.36	0.29	0.34	1.34	0.16	0.21	1.34	0.12	0.16	0.77	0.18	0.19
	S^*	1.56	0.36	0.41	1.39	0.32	0.36	1.36	0.33	0.37	0.77	0.37	0.38
	I_{NP}	1.38	0.26	0.31	1.35	0.19	0.23	1.34	0.16	0.2	0.77	0.22	0.23
	EPA	1.99	0.58	0.66	1.5	0.58	0.63	1.4	0.45	0.49	0.78	0.51	0.53
	ASI	1.41	0.29	0.34	1.37	0.27	0.31	1.36	0.29	0.32	0.77	0.34	0.35
	I_H	2.19	0.7	0.79	1.63	0.76	0.83	1.47	0.6	0.65	0.78	0.68	0.7
Amplitude-based	**PGA**	1.59	0.46	0.52	1.41	0.38	0.43	1.43	0.52	0.55	0.77	0.48	0.49
	PGV	2.12	0.65	0.74	1.61	0.7	0.77	1.4	0.5	0.54	0.78	0.54	0.55
Duration-based	**I_A**	1.63	0.39	0.45	1.44	0.5	0.55	1.42	0.47	0.51	0.78	0.47	0.48
	CAV	1.88	0.59	0.65	1.64	0.76	0.83	1.48	0.59	0.64	0.78	0.64	0.65
	SCAV	1.74	0.48	0.53	1.82	0.69	0.79	1.64	0.68	0.75	0.78	0.83	0.83
	a_{RMS}	2.16	0.68	0.78	1.71	0.72	0.8	1.63	0.72	0.78	0.76	1.03	1.04
	I_C	1.72	0.41	0.49	1.65	0.67	0.74	1.6	0.67	0.73	0.74	1.02	1.03

Table 2.11 *EC8-FRAME: Logarithmic Standard deviation (β) of the residual*

		Large magnitude						*Small magnitude*					
		Short distance			*Long distance*			*Short distance*			*Long distance*		
Damaging records		*32 of 34*			*100 of 322*			*75 of 403*			*64 of 1,286*		
IM type	IM	D_m	μ_{max}	*MIDR*	D_m	μ_{max}	*MIDR*	D_m	μ_{max}	*MIDR*	D_m	μ_{max}	*MIDR*
Frequency response-based	**ASA_{20}**	**0.38**	**0.4**	**0.3**	**0.58**	**0.26**	**0.22**	**0.63**	**0.27**	**0.21**	**0.51**	**0.32**	**0.29**
	ASA_{40}	**0.39**	**0.36**	**0.28**	**0.59**	**0.29**	**0.24**	**0.63**	**0.3**	**0.24**	**0.52**	**0.35**	**0.32**
	$S_{pa}(T_1)$	0.39	0.47	0.35	0.58	0.26	0.22	0.63	0.25	0.2	0.51	0.29	0.25
	S^*	0.39	0.41	0.28	0.61	0.33	0.3	0.64	0.34	0.28	0.52	0.39	0.36
	I_{NP}	0.38	0.42	0.3	0.57	0.25	0.21	0.63	0.26	0.18	0.51	0.31	0.27
	EPA	0.42	0.43	0.29	0.61	0.36	0.33	0.69	0.48	0.41	0.52	0.46	0.43
	ASI	0.5	0.64	0.56	0.69	0.52	0.51	0.81	0.75	0.7	0.55	0.68	0.67
	I_H	0.43	0.43	0.3	0.68	0.44	0.41	0.66	0.4	0.33	0.52	0.43	0.4
Amplitude-based	**PGA**	0.5	0.63	0.52	0.7	0.51	0.5	0.87	0.92	0.87	0.55	0.78	0.76
	PGV	0.44	0.47	0.27	0.7	0.49	0.47	0.7	0.55	0.48	0.52	0.5	0.47
Duration-based	**I_A**	0.49	0.56	0.5	0.64	0.42	0.4	0.79	0.75	0.7	0.54	0.62	0.6
	CAV	0.53	0.62	0.64	0.76	0.53	0.52	0.76	0.69	0.64	0.53	0.57	0.55
	SCAV	0.5	0.57	0.55	0.82	0.68	0.67	0.93	1	0.97	0.53	0.98	0.97
	a_{RMS}	0.56	0.72	0.62	0.79	0.71	0.7	0.91	1.02	0.98	0.53	1.11	1.11
	I_C	0.5	0.59	0.48	0.76	0.68	0.67	0.89	1	0.95	0.52	1.1	1.1

In considering Tables 2.9-2.11:

PGA efficiency remains lower than that of *PGV* only in the long-period case of the EC8-FRAME structure. *PGA* is always less efficient than $S_{pa}(T_1)$: an observation of the standard deviation of residuals, as obtained with respect to the three test cases, indicates that *PGA* efficiency is higher for shorter fundamental period structures, which could have been expected in as much as $\lim_{T_1 \to 0} S_{pa}(T_1) = PGA$.

Among duration-based IMs, I_A demonstrates the best performance; however, the efficiency of this IM class is typically lower than that of frequency response-based IMs.

The IMs exhibiting the highest efficiency are in the structure-specific class, i.e. those including information on the fundamental structure period (S_{pa}, S^*, I_{NP} and ASA_{40}). IMs based solely on the ground motion time-history data show lower efficiency, which confirms that the total earthquake signal energy (to damage the structure) is not as important as the amount of energy the earthquake signal is able to transmit to the structure (Newmark and Hall, 1982). Moreover, the superiority of this IM class has been confirmed by the Tan and Irfanoglu (2012) study, which is based on damage data stemming from the inspections of thousands of American buildings following the 1994 Northridge earthquake.

Among the frequency-based IMs, I_H shows the weakest performance, except in the case of the low-frequency EC8-FRAME structure. These results are in agreement with the findings of Masi *et al.* (2011) on a similar low-frequency frame building.

When ground motions are unable to produce significant structural damage (i.e. the structure remains elastic), as it is the case for the majority of records belonging to the LM-LR, SM-SR and SM-LR bins, $S_{pa}(T_1)$ reveals a high efficiency with respect to both max inter-story drift ratio and maximum ductility demand. Put otherwise, when the LM-SR bin (containing many records capable of producing relevant structural damage) is considered, $S_{pa}(T_1)$ efficiency drastically decreases, thus confirming that the pseudo-spectral acceleration at the fundamental period of the structure is a highly efficient IM should the structure behave elastically or experience a small amount of non-linearity. If such a condition is not satisfied (i.e. fragile structures and/or strong ground motions), then the $S_{pa}(T_1)$ efficiency declines significantly.

In the case of S^* and I_{NP}, when coupled to $S_{pa}(T_1)$, a factor accounting for the spectral shape within the period lengthening zone reveals an improvement in the performance of $S_{pa}(T_1)$ when considered alone. This improvement is more apparent in I_{NP}, where the "shape

factor" turns out to be less biased compared to the *S** case, since it is being computed over multiple periods (three in this case) rather than over a single period. These results are in agreement with the findings of Buratti (2012) in his comprehensive comparative study.

An observation of the correlation coefficients of *EPA* and *ASI* reveals the importance of the period (frequency) range considered when integrating the response spectrum. From Table 2.9, *ASI* has a higher efficiency with respect to *EPA* given its smaller integration interval more highly concentrated around the fundamental period of the structure. This same rationale can be applied to the results presented in Table 2.10. Nevertheless, when considering Table 2.11, *ASI* now shows less efficiency with respect to *EPA* (and moreover it has one of the lowest efficiency among all IMs). The reason behind this performance decline is that in this latter case, the fundamental period of the structure lies outside the range considered in *ASI* yet still within the range considered by *EPA*.

Table 2.12 *Damaging records ($\mu_{max} \geq 2$): Logarithmic Standard deviation (β) of the residual*

		CAMUS1			*CAMUS1-SSI*			*EC8-FRAME*		
Damaging records		*106*			*119*			*271*		
IM type	IM	D_m	μ_{max}	*MIDR*	D_m	μ_{max}	*MIDR*	D_m	μ_{max}	*MIDR*
Frequency response-based	**ASA_{20}**	**0.25**	**0.45**	**0.36**	**0.27**	**0.22**	**0.22**	**0.25**	**0.27**	**0.36**
	ASA_{40}	**0.23**	**0.36**	**0.29**	**0.28**	**0.22**	**0.21**	**0.24**	**0.28**	**0.36**
	$S_{pa}(T_1)$	0.31	0.52	0.41	0.33	0.28	0.28	0.32	0.31	0.38
	S^*	0.27	0.39	0.31	0.36	0.31	0.29	0.3	0.33	0.38
	I_{NP}	0.26	0.42	0.34	0.3	0.24	0.23	0.26	0.28	0.36
	EPA	0.33	0.52	0.39	0.39	0.37	0.34	0.33	0.34	0.39
	ASI	0.26	0.38	0.29	0.32	0.27	0.26	0.53	0.49	0.47
	I_H	0.36	0.58	0.43	0.43	0.42	0.4	0.34	0.36	0.4
Amplitude-based	**PGA**	0.29	0.46	0.35	0.38	0.36	0.35	0.52	0.48	0.47
	PGV	0.34	0.55	0.42	0.42	0.4	0.38	0.36	0.38	0.41
Duration-based	**I_A**	0.3	0.44	0.34	0.35	0.33	0.32	0.44	0.42	0.44
	CAV	0.34	0.54	0.41	0.43	0.43	0.41	0.52	0.49	0.47
	SCAV	0.33	0.51	0.39	0.4	0.4	0.38	0.49	0.46	0.44
	a_{RMS}	0.36	0.59	0.45	0.45	0.45	0.43	0.66	0.6	0.52
	I_C	0.29	0.42	0.33	0.34	0.32	0.31	0.63	0.58	0.5

Lastly, the herein introduced ASA_R shows a slightly lower efficiency than $S_{pa}(T_1)$ when considering the non-damaging record bins (LM-LR, SM-SR and SM-LR). In these cases, the "intensity" of most ground motion is insufficient to produce structural damage, therefore inducing no frequency drop, while formulation (Eq. 2.1) of the ASA_R introduces bias with respect to $S_{pa}(T_1)$. This fact is highlighted by the higher performance of ASA_{20} on ASA_{40}.

ASA_{40} however exhibits the highest efficiency when considering the LM-SR "damaging" bin. When the analysis is restricted to only those records capable of damaging the structure (Table 2.12), independently of the bin classification, the ASA_{40} efficiency is seen to rise to 31% above that of $S_{pa}(T_1)$ when predicting maximum ductility demand (Fig. 2.20) and to 26% and 29% higher when predicting frequency drop and maximum inter-story drift respectively. Moreover, in considering damage records, the ASA_{40} efficiency is typically higher than that of S^* and I_{NP}: focusing on the average spectral acceleration over a well-defined frequency drop interval proves to be a better approach compared with coupling a spectrum "shape factor" to $S_{pa}(T_1)$.

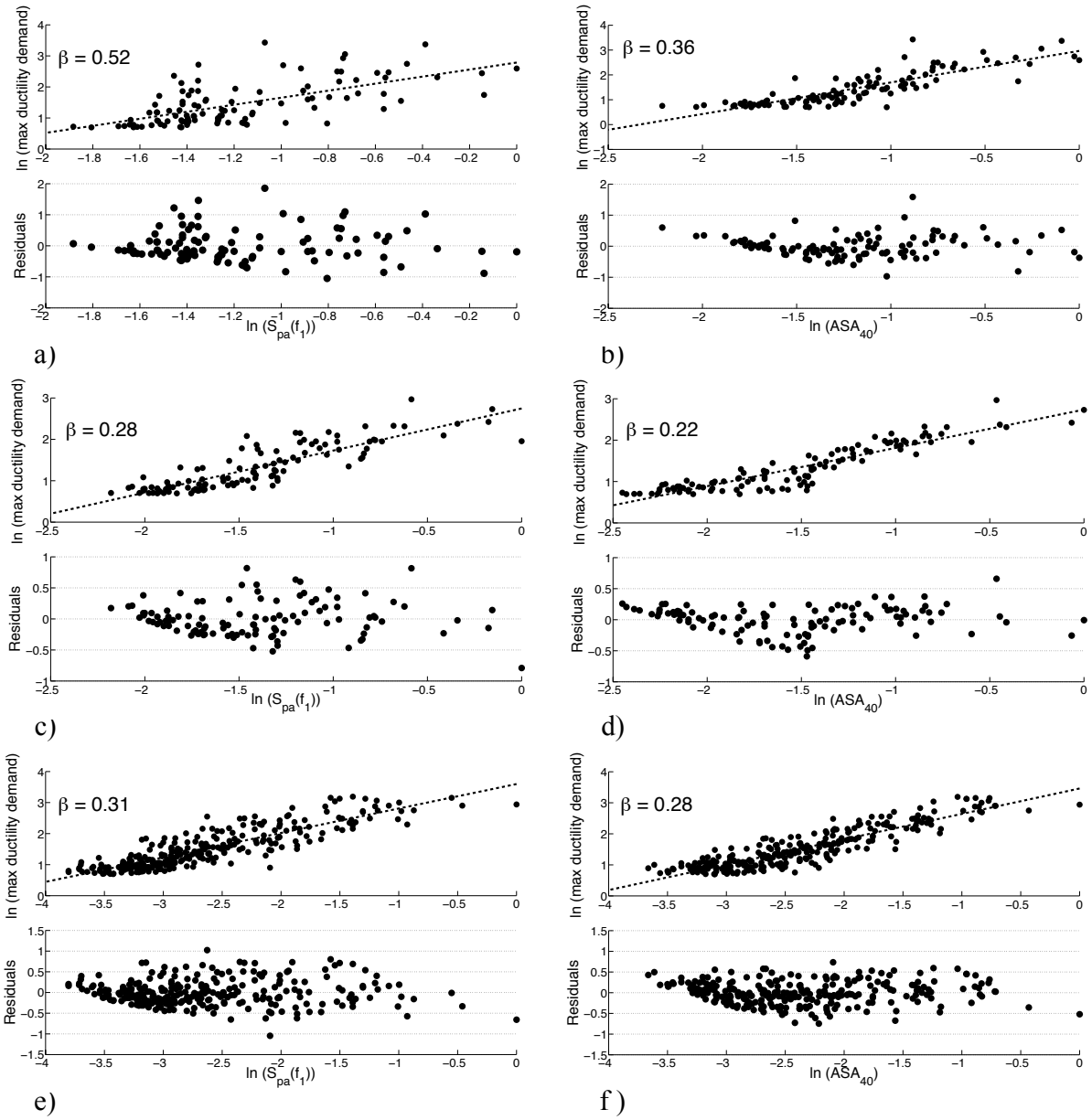

Figure 2.20 *Damaging records ($\mu_{max} \geq 2$) - Scatter plots, regression and standard deviation of the residual with respect to the maximum ductility demand for: a) CAMUS1, $S_{pa}(f_1)$; b) CAMUS1, ASA_{40}; c) CAMUS1-SSI, $S_{pa}(f_1)$; d) CAMUS1-SSI, ASA_{40}; e) EC8-FRAME, $S_{pa}(f_1)$; f) EC8-FRAME, ASA_{40}*

2.3.5.2 IM sufficiency evaluation

Results of the comparative statistical analysis relative to IM sufficiency are presented in Table 2.13 for the 2,045 records composing the four ground motion bins.

Table 2.13 *IM sufficiency: Spearman rank correlation coefficient. (The EDP considered is the μ_{max}). The closer to zero the value, the better the sufficiency; the value highlighted in bold evidence the worst insufficiencies.*

		CAMUS1			*CAMUS1-SSI*			*EC8-FRAME*		
IM type	IM	M_w	R_{hyp}	V_{S30}	M_w	R_{hyp}	V_{S30}	M_w	R_{hyp}	V_{S30}
Frequency response-based	**ASA_{20}**	-0.1	-0.15	0.06	-0.1	-0.19	0.06	0.01	-0.12	0.08
	ASA_{40}	-0.18	-0.22	0.12	-0.15	-0.26	0.09	-0.06	-0.18	0.09
	$S_{pa}(T_1)$	0.06	0.01	-0.01	0.16	0.09	-0.01	0.07	-0.03	0.01
	S^*	-0.23	-0.26	0.15	-0.19	-0.26	0.15	-0.13	-0.24	0.05
	I_{NP}	-0.14	-0.11	0.08	-0.07	-0.1	0.06	0.05	0.01	-0.01
	EPA	-0.26	**-0.45**	0.22	-0.2	-0.33	0.1	0.15	0.21	-0.16
	ASI	-0.22	-0.25	0.15	0.09	0.07	-0.06	0.43	0.31	-0.22
	I_H	-0.2	**-0.54**	0.21	-0.19	**-0.47**	0.14	-0.08	-0.1	-0.06
Amplitude-based	**PGA**	-0.05	-0.07	0.04	0.26	0.15	-0.13	**0.5**	0.3	-0.23
	PGV	-0.22	-0.44	0.19	-0.13	-0.31	0.06	0.16	0.18	-0.17
Duration-based	**I_A**	-0.28	-0.4	0.17	-0.13	-0.21	-0.01	0.27	0.2	-0.19
	CAV	-0.23	**-0.59**	0.21	-0.18	**-0.51**	0.11	0.03	-0.14	-0.07
	SCAV	0.12	-0.28	0.06	0.3	-0.13	-0.04	**0.53**	0.07	-0.15
	a_{RMS}	0.22	-0.33	0.02	0.37	-0.2	-0.13	**0.56**	-0.02	-0.12
	I_C	0.2	-0.33	0.03	0.35	-0.19	0.06	**0.55**	-0.02	-0.13

In considering Table 2.13:

With the exception of some correlation for I_H (Fig. 2.22b) and *EPA*, an analysis of these results reveals no significant correlation between the frequency response-based IMs and M_w or R_{hyp}. This lack of correlation indicates the practical sufficiency of this class of IMs (including ASA_R, see Figures. 2.21a-2.21b) as regards the Magnitude and source-to-site distance (see also Appendix B).

In contrast, a noticeable degree of insufficiency with respect to the moment Magnitude has been exposed in the case of the low-frequency frame structure, for *S-CAV*, a_{RMS}, I_C and *PGA* (Fig. 2.22a). In addition, a perceptible degree of insufficiency with respect to distance has been shown in the case of CAMUS1 structures, for *CAV* (Fig. 2.22c).

Lastly, it is important to note that none of the considered IMs display a significant degree of insufficiency relative to soil type, i.e. V_{s30} (Fig. 2.23).

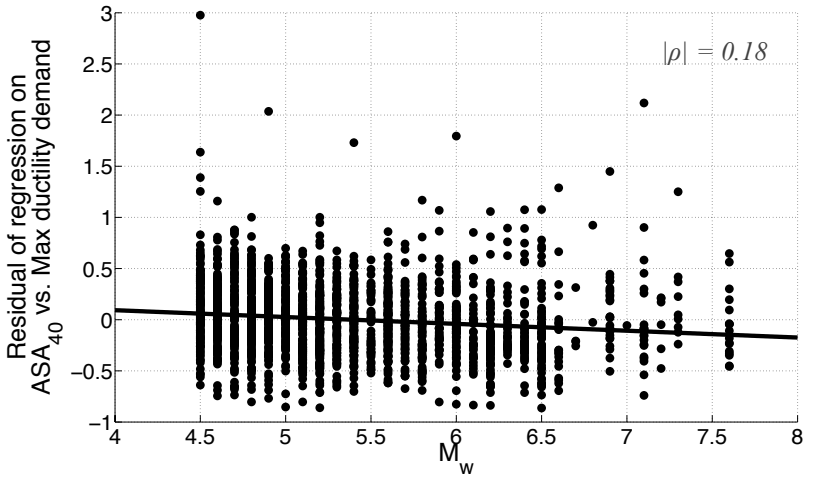

a)

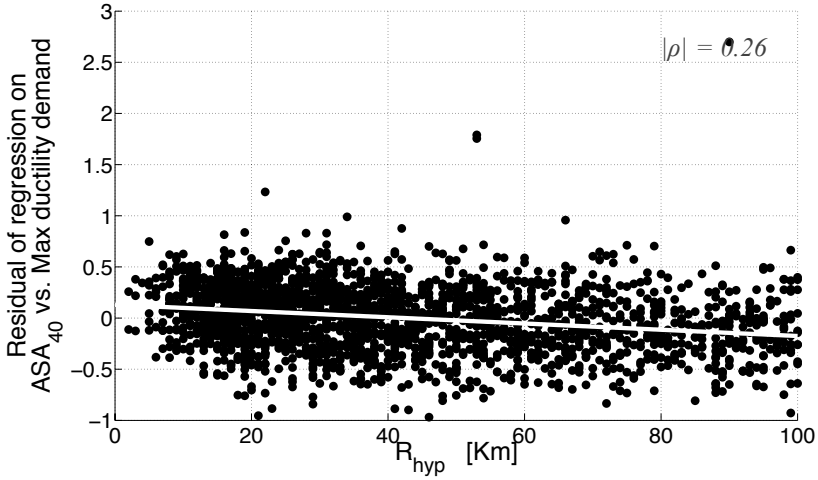

b)

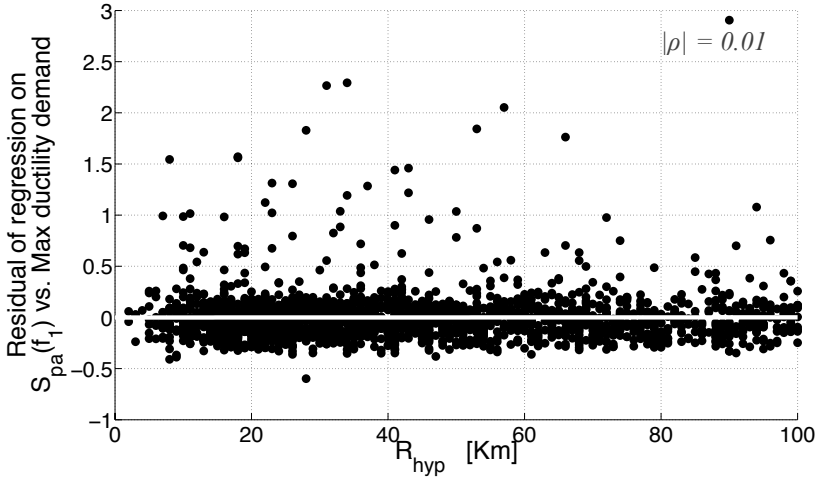

c)

Figure 2.21 *The sufficiency can be appreciated observing the slope of the regression line (lower the slope, higher the sufficiency): a) CAMUS1 ASA_{40} vs. M_w; b) CAMUS1-SSI ASA_{40} vs. R_{hyp}; c) CAMUS1, $S_{pa}(f_1)$ vs. R_{hyp}.*

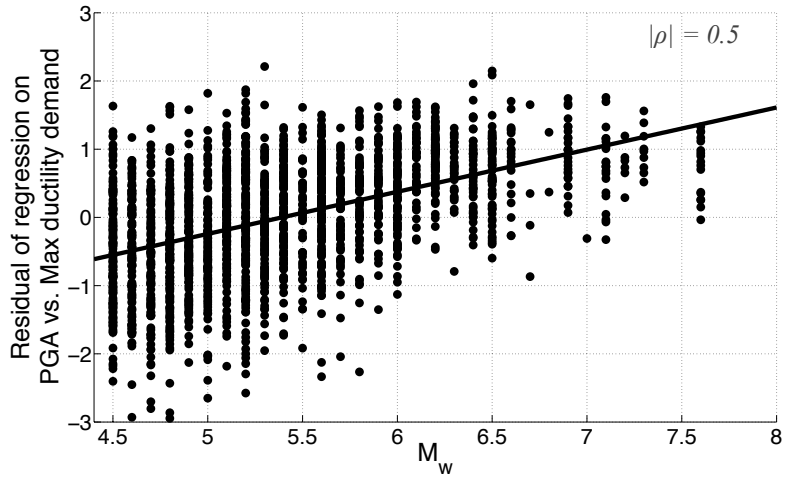

a)

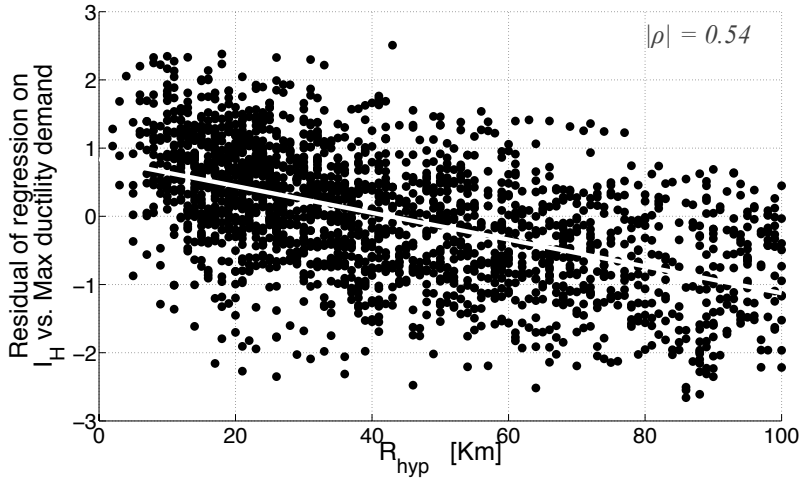

b)

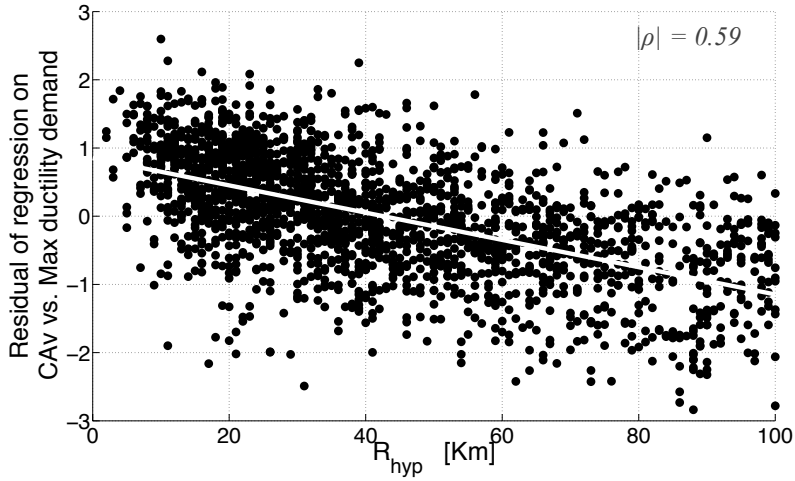

c)

Figure 2.22 *The sufficiency can be appreciated observing the slope of the regression line (lower the slope, higher the sufficiency): a) EC8-FRAME PGA vs. R_{hyp}; b) CAMUS1 I_H vs. R_{hyp}; c) CAMUS1, CAV vs. R_{hyp}.*

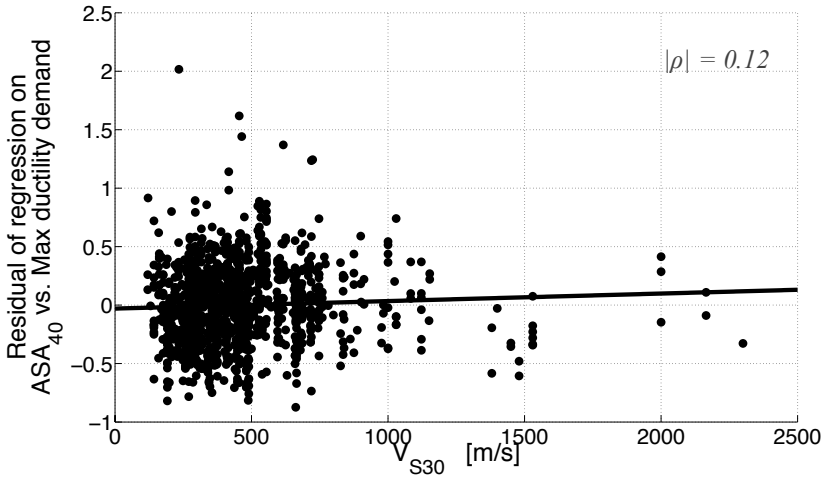

a)

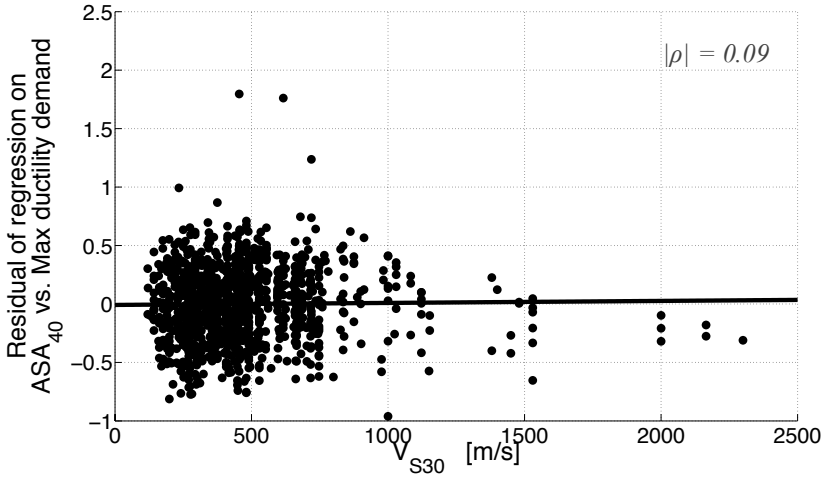

b)

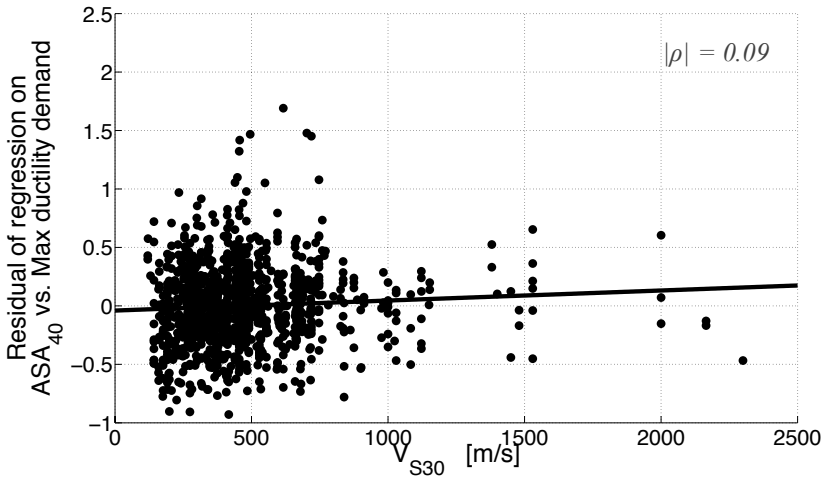

c)

Figure 2.23 *The sufficiency can be appreciated observing the slope of the regression line (lower the slope, higher the sufficiency a) CAMUS1 ASA_{40} vs. V_{S30}; b) CAMUS1-SSI ASA_{40} vs. V_{S30}; and c) EC8-FRAME, ASA_{40} vs. V_{S30}.*

2.3.6 ASA_R optimum

Given that ASA_R has been proposed for application to nonlinear behaving RC structures, the results of analyses associated with the "damaging records" will be considered herein for the purpose of establishing a general and optimal value of the reduction factor R in the ASA_R definition (Eq. 2.1).

With respect to the abovementioned results, the values of frequency drop and maximum ductility demand (as computed using the first yield) are given in Figure 2.24, which also exhibits the correlation between f_D and μ_{max}. The relationship between maximum ductility demand and maximum inter-story drift ratio is then shown in Figure 2.25: the good linear fit for the CAMUS1 test cases indicates a nearly uniform inter-story drift distribution along the height of the structure (Ghobarah, 2004).

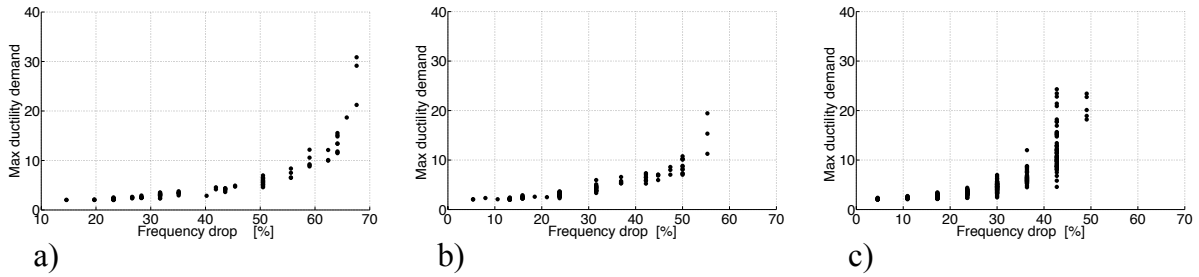

Figure 2.24 *Damaging records ($\mu_{max} \geq 2$), frequency drop vs. maximum ductility demand: a) CAMUS1, b) CAMUS1-SSI, and c) EC8-FRAME.*

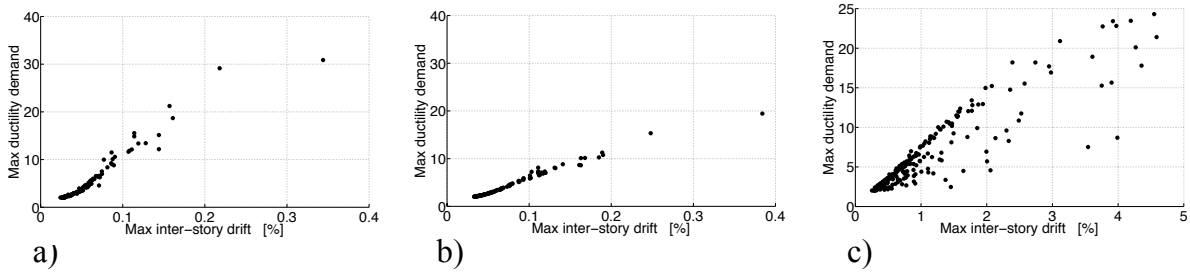

Figure 2.25 *Damaging records ($\mu_{max} \geq 2$), maximum inter-story drift vs. maximum ductility demand: a) CAMUS1, b) CAMUS1-SSI, and c) EC8-FRAME.*

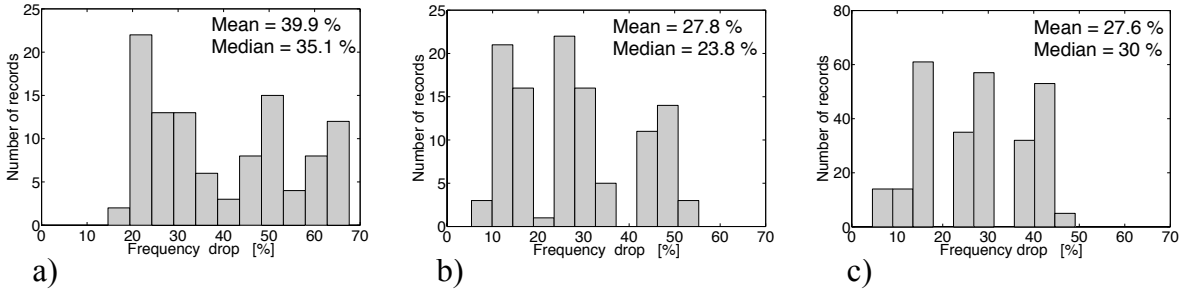

Figure 2.26 *Damaging records ($\mu_{max} \geq 2$), frequency drop distribution histograms: a) CAMUS1, b) CAMUS1-SSI, and c) EC8-FRAME.*

So, in order to proceed with selecting the optimum reduced fundamental frequency (i.e. the R value in Equation 2.1), the ASA_R has been computed for several reduction values (R), i.e. ASA_{20}, ASA_{30}, ASA_{40}, ASA_{50} and ASA_{60}.

It can be observed from Table 2.14 that ASA_{40}, with a reduction value (R) of 40%, yields a slightly higher efficiency for most considered test cases and EDPs. The mean and median of the frequency drop value distributions (Figure 2.26) confirm the results shown in Table 2.14.

Table 2.14 *ASA_R sensitivity study: damaging records ($\mu_{max} \geq 2$), Logartithmic Standard deviation (β) of the residual*

	CAMUS1			*CAMUS1-SSI*			*EC8-FRAME*		
IM	D_m	μ_{max}	*MIDR*	D_m	μ_{max}	*MIDR*	D_m	μ_{max}	*MIDR*
ASA_{20}	0.25	0.45	0.36	**0.27**	**0.22**	**0.22**	0.25	**0.27**	**0.36**
ASA_{30}	**0.24**	0.41	0.32	**0.27**	**0.21**	**0.21**	**0.23**	**0.27**	**0.35**
ASA_{40}	**0.23**	**0.36**	0.29	**0.28**	**0.22**	**0.21**	**0.24**	**0.28**	**0.36**
ASA_{50}	**0.23**	**0.35**	**0.28**	0.3	0.24	0.23	0.25	0.29	**0.36**
ASA_{60}	**0.24**	**0.35**	**0.27**	0.32	0.26	0.24	0.26	0.3	0.37

Moreover, it is important to highlight that a 40% frequency drop matches the mean values identified on RC buildings by both post-earthquake observations (CALTECH, 1975; Naeim, 1988; Mucciarelli *et al.*, 2004) and numerical studies (Crowley and Pinho, 2004).

Results of the sensitivity analysis, as supported by the literature, therefore encourage the author to consider that a 40% fundamental frequency drop be considered as a general/optimal value in the definition of ASA_R; Equation (2.1) then assumes the following form:

$$ASA_{40}(f_1) = \frac{2.5}{f_1} \int_{0.6 f_1}^{f_1} S_{pa}(f, \xi) \; df \tag{2.20}$$

Similarly, Equation (2.3) assumes the form:

$$ASA_{40}(T_1) = 2.5 \cdot T_1 \int_{T_1}^{1.67 \cdot T_1} \frac{S_{pa}(T, \xi)}{T^2} dT \tag{2.21}$$

Ultimately, formulations (2.20) and (2.21) allow computing ASA_{40} in only knowing the fundamental frequency (period) of the structure, like in the case of $S_{pa}(f_1)$.

2.4 MAIN SOURCE OF IMs' EFFICIENCY LIMITATION

In the previous paragraphs the performance of a large panel of IMs have been compared, and the superiority of the herein introduced ASA_R in predicting structural demand for non-linear behaving structures has been highlighted. However, despite its promising performance ASA_R is not perfect (i.e., $\beta = 0$) and therefore, the aim of this paragraph is to depict and analyze the main source of its efficiency limitation, so to highlight some ideas for future improvements.

Figure 2.27 shows the scatter plot of ASA_{40} vs. frequency drop for the CAMUS1 structure exposed to the 2,045 ground motion records considered in the comparative analyses. As it can be observed, there are few cases in which records characterized by nearly the same ASA_{40} produce quite different structural demand (i.e., frequency drop), and inversely there are few cases in which records characterized by quite different ASA_{40} produce almost the same structural demand. The same evidence of dispersion is visible in the analogous scatter plots of ASA_{40} vs. Max Inter-Story Drift (Figure 2.28) and ASA_{40} vs. μ_{max}.

It is worth reminding that (as illustrated in paragraph 2.3.5.1) a part of the scatter is due to the impossibility to know a priori the value of the structure's softened frequency, and then to assign the "exact" R value in the formulation of ASA_R (Eq. 2.1). Indeed, the "general" optimum R value (paragraph 2.3.6), even if statistically optimum, introduces bias in most of the cases.

However, the aforementioned is not the only source of uncertainty affecting the ASA_R's demand prediction: another important part of bias originates from the *non-stationary character, in amplitude and frequency content, of ground motion records*. This last source of uncertainty is particularly important because, as it is proven in the final part of the section, it affects all the IMs considered in this study.

So, in order to explain how the non-stationary character of ground motions biases IMs' demand prediction, detailed analyses of the evolution (during the seismic loading) of the CAMUS1' fundamental-frequency are here presented. Such analyses are performed on two sets of ground motions (highlighted in Figure 2.27), which have been selected because they are the ones showing the largest variability in the ASA_R demand prediction.

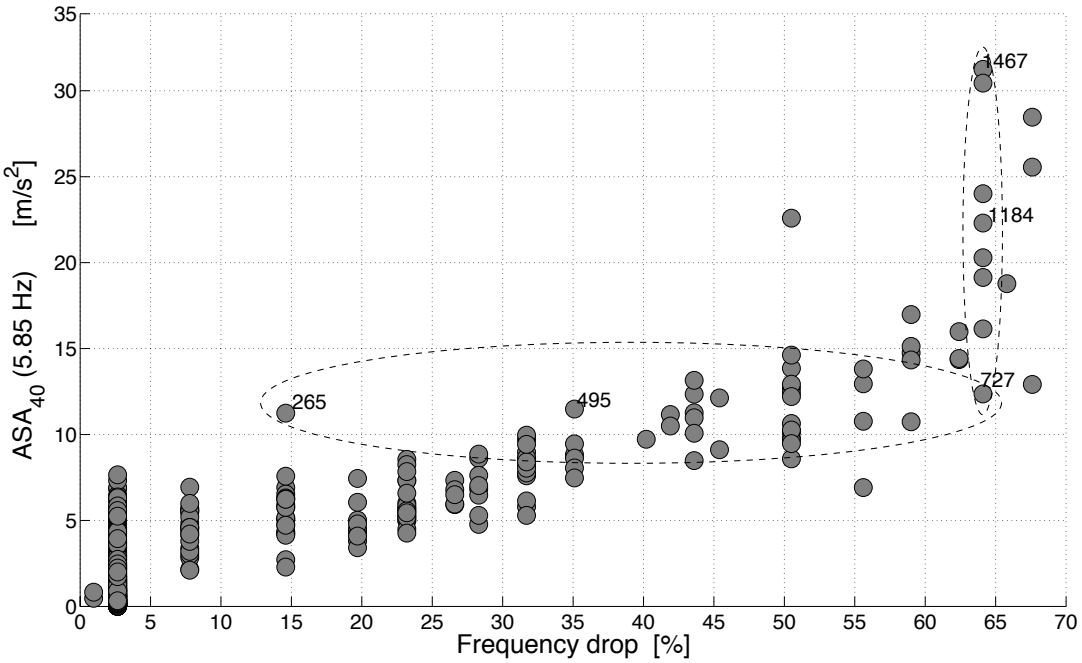

Figure 2.27 *CAMUS1: Scatter plot, ASA_{40}(5.85 Hz) vs. Frequency drop. (The distribution of the data in vertical arrays, is due to the resolution (0.1 Hz) of the method used to extract the softened frequency, see end of paragraph 2.3.4.1. The same explanation for the position, at 2.5% frequency-drop, of the points corresponding to the runs which do not produce structural damage.)*

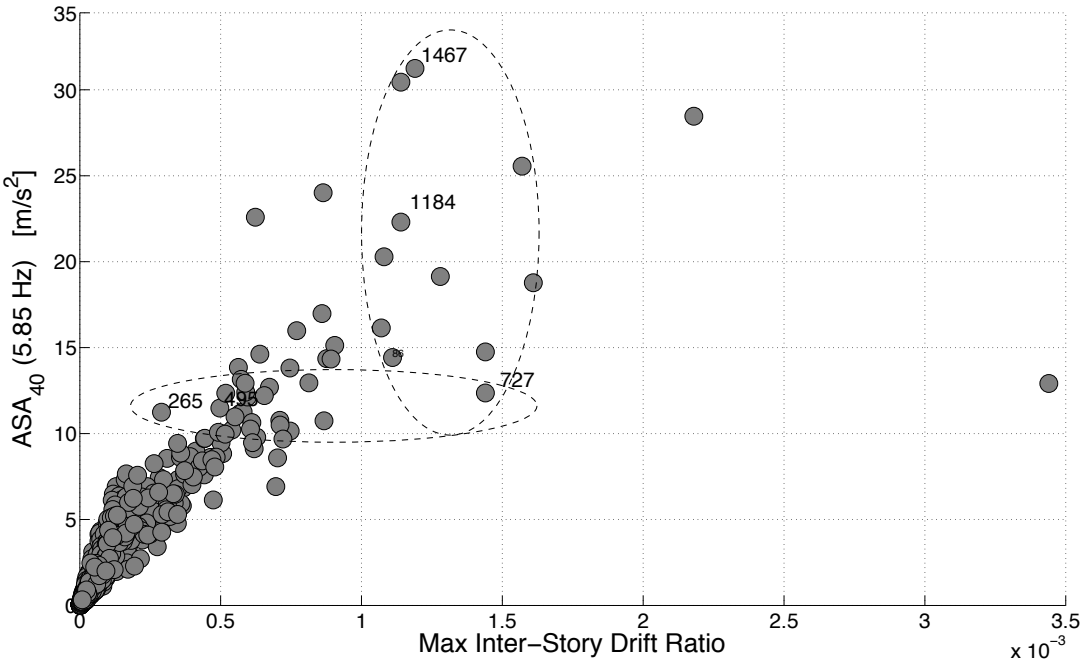

Figure 2.28 *CAMUS1: Scatter plot, ASA_{40}(5.85 Hz) vs. MIDR.*

The records 1467, 1184 and 727 (the response spectra of which are reported in Figure 2.29) are characterized by rather different values of $ASA_{40}(5.85\ Hz)$, nevertheless they produce the same amount of frequency drop (Figure 2.27). Figures 2.30, 2.31 and 2.32 show the time evolutions of the CAMUS1 fundamental frequency with respect to the three ground motion records.

For each record, the fundamental frequency evolution is computed by performing *n* time-history analyses, where *n* is equal to the ratio between the length of the record and a time-window of 0.5 seconds (arbitrarily chosen). Thus, for each of the *n* simulations, which simulate the response of the structure for increasing time length (i.e., *n**0.5 seconds), the method described in paragraph 2.3.4.1 is applied to extract the softened frequency.

Referring to the record 1467 (i.e., Figure 2.30), it is worth noting that the damage process stops after about 8.5 seconds, i.e. the remaining part of the record does not further damage the structure. The same remark can be made with respect to the record 1184 (i.e., Figure 2.31), in which the damage process clearly stops at 14.5 seconds before the highest peaks of the record's acceleration time history, and with respect to the record 727 (i.e., Figure 2.32), which stops damaging the structure after 11 seconds.

Figures 2.33-2.35, instead, report the response spectra, respectively of records 1467, 1184 and 727, computed on both the whole length of the records, and a portion of them. This last encompasses the ground motion record from its beginning until the instant the damage process (on the test-case structure) stops.

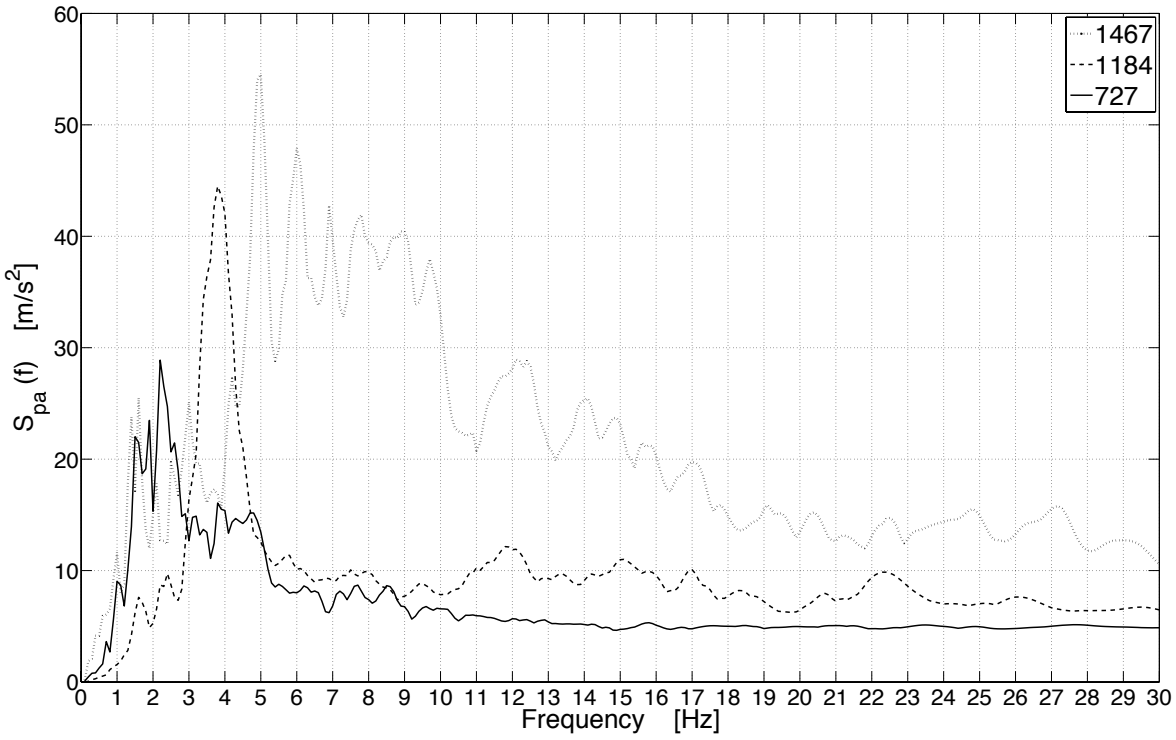

Figure 2.29 *Response spectra (2 % damping) comparison: records 1467, 1184 and 727. The three records, having different ASA_{40}(5.87 Hz) values, produce the same frequency drop.*

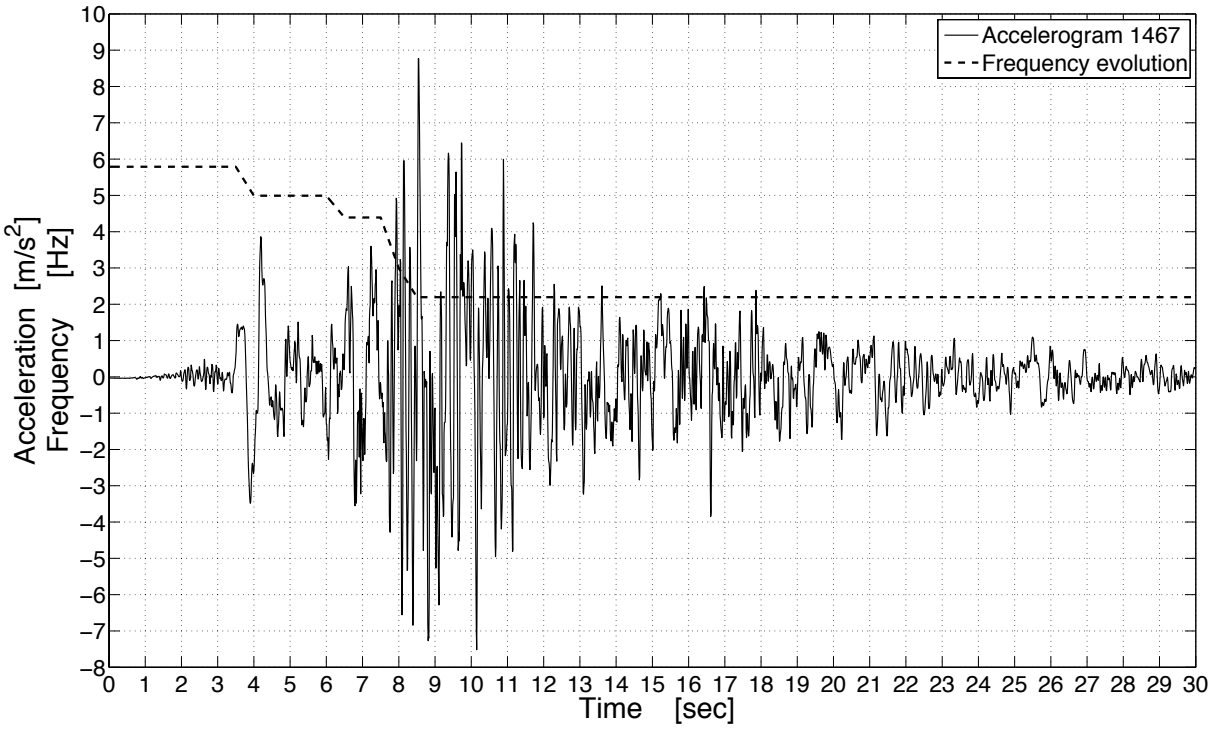

Figure 2.30 *CAMUS1 loaded with record 1467: fundamental frequency evolution.*

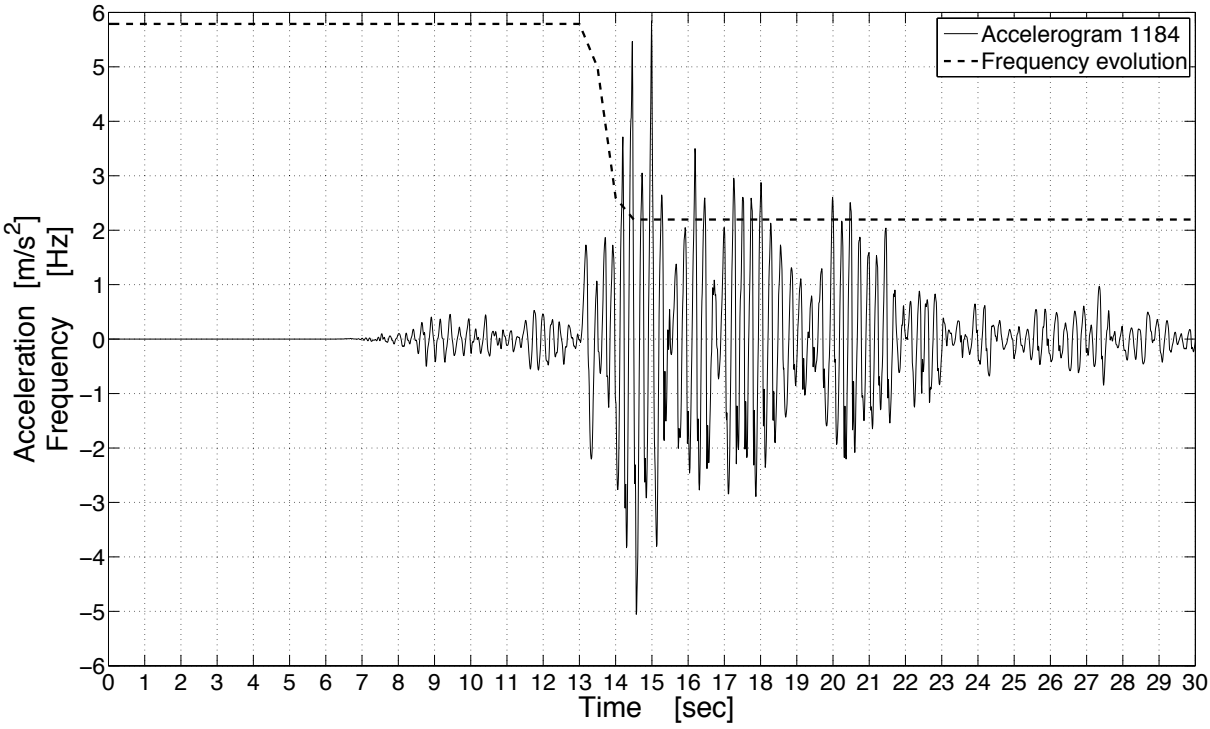

Figure 2.31 *CAMUS1 loaded with record 1184: fundamental frequency evolution.*

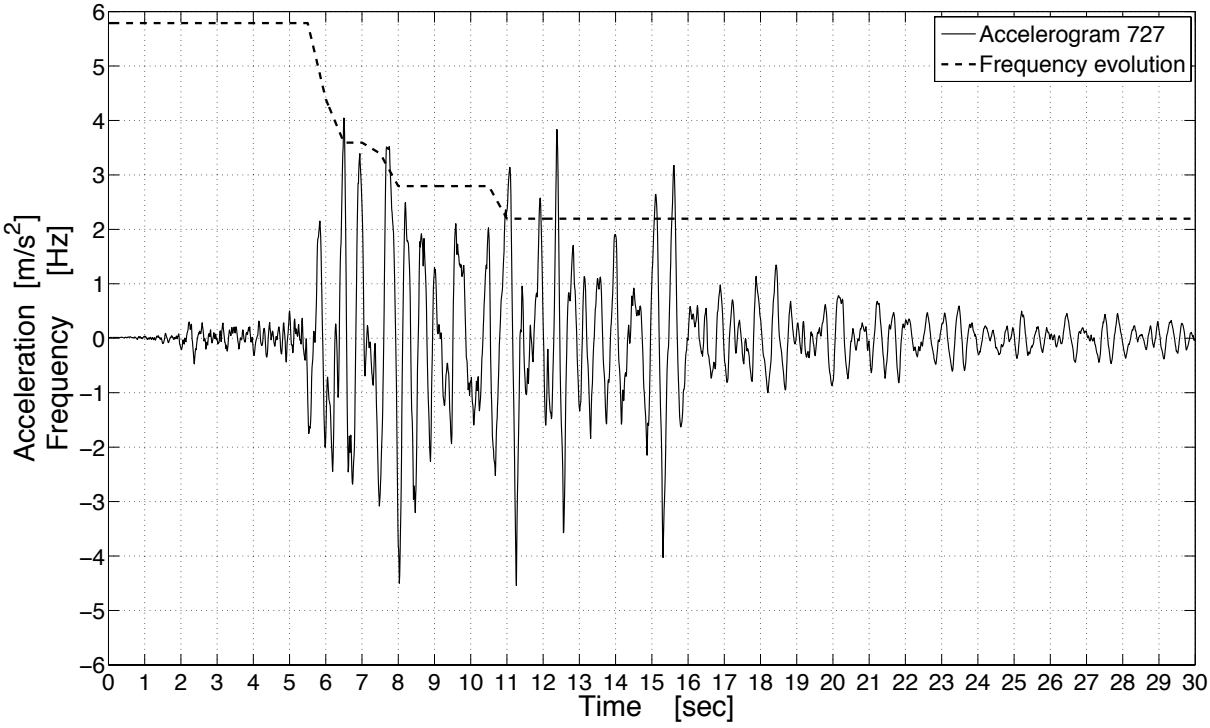

Figure 2.32 *CAMUS1 loaded with record 727: fundamental frequency evolution.*

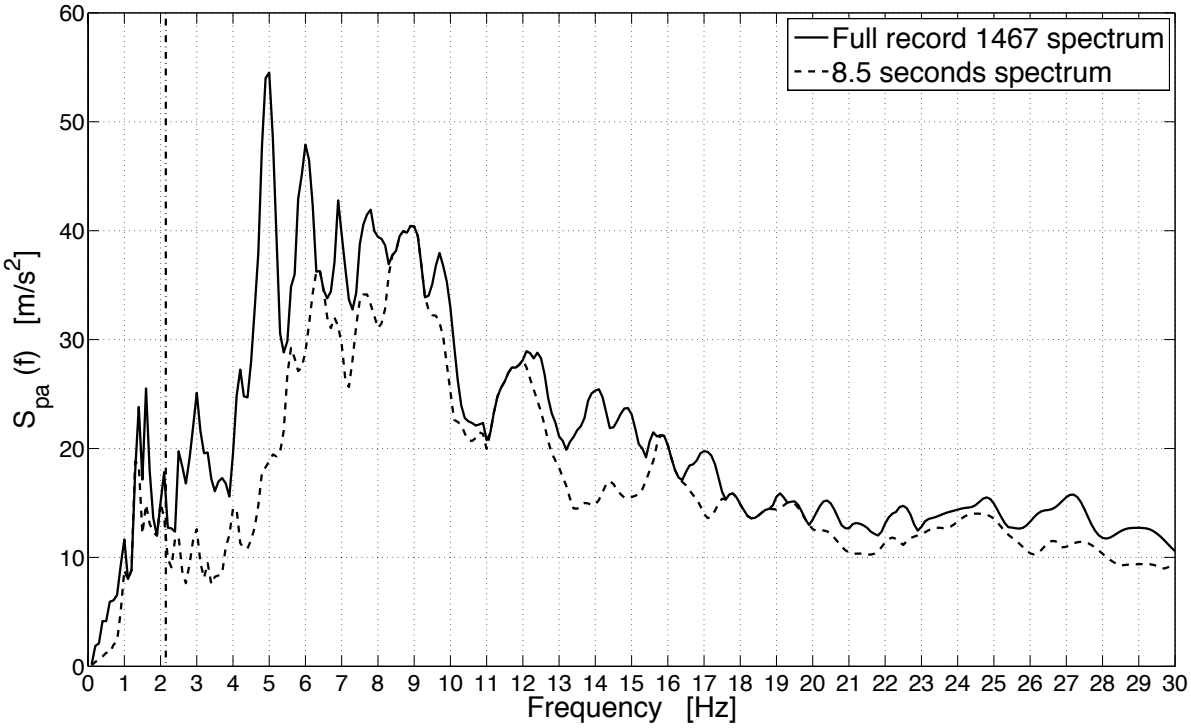

Figure 2.33 *Record 1467:"full" and "partial" response spectra (2 % damping). The vertical line indicates the structure's fundamental frequency at 8.5 seconds.*

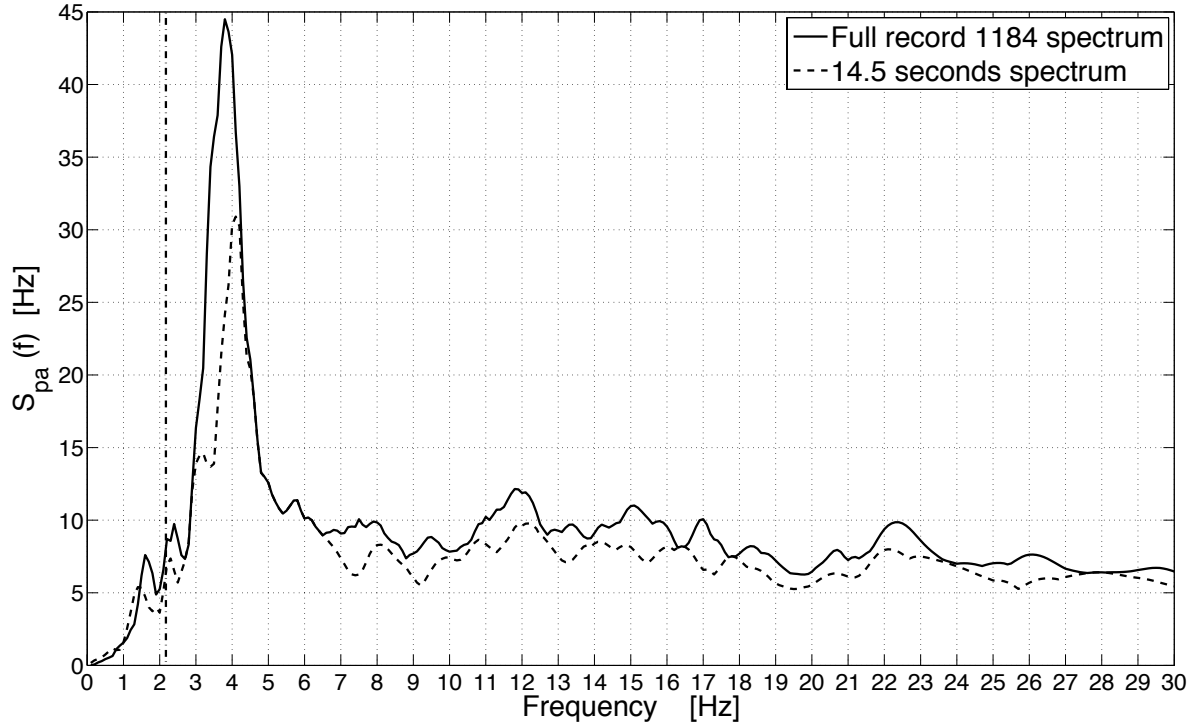

Figure 2.34 *Record 1184:"full" and "partial" response spectra (2 % damping). The vertical line indicates the structure's fundamental frequency at 14.5 seconds.*

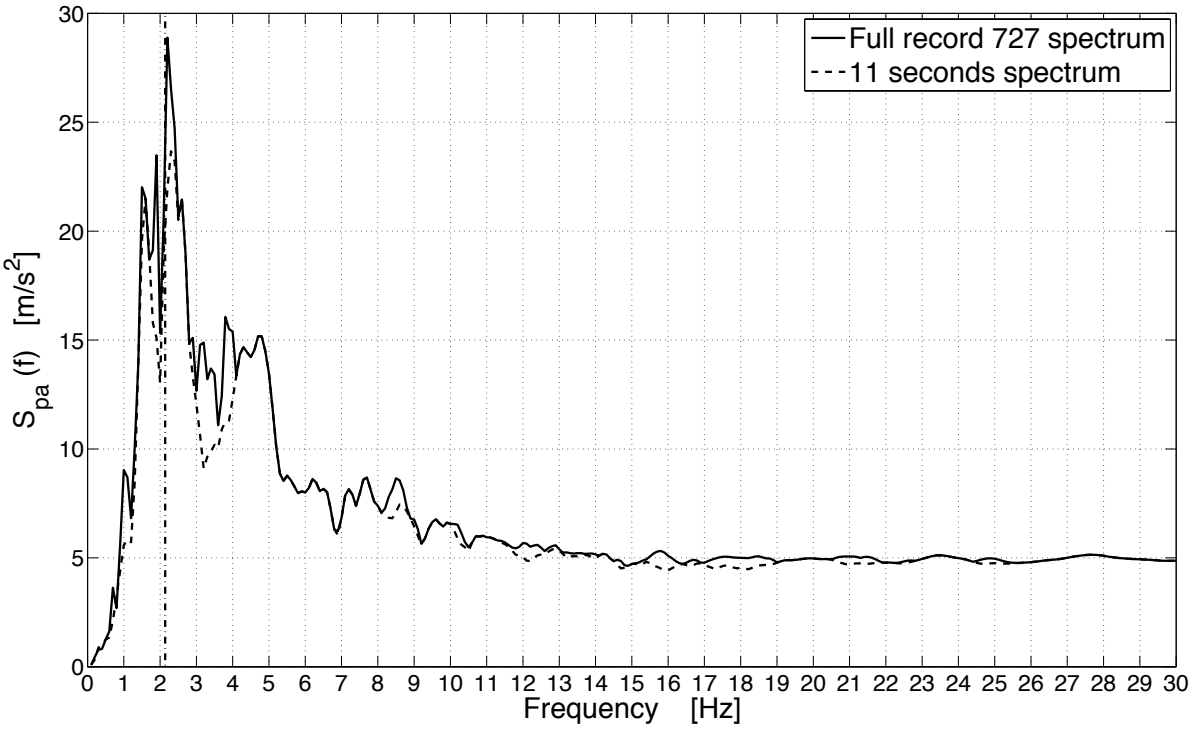

Figure 2.35 *Record 727:"full" and "partial" response spectra (2 % damping). The vertical line indicates the structure's fundamental frequency at 11 seconds.*

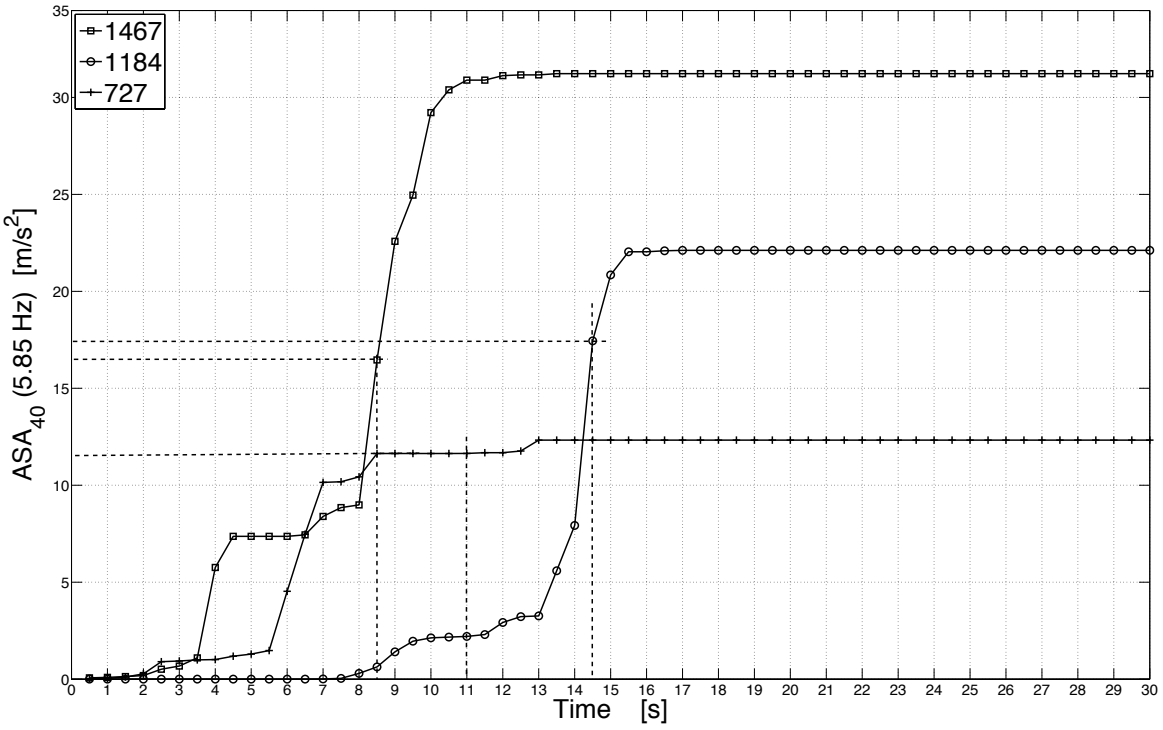

Figure 2.36 *ASA_{40}(5.87 Hz) time evolution for records 1467, 1184, 727.*

A large part of the bias generated by ASA_R in discriminating the damage potential of the three considered records (which have different values of $ASA_{40}(5.85\ Hz)$ but produce the same structural demand) is due to the fact that its value does not stop growing at the same time-instant the damage process stops. Indeed, when the damage-process stops, the response spectra ordinates continue growing (Figures 2.33-2.35) in the frequency range (3.51-5.85 Hz) over which the $ASA_{40}(5.85\ Hz)$ is computed, even if such "additional" part of the spectra evidently "does not affect" the structure anymore. For instance, in the case of record 1467 the $ASA_{40}(5.85\ Hz)$ value is multiplied by nearly a factor 2 after the damage process stops.

Likewise, in Figures 2.33-2.35, one can notice (at least for the examined cases) that the additional part of spectrum (i.e., the one arriving once the damage process stops) is for large part far, and at higher frequencies, with respect to the current fundamental frequency of the structure. Indeed, as it has been shown in section 2.1.1.1, the structure is less likely to be damaged by ground motion cycles which frequency is not tuned with the current structure's fundamental frequency.

Besides, the foregoing arguments are supported by the plots of the $ASA_{40}(5.85\ Hz)$ time-evolution for the three examined records (Figure 2.36): if the computation of the $ASA_{40}(5.85\ Hz)$ is stopped at the time the structure stops being damaged, the values of $ASA_{40}(5.85\ Hz)$ for the three records (which produce the same structural demand) become much closer (i.e. the spread of $ASA_{40}(5.85\ Hz)$ moves from 12÷31 m/s^2 to 11÷17 m/s^2), indicating a reduction of bias of 70 %.

The abovementioned argumentations can be applied to (and verified by) other "biased" cases, for instance the records 727, 265 and 495. These three records (which response spectra are compared in Figure 2.37) have nearly the same value of $ASA_{40}(5.85\ Hz)$, nevertheless they produce clearly different frequency drops, respectively 65%, 35%, and 15% (Figure 2.27). The record 727 stops damaging after 11 sec (Figure 2.32), the record 265 stops damaging after 9 sec (Figure 2.39), and the record 495 stops damaging after 7.5 sec (Figure 2.41). If the computation of the $ASA_{40}(5.85\ Hz)$ is stopped at the aforementioned time instants, the $ASA_{40}(5.85\ Hz)$ is not anymore biased by the "non-damaging" evolution of the response spectra (Figures 2.35, 2.40, 2.42) and therefore, it is able to better discriminate the damage potential of the three ground motions (i.e., in Figure 2.38 the values of $ASA_{40}(5.85\ Hz)$ for the three records "move" farther away from each other and their arrangement is consistent with the damage order visible in Figure 2.27).

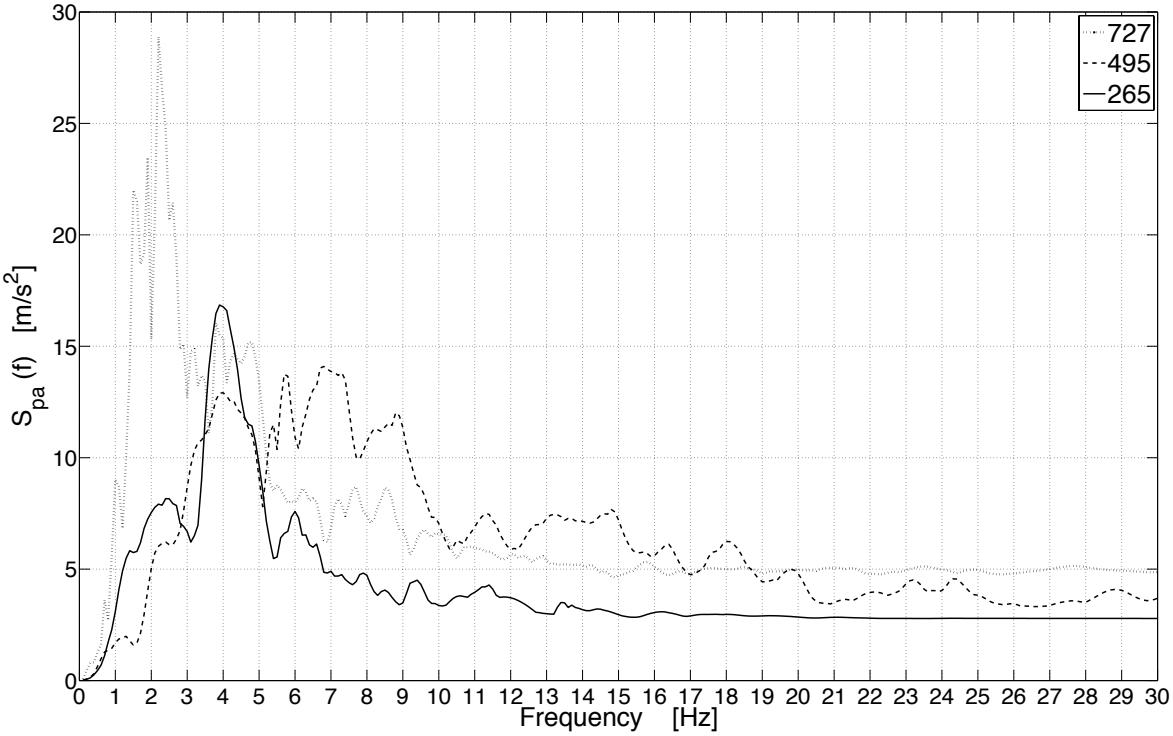

Figure 2.37 *Response spectra (2 % damping) comparison: records 727, 495 and 265. The tree records, having quite similar ASA_{40}(5.87 Hz) values, produce rather different frequency drop.*

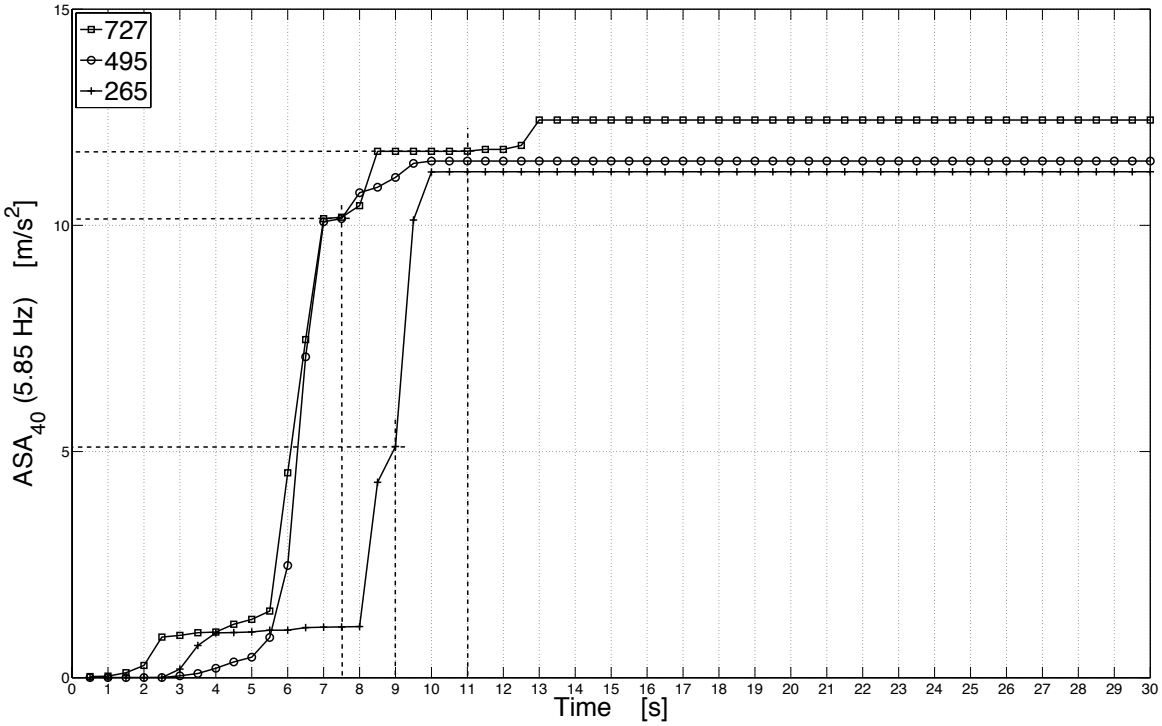

Figure 2.38 *ASA_{40}(5.87 Hz) time evolution for records 727, 495, 265.*

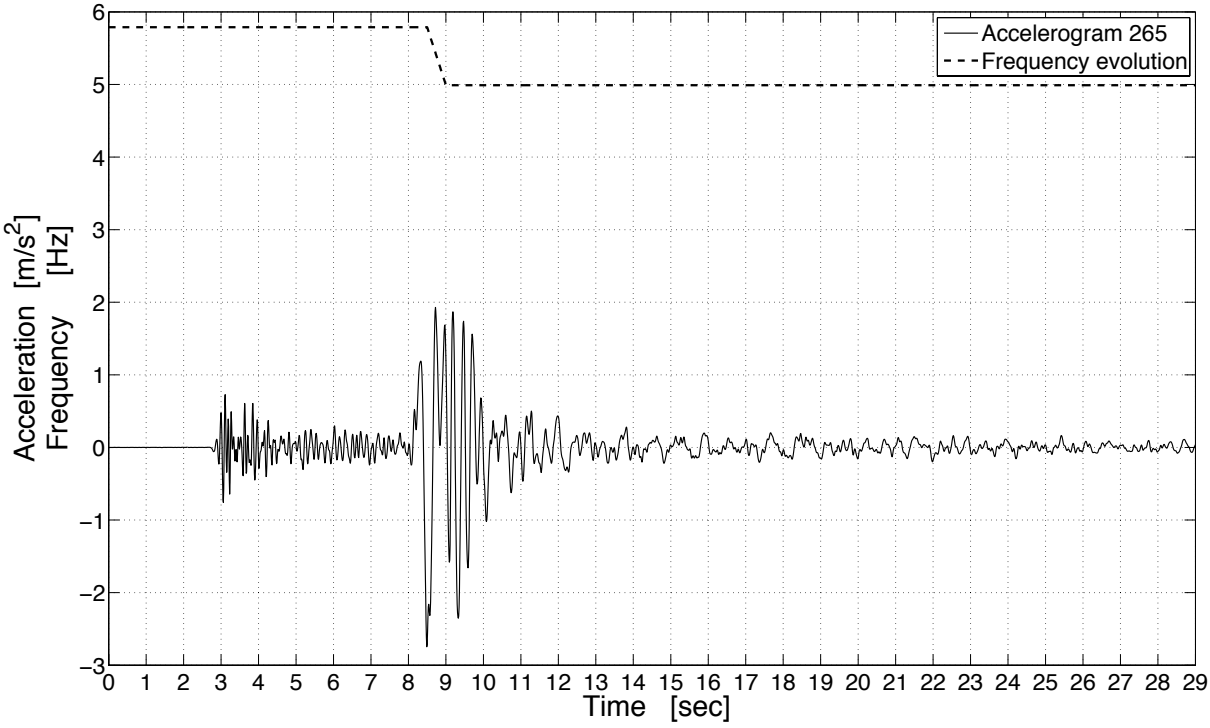

Figure 2.39 *CAMUS1 loaded with record 265: fundamental frequency evolution.*

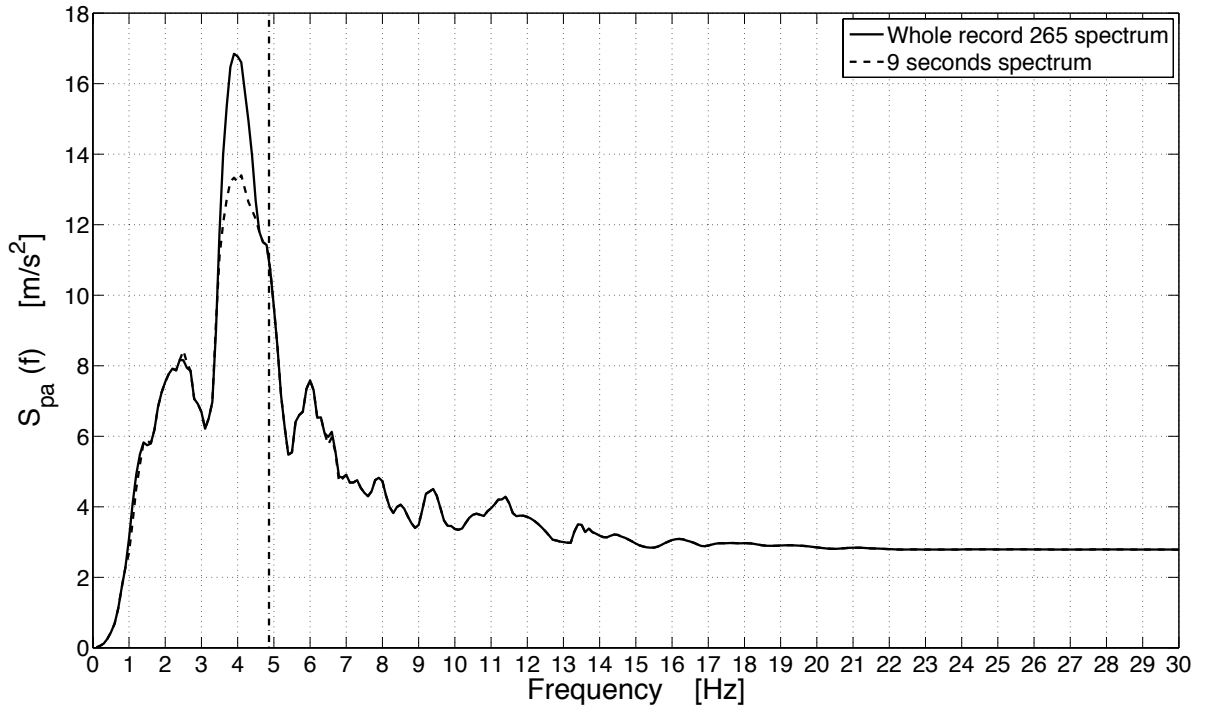

Figure 2.40 *Record 265: "whole" and "partial" response spectra (2 % damping). The vertical line indicates the structure's fundamental frequency at 9 seconds.*

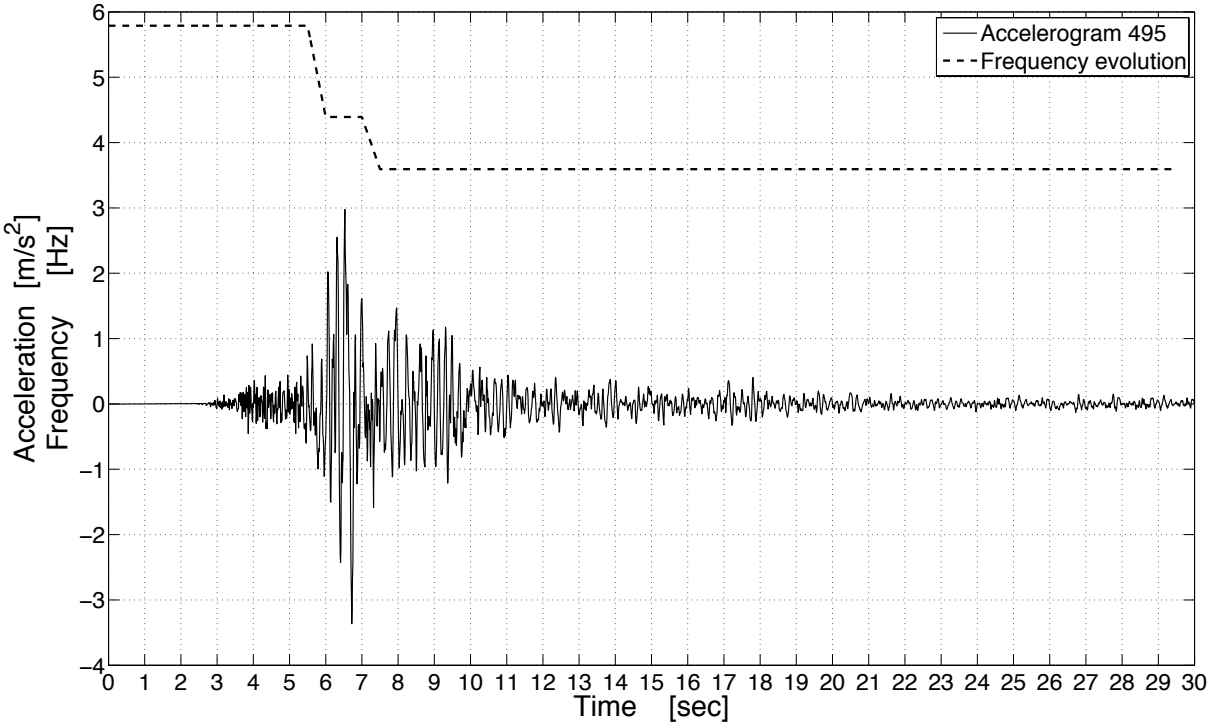

Figure 2.41 *CAMUS1 loaded with record 495: fundamental frequency evolution.*

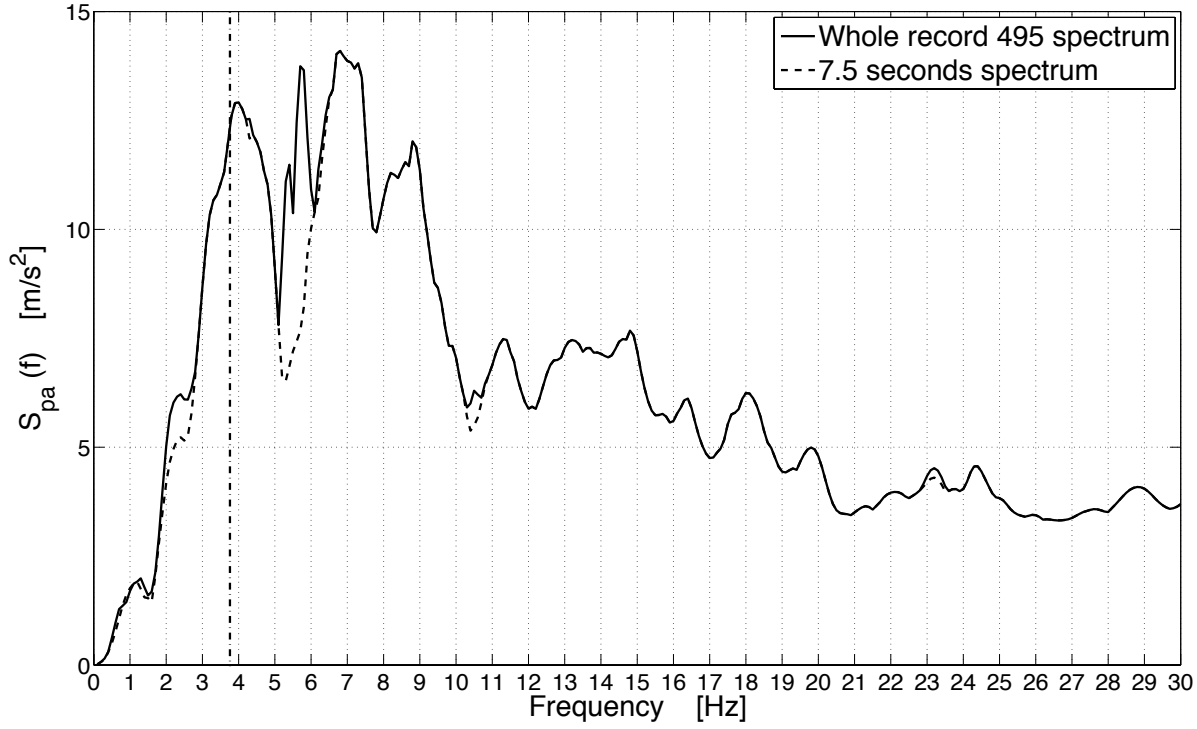

Figure 2.42 *Record 495: "whole" and "partial" response spectra (2 % damping). The vertical line indicates the structure's fundamental frequency at 7.5 seconds.*

Lastly, in order to further stress the previous arguments and their impact on IMs' structural demand prediction, an additional (heuristic) example is herein provided. In this, the CAMUS1 structure has been loaded with two simple excitations (Fig. 2.43), which are both constituted by the sequence of two sinuses: in the first sequence, a sinus at frequency 3 Hz follows, after two seconds without excitation, a sinus of frequency 5.85 Hz; in the second sequence, a sinus at frequency 5.85 Hz follows, after two seconds without excitation, a sinus of frequency 3 Hz. Indeed, the second sequence is exactly the "mirror copy" of the first one.

The two loading sequences produce structural demand differing of about 17 % in terms of frequency drop, and 30 % in terms of Max Inter-story Drift Ratio (Table 2.15).

Table 2.15 *CAMUS1: response to two "mirror" sequences of loading*

Signal	MIDR	Frequency drop [%]
Sequence 1	8.9E-4	54.0
Sequence 2	6.2E-4	45.0

What it is emblematic to note is that no one of the IMs considered in this study is able to distinguish the two loading sequences (i.e. the values of IMs for the sequence 1 are exactly the same of sequence 2), which produce exactly the same response spectra (Figure 2.44).

Hence, conclusively, other than to evidence the sources of bias affecting the ASA_R structural prediction, the foregoing analyses emphasize two central aspects in the process of characterization of seismic ground motion through IMs:

1. *The duration of the ground motion is a misleading parameter*: the considered examples have shown (on the basis of the CAMUS1 RC structure) that the damage process is not directly correlated with the duration of the strong ground motion, thus confirming the finding of Iervolino *et al*. (2006), about its statistical insignificance in the characterization of the ground motion damaging potential.
2. *The non-stationary character, in amplitude and frequency content, of ground motions is a main source of bias affecting all "simple" IMs:* the foregoing examples have shown that the structural damage process is related to complex time-dependent interactions between the current structural frequency and the current amplitude and frequency content of the loading. Simple IMs, as the ones considered in this study, are far from being able to account for such phenomena.

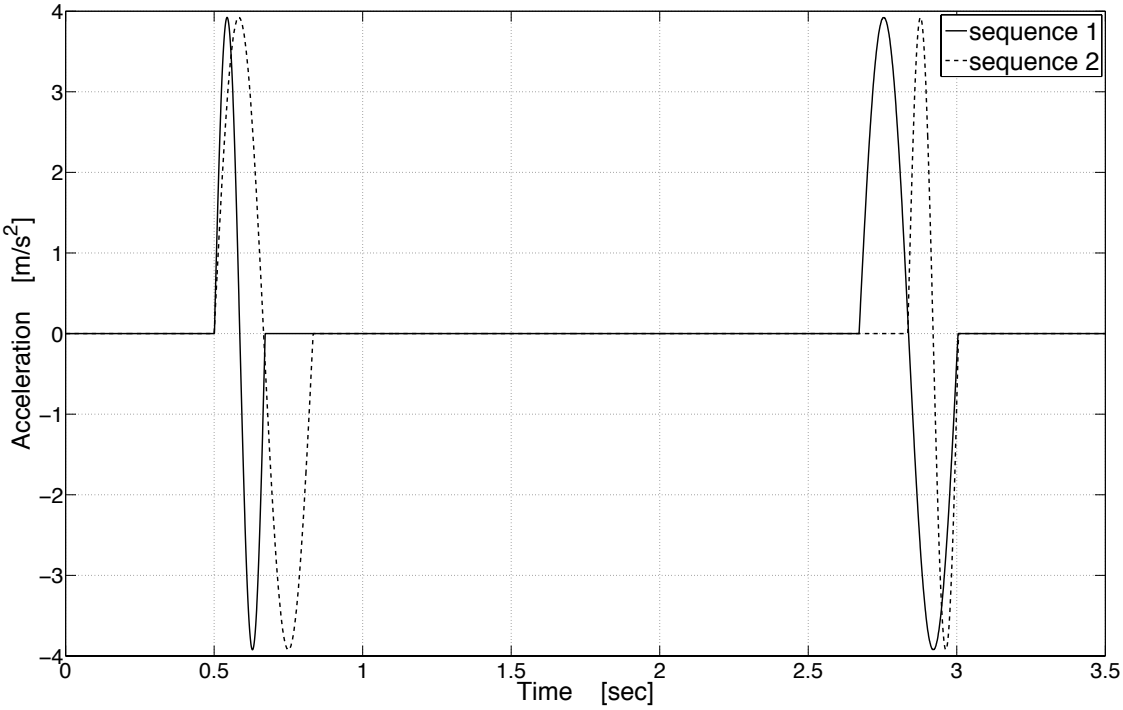

Figure 2.43 *Acceleration tine-histories of double-sinus sequences with same values of IMs.*

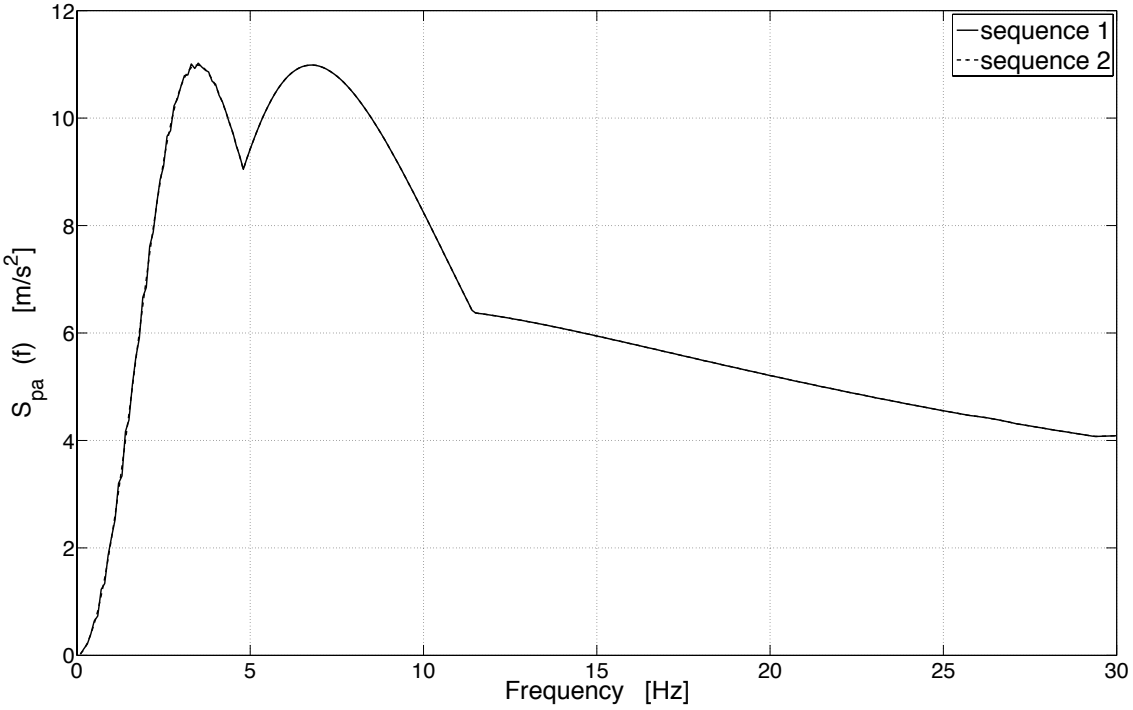

Figure 2.44 *Response spectra (5% damping) of double-sinus sequences with same values of IMs.*

2.5 CONCLUSIONS

In this chapter, a new structure-specific IM, namely the *Relative Average Spectral Acceleration* (ASA_R), has been proposed. The ASA_R is based on the pseudo-spectral acceleration values averaged over a definite, structure-specific, frequency range (period). Such a range covers the evolution of the structure's fundamental frequency (period) caused by the ground motion-induced damage process.

The efficiency of ASA_R has been revealed by means of comparative statistical analyses of the results of nonlinear dynamic simulations performed on two reinforced concrete structures on a large database of recorded seismic ground motions. Among the considered IMs, ASA_R exhibits the highest efficiency in discriminating damaging earthquake ground motion records: its efficiency rises to 31% higher compared with the widely used $S_{pa}(T_1)$.

It has been shown that the ASA_R efficiency is robust with respect to the type of building (load-bearing wall vs. frame; high vs. low frequency) and with respect to linear Soil-Structure Interaction effects.

The sufficiency of ASA_R relative to magnitude, source-to-site distance and soil type (V_{S30}) has also been demonstrated by statistical analyses. Such sufficiency implies that if the ASA_R of interest is given (through Hazard Analysis), then no concerns need to be raised regarding the M, R and V_{S30} of the records used in structural analyses, provided the selected records match the given ASA_R value.

The ASA_R can be computed, like for $S_{pa}(T_1)$, by simply knowing the fundamental frequency (period) of the structure. This looser restriction offers a practical advantage when working with more complex structure-specific IMs. For an actual structure, the fundamental frequency (period) is indeed typically known or else easy to know by means of in-situ tests; for regular buildings, it can be roughly estimated using an empirical code-based approach.

Furthermore, the simple formulation of ASA_R, based exclusively on spectral pseudo-acceleration values, allows performing PSHA by employing the common ground motion prediction models currently available for $S_{pa}(T_1)$.

Lastly, it has been shown how the inner non-stationary character of ground motions imposes limitations to the efficiency of the IMs examined in this study, and how the concept of strong motion duration can drive towards misleading judgment about ground motions destructive potential.

.

3 IMs for Non-Structural demand

NOTE: An adaptation of this chapter has been submitted for publication as: De Biasio M., Grange S., Dufour F., Allain F., Petre-Lazar I., (2014). Intensity Measures for Probabilistic Risk Assessment of Non-Structural Components Acceleration Demand. Earthquake Engineering and Structural Dynamics (SUBMITTED).

Non-Structural Components (NSCs, also denoted as Secondary Systems) are those elements housed-on or attached-to the floors and walls of a building or industrial facility which are not part of the main load-bearing structural system (Fig. 3.1). NSCs are usually classified into three ”functional” categories (Villaverde, 1996): architectural components (stairways, parapets, partitions, suspended ceiling, etc.), mechanical and electrical equipment (piping systems, antennas, computer and data acquisition systems, control panels, transformers, switchgears, emergency power systems, fire protection systems, etc.) and building contents (bookshelves, storage racks, furniture, etc.).

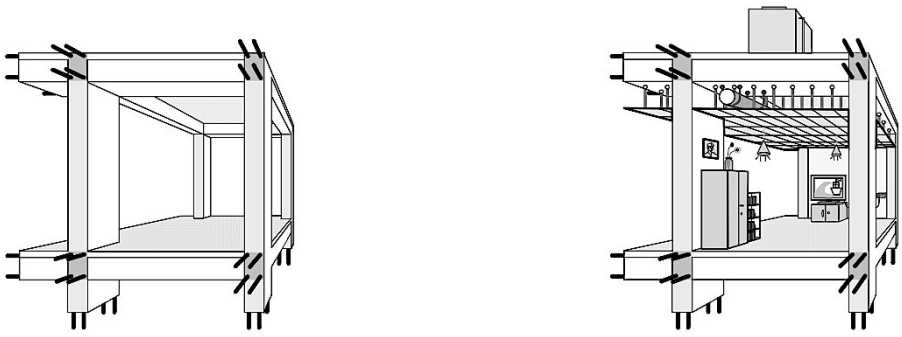

Figure 3.1 *Items employed in a Building: (a) Structure only, and (b) Structure and NSCs.*

Other than with respect to their function, Non-Structural Components may also be classified with respect to their “source of damage”. For instance, in FEMA (1997) the NSCs considered primarily sensitive to inertial loading are classified as *acceleration-sensitive* components. Instead, the Nonstructural components considered primarily sensitive to deformation imposed by inter-story drifts of the structure are classified as *deformation-sensitive* components. The components that are considered sensitive to both inertial loading and inter-story drifts are also classified with the more sensitive effect denoted as Primary (P)

and the less significant effect denoted as Secondary (S). Table 3.1 summarizes inertial and/or deformation sensitivity of selected nonstructural components as identified in FEMA (1997).

It is recognized that in the event of an earthquake, the economical losses are primarily produced by NSCs damage (Taghavi and Miranda, 2003; Fig. 3.2). Indeed, the U.S. Applied Technology Council (ATC, 2004) reported that over 50% of the total losses in recent earthquakes in the United States are associated with NSCs: for example in occasion of the 1994 Northridge earthquake the cost related to nonstructural components represented over 50% of the total damage cost of $18.5 billion for that event (Kircher, 2003). Moreover, the survival of NSCs during an earthquake, which is important for maintaining the operation of emergency services and/or the continuing functionality of critical facilities (e.g. Hospitals, Nuclear Power Plants, etc.), is a public-safety issue.

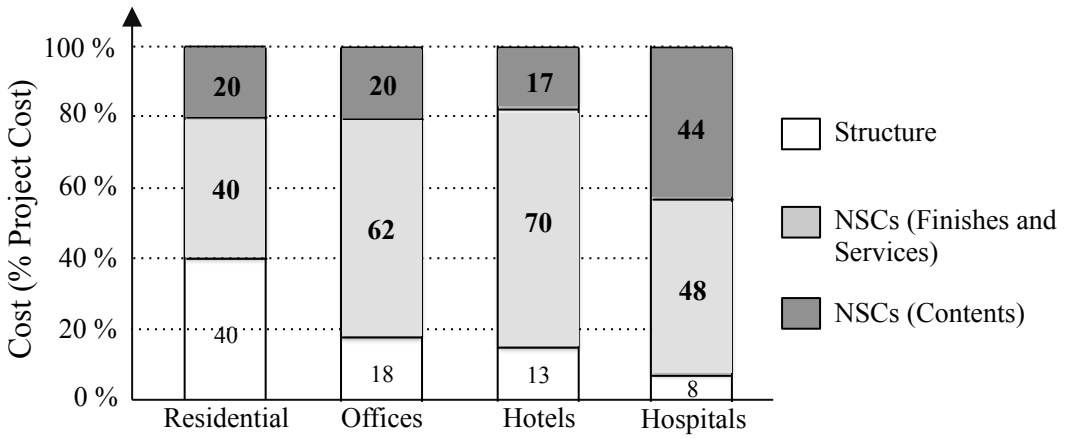

Figure 3.2 *Cost shares of structure and NSCs in building projects implemented in USA and Japan. Adapted from Takahashi and Shiohara, (2004).*

The importance of NSCs seismic assessment is also highlighted by the fact that damage to NSCs usually initiates at levels of ground shaking much smaller than those required to cause structural damage. This means that with respect to structural-damaging earthquake events, larger geographical areas are affected. Besides, the NSCs damage risk can be considered higher, being low-to-moderate earthquake events more frequent than large ones.

However, despite the importance of NSCs and contrarily to the large amount of research focused on IMs aiming to assess structural-deformation-demand, the specific literature about IMs for floor-acceleration-demand estimation is quite limited. The few studies available (e.g., Taghavi and Miranda, 2006; Zentner *et al*., 2011) denote the *PGA* as the most efficient IM, yet these studies have the common drawback to be mainly realized on the base of low-frequency frame structures (De Biasio *et al*., 2014b). For instance, in their comprehensive

study Taghavi and Miranda (2006) considering numerical models with fundamental frequency ranging from 0.25 Hz to 2 Hz and few IMs, conclude that the *PGA* is more efficient than the IMs based on the spectral acceleration at the fundamental frequency of the structure $S_{pa}(f_1)$, despite these latter are accepted as the most efficient with respect to structural demand (NUREG, 1986; Buratti, 2012; De Biasio *et al*., 2014a). The lack of performance provided by $S_{pa}(f_1)$-based IMs is typically justified by the fact that as opposed to structural demand, which is mainly dictated by the structure's first vibration mode, floor acceleration demand is also strongly dependent on the higher vibration modes.

Therefore, being a sizeable part of Non-Structural Components sensible to inertial failure (i.e. electronic devices, piping systems, ceiling systems, ventilation ducts, machinery, bookcases (FEMA, 1997)), here the aim is to propose a new Intensity Measure, which will be expressly designed for NSCs acceleration demand, and to compare its efficiency and sufficiency to the ones of well-known IMs (paragraph 1.2.2).

Table 3.1 *Response sensitivity of selected Non Structural Components. Adapted from FEMA (1997)*

ARCHITECTURAL COMPONENTS			*MECHANICAL EQUIPMENT*		
	Acc. sensitive	Def. sensitive		Acc. sensitive	Def. sensitive
Exterior Skin			**Mechanical equipment**		
Adhered veneer	S	**P**	Boilers and furnaces	**P**	
Anchored veneer	S	**P**	General Mfg. and process machinery	**P**	
Glass blocks	S	**P**	HVAC equipment, vibration isolated	**P**	
Prefabricated Panels	S	**P**	HVAC equipment, non vibration isolated	**P**	
Glazing systems	S	**P**	HVAC Equipment, mounted in line with ductwork	**P**	
Partitions			**Storage vessels and water heaters**		
Heavy	S	**P**	Structurally supported vessels	**P**	
Light	S	**P**	Flat bottom vessels	**P**	
Interior veneers			**Pressure piping**	**P**	S
Stone, marble	S	**P**	**Fire suppression piping**	**P**	S
Ceramic tile	S	**P**	**Fluid piping, not fire suppression**		
Ceilings			Hazardous materials	**P**	S
Directly applied to structure	**P**		Non-hazardous materials	**P**	S
Dropped, furred, gypsum board	**P**		**Ductwork**	**P**	S
Suspended lath and plaster	S	**P**			
Suspended integrated ceiling	S	**P**			
Parapets and appendages	**P**				
Exterior Skin	**P**				
Canoples and marquees	**P**				
Chimneys and stacks	**P**				
Stairs	**P**	S			

3.1 GROUND MOTIONS NSCs DAMAGING FEATURES

In order to emphasize the ground motions' features affecting the NSCs acceleration demand, here is studied the modal recombination of the response of a generic linear MDOF system (representing a generic building) having a linear SDOF system (representing a generic Non-Structural Component) attached to the structural node *k*. The weight of the SDOF is assumed to be negligible with respect to the weight of the MDOF, i.e. the dynamic interaction between the primary (MDOF) system and the secondary (SDOF) system is neglected.

By means of the Complete Quadratic Combination (CQC) rule (Wilson *et al.*, 1981) the max acceleration of the SDOF (i.e. Non-Structural Component) can be written (Igusa and Der Kiureghian, 1985) as:

$$\max\left(\ddot{u}_k\right) = \left(\sum_{i=1}^{N} \sum_{j=1}^{N} A_{ik} \cdot \rho_{ij} \cdot A_{jk} \cdot S_{pa}(f_i, \xi_i^*) \cdot S_{pa}(f_j, \xi_j^*) \right)^{1/2} \tag{3.1}$$

Where, ρ_{ij} represent the cross-correlation between modes *i* and *j* and where, being φ_{ik} the modal displacement of the structural node *k* and being Γ_i the modal participation factors, the coefficients A_{ik} stand:

$$A_{ik} = \alpha_i \cdot \varphi_{ik} \cdot \Gamma_i \tag{3.2}$$

The α_i are amplification factors accounting for the dynamic interaction of the secondary system with the supporting structure. These are expressed (Eq. 3.3) as function of the secondary system's fundamental frequency f_e and the supporting structure's natural frequencies f_i.

$$\alpha_i = \frac{f_e^2}{\left| f_e^2 - f_i^2 \right|} \tag{3.3}$$

S_{pa} is the spectral pseudo-acceleration at the frequency f_i and the damping ratio ξ^* (Eq. 3.4) is equal to the average of the supporting structure ξ_i and the secondary system ξ_e damping ratios.

$$\xi_i^* = \frac{\xi_e + \xi_i}{2} \tag{3.4}$$

Equation 3.1, besides showing excellent predictive capability of the floor response spectra (e.g. Figure 3.3), gives useful insight on the factors affecting NSCs response and how the

different structural modes contribute to it. From (Eq. 3.2), the contribution of each structural mode to the NSCs' response is equal to the contribution of that mode to the acceleration of the attachment node multiplied by an amplification factor that depends on the natural frequencies of the mode and the equipment. From (Eq. 3.3), if one of the modal frequencies f_i is very close to the NSC frequency then α_i is very large, indicating that the NSC endures an amplification of the motion of mode i. If f_i is much higher than the NSC frequency, α_i is smaller than the unity, which indicates that the NSC experiences a de-amplification of the motion of mode i. If f_i is much lower than the NSC frequency, α_i value is approximately one, which indicates that the NSC responds statically to the motion of mode i.

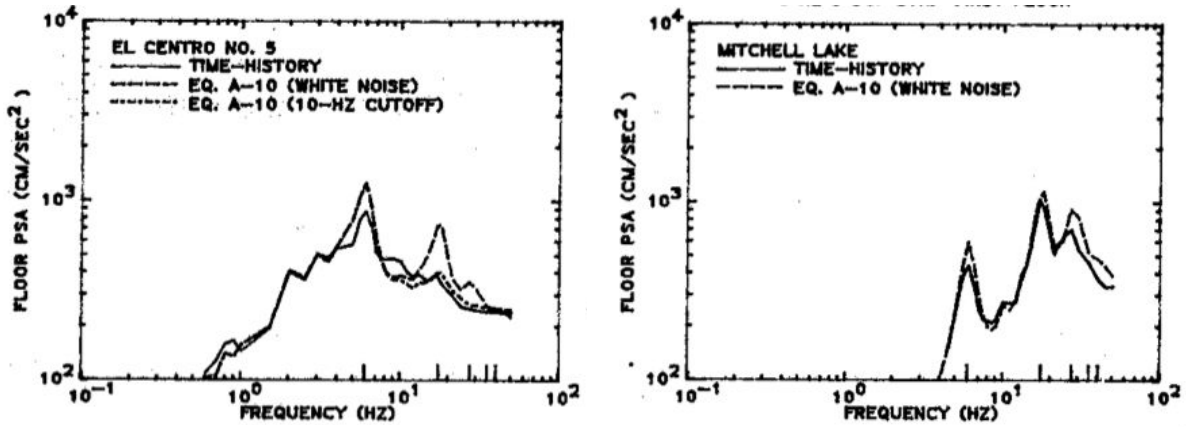

Figure 3.3 *Comparison of Floor Response Spectra obtained trough time history analyses and through Eq. 3.1. Reproduced from EPRI (1989).*

Thus, the presence of the factors α_i in (Eq. 3.2) highlights the importance of the higher order vibration modes and the impossibility to neglect them (at least "a priori") in the evaluation of NSCs acceleration demand.

Nevertheless, it must be considered that the participation factors Γ_i are usually negligible for higher (horizontal) vibration modes. Then in order to "weigh" the combined effect of the α_i and Γ_i, a factor λ_i is herein introduced as:

$$\lambda_i = \alpha_i \cdot \Gamma_i \tag{3.5}$$

The practical role of the factor λ_i is to discriminate, with respect to frequency, the ground motion spectral acceleration ordinates having (or not) influence on the Floor Response Spectra ordinates. In other words, when λ_i are negligible, their associated ground motion response spectra ordinates (i.e., $S_{pa}(f_i, \xi)$) can be neglected in the computation of (Eq. 3.1);

instead, the ground motion response spectra ordinates associated to large λ_i values should be considered, due to the large "weight" they have in the computation of (Eq. 3.1).

3.1.1 A new IM: the E-ASA$_R$

An attempt to identify an efficient IM for NSCs acceleration demand is done here. Based on the foregoing, it can appear intuitive to consider (as "significant") the ground motion spectral ordinates associate to the modal frequencies giving the highest λ_i values. Following this thought, a new IM could be defined (Eq. 3.6) under the simple form of a normalized summation of the n values of $S_{pa}(f_n, \xi)$ corresponding to the n highest λ_i values:

$$IM_{\lambda} = \frac{1}{n}\sum_{i=1}^{n} S_{pa}(f_i, \xi) \tag{3.6}$$

Nevertheless an IM stated as in equation 3.6 requires for its definition the computation of the λ_i values. These last necessitate, in order to be computed, the knowledge of n-natural frequencies and participation factors of the supporting structure other than the fundamental frequency(s) of the secondary system(s). Thus, even if hypothetically high efficient, the "IM_{λ}" could not be practically implemented in PSHA and then used in Seismic Probabilistic Risk Analysis.

For such a reason, following the same philosophy adopted in the study about Structural demand (chapter 2), here the purpose is to define an IM that is independent from the dynamic characteristics of the NSCs and in which the only required structural characteristic is the fundamental frequency of the supporting structure.

Having in mind this aim, the author highlights three points: a) generally the evolution with the frequency of the (horizontal) participation factors Γ_i is such that higher values of Γ_i appear at lower natural frequencies; b) the dynamic amplification factors α_i assume higher values in correspondence of the NSCs frequencies; c) generally the frequency content of earthquake ground motions is such that higher modes are less likely to be excited with respect to the lower ones. These facts suggest that for every structure it is possible to "roughly" identify a, here-called, "*dominant-frequencies interval*" that contains the factors λ_i (Eq. 3.5) with the highest (dominant) values.

Thus, the key-idea is to consider such a structure-relative's dominant-frequencies interval as the "core" of the IM. The dominant-frequencies interval can be "approximately" defined

knowing only the fundamental frequency value: the lower bound corresponds to the fundamental frequency of the structure and the upper bound could be evaluated as percentage of the fundamental frequency value.

In practice, this can be done taking the ASA_R (introduced in chapter 2, Eq. 2.1), and modifying it in order to consider the structure-relative's dominant-frequencies interval. In (Eq. 2.1), f_1 is the fundamental frequency of the structure, $X_f < 1$ is a factor accounting for the drop, due to damage, of the fundamental frequency f_1, S_{pa} is the spectral pseudo-acceleration and ξ is the structural damping value. The suffix R indicates the chosen percentage of drop of the fundamental frequency ($X_f = 1-(R/100)$).

In order to consider the dominant-frequencies interval instead of the frequency drop one (Figure 3.4), the formulation (Eq. 2.1) is kept identical but a modification is done by taking $X_f > 1$. Now X_f represents a factor accounting for the width of the dominant-frequencies range and the suffix R indicates the width of the dominant-frequencies range as percentage of the fundamental frequency ($X_f = 1+(R/100)$).

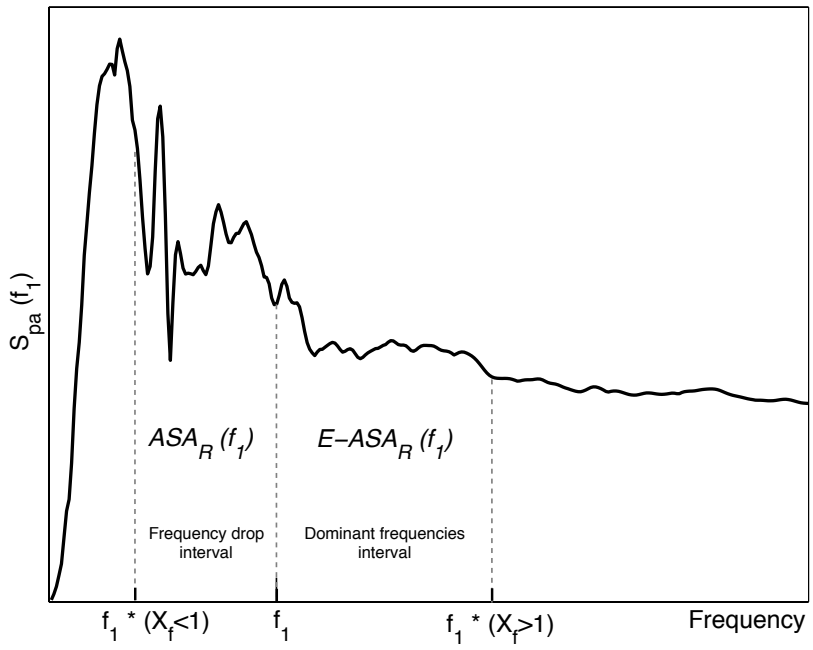

Figure 3.4 *ASA_R and E-ASA_R (f_1 is the structure's fundamental frequency)*

Therefore, the proposed IM (De Biasio *et al.*, 2014c), named *Equipment Relative Average-Spectral-Acceleration (E-ASA_R)*, is defined as the average spectral pseudo-acceleration over the dominant-frequencies interval of the structure:

$$E-ASA_R(f_1) = \frac{1}{f_1(X_f-1)} \int_{f_1}^{X_f \cdot f_1} S_{pa}(f,\xi)\,df \qquad with\ X_f > 1 \tag{3.8}$$

The formulation (Eq. 3.8) of $E\text{-}ASA_R$ captures the presence of significant spectral acceleration ordinates over the structure‘s dominant-frequencies interval. According to (Eq. 3.1), this is a key feature that a seismic signal must have in order to produce high Floor Response Spectra ordinates.

In (Eq. 3.8), the value of X_f depends on the dynamic characteristics of the structure that, in turn, depend on its design properties. A general and optimum X_f value issued from numerical sensibility analyses is suggested in the final part of the chapter.

It is important to note that, similar to ASA_R (paragraph 2.2.1), the formulation (Eq. 3.8) of the $E\text{-}ASA_R$ is exclusively based on spectral pseudo-acceleration values, which means it allows (Bazzurro and Cornell, 2002; Stewart *et al*., 2002; Baker and Cornell, 2006b; Inoue and Cornell, 1990) performing PSHA with respect to $E\text{-}ASA_R$ by means of widespread ground motion prediction models available for $S_{pa}(f_1)$.

3.2 COMPARATIVE ANALYSES

In order to compare the performance of the IMs with respect to NSCs acceleration demand prediction, numerical analyses are performed on three test case structures. The same approach adopted in the part of the study relative to structural demand (i.e., chapter 2) has been herein used to select the test-case structures. Then, among these two have been experimentally tested: this set-up offers the advantage of a validation tool for the numerical models, which under the condition of sufficiently close agreement between numerical simulation runs and experimental testing, lends credibility to the results derived from numerical models. Also, the chosen test cases have different design characteristics and therefore different dynamic properties: two are stiff, high frequency, structural-wall structure, the SMART (CEA, 2013) mock-up and the, here called, TC3 (i.e. Test-Case n^{o}3) building; the third one is the ductile, low frequency, frame structure described in paragraph 2.3.3 (i.e., EC8-FRAME). The choice of the SMART and the EC8-FRAME allows to evaluate the robustness of the IMs. The TC3 instead permits to investigate the performance of the IMs with respect to a test case characterized by a very complex (and uncommon) dynamic behaviour (multiple-coupled natural modes), i.e. a kind of “worst-situation” test case.

It is important to note that in this part of the study (i.e. IMs for NSCs acceleration demand), *linear-elastic modelling* of the test-case structures has been adopted. Indeed, being in this chapter the interest focused on the response of Non-Structural Components to low-to-

moderate earthquakes, it is assumed that such earthquakes are not able to significantly damage a well-engineered reinforced concrete structure. Additionally, this choice allows to use (for the resolution of the FE dynamic problem) the time-efficient *modal superposition analysis* technique (Chopra, 2007) at the place of the (much) more computational demanding time-history analysis, which has been adopted in Chapter 2.

3.2.1 Test case structure: SMART2013

3.2.1.1 Structure presentation

SMART (Fig. 3.5a) is a ¼ scaled model, designed in accordance with the current French nuclear regulation, tested in 2013 on the shaking table of the French Atomic Energy Agency (i.e., CEA) and also object of an international blind contest. The mock-up is a trapezoidal, three-story, reinforced concrete structure representative of a typical simplified half part of an electrical nuclear building. The mock-up is designed and tested following precise similitude criteria that allow doing its behavior representative of a full-scale structure (Table 2.6).

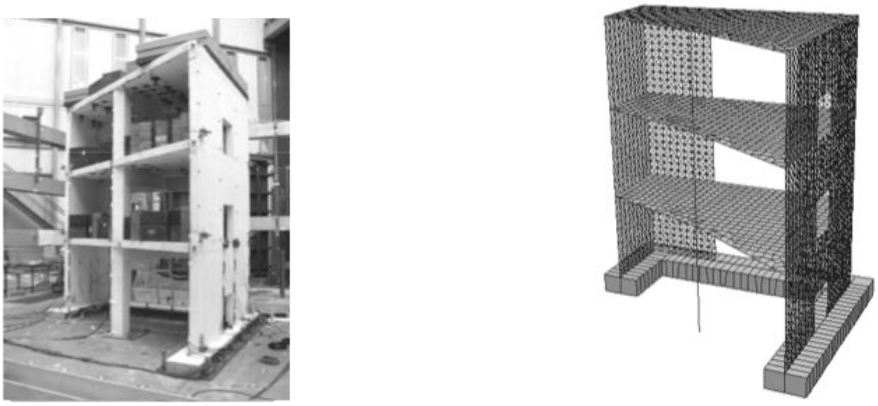

a) b)

Figure 3.5 *SMART2013 test case: a) structure; b) numerical model*

3.2.1.2 Numerical model & Equivalent Reinforced Concrete modeling

In the Finite Element SMART numerical model (Fig. 3.5b), both columns and beams have been modeled by means of Timoshenko beam elements whilst the slabs have been represented through shell elements. Instead, for the modeling of the structural walls, a lattice modelling technique derived from the Equivalent Reinforced Concrete (ERC) approach of Kotronis *et al*. (2003) has been used.

The ERC modeling method uses lattice meshes to predict the linear and non-linear behavior of shear RC walls, and is based on the framework method proposed by Hrennikoff (1941). The basic idea of the framework method consists in replacing the continuum material of the elastic body under investigation by a framework of bars arranged according to a definite pattern (Fig. 3.6), whose elements have suitable elastic properties. Set up for linear elastic behavior, the criterion of suitability is associated, at a given deformation, to energy equivalence between the framework pattern and the continuum material. If the unit size of the pattern of such a framework is made infinitesimal, then the latter will be representative of a complete mechanical model of the solid prototype, with identical displacements, strains and unit stresses.

The main interest of the ERC model is that, being based on uniaxial behavior, it makes the application to inelastic calculation easy and robust. This is not always the case for 2D or 3D damage or smeared crack approaches, particularly under severe shear where localization phenomena can compromise the robustness. Despite the fact that linear elastic modeling is herein considered, parallel research work involving the author in the SMART 2013 international benchmark (CEA, 2013) has encouraged the use/development of the ERC modeling technique also in the present study.

With respect to a linear-elastic modeling (i.e., the one herein adopted), the ERC model works under the following assumptions (Kotronis *et al*., 2003):

- An elementary volume of reinforced concrete can be separated into a concrete element and a horizontal and a vertical reinforcement bars (S_H and S_V, respectively). Concrete and steel are then modeled separately by using two different lattices (Fig. 3.6).
- The sections (A_h, A_v, and A_d) of the bars simulating concrete can be derived directly from the framework method (Fig. 3.7).
- A lattice composed of horizontal and vertical bars simulates steel (Fig. 3.6). The section and position of the bars coincide with the actual section and position of the reinforcement. To simplify the mesh, a method of distribution can be used where the bar sections are proportionally increased in order to obtain in a given zone the same global surface area of reinforcement. The mesh is thus independent of the geometry of the specimen.
- Perfect bonding is assumed between concrete and steel.

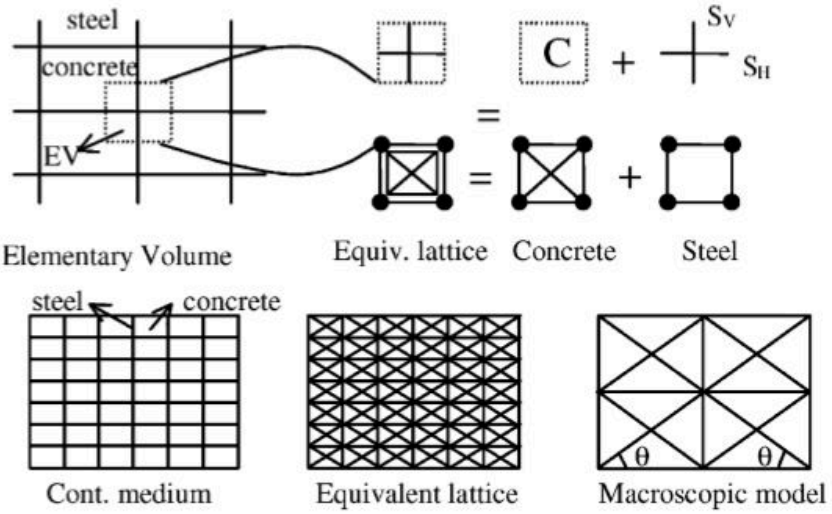

Figure 3.6 *Equivalent Reinforced Concrete modeling. Reproduced from Kotronis et al. (2003)*

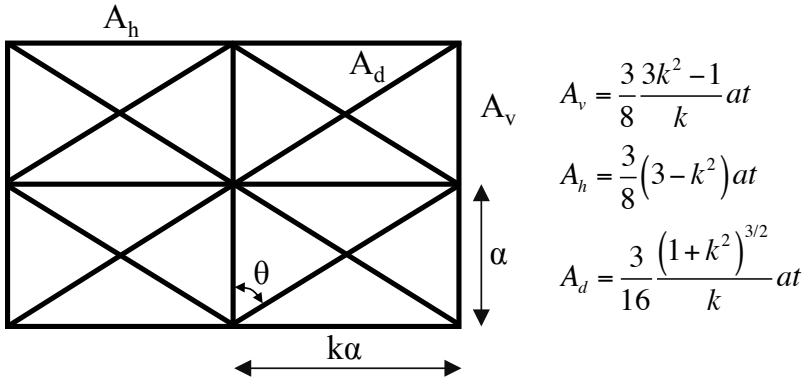

Figure 3.7 *Equivalent Reinforced Concrete modeling, "concrete" bars: k is the ratio of the "squares' sides" (k=1.192 has been used in this study, i.e. θ = 40°); t is the wall thickness; A_h, A_v, and A_d are, respectively, the cross section area of the horizontal, vertical and diagonal "concrete" bars.*

Nevertheless, a problem arises with the practical use of the ERC method: being exclusively based on bar elements arranged in a plane, the ERC is strictly a two-dimensional modeling technique. Therefore, in order to be suitable for the modeling of the three-dimensional SMART structure, the ERC modeling necessitates to be enriched with out-of plane stiffness. This is herein achieved by superposing to the pattern of bars (horizontal and vertical only) an additional "layer" constituted, this time, by beam elements. These have the elastic properties of concrete (Young modulus and Poisson ratio, appendix A4) and zero cross sectional area (i.e. no axial stiffness). The torsion constant (J_t) and the moments of inertia (J_{xx}, J_{yy}) are tuned against an equivalent-mesh-size shell-elements model representing an elementary section of wall, which dimensions have been arbitrarily chosen (Fig. 3.8).

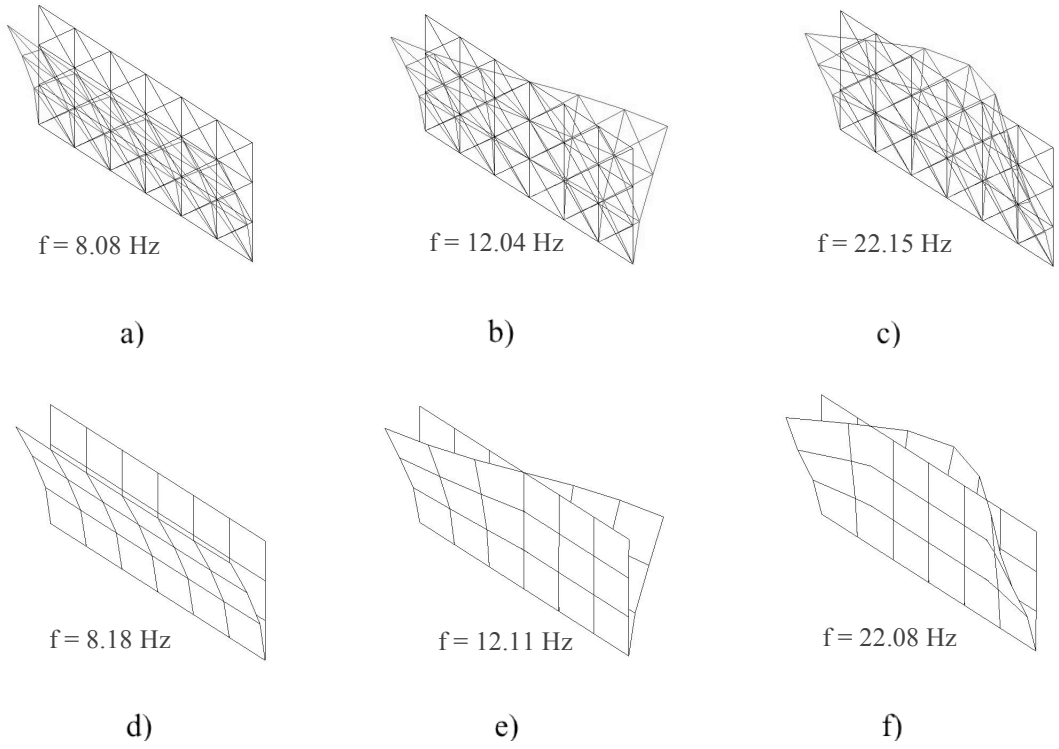

Figure 3.8 *Tuning of the out-of-plane stiffness in the Enriched-ERC modeling. The Enriched-ERC model (a, b, c) has same dimensions, mass and mesh-size of the shell model (d, e, f). The moments of inertia (J_{xx} and J_{yy}) and the torsion constant (J_T) of the added beam-layer are tuned in order to reproduce (a, b, c) the first three modal frequencies & shapes of the "reference" shell model (d, e, f).*

Finally, the masses are distributed on the elements (beams, column, slabs and walls) and modal numerical damping is introduced in the model with a value of 2 % on the first twenty natural frequencies (i.e. herein used in the modal superposition analysis technique).

3.2.1.3 Model validation

The predictive capabilities of the SMART numerical model have been checked with the results stemming from the "elastic part" of the experimental campaign of the structure, which has been performed with respect to a white noise signal (shaking-table test1) and an artificial low-intensity signal (shaking-table test2, Figure 3.9), in terms of Floor Response Spectra.

Being the available experimental data referred to the mock-up placed on the shaking-table (CEA, 2013), the numerical modeling of this device has been necessary in order to correctly compare numerical and experimental results. Due to the differences in the loadings (2D for SMART, 1D for CAMUS1) and in the mock-ups geometry (SMART is asymmetric, CAMUS1 is symmetric), the shaking-table model adopted in paragraph 2.3.3.1 for the CAMUS1 structure (which has been tested on the same shaking-table) is not adequate for the

simulation of the SMART structure. Consequently, the full 3D FE model of the shaking table (provided by CEA, 2013) has been herein used (Figure 3.10).

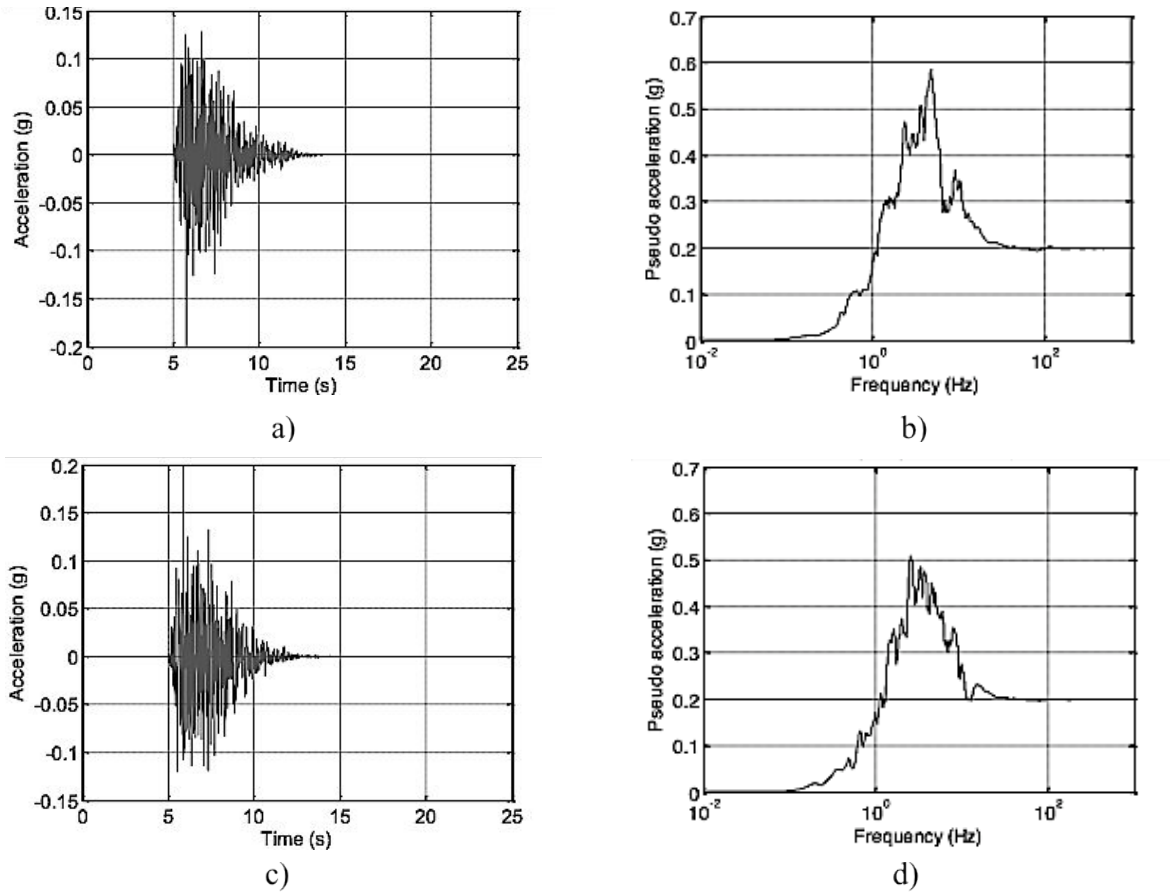

Figure 3.9 *Shaking table test2, input signal: a) x-direction time-history; b) x-direction Response spectrum (5% damping); c) y-direction time-history; d) y-direction Response spectrum (5% damping). Reproduced from CEA (2013).*

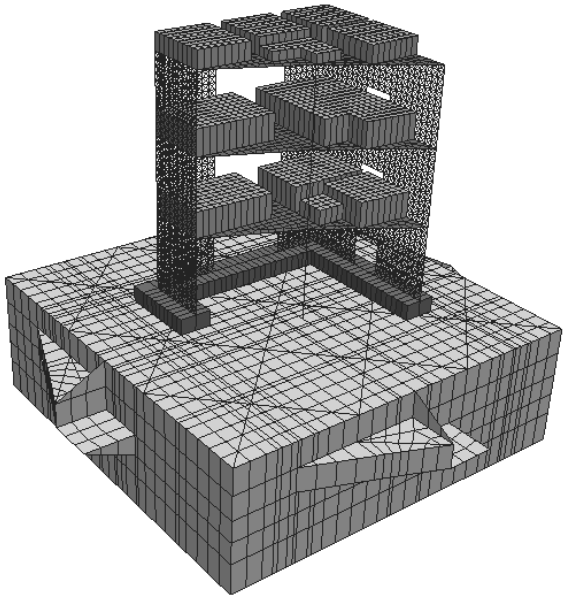

Figure 3.10 *SMART, numerical model with shaking table.*

Note that the validation of the SMART numerical model has been performed with respect to the ¼ scaled mock-up. Nevertheless, once created and validated, the SMART numerical model has been rescaled to full-scale (Table 2.5) in order to avoid having to scale the entire ground motion dataset. The dynamic characteristics of the full-scale numerical model are reported in Table 3.3.

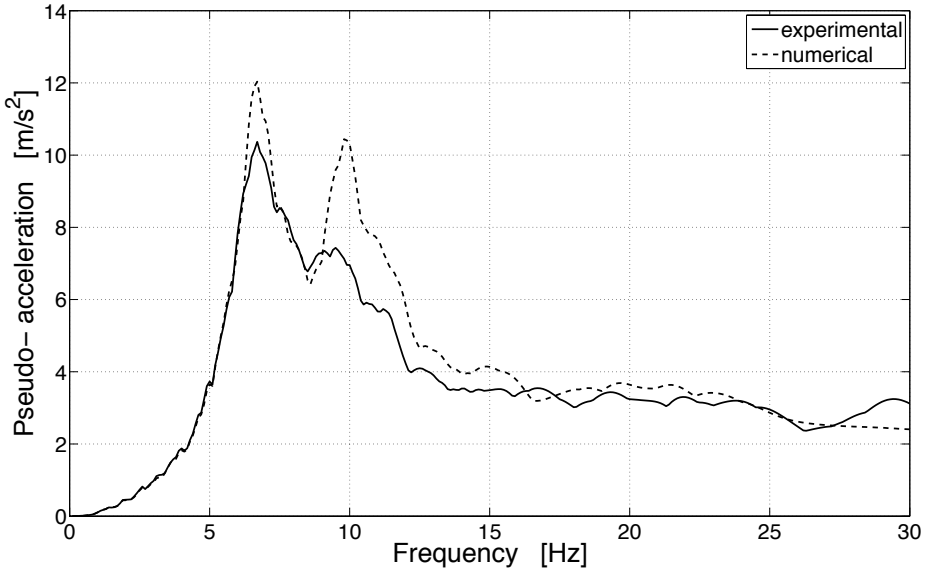

a)

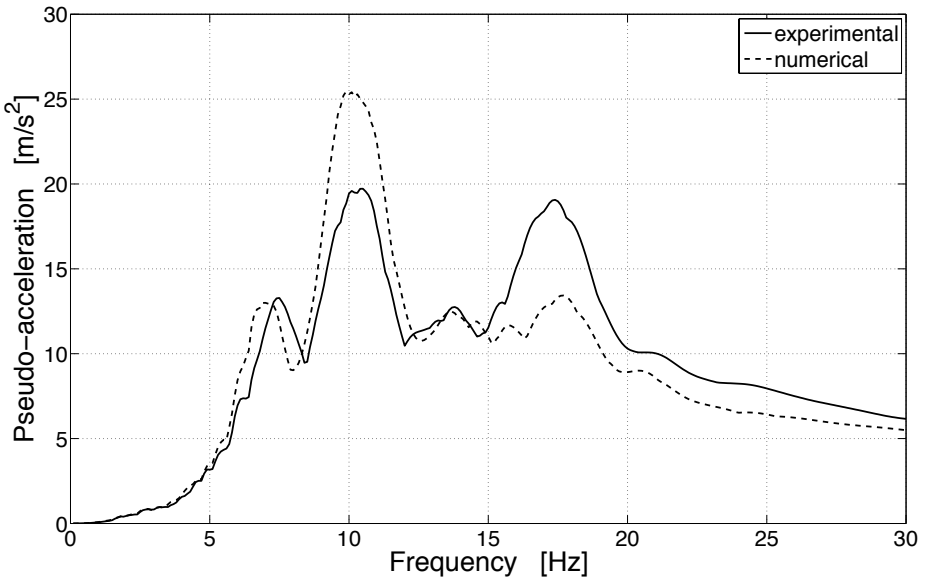

b)

Figure 3.11 *SMART-2013 numerical model validation, shaking table test1: a) FRS (5 % damping) at the roof along the X- direction ; b) FRS (5 % damping) at the roof along the Y-direction.*

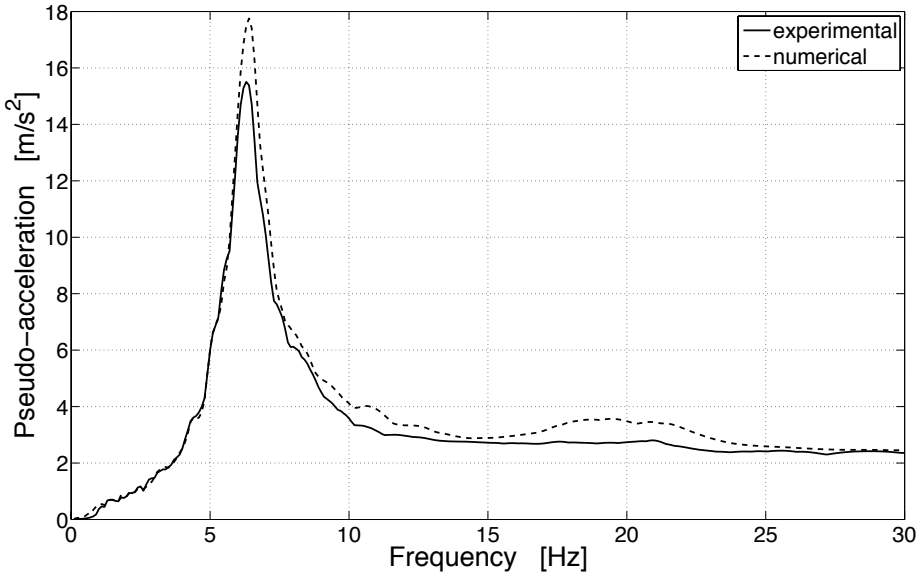

a)

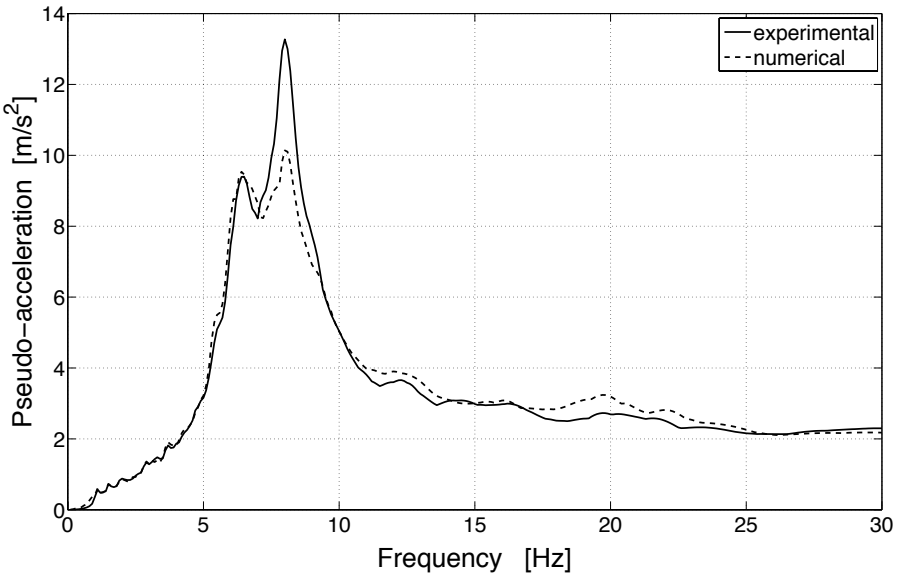

b)

Figure 3.12 *SMART-2013 numerical model validation, shaking table test2: a) FRS (5 % damping) at the roof along the X- direction; b) FRS (5 % damping) at the roof along the Y-direction.*

Finally, the comparison of numerical and experimental results has shown the ability of the numerical model to predict with good agreement the structure's linear behaviour qualitatively and quantitatively (Figures 3.11-3.12).

3.2.2 Test case structure: TC3

3.2.2.1 Structure presentation

The TC3 (Fig. 3.13a) is an existing thirteen-story, European, RC industrial building characterized by strongly irregular plan/slabs distributions. The specific feature of this stiff structural wall building is its particular design, which makes its dynamic behavior particularly complex and unusual. This offers the possibility to test the IMs with respect to a "worst situation" case.

a) b)

Figure 3.13 *TC3 test case: a) structure; b) numerical model*

3.2.2.2 Numerical model & torsional-stick modeling

The TC3 building has been modeled by means of a stick model able to take into account the torsional characteristics of the structure. In this model the slabs are assumed rigid and the walls give in-plane and out-of-plane stiffness contribution to the equivalent beams, the axes of which pass through the gravity centres of the stories. The masses of the slabs are represented by lumped masses and inertia (highlighted in Fig. 3.13b) located at the slabs' gravity centres, whilst the masses of the half-stories at each side of every slab are reduced to the mean-layers of these.

The characteristics of the equivalent beams are therefore computed starting from the plans of the building (example in Figure 3.14) in considering the building cross-section as a beam. Consequently for each story, the cross-section area (A), the gravity centre (G), the moments of inertia (J_{xx} and J_{yy}), the shear coefficients (k_x and k_y) and the torsion constant (J_T) are

computed and assigned to the corresponding equivalent beam, the length of which equals the height of the story.

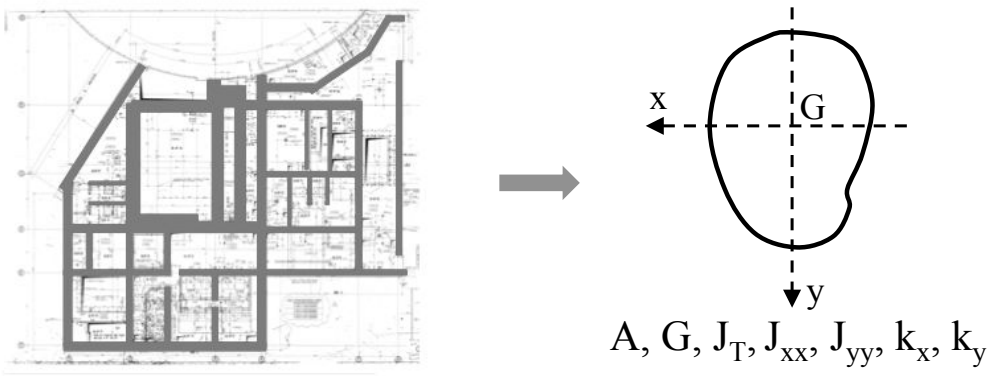

Figure 3.14 *TC3 test case, from the stories to the equivalent beams*

The adequacy of the performance associated to the stick-torsional modeling technique have been shown by Ravet (2009) on the basis of several test cases and with respect to the modeling of the linear structural behavior of complex multi-story buildings.

Regarding the material characteristics, they have been assigned as recommended by the building owner (i.e., Young modulus=33 GPa, Poisson modulus=0.2). Then, the dynamic characteristics of the numerical model are reported in Table 3.4.

Lastly, modal numerical damping has been introduced in the model with a value of 2 % on the first twenty natural frequencies (i.e. herein used in the modal superposition analysis technique).

Finally, the reader must note that the unavailability of experimental data about the dynamic behavior of the TC3 building precludes performing the validation of the numerical model, as instead it has been done for the others test case buildings.

Table 3.2 *EC8-FRAME: dynamic characteristics (the modes higher than the 10th are not reported cause they all give values of λ_i approaching zero).*

Mode	Frequency [Hz]	Γ_x	Γ_y	α_i				$\lambda_i = \alpha_i * (\Gamma_x + \Gamma_y)$			
				1hz	5hz	10hz	20hz	1hz	5hz	10hz	20hz
1	**1.57**	1.21	0.00	0.68	1.11	1.03	1.01	**0.82**	**1.34**	**1.24**	**1.21**
2	**1.59**	0.00	1.31	0.65	1.11	1.03	1.01	**0.85**	**1.45**	**1.34**	**1.31**
3	2.07	0.00	0.12	0.30	1.21	1.04	1.01	0.04	0.14	0.12	0.12
4	**5.47**	0.28	0.00	0.03	5.08	1.43	1.08	0.01	**1.44**	**0.40**	**0.31**
5	**5.53**	0.00	0.30	0.03	4.48	1.44	1.08	0.01	**1.35**	**0.43**	**0.33**
6	7.16	0.00	0.03	0.02	0.95	2.05	1.15	0.00	0.03	0.06	0.03
7	10.75	0.11	0.00	0.01	0.28	6.43	1.41	0.00	0.03	**0.70**	0.15
8	10.87	0.00	0.12	0.01	0.27	5.51	1.42	0.00	0.03	**0.64**	0.16
9	12.68	0.03	0.00	0.01	0.18	1.65	1.67	0.00	0.01	0.05	0.05
10	13.81	0.00	0.01	0.01	0.15	1.10	1.91	0.00	0.00	0.01	0.02

Table 3.3 *SMART (full-scale): dynamic characteristics.*

Mode	Frequency [Hz]	Γ_x	Γ_y	α_i				$\lambda_i = \alpha_i * (\Gamma_x + \Gamma_y)$			
				1hz	5hz	10hz	20hz	1hz	5hz	10hz	20hz
1	**5.35**	1.69	0.62	0.04	6.90	1.40	1.08	**0.08**	**15.97**	**3.24**	**2.49**
2	**9.54**	0.81	1.40	0.01	0.38	11.13	1.29	0.02	0.84	**24.60**	**2.86**
3	**16.76**	0.57	0.76	0.00	0.10	0.55	3.36	0.00	0.13	0.73	**4.46**
4	**19.74**	0.68	0.22	0.00	0.07	0.35	38.71	0.00	0.06	0.31	**34.73**
5	22.87	0.03	0.12	0.00	0.05	0.24	3.25	0.00	0.01	0.04	0.49
6	28.02	0.37	0.14	0.00	0.03	0.15	1.04	0.00	0.02	0.08	0.54
7	28.55	0.19	0.08	0.00	0.03	0.14	0.96	0.00	0.01	0.04	0.26
8	28.93	0.30	0.72	0.00	0.03	0.14	0.92	0.00	0.03	0.14	0.93
9	29.66	0.49	0.77	0.00	0.03	0.13	0.83	0.00	0.04	0.16	1.05
10	30.59	0.31	0.25	0.00	0.03	0.12	0.75	0.00	0.02	0.07	0.42

Table 3.4 *TC3: dynamic characteristics.*

Mode	Frequency [Hz]	Γ_x	Γ_y	α_i				$\lambda_i = \alpha_i * (\Gamma_x + \Gamma_y)$			
				1hz	5hz	10hz	20hz	1hz	5hz	10hz	20hz
1	**6.42**	1.80	0.11	0.02	1.54	1.70	1.11	**0.05**	**2.94**	**3.25**	**2.13**
2	**8.03**	0.12	1.90	0.02	0.63	2.82	1.19	**0.03**	**1.28**	**5.69**	**2.41**
3	**10.78**	0.08	0.11	0.01	0.27	6.17	1.41	0.00	0.05	**1.17**	0.27
4	**15.87**	1.30	0.09	0.00	0.11	0.66	2.70	0.01	0.15	**0.91**	**3.74**
5	**17.56**	0.08	0.89	0.00	0.09	0.48	4.36	0.00	0.09	0.47	**4.24**
6	**18.09**	0.06	0.66	0.00	0.08	0.44	5.50	0.00	0.06	0.32	**3.94**
7	24.96	0.05	0.24	0.00	0.04	0.19	1.79	0.00	0.01	0.06	0.52
8	26.93	0.55	0.04	0.00	0.04	0.16	1.23	0.00	0.02	0.09	0.73
9	32.53	0.19	0.48	0.00	0.02	0.10	0.61	0.00	0.02	0.07	0.41
10	33.79	0.63	0.30	0.00	0.02	0.10	0.54	0.00	0.02	0.09	0.50

3.2.1 Selected Engineering Demand Parameters

In order to define the EDPs used in this part of the study, it is useful to introduce the two basic approaches that currently exist for the seismic design and analysis of acceleration sensitive Non-Structural Components. These methods are the "conventional" Floor Response Spectrum (FRS) approach, and the combined Primary-Secondary system approach. The latter consists in the full modeling of both the supporting structure and the NSCs, and consequently in the "coupled" analysis of them. Although it is the most comprehensive, the engineering use of this method is limited to very few particular applications.

Differently, in the (nowadays conventional) method of Floor Response Spectra the response of the primary and secondary systems are decoupled and analyzed separately. Indeed, the response behavior of the primary structural system at the support points of a secondary system is determined while neglecting the effect of the secondary system. To obtain the Floor Response Spectra, horizontal and vertical time histories at support points of a secondary system are first calculated based upon time domain analysis of the primary system. Then, these time histories are used to generate the required floor response spectrum for secondary system response analysis (Figure 3.15).

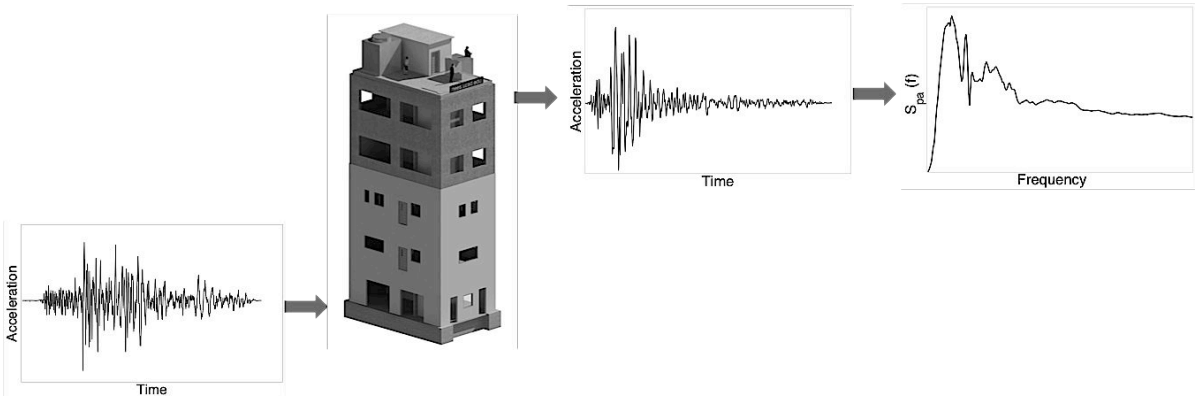

Figure 3.15 *Floor Response Spectra (FRS) approach.*

However, while the method of Floor Response Spectra provides a relatively simple procedure for response calculations of secondary systems, the use of this approach leads to a number of deficiencies. The most serious is the fact that it ignores the interaction between primary and secondary systems. This phenomenon become significant when the masses of the secondary systems become more than negligible or when the frequencies of the two systems are tuned to each other. Therefore the Floor Response Spectrum method gives acceptable results for secondary systems with relatively small masses and with frequencies

which are not tuned to a frequency of the primary structural system (Taghavi and Miranda, 2008).

A design criterion is currently employed in engineering practice in deciding whether the decoupled or the coupled approach is required, i.e. to judge on the significance of dynamic interaction between primary and secondary systems (Chen and Soong, 1988). The secondary system vs. primary system mass ratio μ and frequency ratio η, may be defined respectively as:

$$\mu = M_s / M_p \tag{3.9}$$

$$\eta = \omega_s / \omega_p \tag{3.10}$$

where M_s is the total mass of the secondary system and M_p is the total modal mass of the primary structure associated with the dominant frequencies, and where ω_s is the fundamental frequency of the secondary system and ω_p is the dominant frequency(ies) of the primary structure.

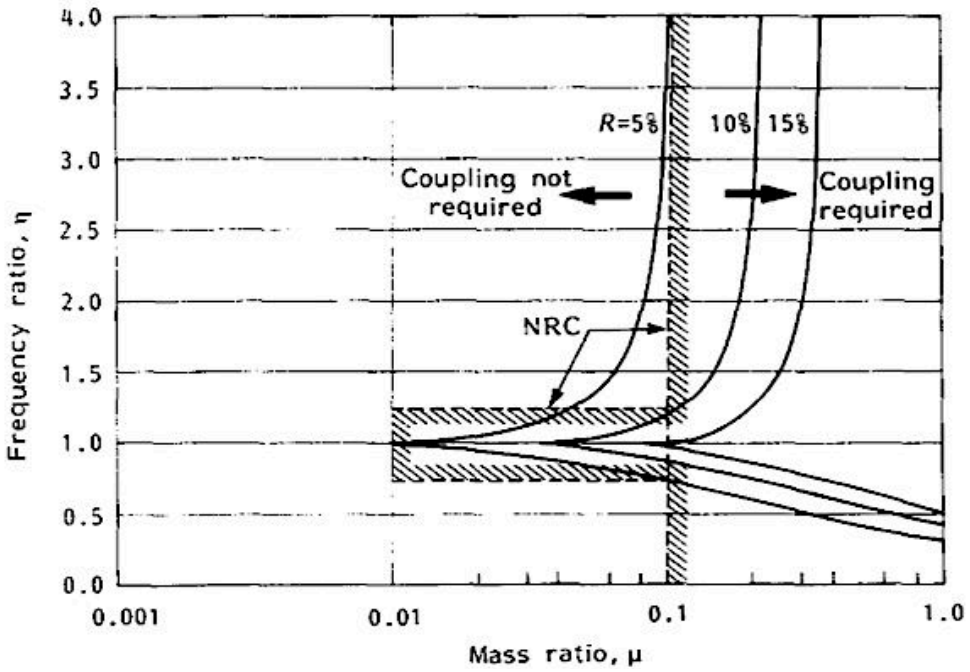

Figure 3.16 *Frequency error region. Reproduced from Cheen and Soong, 1988.*

A greater primary-secondary system interaction is expected as μ increases and as η approaches one. Thus, regions of validity of decoupled and coupled analysis can be determined according to the values of μ and η. A typical base for a design rule is indicated in Figure 3.16, which results from a two-degree-of-freedom system analysis, i.e. a single-degree-of-freedom secondary system mounted on a single-degree-of-freedom primary

structure. In Figure 3.16, being ω_c the natural frequency of the combined system, R is defined as:

$$R = \left|\omega_c - \omega_p\right| / \omega_p \tag{3.11}$$

Finally, the use of the FRS method (i.e. to uncouple the response of the supporting structure from that of the non-structural component) is acceptable for NSCs whose mass is less than 1% of that of the structure supporting them (Singh and Ang, 1974; USNRC, 1978; Taghavi and Miranda, 2008).

Then, coming back to the choice of the EDPs, the (horizontal) NSCs acceleration demand has been measured in the numerical models as the maximum of the 5% damped acceleration Floor Response Spectra over all the floors and over four frequency ranges: 0.9 to 1.1 Hz, 4.5 to 5.5 Hz, 9 to 11 Hz and 18 to 22 Hz. These frequency ranges reflect the hypothetical presence of NSCs with fundamental frequency standing respectively 1 Hz, 5 Hz, 10 Hz, and 20 Hz, with an interval of confidence of ± 10 % on these values (e.g. Figure 3.17).

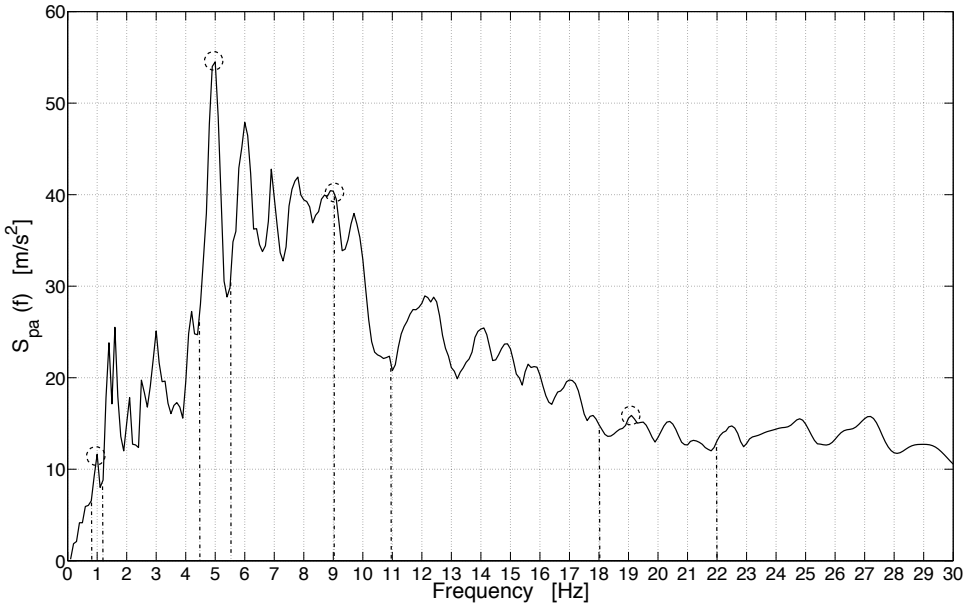

Figure 3.17 *EDPs for NSCs acceleration demand.*

Lastly, it is important to remind that this study considers linear-supported Non-Structural Components hosted on linear behaving buildings. For details about the effectiveness of the FRS with respect to the characterization of equipment with linear/non-linear behaving supports installed in linear/non-linear behaving structures, the reader can refer to more specific documents (e.g., Sewell, 1989; EPRI, 1989).

3.2.2 Results

3.2.2.1 IMs efficiency comparison

The results of the comparative statistical analysis about the IMs' efficiency are presented (Table 3.5) with respect to the 2,045 records composing the four ground-motion bins (i.e., paragraph 1.4.2). These results do not show significant discrepancies with the results obtained with respect to the four ground-motions bins taken one-by-one, which consequently are not reported.

For the comparison with the other IMs, the $E\text{-}ASA_R$ has been computed with an R value of 67 % (i.e., $E\text{-}ASA_{67}$). The choice of an optimum R value is addressed in the final part of the chapter. The IM_λ has been computed (distinctly for each EDP vs. test-case couple) considering the structural vibration modes highlighted in bold in Tables 3.2-3.4.

Table 3.5 *Efficiency analysis on all the 2,045 ground motions: Logarithmic Standard deviation (β) of the residuals.*

Max FRS at:	IMs												
	Frequency Response Based								*Peak Based*		*Duration Based*		
	IM_λ	***$E\text{-}ASA_{67}$***	*ASA_{40}*	***S_{pa}***	*S**	*I_{NP}*	*ASI*	*EPA*	***PGA***	*PGV*	*I_A*	*CAV*	*SCAV*
EC8 FRAME (f_1 = 1.57 Hz)													
1Hz±10%	**0.27**	**0.49**	0.25	**0.25**	0.33	0.24	0.87	0.51	**1.01**	0.59	0.74	0.66	1.24
5Hz±10%	**0.25**	**0.59**	0.77	**0.73**	0.79	0.71	0.27	0.53	**0.35**	0.56	0.42	0.67	0.77
10Hz±10%	**0.19**	**0.58**	0.74	**0.69**	0.76	0.67	0.3	0.49	**0.22**	0.5	0.34	0.65	0.76
20Hz±10%	**0.29**	**0.51**	0.67	**0.62**	0.69	0.6	0.31	0.43	**0.28**	0.44	0.3	0.59	0.77
SMART (f_1 = 5.35 Hz)													
1Hz±10%	**0.29**	**0.37**	0.34	**0.26**	0.36	0.25	0.35	0.61	**0.32**	0.62	0.46	0.75	0.81
5Hz±10%	**0.42**	**0.46**	0.53	**0.42**	0.59	0.45	0.61	0.87	**0.61**	0.89	0.75	0.97	0.94
10Hz±10%	**0.56**	**0.51**	0.81	**0.69**	0.88	0.73	0.85	1.14	**0.75**	1.14	0.99	1.22	1.06
20Hz±10%	**0.46**	**0.42**	0.72	**0.58**	0.79	0.62	0.77	1.07	**0.65**	1.07	0.91	1.16	1.00
TC3 (f_1 = 6.42 Hz)													
1Hz±10%	**0.22**	**0.28**	0.44	**0.35**	0.46	0.35	0.41	0.67	**0.3**	0.67	0.51	0.8	0.77
5Hz±10%	**0.35**	**0.35**	0.6	**0.46**	0.67	0.5	0.66	0.97	**0.6**	0.98	0.82	1.06	0.94
10Hz±10%	**0.48**	**0.39**	0.79	**0.67**	0.85	0.71	0.83	1.12	**0.73**	1.12	0.97	1.20	1.04
20Hz±10%	**0.55**	**0.49**	0.82	**0.72**	0.88	0.75	0.85	1.10	**0.73**	1.10	0.96	1.19	0.97

In considering Table 3.5:

In agreement with the literature, the present study finds a noticeable efficiency of the *PGA* in the case of the tested frame structure (Fig. 3.19a). It is the opinion of the author that such efficiency originates from the observed (Fig. 3.18a) strong correlation between the *PGA* and the spectral acceleration ordinates in the range 2-10 Hz. Indeed such frequency interval roughly coincides with the *dominant-frequency interval* of the EC8 FRAME (Table 3.2). Evidently the *PGA* is not well correlated (Fig. 3.18b) with the $S_{pa}(f_1)$ which exhibits the highest efficiency for NSCs frequency lower than the structure fundamental frequency. The same argument can be used to explain the efficiency of the *PGA* with respect to low frequency FRS ordinates in the case of the SMART and TC3 test cases.

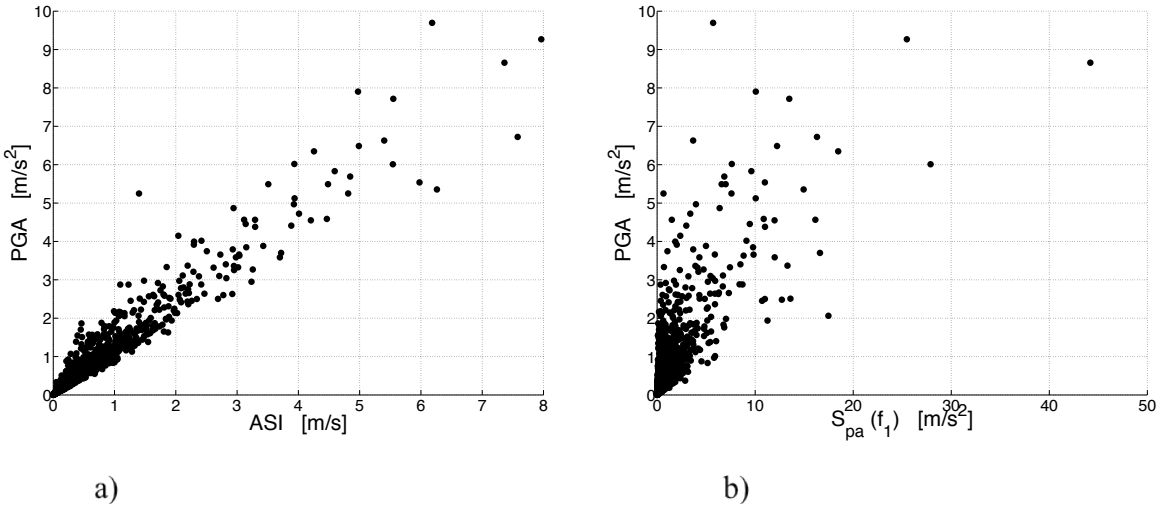

Figure 3.18 *Scatter plots, all (2,045) records: (a) PGA vs. ASI (i.e. spectral acceleration between 2 and 10 Hz); (b) PGA vs. $S_{pa}(f_1)$ (computed at the fundamental frequency of the EC8-FRAME).*

The *PGV*'s efficiency is sensibly lower than the *PGA*'s; among the duration based IMs, the I_A shows the best performance. Nevertheless, the efficiency of this class of IMs, which has been found slightly higher in the case of the EC8-FRAME structure, is generally lower than the one of the frequency-response and peak based ones. Such result was predictable in considering equation 3.1 and the linear-elastic "nature" of the performed analyses.

The IMs based on the spectral acceleration at the fundamental frequency of the structure $S_{pa}(f_1)$ exhibit high efficiency in predicting FRS ordinates at frequency lower than the fundamental one. Indeed in such situation, based on equation 3.1, the equipment de-amplifies all the motions of the structure being the first-mode motion the least de-amplified and therefore the one leading the equipment response (i.e. higher λ_i values).

For equipment frequencies higher than the structure fundamental frequency, the efficiency of the $S_{pa}(f_1)$ is lower than the *PGA*'s for the EC8-FRAME, but it is higher to this last for the other two (structural wall) test-case buildings (Fig. 3.19a-3.20a-3.21a). Still, this result can be explained by considering the non-negligible values of λ_i for the modes 4-5 and 7-8 in the case of EC8-FRAME (Table 3.2). The contribution of these modes is not captured by the $S_{pa}(f_1)$-based IMs, but instead is done by the *ASI*, *EPA* and *PGA* that consequently have high efficiency in the frame-building test case.

In the case of S^* and I_{NP}, to couple to the $S_{pa}(T_1)$ a factor accounting for the spectral shape in the period lengthening zone reveals to slightly decrease the performances of $S_{pa}(T_1)$ considered alone. Similarly, the ASA_{40}, which considers spectral acceleration ordinates along the structure frequency drop interval, shows minor performance with respect to the $S_{pa}(f_1)$. Nevertheless for both the structural-wall buildings tested, the ASA_{40} and the I_{NP} have efficiency comparable to the *PGA*'s.

The observation of the standard deviation values of the *EPA* and *ASI* reveals the effect of the width of the dominant-frequency interval: the *ASI* is computed on the range 2 to 10 Hz and the *EPA* is computed on the range 0.4 to 10 Hz. From Table 3.5, in the case of the EC8-FRAME the *ASI* has higher efficiency with respect to the *EPA* being its interval of integration smaller and more centered around the dominant-frequencies interval of the structure. The same argumentation can be used with respect to the results relative to the SMART and the TC3 test cases.

As hypothesized, the IM_λ possesses high efficiency in all the test cases and with respect to all the selected FRS frequency values (EDPs).

Finally, the herein introduced $E\text{-}ASA_{67}$ with respect to the *PGA* is less efficient in the case of the frame structure. This is essentially due to the chosen (low) value of *R*, not able to cover the frequencies related to the modes 4-5 and 7-8 (Table 3.2), which are associated with high λ_i values. Nevertheless the $E\text{-}ASA_{67}$ is very efficient in the cases of structural wall buildings where its efficiency is up to 52% higher than the one of *PGA* (Figure 3.20c-3.21c).

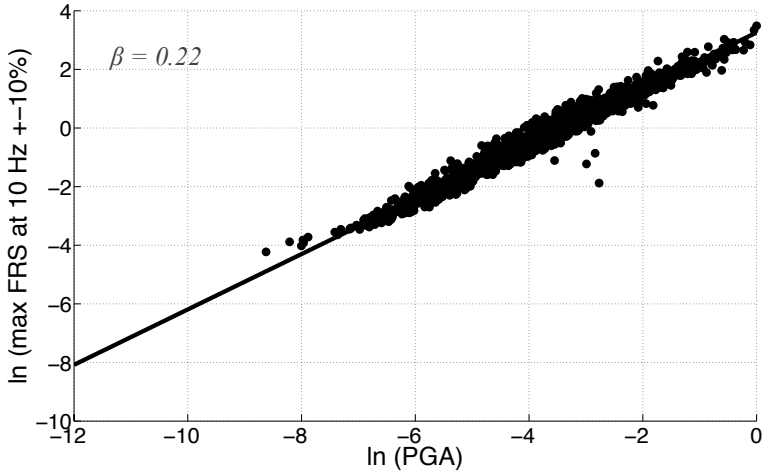

a)

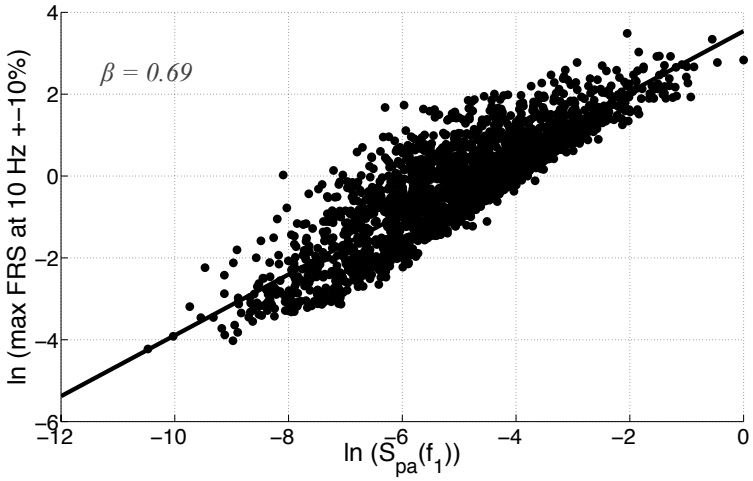

b)

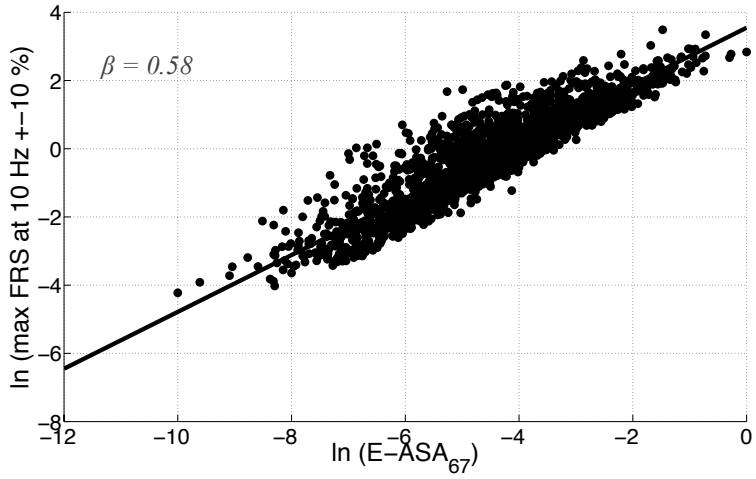

c)

Figure 3.19 *Regression plots, IMs vs. Max FRS in the range 10Hz±10% for EC8-FRAME: (a) PGA b) $S_{pa}(f_1)$; (c) E-ASA_{67}.*

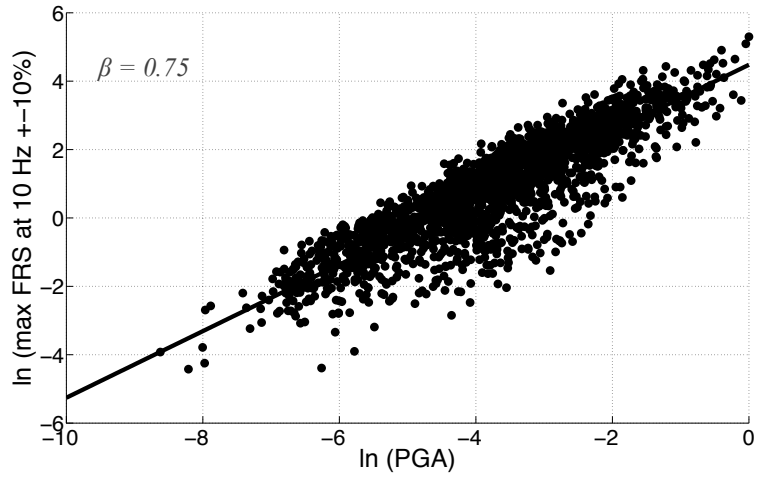

a)

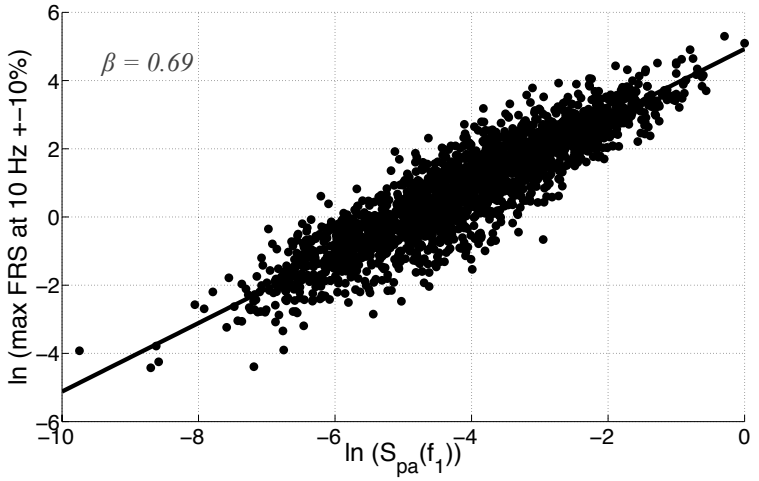

b)

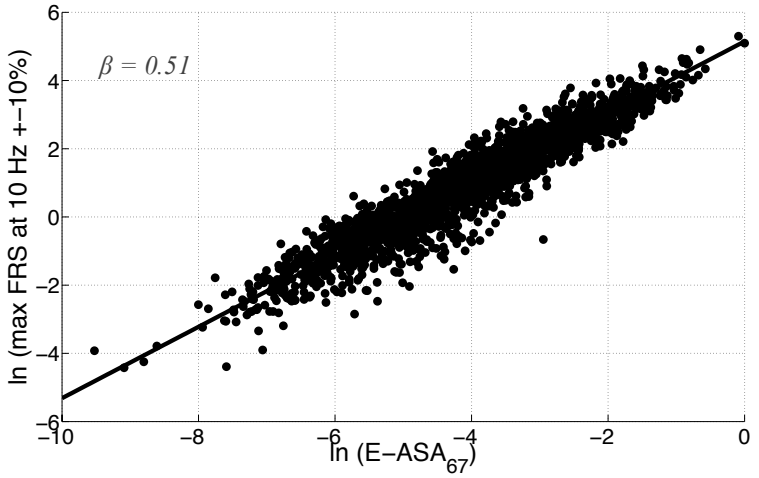

c)

Figure 3.20 *Regression plots, IMs vs. Max FRS in the range 10Hz±10% for SMART (a) PGA b) $S_{pa}(f_1)$; (c) E-ASA_{67}.*

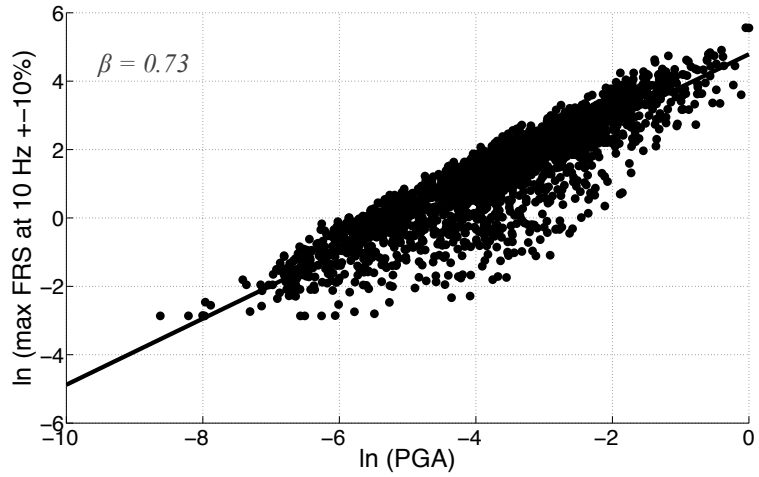

a)

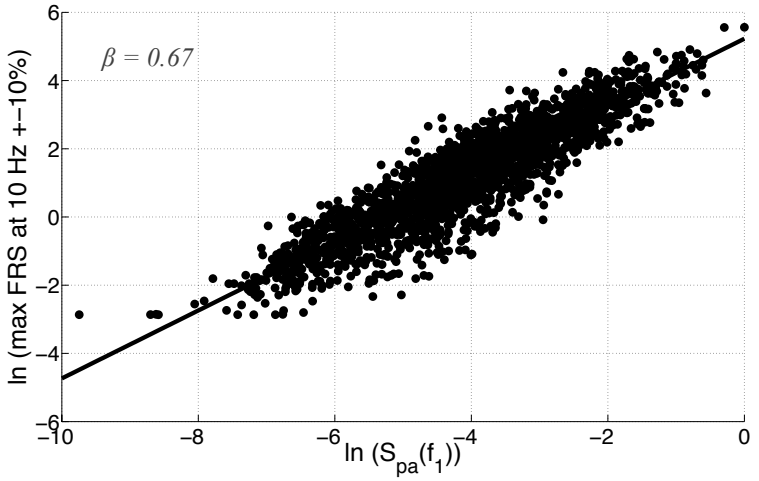

b)

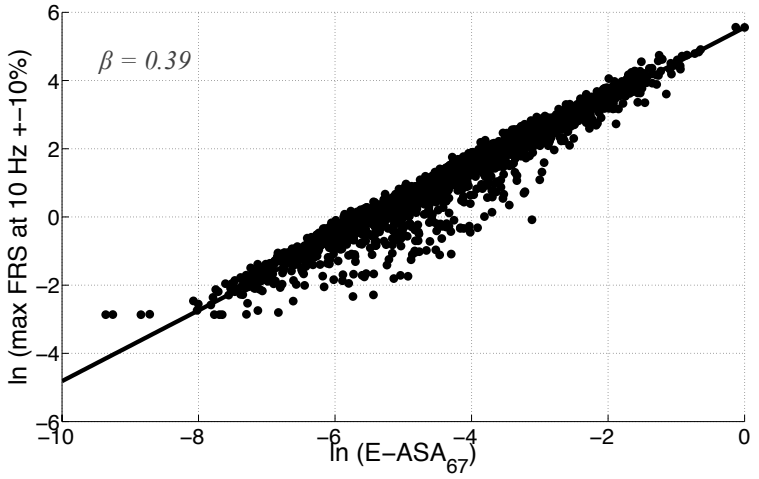

c)

Figure 3.21 *Regression plots, IMs vs. Max FRS in the range 10Hz±10% for TC3: (a) PGA b) $S_{pa}(f_1)$; (c) E-ASA_{67}.*

3.2.2.2 IMs sufficiency evaluation

The results of the comparative statistical analysis concerning the IMs' sufficiency are presented (Table 3.6) for the 2,045 records composing the four ground-motions bins, with respect to the max of the 5% damped FRS at 20 Hz ± 10%. Analogous results have been found for the other considered EDPs.

Table 3.6 *Sufficiency analysis on all the 2,045 ground motions: Spearman rank correlation coefficients*

	IMs												
	Frequency Response Based								*Amplitude Based*		*Duration Based*		
	IM$_\lambda$	***E-ASA$_{67}$***	*ASA$_{40}$*	***S$_{pa}$***	*S**	*I$_{NP}$*	*ASI*	*EPA*	***PGA***	*PGV*	*I$_A$*	*CAV*	*SCAV*
EC8 FRAME													
M$_w$	**0.08**	**-0.13**	-0.18	**-0.15**	-0.2	-0.18	0.12	-0.31	**0.36**	-0.26	-0.29	-0.26	0.29
R$_{hyp}$	**-0.07**	**-0.5**	-0.6	**-0.58**	-0.61	-0.58	-0.06	-0.52	**0.19**	-0.5	-0.44	-0.66	-0.19
V$_{S30}$	**0.01**	**0.22**	0.27	**0.26**	0.24	0.26	0.01	0.22	**-0.14**	0.18	0.11	0.2	0.00
SMART													
M$_w$	**-0.3**	**-0.28**	-0.29	**-0.28**	-0.3	-0.3	-0.3	-0.26	**-0.27**	-0.25	-0.33	-0.23	-0.03
R$_{hyp}$	**-0.21**	**-0.23**	-0.41	**-0.34**	-0.43	-0.36	-0.41	-0.56	**-0.31**	-0.56	-0.55	-0.66	-0.44
V$_{S30}$	**0.18**	**0.14**	0.25	**0.23**	0.26	0.24	0.26	0.28	**0.22**	0.26	0.27	0.27	0.16
TC3													
M$_w$	**-0.27**	**-0.26**	-0.27	**-0.26**	-0.28	-0.27	-0.28	-0.24	**-0.27**	-0.24	-0.3	-0.21	-0.05
R$_{hyp}$	**-0.28**	**-0.28**	-0.44	**-0.38**	-0.46	-0.4	-0.45	-0.58	**-0.37**	-0.58	-0.56	-0.67	-0.5
V$_{S30}$	**0.14**	**0.08**	0.21	**0.17**	0.22	0.19	0.22	0.25	**0.19**	0.24	0.24	0.25	0.16

In considering Table 3.6:

Excluding a light correlation in the case of the EC8-FRAME (Figure 3.22b) and with respect to the R_{hyp}, the analysis of these results evidences no significant correlation between the proposed IM and the M_w or the R_{hyp}. Moreover, excluding the case of the EC8-FRAME, the *E-ASA$_{67}$* shows always lower correlation than the $S_{pa}(f_1)$ and the *PGA*. The lack of correlation indicates the sufficiency of the *E-ASA$_{67}$* (Fig. 3.23a-3.23b-3.24a-3.24b) with respect to magnitude and source-to-site distance (see also Appendix B).

All the test cases show a pronounced lack of sufficiency of the *CAV* with respect to the R_{hyp}. Such insufficiency was also noted (chapter 2, paragraph 2.3.5.2) considering structural demand parameters (i.e. MIDR, global ductility, frequency drop).

Lastly, it is important to notice that none of the considered IMs shows an appreciable degree of in-sufficiency with respect to the soil-type, i.e. V_{s30} (Figure 3.22c-3.23c-3.24c).

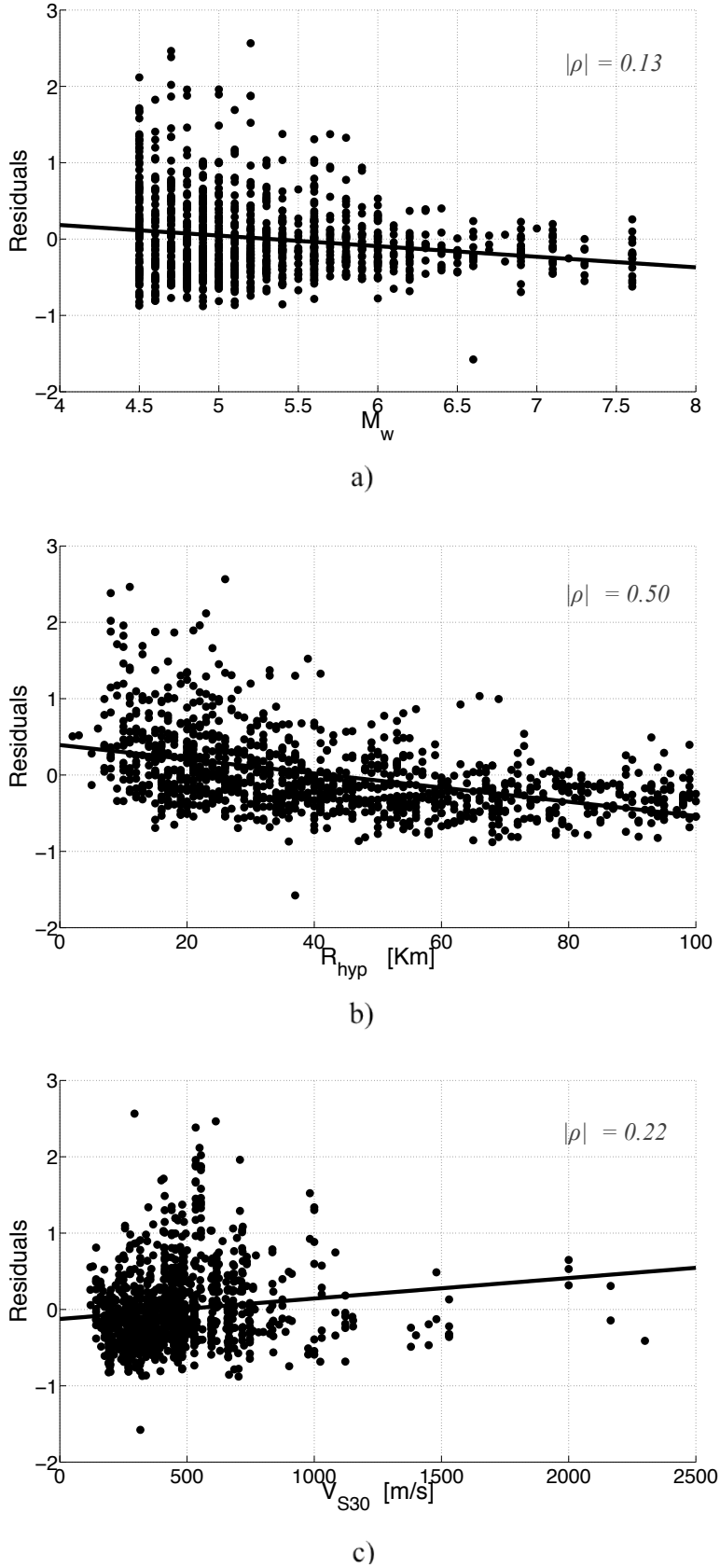

Figure 3.22 *Sufficiency analysis, all records – EC8-FRAME: (a) E-ASA$_{67}$ vs. M_w; (b) E-ASA$_{67}$ vs. R_{hyp}; (c) E-ASA$_{67}$ vs. V_{S30}.*

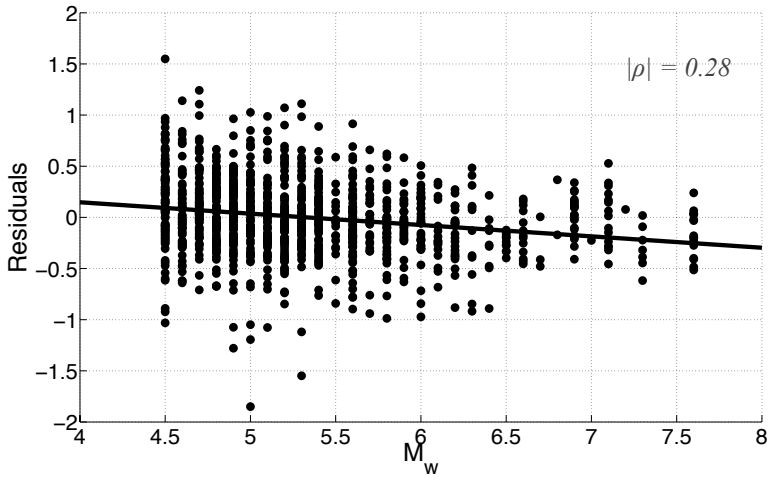

a)

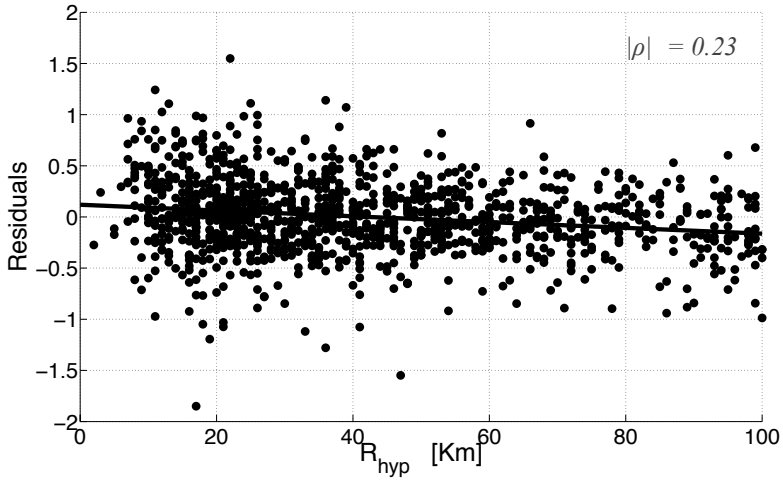

b)

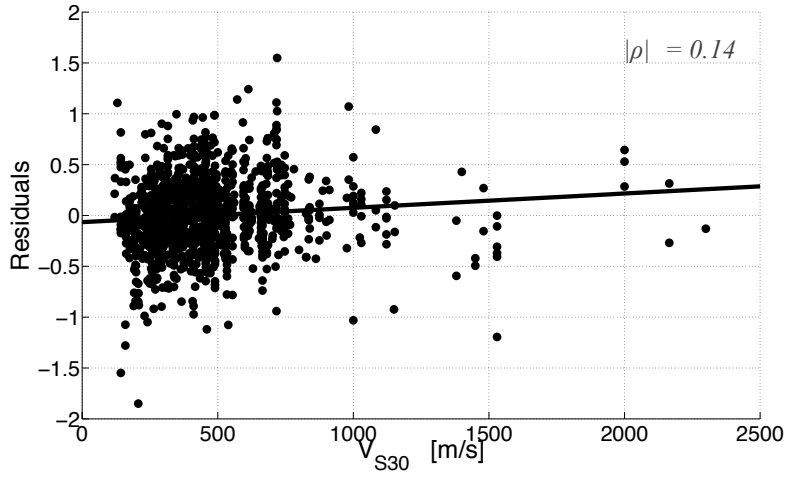

c)

Figure 3.23 *Sufficiency analysis, all records - SMART: (a) E-ASA$_{67}$ vs. M$_w$; (e) E-ASA$_{67}$ vs. R$_{hyp}$; (f) E-ASA$_{67}$ vs. V$_{S30}$.*

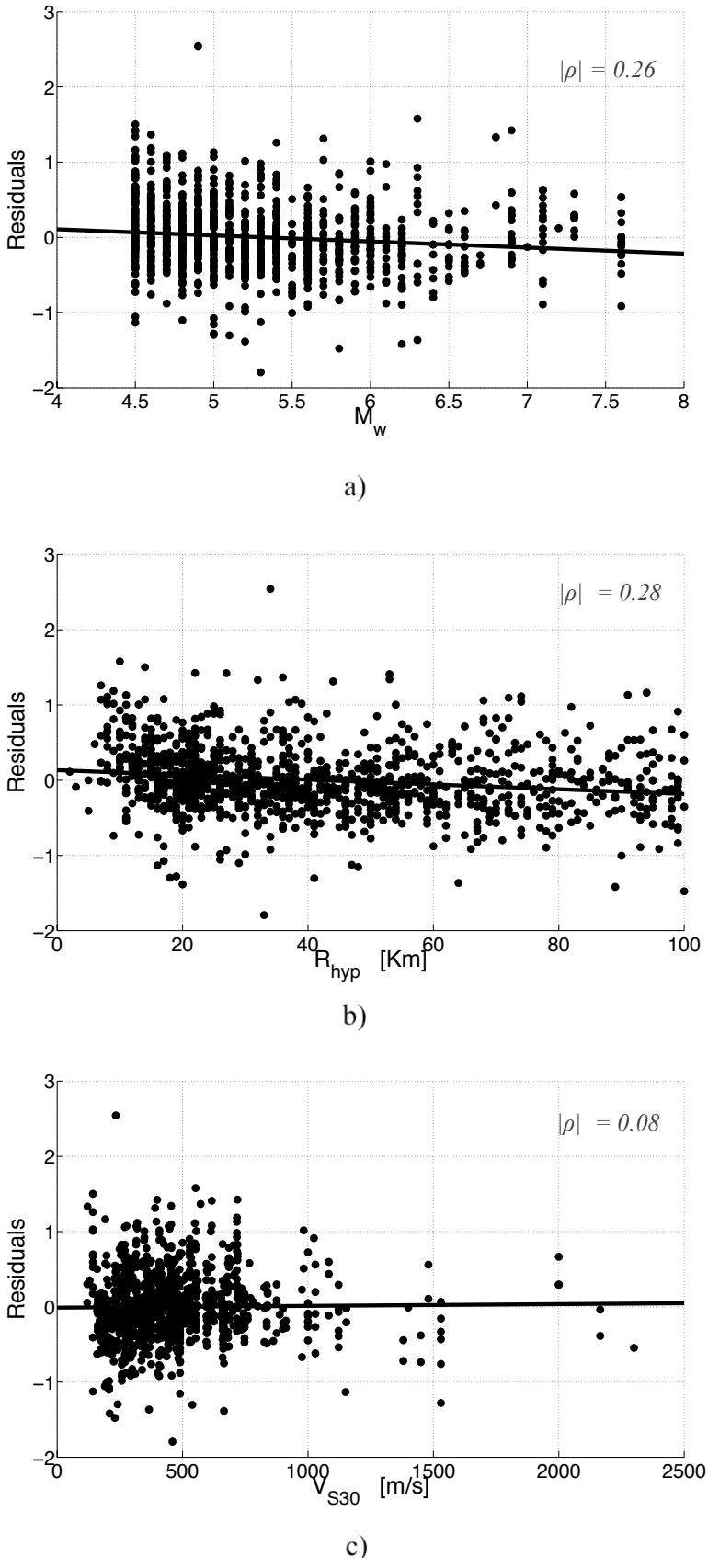

Figure 3.24 *Sufficiency analysis, all records – TC3: (a) E-ASA$_{67}$ vs. M_w; (e) E-ASA$_{67}$ vs. R_{hyp}; (f) E-ASA$_{67}$ vs. V_{S30}.*

3.2.3 *E-ASA$_R$ optimum*

In order to analyze the sensitivity to the choice of the width of the dominant-frequencies range (i.e. R factor in equation 3.8), the *E-ASA$_R$* has been computed for several values of width, i.e. *E-ASA$_{40}$*, *E-ASA$_{67}$*, *E-ASA$_{80}$*, *E-ASA$_{100}$*, *E-ASA$_{150}$* and *E-ASA$_{200}$* (Table 3.7).

Table 3.7 *E-ASA$_R$ sensibility study: efficiency analysis on all the 2,045 ground motions (Logarithmic standard deviation (β) of the residuals).*

Test-Case	IM	X_f	Max FRS 1Hz±10%	Max FRS 5Hz±10%	Max FRS 10Hz±10%	Max FRS 20Hz±10%
EC8 FRAME	***E-ASA$_{40}$***	*1.4*	**0.41**	0.65	0.63	0.55
	E-ASA$_{67}$	*1.67*	0.49	0.59	0.58	0.51
	E-ASA$_{80}$	*1.8*	0.52	0.56	0.56	0.5
	E-ASA$_{100}$	*2*	0.57	0.53	0.54	0.47
	E-ASA$_{150}$	*2.5*	0.67	0.44	0.47	0.42
	E-ASA$_{200}$	*3*	0.77	**0.34**	**0.41**	**0.38**
SMART	***E-ASA$_{40}$***	*1.4*	**0.35**	**0.42**	0.56	0.46
	E-ASA$_{67}$	*1.67*	**0.37**	**0.46**	0.51	0.42
	E-ASA$_{80}$	*1.8*	0.38	0.47	0.49	0.4
	E-ASA$_{100}$	*2*	0.39	0.49	**0.46**	**0.38**
	E-ASA$_{150}$	*2.5*	0.41	0.51	**0.45**	**0.37**
	E-ASA$_{200}$	*3*	0.42	0.53	**0.47**	**0.37**
TC3	***E-ASA$_{40}$***	*1.4*	**0.26**	**0.32**	**0.4**	0.51
	E-ASA$_{67}$	*1.67*	**0.28**	**0.35**	**0.39**	**0.49**
	E-ASA$_{80}$	*1.8*	0.29	0.36	**0.39**	**0.48**
	E-ASA$_{100}$	*2*	0.3	0.38	0.4	**0.48**
	E-ASA$_{150}$	*2.5*	0.31	0.41	0.44	**0.47**
	E-ASA$_{200}$	*3*	0.31	0.43	0.47	**0.47**

It can be noticed (Table 3.7) that the optimal R value is function of the Non-Structural Component fundamental frequency. Indeed, this last through the α_i (Eq. 3.3) influences the extent of the dominant-frequencies interval. Accordingly, the best performing R values (Table 3.7) are the ones that allow "to cover" the natural modes of the buildings associated to the higher λ_i (Eq. 3.5) values (highlighted in bold in Tables 3.2-3.4).

Therefore, looking for the maximum efficiency of the *E-ASA$_R$*, the analysis of the results shown in Table 3.7 suggests that the optimal R should be chosen such to extend the lower bound of integration in Eq. 3.8 up to the value of f_e (i.e. the fundamental frequency of the NSC). Nevertheless, although this procedure maximizes the efficiency of the *E-ASA$_R$* and

keeps its formulation simpler than the one of the IM_λ (Eq. 3.6), the introduced dependency on the f_e values translates in a loss of exploitability.

Consequently, if the objective is to have a highly exploitable IM, and a minor decrease in efficiency is tolerable, the proposed solution is to select the value of R on the base of the kind of structure hosting the NSCs, independently from the NSCs fundamental frequencies. For instance, practical considerations lead to suggest the $E\text{-}ASA_{67}$ (i.e. R = 67 %) as general optimum IM for NSCs acceleration demand prediction in high-frequency structural wall buildings. The main reason is due to the noticeable (Table 3.5) global performance (i.e. on the two structural-wall buildings and for the four FRS frequency targets) of the $E\text{-}ASA_{67}$. An additional reason comes from the direct relation (Eq. 3.12) between $E\text{-}ASA_{67}$ (3.8) and ASA_{40} (2.1).

$$E - ASA_{67}(f_1) = ASA_{40}(1.67 f_1) \tag{3.12}$$

Indeed the ASA_{40} has shown (chapter 2, paragraph 2.3.5) to be a very high efficient IM with respect to structural damage prediction and specific GMPEs in its terms have been already developed (Koufoudi *et al*., 2014). This means that (because of the relation 3.12) PSHA could be advantageously performed by means of the same GMPE with the aim to specify both the structural and the non-structural seismic hazard.

3.3 CONCLUSIONS

In this chapter, a new IM has been proposed in order to predict NSCs acceleration demand. The proposed IM, namely *Equipment Relative Average-Spectral-Acceleration* ($E\text{-}ASA_R$), is based on the pseudo-spectral acceleration values along a definite, structure-specific, frequency range. Such range corresponds to the here-called structure's "*dominant-frequencies interval*". This last has been defined as the frequency range that includes the first n-vibration modes such that the product between the participation factors of those modes and the dynamic amplification factors related to those modes assumes a dominant value. It has been shown that the dominant-frequencies interval can be effectively defined based on the fundamental frequency of the structure.

The efficiency of $E\text{-}ASA_R$ has been demonstrated by comparative statistical analysis of the results of linear dynamic simulations performed on three reinforced concrete structures over a database of thousands recorded seismic ground motions. The $E\text{-}ASA_R$ exhibits high efficiency in predicting non-structural components' acceleration demand: it has been shown that such

efficiency is robust with respect to the structure's type (structural wall vs. frame; high vs. low frequency) and with respect to the fundamental frequency of the non-structural component.

The sufficiency of $E\text{-}ASA_R$ with respect to Magnitude, source-to-site distance and soil-type (*Vs30*) has also been shown by statistical analysis. Such sufficiency implies that if the $E\text{-}ASA_R$ of interest is given (by Hazard Analysis), there is no need to be concerned about the *M, R* and *Vs30* of the records to be used in structural analyses provided that the selected records match the given $E\text{-}ASA_R$ value.

$E\text{-}ASA_R$ can be computed, as ASA_R and $S_{pa}\ (f_1)$, by only knowing the fundamental frequency of the structure. This represents a useful advantage with respect to more complex structure-specific IMs: indeed, for an actual structure the fundamental frequency is usually known or easily assessable through in-situ tests and/or empirical code-based approaches.

The simple formulation of $E\text{-}ASA_R$ based exclusively on spectral pseudo-acceleration values, allows performing PSHA by means of common ground motion prediction models currently available for $S_{pa}\ (T_1)$. Moreover, the straightforward link between $E\text{-}ASA_R$ and ASA_R, which revealed (Chapter 2) to be a high efficient IM for structural demand prediction, enable to use the same GMPE form for both structural and non-structural demand oriented PSHA/SPRA studies.

.

4 General Conclusions and Perspectives

4.1 GENERAL CONCLUSIONS

In the present study, the performance of a large panel of Intensity Measures, which are suitable for Probabilistic Seismic Risk Analysis, have been compared with respect to the ability in predicting Structural and Non-Structural demand. The comparison is based on the use of a large dataset of recorded earthquake ground motions, numerical analyses performed on experimentally validated three-dimensional numerical models, and systematic statistical analysis of the results.

In agreement with literature and with respect to the considered Engineering Demand Parameters, it has been found that the *Intensity Measures based on the spectral acceleration ordinates* are the ones displaying better performance. Among these, the structure-specific IMs (i.e. including the information about the structure's fundamental frequency) are the best performing. This result involves both Structural and Non-Structural demand.

The study (Chapter 2) confirmed that the widespread spectral acceleration at the fundamental frequency of the structure $S_{pa}(f_1)$ is an excellent IM for structural demand prediction, provided that the examined structure experiences small or zero damage. In the case the structure experiences damage (and this may happen in case of "strong" ground motion or "weak" structure), the performance of the $S_{pa}(f_1)$ declines. With the specific aim to handle such situations, *a new Intensity Measure* based on the pseudo-spectral acceleration values along a definite, structure-specific, frequency range has been herein introduced. Such IM, namely *Relative Average-Spectral-Acceleration* ASA_R, results to be up to 30% more efficient in predicting structural demand than the $S_{pa}(f_1)$.

Therefore, the use of ASA_R may be particularly advantageous when, due to location and/or structural design, the earthquake engineer expects *nonlinear structural behavior*. Under such conditions, the high ASA_R efficiency helps reducing the number of records needed to simulate the time-history response within a specified confidence interval. This advantage can be especially valuable when evaluating seismic retrofitting strategies since several solutions can be assessed, causing a significant increase in the number of analyses to be performed.

Regarding non-structural demand (Chapter 3), the study confirmed that the Peak Ground Acceleration *PGA* is a valuable IM when used to predict acceleration demand of components housed on low-frequency frame building. However, the study revealed that *PGA*'s performance is not adequate in case of components housed on high-frequency structural wall buildings. Therefore, *a new Intensity Measure* based on the pseudo-spectral acceleration values along a definite, structure-specific, frequency range has been herein specifically developed for the prediction of Non-Structural Components acceleration demand. This IM, namely *Equipment Relative Average Spectral Acceleration E-ASA,* has shown to be up to 50% more efficient than the *PGA* in predicting Non-Structural Components acceleration demand.

Due to its robust efficiency, the use of $E\text{-}ASA_R$ may be particularly advantageous when the earthquake engineer has to handle with *several kinds of acceleration-sensitive non-structural components* (i.e. characterized by different fundamental frequency values). In such case the use of $E\text{-}ASA_R$ turn in using a single high-efficiency IM for the whole panel of non-structural components housed in the building.

Besides, the efficiency of both ASA_R and $E\text{-}ASA_R$ in predicting the system response with the least scatter using the smallest number of response analyses can be valuable in the *formulation of fragility curves*.

Other than efficiency, both ASA_R and $E\text{-}ASA_R$ have shown to own the characteristic of *sufficiency* with respect to Magnitude, source-to-site distance and soil-type (Vs_{30}). Such feature implies that the use of ASA_R (or $E\text{-}ASA_R$) can be associated to loosen restrictions in ground motions selection procedures (i.e., no need to be concerned about Magnitude, source-to-site distance and soil- type) provided that the selected records match the ASA_R (or the $E\text{-}ASA_R$) value for the site of interest.

Moreover, both the introduced IMs possess the valuable characteristics to need (in order to be computed) merely the knowledge of the building's fundamental frequency, exactly as it is for the wide-spread spectral acceleration $S_{pa}(f_1)$. This key characteristic makes both ASA_R and $E\text{-}ASA_R$ *easily exploitable in Probabilistic Seismic Hazard Analysis*. Indeed, nowadays such possibility of exploitation is a condition *sine qua non* for the use of IMs in Seismic Probabilistic Risk Analysis methods. Encouragingly, at the time of the publication of this manuscript, Ground Motion Prediction Equations are already under development for both

ASA_R and $E\text{-}ASA_R$. Promisingly, such implementation could translate into the diffusion in the engineering practice of the herein introduced IMs.

Additionally, it is worth to highlight that the proven capability of both ASA_R and $E\text{-}ASA_R$ in discriminating ground motions "intensity" makes them valuable also for deterministic seismic vulnerability assessment, when "worst case scenario" ground motions have to be selected.

In conclusion, the introduction of both ASA_R and $E\text{-}ASA_R$ is associated with a substantial reduction of the record-to-record variability of both structural and non-structural demand prediction, i.e., reduction of uncertainty in the characterization of seismic ground motions. Therefore, due to their proven efficiency, sufficiency, robustness and applicable formulation, both ASA_R and $E\text{-}ASA_R$ can be considered as worthy candidates in the near future for defining seismic hazard within the frameworks of both Probabilistic and Deterministic Seismic Risk Analysis.

4.2 PERSPECTIVES

The IMs introduced in this study have shown promising performance, however, further work could still improve such performance and contribute to the reduction of uncertainty in the characterization of seismic ground motions. Some suggestion for future development is listed herein:

- In order to be computed, both ASA_R and $E\text{-}ASA_R$ need the definition of structure-specific frequency ranges. Despite general-optimum frequency ranges have been recommended for both the proposed IMs, further research could result in more specific *strategies of identification of the optimum frequency ranges*. These could, in turn, lead to further improving of the performance of both ASA_R and $E\text{-}ASA_R$.

- It has been shown that ASA_R's performance is robust with respect to the type of building. However the study did not consider structures whose dynamic behavior is recognized to be strongly influenced by higher vibration modes, e.g., *high-rise and super high-rise buildings*. Besides, nowadays such kinds of buildings are largely diffuse and, with respect to them, current IMs do not have shown to be together efficient and exploitable. Hence, assessments of ASA_R performance for such type of buildings is advisable. Indeed, it is conceivable that a strategy of identification of the

frequency range based on the consideration of several modes could lead to obtain interesting performance, which in turn could support the use of ASA_R also for tall buildings.

- It has been shown that ASA_R's performance is robust with respect to linear Soil-Structure Interaction effects. However, could be useful to perform further investigation considering more advanced non-linear SSI models.

- In the part of the study relative to Non-Structural Components demand, it has been chosen to evaluate the IMs' performance with respect to NSCs housed on linear behaving structures. Future works could investigate the case of *NSCs housed on non-linear behaving structures, and/or NSCs with non-linear behaving supports* (i.e., links with the structure).

- It is worth to note that the $E\text{-}ASA_R$ is currently, in the knowledge of the author, the only IM exclusively developed to predict Non-Structural Components acceleration demand. Auspiciously, this study may open *a new research path* that could lead to advances in the prediction of the response of acceleration-sensitive secondary systems, which represent an important part of the seismic assessment problem.

- An additional IMs' characteristic, which could be required by engineers, is *scaling robustness*: this property implies that ground motions which are scaled to a target IM value induce results in terms of EDP which are unbiased compared to results given by the un-scaled ground motions. Considering that the scaling robustness of $S_{pa}(f_1)$ has been extensively demonstrated, and the herein proposed IMs can be assimilated to average spectral acceleration values, the scaling robustness for ASA_R and $E\text{-}ASA_R$ has not been explicitly investigated in this study. However, it could be suitable, in order to facilitate their diffusion, to provide clear demonstration of the scaling robustness of the proposed IMs.

- Lastly, in chapter 2 it has been shown that ASA_R and the other examined IMs have a inner efficiency limit, which is due to their inability to follow (during the seismic excitation) the evolution and the interaction of the dynamic characteristics of both the structure and the ground motion excitation. Indeed, it is evident that such limitation is common to all the Intensity Measures nowadays considered as

practically exploitable. Hence, it appears that such a limit can be overcome only through the consideration/development of *more complex IMs*. In order to succeed, these would have to consider more structural information that the building's natural frequency and, ideally, would have to be derived from non-linear dynamic time history analyses of inelastic Single Degree of Freedom systems.

Nevertheless regarding this last point, even if such IMs can be currently developed (and in some form they already exist, e.g., Conte *et al*., 2003), until the day it will become ordinary to perform Probabilistic Seismic Hazard Analysis in their terms, engineers will continue to use simpler IMs which as it is proven by the ASA_R and the $E\text{-}ASA_R$ continue to gain performance day after day.

.

REFERENCES

Abbasi, V., Daudeville, L., Kotronis, P., and Mazars, J., 2003. Using damage mechanics to model a four story RC framed structure submitted to earthquake loading," *Proc. 5th International Conference on Fracture Mechanics of Concrete and Concrete Structures FRAMCOS V*, Vail, Colorado, USA.

Akkar, S., Sandıkkaya, M.A., Şenyurt, M., Azari Sisi, A., Ay, B.Ö., Traversa, P., Douglas, J., Cotton, F., Luzi, L., Hernandez, B., and Godey, S., 2013. Reference database for seismic ground-motion in Europe (RESORCE), Bulletin of Earthquake Engineering, DOI: 10.1007/s10518-013-9506-8

Ang, A. H. S., 1987. Basis for earthquake resistant design with tolerable structural damage. Proceedings of the 5th *International Conference on Applications of Statistics and Probability to Soil and Structural Engineering*. Vancouver, Canada.

Ang, A. H. S., 1990. Reliability bases for seismic safety assessment and design. Proceedings of the *Fourth U.S. National Conference on Earthquake Engineering*. Palm Springs, California, USA.

Arias, A., 1970. A measure of earthquake intensity. *Seismic design for nuclear power plants*. Cambridge, MA: MIT Press, 1970:438–69.

ATC, 1978. Tentative Provisions for the Development of Seismic Regulations for Buildings. ATC-3-06 Report, Applied Technology Council, Redwood City, CA.

ATC, 2004. Engineering Demand Parameters for Nonstructural Components, ATC-58, Project Task Report, Phase 2, Task 2.3, Redwood City, CA.

Baker, J. W., Cornell, C. A., 2004. Choice of a vector of ground motion intensity measures for seismic demand hazard analysis. *13th World Conference on Earthquake Engineering, Vancouver, Canada 2004.*

Baker, J. W., Cornell, C. A., 2006a. Which spectral acceleration are you using?. *Earthquake Spectra*, Volume 22, No. 2, pages 293–312, May 2006; Earthquake Engineering Research Institute

Baker, J. W., Cornell, C. A., 2006b. Spectral shape, epsilon and record selection. *Earthquake Engineering and Structural Dynamics* . 2006; 35:1077–1095.

Baker, J. W., 2008. An introduction to Probabilistic Seismic Hazard Assessment. Support of the PSHA lectures, Stanford University, Stanford, USA.

Bazzurro, P., Cornell, C. A., 2002. Vector-valued probabilistic seismic hazard analysis. *Proceedings of the 7th US national conference on earthquake engineering*. Earthquake Engineering Research Institute, Boston, MA; 2002.

Benjamin, J., Cornell, C. A., 1970. Probability, statistics and decisions for civil engineers. *Mc-Graw Hill Companies.*

Beyer, K., Dazio, A., Priestley, M. J. N., 2011. Shear Deformations of Slender Reinforced Concrete Walls under Seismic Loading. *ACI Structural Journal,* V. 108, No. 2, March-April 2011

Blume, J. A., 1979. On instrumental versus effective acceleration and design coefficients. Proceedings of the *2nd U.S. National Conference on Earthquake Engineering*. Stanford, California, USA.

Bojorquez, E., Iervolino, I., 2011. Spectral shape proxies and nonlinear structural response. *Soil Dynamics and Earthquake Engineering 31 (2011) 996–1008*

Bolt, B. A., 1969. Duration of Strong Motion*, Proceedings of 4th World Conference Earthquake Engineering*, 1304-1314, Santiago, Chile.

Bommer, J. J., and Acevedo, A. B., 2004. The Use of Real Earthquake Accelerograms as Input to Dynamic Analysis. *Journal of Earthquake Engineering, 8 (Special Issue 1), 43-9*

Bommer, J.J., and Abrahamson, N.A., 2006. Why do modern probabilistic seismic-hazard analyses often lead to increase hazard estimates?. *Bulletin of Seismological Society of America* 96:6, 1967–1977.

Boore, D. M., 2004. Can site response be predicted?. *Journal of Earthquake Engineering, 8 (Special Issue 1), 43-91.*

Barenberg, M. E., Foutch, D. A., 1998. Evaluation of seismic design procedures for highway bridge. *Journal of Structural Engineering*. ASCE Vol. 111:4, 1588-1605.

Bracci, J. M., Reinhorn, A. M., Mander, J. B., Kunnath, S. K., 1989. Deterministic Model for Seismic Damage Evaluation of Reinforced Concrete Structures. Rep. No. NCEER-89-0033, National Center for Earthquake Engineering Research, State Univ. of New York, Buffalo, NY, USA.

Brincker, R., Zhang, L., Andersen, P., 2001. Modal Identification of Output Only Systems using Frequency Domain Decomposition. *Smart Materials and Structures*, 10, 441-445.

Buratti, N., 2012. A comparison of the performances of various ground–motion intensity measures. *15th World Conference on Earthquake Engineering*. Lisbon, Portugal

CALTECH, 1975. Dynamic response of six multistory buildings during the San Fernando earthquake. *Report No. EERL 75-02*. California Institute of Technology. USA.

Cakmak, A. S., Rodriguez-Gomez, S., DiPasquale E., 1991. Seismic damage assessment for reinforced concrete structures. Proceedings of the first International Conference on Soil Dynamics and Earthquake Engineering, Karlsruhe, Germany.

Campbell, K. W., Bozorgnia, Y., 2010. A Ground Motion Prediction Equation for the Horizontal Component of Cumulative Absolute Velocity (CAV) Based on the PEER-NGA Strong Motion Database. *Earthquake Spectra*, Volume 26, No. 3, pages 635–650, August 2010; Earthquake Engineering Research Institute.

Carvalho E.C., 1998 .Invited Lecture: Seismic testing of Structures. Proceedings of the 11th European Conference on Earthquake Engineering, Paris, France.

CEA, 1998a. CAMUS international benchmark, Report I, Specimen and loading characteristics. Specification for the participants report. SEMT/EMSI/RT/98-066A, CEA, Saclay, France.

CEA, 1998b. CAMUS international benchmark, Report II, experimental results. Synthesis of the participant reports. SEMT/EMSI/RT/98-067A, CEA Saclay, France.

CEA, 2013. Presentation of the SMART 2013 international benchmark. Report DEN/DANS/DM2S/SEMT/EMSI/ST/12-017/E, CEA, Saclay, France.

Chen, Y., Soong, T. T., 1988. State-of-the-art review: Seismic response of secondary systems. *Engineering Structures, Vol. 10, 1988.*

Chopra, A. K., 2007. Dynamics of structures: theory and applications to earthquake engineering (3rd ed.). Englewood Cliffs, NJ: Prentice Hall.

Ciampoli M., Giannini R., Nuti C., Pinto P. E., 1989. Seismic reliability of non-linear structures with stochastic parameters by directional simulation. Proc. 5th Intern. Conf. on Structural Safety and Reliability ICOSSAR '89, S.Francisco, pp. 1121–1126

Cimellaro GP., Christovasilis IP., Reinhorn AM., Kirova T. (2010). "L'Aquila earthquake of April 6, 2009: rebuilding a resilient city to multiple hazard". MCEER-10-0010. University of Buffalo. USA.

Combescure, D., 2001. Modélisation des structures de génie civil sous chargement sismique à l'aide de castem 2000, CEA, Direction de l'énergie nucleaire, département modélisation de systèmes et structures, service d'études mécaniques et thermiques, Rapport DM2S. 2000.

Comerio, M.C., 2005. PEER testbed study on a laboratory building: exercising seismic performance assessment. PEER Report. PEER 2005/12.

Conte, J. P., Pandit, H., Stewart, J. P., Wallace, J. W., 2003. Ground motion intensity measures for performance based earthquake engineering. *Ninth International Conference on Applications of Statistics and Probability in Civil Engineering (ICASP9) July 6-9, 2003, San Francisco, USA.*

Cordova, P.P., Deierlein, G.G., Mehanny, S.S.F., and Cornell, C.A., 2001. Development of a two-parameter seismic intensity measure and probabilistic assessment procedure. *2nd U.S.-JapanWorkshop on PBEE Methodology for Reinforced Concrete Building Structures.*

Cornell C.A., 1968. Engineering seismic risk analysis, *Bulletin of the Seismological Society of America*, 58(5), 1583-1606.

Cornell, C. A., 2004. Hazard, ground motions and probabilistic assessment for PBSD. *Performances based seismic design concepts and implementation, International workshop. 28 June-1 July 2004, Bled, Slovenia.*

Cornell, C.A., Jalayer, F., Hamburger, R.O., and Foutch, D.A., 2002. Probabilistic basis for 2000 SAC federal emergency management agency steel moment frame guidelines. *Journal of Structural Engineering*. 128:4, 526 - 533.

Crowley, H. and Pinho, R., 2004. Period-Height Relationship for Existing European Reinforced Concrete Buildings, *Journal of Earthquake Engineering*, 8(Special Issue 1), 93-119.

De Biasio, M., Grange, S., Dufour, F., 2012. The role of model calibration in seismic FE analysis: the case study of an old reinforced concrete structure by using ambient noise modal analysis. *Proceedings of the 15th World Conference on Earthquake Engineering. 24-28 September, Lisbon, Portugal.*

De Biasio, M., Grange, S., Dufour, F., Allain, F., Petre-Lazar I., 2013. Correlation between seismic ground motions and structural damage. *Proceedings of the 22nd Conference in Structural Mechanics in Reactor Technology. 18-23 August, San Francisco, USA.*

De Biasio, M., Grange, S., Dufour, F., Allain, F., Petre-Lazar I., 2014a. A simple and efficient intensity measure to account for nonlinear structural behavior. *Earthquake Spectra (in press).*

De Biasio, M., Grange, S., Dufour, F., Allain, F., Petre-Lazar I., 2014b. Correlation between seismic ground motions and floor acceleration demand for frame and structural wall buildings. *Proceedings of the 2nd European Conference on Earthquake Engineering and Engineering Seismology. 25-29 August, Istanbul, Turkey.*

De Biasio, M., Grange, S., Dufour, F., Allain, F., Petre-Lazar I., 2014c. Intensity Measures for Probabilistic Assessment of Non-Structural Components Acceleration demand. *Earthquake Engineering and Structural Dynamics (Submitted).*

DiPasquale, E., and Cakmak, A. S., 1987. Detection and Assessment of seismic structural damage. Rep. No. NCEER-87-0015, National Center for Earthquake Engineering Research, State Univ. of New York, Buffalo, NY, USA.

DiPasquale, E., and Cakmak, A. S., 1989. On the relation between global and local damage indices. Rep. No. NCEER-89-0034, National Center for Earthquake Engineering Research, State Univ. of New York, Buffalo, NY, USA.

Dowell, E. H., 1979. On Some General Properties of Combined Dynamical Systems. *Journal of Applied Mechanics* 46(4), 964-965.

EC8, 1988. Eurocode No. 8 Structure in Seismic Regions -Design-), Part1, General and Building, May 1988 edition, Report EUR 12266 EN, Commission of the European Communities.

Elnashai, A. S., El Ghazouli, A. Y., Dowling P. J., 1990. Verification of pseudo dynamic testing of steel members. *Journal of Construction Steel Research* 16(1990), 153-161.

EPRI, 1988. A criterion for determining exceedance of the operating basis earthquake. EPRI NP-5930. Electric Power Research Institute, USA.

EPRI, 1989. Linear and Nonlinear Response of Structures and Equipment to California and Eastern United States Earhquakes. EPRI NP-5566. Electric Power Research Institute, USA.

EPRI, 1991. Standardization of the Cumulative Absolute Velocity. EPRI TR-100082. Electric Power Research Institute. USA.

EPRI, 1994. Methodology for Developing Seismic Fragilities. EPRI TR 103959, Electric Power Research Institute (EPRI), Palo Alto, California, USA,June 1994.

EPRI, 2002. Seismic Fragility Application Guide. EPRI 1002988, Electric Power Research Institute (EPRI), Palo Alto, California,USA, December 2002.

EPRI, 2009. Seismic Fragility Applications Guide Update. EPRI, Palo Alto, CA, USA: 2009. Product ID Number 1019200.

FEMA, 1997. NEHRP commentary on the guidelines for the seismic rehabilitation of buildings, FEMA 274. Prepared by the Applied Technology Council for the Building Seismic Safety Council, Washington D.C., USA.

FEMA, 2000. Prestandard and Commentary for the Seismic Rehabilitation of Buildings, FEMA 356. Prepared by the American Society of Civil Engineers for the Federal Emergency Management Agency, Washington D.C., USA.

FEMA, 2012. Seismic Performance Assessment of Buildings, FEMA P-58. Prepared by the Applied Technology Council for the Federal Emergency Management Agency, Washington D.C., USA.

Fontara, I.K.M., Athanatopoulou, A.M., Avramidis I.E., 2012. Correlation between advanced, structure-specific ground motion intensity measures and damage indices. *15th World Conference on Earthquake Engineering, Lisbon 2012.*

Gazetas, G., 1991. Foundation Engineering Handbook. Fang H-Y (ed.), van Nostrand Reinhold, New York.

Ghobarah, A., 2004. On drift limits associated with different damage levels. *Performances based seismic design concepts and implementation, International workshop. 28 June-1 July 2004, Bled, Slovenia.*

Grange, S., 2008. Modélisation simplifiée 3D de l'interaction sol-structure : application au génie parasismique. Ph. D. Thesis Report. Institut National Polytechnique de Grenoble, France.

Grange, S., Mazars, J., Dufour F., De Biasio, M., 2012. 15WCEE blind prediction contest: modeling strategy using multifiber Timoshenko beams and 3D constitutive law in concrete for shear - Contribution of Team 104, 3SR Lab - Grenoble. Report. 3SR Lab, Grenoble, France.

Guedes J., Pégon P., Pinto A., 1994. "A fibre Timoshenko beam element in CASTEM 2000". Special publication Nr. I.94.31, J.R.C., I-21020, Ispra, Italy.

Gunay, M. S., Mosalam, K. M., 2012. PEER Performance Based Earthquake Engineering methodology, revisited. *15th World Conference on Earthquake Engineering. Lisbon, Portugal*

Hamburger, R.O., Foutch, D.A., and Cornell, C.A., 2003. Translating research to practice: FEMA/SAC performance-based design procedures. *Earthquake Spectra, 19 (2), 255*!*267*.

Haselton, C.B., Goulet C. A., Mitrani-Reiser J., Deierlein G. G., Porter K. A., Stewart J. P., Taciroglu E., 2008. An Assessment to Benchmark the Seismic Performance of a Code-Conforming Reinforced Concrete Moment-Frame Building. PEER Report. PEER 2007/12.

Hrennikoff, A., 1941. Solution of problem of elasticity by the Framework Method. *Journal of Applied Mechanics*, A169-A175.

Housner, G. W., 1959. Behaviour of structures during earthquakes. *Journal of the Engineering Mechanics Division*, ASCE 1959: 85(4): 109–129.

Housner, G. W., and Jennings, P.C., 1964. Generation of artificial earthquakes. *Journal of the Engineering Mechanics Division*. **90**:Proceedings paper 3806.

Housner, G. W., and Jennings, P.C., 1977. Earthquake design criteria for structures. Report No. EERL 76-06, EERL, California Institute of Technology, Pasadena, California, USA.

Housner, G. W., 1975. Measures of severity of Earthquake ground shaking. Proceedings of the *1st U.S. National Conference on Earthquake Engineering*. Ann Harbor, Michigan, USA.

IAEA, 2013. "Seismic instrumentation for exceedance criteria, plant shutdown and restart. DRAFT". *IAEA-TECDOC-ISCC EBP-WA4* International Atomic Energy Agency. Vienna, Austria.

Iervolino I., Manfredi, G., Cosenza E., 2006. Ground motion duration effects on nonlinear seismic response. *Earthquake Engineering and Structural Dynamics 2006; 35:21–38*

Igusa T., Der Kiureghian A., 1985. Dynamic characterization of two-degree-of freedom equipment structure systems. *Journal of Engineering Mechanics. ASCE, vol. 111, No. 1, January 1985*.

Inoue, T., Cornell, C. A., 1990. Seismic hazard analysis of multi-degree-of-freedom structures. Reliability of marine structures, RMS-8. Stanford, CA; 1990.

JRC, 1994. Tests on a Four-Storey Full-Scale R/C Frame Designed According to Eurocodes 8 and 2: Preliminary Report. EUR 15879, 1994, Ispra, Italy.

Katsanos EI, Sextos AG, Manolis GD (2010). Selection of earthquake ground motion records: a state-of-the-art review from a structural engineering perspective. *Soil Dynamics and Earthquake Engineering* 2010;30(4):157–69.

Kennedy, R.P., et al., 1980. Probabilistic seismic safety of an existing nuclear power plant. *Nuclear Engineering Design*, 59, 315 338.

Kennedy, R. P., 1984. Engineering characterization of ground motion. Task 1:Effects of characteristics of free-field motion on structural response. Office of Nuclear Regulatory Research. U.S. NUREG/CR-3805, Vol. 5

Kennedy, R. P., Wesley D. A., Tong, W.H., 1988. Probabilistic evaluation of the Diablo Canyon turbine building seismic capacity using non-linear time history analysis. Pacific Gas & Electric Company 1988 -Report 1643.1.

Kircher, C. A., 2003. It makes dollars and sense to improve nonstructural system performance, Proc. ATC 29-2 Seminar on Seismic Design, Performance, and Retrofit of Nonstructural Components in Critical Facilities, 23–24 October 2003, Newport Beach, CA.

Kotronis, P., Mazars, J., Davenne, L., 2003. The equivalent reinforced concrete model for simulating the behaviour of walls under dynamic shear loading. *Engineering Fracture Mechanics*. Vol. 70, Issues 7-8, May 2003, Pages 1085-1097

Kotronis, P., Ragueneau, F., Mazars, J., 2005. A simplified modelling strategy for R/C walls satisfying PS92 and EC8 design. *Engineering Structures* 27 (2005) 1197–1208

Koufoudi E., Ktenidou O.J., Cotton F., Dufour F., Grange S., 2014. Empirical Ground-Motion Models adapted to a new intensity measure (ASA_{40}). *Bulletin of Earthquake Engineering*, (Submitted)

Kramer, S. L., 1996. Geotechnical Earthquake Engineering. Prentice-Hall International series.

Krawinkler, H., and Miranda E., 2004. Performance-based earthquake engineering. In Y. Bozorgnia and V. V. Bertero (Eds.), Earthquake engineering: from engineering seismology to performance-based engineering. Boca Raton: CRC Press.

Krawinkler, H., 2005. Van Nuys Hotel building testbed report: exercising seismic performance assessment. PEER Report. PEER 2005/11.

La Borderie, C., Mazars, J., Pijauder-Cabot, G., 1994. Damage Mechanics model for reinforced concrete structures under cyclic loading. *ACI 134*, 147-172

Lee, T. H., and Mosalam, K.M., 2006. Probabilistic seismic evaluation of reinforced concrete structural components and systems. PEER Report. PEER 2006/04.

Luco, N., 2002. Probabilistic seismic demand analysis, SMRF connection fractures, and near-source effects. Ph.D. Thesis dissertation, Stanford University, California, USA

Luco, N., and Cornell, C. A., 2007. Structure-Specific Scalar Intensity Measures for Near-Source and Ordinary Earthquake Ground Motions. *Earthquake Spectra*: May 2007, Vol. 23, No. 2, pp. 357-392.

Masi, A., Vona, M., Mucciarelli, M., 2011. Selection of Natural and Synthetic Accelerograms for Seismic Vulnerability Studies on Reinforced Concrete Frames. *Journal of Structural Engineering DOI: 10.1061/(ASCE)ST.1943-541X.0000209*

McCann, M. W. and Shah H. C., 1979. RMS acceleration for seismic risk analysis: an overview. Proceedings of the *2nd U.S. National Conference on Earthquake Engineering*. Stanford, California, USA.

Mehanny, S. S. F., 2009. "A broad range power law form scalar based seismic intensity measure". *Engineering Structures*. 31 (2009) 1354–1368

Menegotto, M., and Pinto, P. E., 1973. Method of analysis for cyclically loaded r. c. plane frames including changes in geometry and non-elastic behavior of elements under combined normal force and bending. *Preliminary Report, IABSE Symposium: Resistance and Ultimate Deformability of Structures Acted on by Well Defined Repeated Loads* - IABSE, Vol. 13, Lisbon 1973.

Michel, C., Gueguen, P., El Arem, S., Mazars, J., Kotronis, P., 2010. Full-scale dynamic response of an RC building under weak seismic motions using earthquake recordings, ambient vibrations and modelling. *Earthquake Engineering and Structural Dynamics*. 2010; 39:419–441

Mikael A., Gueguen P., Bard P.Y., Roux P, Langlais M. (2013). The Analysis of Long-Term Frequency and Damping Wandering in Buildings Using the Random Decrement Technique. *Bulletin of the Seismological Society of America.* 2014/1.

Mitrani-Reiser, J., Haselton, C.B., Goulet C., Porter, K.A., Beck, J., and Deierlein G.G., 2006. Evaluation of the seismic performance of a code-conforming reinforced-concrete

frame building - part II: loss estimation. *8th NCEE*, San Francisco, California, April 18-22, 10 pp.

Miyamura, M., Kanda K., Kato K., DiPasquale E., Rodriguez-Gomez S., 1989. Global damage indices and nonlinear structural response. Proceedings of the 5th *International Conference on Structural Safety and Reliability*. San Francisco, California, USA.

Moehle, J.P. 2003. A framework for performance-based earthquake engineering. *Proc. ATC-15-9 Workshop on the Improvement of Building Structural Design and Construction Practices*, Maui, HI, June.

Moehle J.P. and Frost J.D., 2012. Earthquake Spectra, Special Issue: June 2012, Vol. 28, No. S1.

Mortgat, C. P., 1979. A probabilistic definition of effective acceleration. Proceedings of the *2nd U.S. National Conference on Earthquake Engineering*. Stanford, California, USA.

Mucciarelli, M., Masi, A., Gallipoli, M. R., Harabaglia, P., Vona, M., Ponzo, F. and Dolce, M., 2004. Analysis of RC Building Response and Soil-Building Resonance based on Data Recorded during a Damaging Earthquake (Molise, Italy, 2002). *Bulletin of the Seismological Society of America*, 94, n° 5, 1943-1953.

Naeim, F., 1998. Research Overview: Seismic Response of Structures, *The Structural Design of Tall Buildings*, 7, 195-215.

Newmark, N. M., 1975. Seismic design criteria for structures and facilities: Trans-Alaska pipeline system. Proceedings of the *1st U.S. National Conference on Earthquake Engineering*. Ann Harbor, Michigan, USA.

Newmark, N. M., Hall, W. J., 1982. Earthquake spectra and design. *Monographs Series (EERI)* Earthquake Engineering Research Institute

Nguyen, X. H., 2006. Vulnérabilité des structures en béton armé à voiles porteurs: expérimentation et modélisation. Ph. D. Thesis Report. Institut National Polytechnique de Grenoble, France.

NUREG, 1986. Engineering characterization of ground motion. Task 2:summary report. Office of Nuclear Regulatory Research. U.S. NUREG/CR-3805, Vol. 5

Park, Y. J., Ang, A. H. S., 1985. Mechanistic seismic damage model for reinforced concrete. *Journal of Structural Engineering*. ASCE Vol. 111:4, 722-739.

Park, Y. J., Ang, A. H. S., Wen, Y.K., 1985. Seismic damage analysis of reinforced concrete buildings. *Journal of Structural Engineering*. ASCE Vol. 111:4, 740-757.

Pinto, P. E., 2014. Existing buildings: the new Italian provisions for a probabilistic seismic performance assessment. *2nd European Conference on Earthquake Engineering and Engineering Seismology. August 24-29, 2014, Istanbul, Turkey.*

Porter, K., 2003. An overview of PEER's performance-based earthquake engineering methodology. *Ninth International Conference on Applications of Statistics and Probability in Civil Engineering (ICASP9) July 6-9, 2003, San Francisco, USA.*

Powell, G. H., 2010. Modeling for structural analysis. Computers and Structures Inc., Berkeley, California, USA.

Ragueneau, F., 1999. Fonctionnement dynamique des structures en béton – Influence des comportements hystérétiques locaux. Ph. D. Thesis Report, Ecole Normale Supérieure de Cachan, France.

Rayleigh (Lord), J. W. S., 1945, The Theory of Sound. 2nd Edition, Dover, New York, 1945.

Ravet, S., 2009, Modélisation séismique des bâtiments nucléaires par une approche brochette-manivelle. EDF/SEPTEN ENGSD080162, Electricité de France, Villeurbanne, France.

Reynouard J. M. and Fardis M. N., 2001. Shear Walls. ECOEST/ICONS Rep. 5. Laboratorio Nacional de Engenharia Civil Publications, Lisbon, ISBN 972-49-1889-0, July 2001, 240p.

SEAOC, 1995. Vision 2000 Committee: Performance-based seismic engineering. SEAOC, Sacramento, CA, USA.

Seco-e-Pinto P. S., 1997. Seismic behavior of ground and geotechnical structures. Balkema, Rotterdam.

Sewell, R., 1989. Damage effectiveness of earthquake ground motion: characterizations based on the performance of structures and equipment. Ph.D. Thesis, Stanford University, California, USA.

Seidel, M. I., Reinhorn, A. M., Park, Y. J., 1989. Seismic Damageability Assessment of R/C Buildings in Eastern US. *Journal of Structural Engineering*. ASCE Vol.115, No.9, pp. 2184-2203.

Shing, P. B., Nakshima, M., Bursi, O. S., 1996. Application of pseudo dynamics test method to structural research. *Earthquake Spectra* 12(1), 29–56.

Shome, N., Cornell, C. A., Bazzurro, P., and Carballo J. E., 1998. Earthquakes, records, and nonlinear responses. *Earthquake Spectra* 14(3), 469–500.

Singh, A. K., Ang A. H. S., 1974. Stochastic Prediction of Maximum Seismic Response of Light Secondary Systems. *Nuclear Engineering and Design* 29(2): 218-230.

Singh, J. P., 1985. Earthquake Ground Motions: Implications for Designing Structures and Reconciling Structural Damage. *Earthquake Spectra*: February 1985, Vol. 1, No. 2, pp. 239-270.

Sommerville P. and Porter. K.A., 2005. Hazard analysis. Chapter 3 in "PEER testbed study on a laboratory building: exercising seismic performance assessment." Comerio M.C. editor. PEER Report PEER 2005/12.

Souid, A., Delaplace, A., Ragueneau, F., Desmorat R., 2009. Pseudodynamic testing and nonlinear substructuring of damaging structures under earthquake loading. *Engineering Structures 31, 5 (2009) 1102-1110*

Spearman, C., 1925. Some Issues in the Theory of "g" (including the Law of Diminishing Returns). *Nature* 116 (2916): 436

Stewart, J. P., Chiou, S. J., Bray, J. D., Graves, R. W., Somerville, P. G., Abrahamson, N. A., 2002. Ground motion evaluation procedures for performance-based design. *Soil Dynamics and Earthquake Engineering* 2002;22:765–72.

Stone, W. C., and Taylor, A. W., 1993. Seismic Performance of Circular Bridge Columns Designed in Accordance with AASHTO/CALTRANS Standards. Gaithersburg, MD: U.S. Dept. of Commerce, National Institute of Standards and Technology.

Taghavi S., Miranda E., 2003. Probabilistic Study of Peak Floor Acceleration Demands in Linear Structures. *Ninth International Conference on Applications of Statistics and Probability in Civil Engineering*, San Francisco, 2**:** 1565-1572.

Taghavi S., Miranda E., 2006. Probabilistic seismic assessment of floor acceleration demands in multistory buildings. *Department of Civil and Environmental Engineering, Stanford University*. Report No. 162.

Taghavi S., Miranda E., 2008. Effect of interaction between primary and secondary systems on floor response spectra. *14th World Conference on Earthquake Engineering*, October 12-17, 2008, Beijing, China.

Takanashi, K., 1975. Nonlinear earthquake response analysis of structures by a computer-actuator on-line system. *Bull. Of Earthquake Resistant Structure Research Center,* 8, Inst. of Ind. Science, Univ. of Tokyo.

Takahashi, N., and Shiohara, H., 2004. Life cycle Economic Loss due Seismic Damage of Nonstructural Elements. Proceeding of 13th World Conference on Earthquake Engineering, Paper No.203, Vancouver, BC, Canada

Tan, A., Irfanoglu, A., 2012. Correlation between ground motion based shaking intensity estimates and actual building damage. *15th World Conference on Earthquake Engineering. Lisbon, Portugal*

USNRC, 1978. Regulatory Guide 1.122. "Development of floor design response spectra for seismic design of floor-supported equipment or components." U.S. Nuclear Regulatory Commission

Villaverde, R., 1996. Earthquake resistant design of secondary systems: a report on the state-of-the-art. Proceedings of the Eleventh World Conference on Earthquake Engineering, Acapulco, Mexico.

Von Thun, J. L., Rochim, L. H., Scott, G. A., and Wilson, J. A., 1988. Earthquake ground motions for design and analysis of dams. *Earthquake Eng. Soil Dyn. II*—Recent Advances in Ground-Motion Evaluation (GSP 20), ASCE, New York, 463–481.

Wakefield, D., Ravindra, M., Merz, K., and Hardy, G., 2003. Seismic probabilistic risk assessment implementa- tion guide. Final Report 1002989, EPRI.

Williams, M. S, and Sexsmith, R. G., 1995. Seismic damage indices for concrete structures: a state-of-the-art review. *Earthquake Spectra*: May 1995, Vol. 11, No. 2.

Wilson, E., L., Der Kiureghian A., Bayo, E., R., 1981. A Replacement for the SRSS Method in Seismic Analysis. *Earthquake Engineering and Structural Dynamics*, Vol. 9, pp. l87-l92, 1981.

Wolf, J. P., 1985. Dynamic Soil Structure Interaction. Prentice Hall International Series, Englewood Cliffs, New Jersey.

Wolf, J. P., 1988. Soil Structure Interaction Analysis in time domain. Prentice Hall International Series, Englewood Cliffs, New Jersey.

Zentner, I., Humbert N., Ravet S., Viallet E., 2011. Numerical methods for seismic fragility analysis of structures and components in nuclear industry - Application to a reactor coolant system. *Georisk: Assesment and Management of Risk for Engineered Systems and Geohazards*, 5: 2, 99-109.

APPENDIX A

Test-case structures' characteristics

In this appendix are reported the characteristics of the test case structures in terms of dimensions, masses, and mechanical properties of materials. The values assigned to the parameters of the constitutive laws are also given.

Due to the owner's request, no data regarding the TC3 building are given.

A1 CAMUS1

Table A1.1 *CAMUS 1 Mock-up: dimensions. Adapted from CAMUS, (1998).*

	Length (m)	Thickness (m)	Height (m)
Walls	1.70	0.06	0.90
Floor	1.70	0.21	-
Footing	2.10	0.1	0.60

Table A1.2 *CAMUS 1 Mock-up: mass balance. Adapted from CAMUS, (1998).*

Structural Element	Weight for element (tons)
Walls (5 storey)	1.1 *2
Footing	1.422+1.390
Floor	1.316
Concrete blocks (lower side)	0.288 *6
Concrete blocks (upper side)	0.240*2
Steel blocks	0.628*4
Total mass of one floor	6.036*5
Lateral bracing system	0.214*5 +0.048
TOTAL WEIGHT	36.31

Table A1.3 *CAMUS 1, materials characteristics from experimental tests. Adapted from CAMUS, (1998).*

Characteristic	Concrete	Steel
Young Modulus	30 GPa	200 GPa
Poisson ratio	0.21	0.
Tension Strength	3.3 MPa	-
Compression Strength	-35 MPa	-
Yield stress	-	414 MPa
Rupture stress	-	494 MPa
Yield strain	-	0.002
Rupture strain	-	0.18

Table A1.4 *CAMUS 1 numerical model: material behavior laws, assigned parameters.*

Characteristic	Concrete	Characteristic	Steel
Young Modulus	30 GPa	Young Modulus	200 GPa
Poisson ratio	0.21	Poisson ratio	0.3
Tension Strength	3.3 MPa	Yield stress	414 MPa
Compression Strength	-35 MPa	Rupture stress	494 MPa
Tension parameter A1	5.E-3	Yield strain	0.002
Tension parameter A2	3.8E-6	Rupture strain	0.18
Compr. parameter B1	1.	A1FA	18.5
Compr. parameter B2	1.1	A2FA	0.15
Crack closure stress	-1.4E6 **	ROFA	20
Tension energy threshold Y1	3.3E2	E_h/E	0.0033
Compr. energy threshold Y2	2.5E3		
Tension inelastic par. BETA1	1.075E6		
Compr. inelastic par. BETA2	-40.E6		

*** value recommended by Ragueneau (1999).*

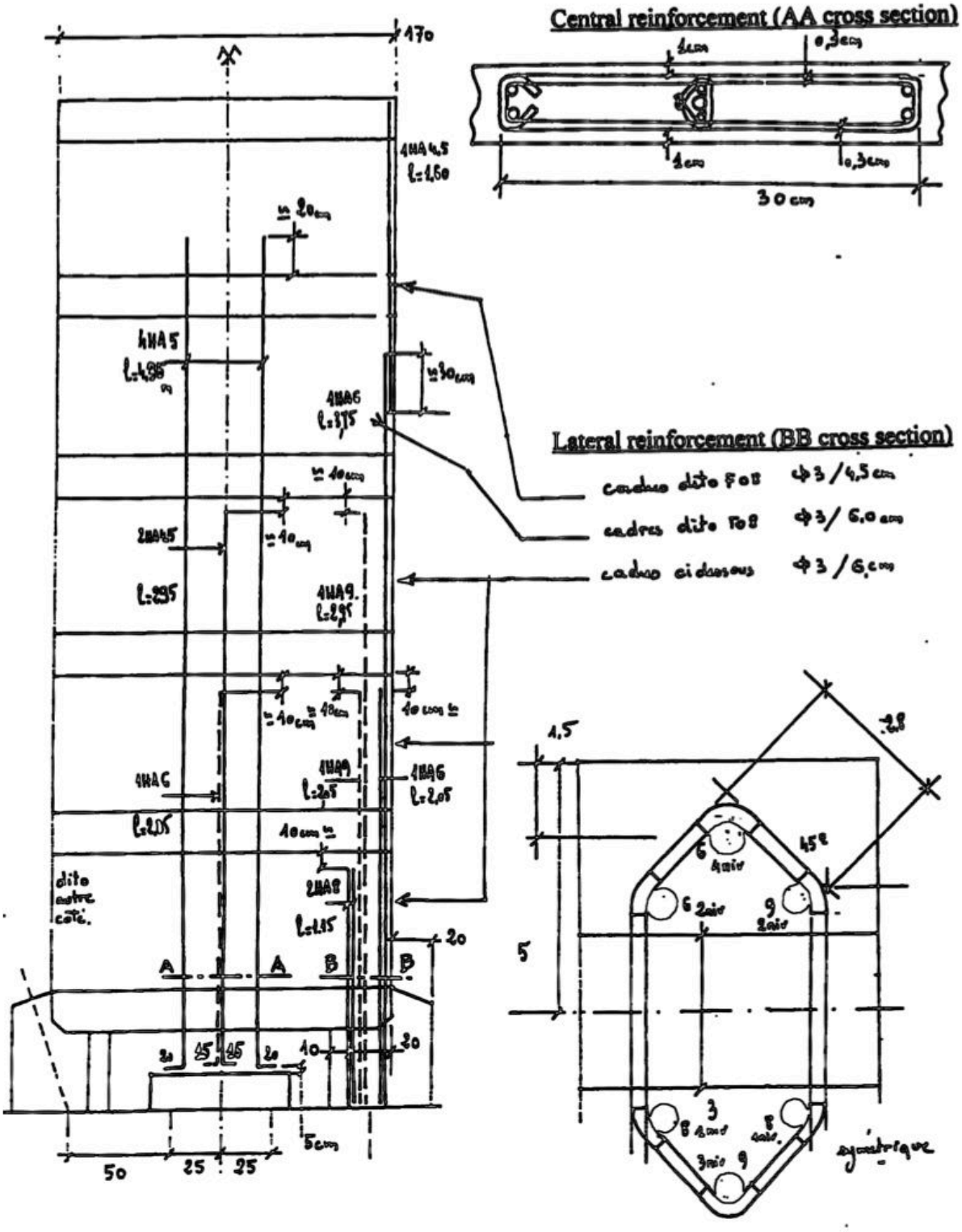

Figure A1.1 *CAMUS1, rebars arrangement. Reproduced from CEA (1998a).*

A2 CAMUS1-SSI

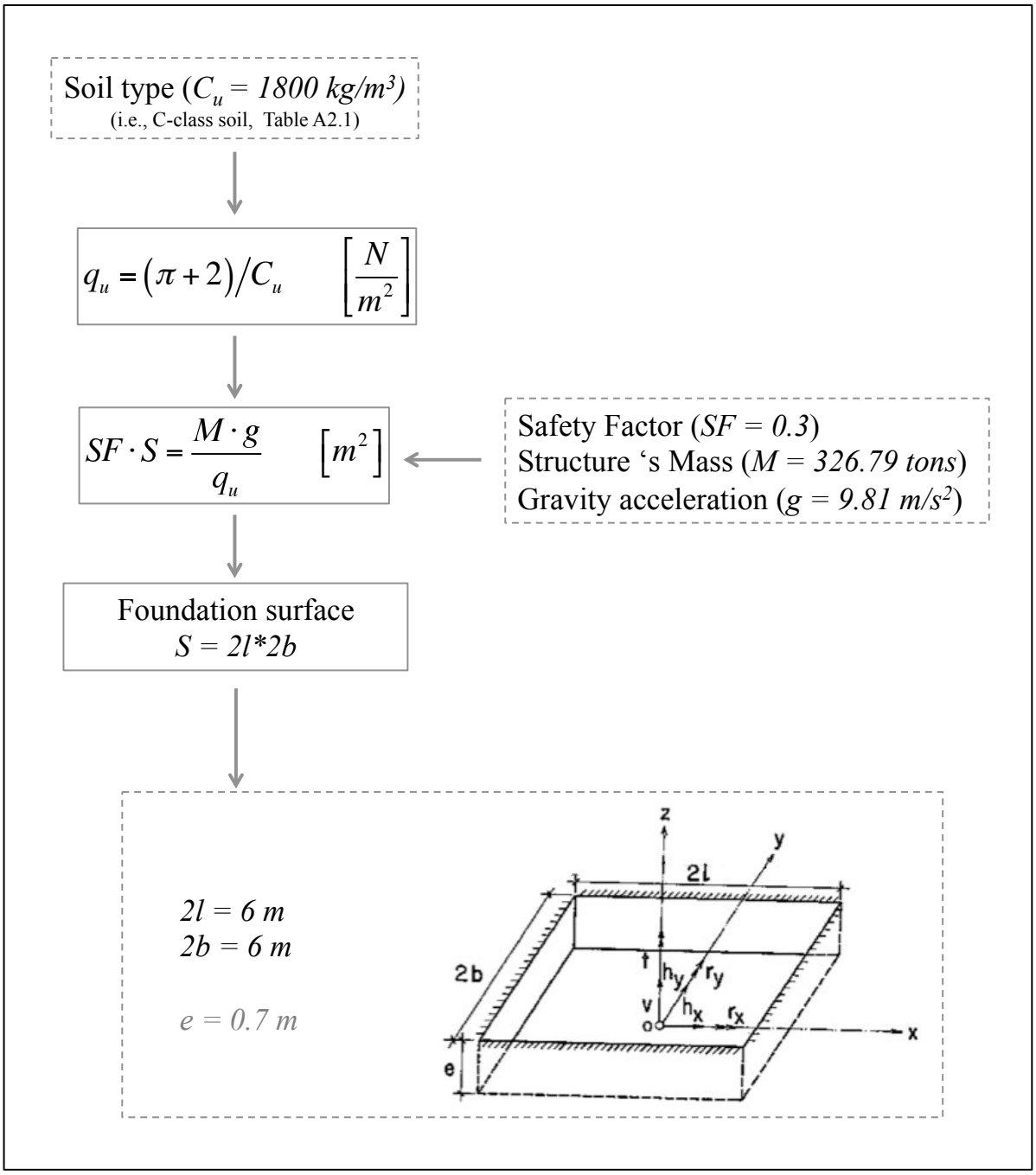

Figure A2.1 *CAMUS1-SS:, spread footing, simplified dimensioning*

***Table A2.1** Eurocode 8, soil classes. Adapted from EC8 (1998).*

Ground type and description	**V_{S30} [m/s]**	**N_{SPT} [blows/30 cm]**	**C_u [kPa]**
A: Rock or other rock-like geological formation, including at most 5 m of weaker material at the surface	> 800	-	-
B: Deposits of very dense sand, gravel, or very stiff clay, at least several tens of meters in thickness, characterized by a gradual increase of mechanical properties with depth.	360 - 800	> 50	> 250
C: Deep deposits of dense or medium dense sand, gravel or stiff clay with thickness from several tens to many hundreds of meters	180 - 360	15 - 50	70 - 250
D: Deposits of loose-to-medium cohesionless soil (with or without some soft cohesive layers), or of predominantly soft-to-firm cohesive soil.	< 180	< 15	< 70

A3 EC8-FRAME

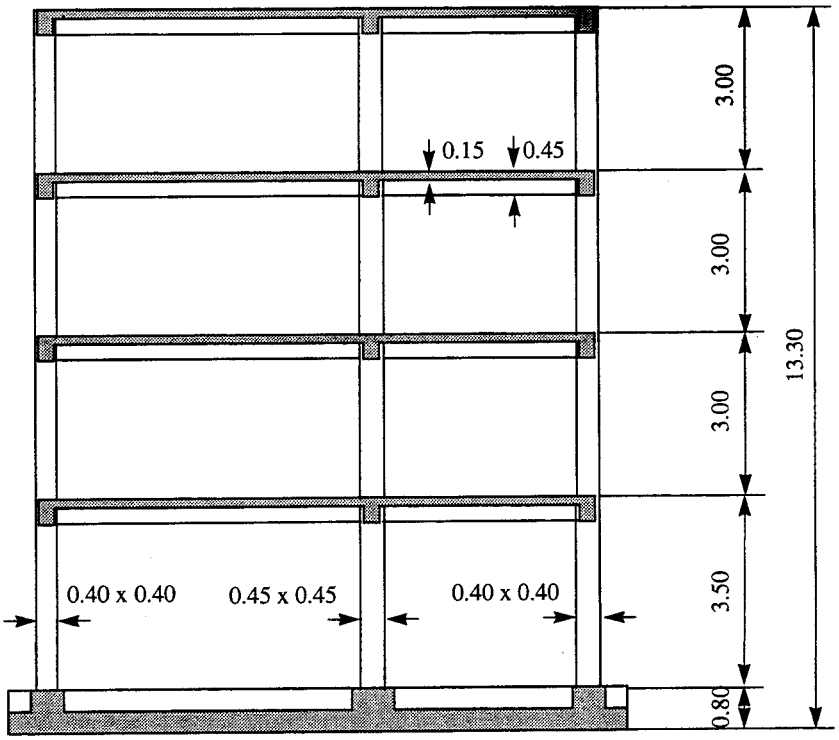

a)

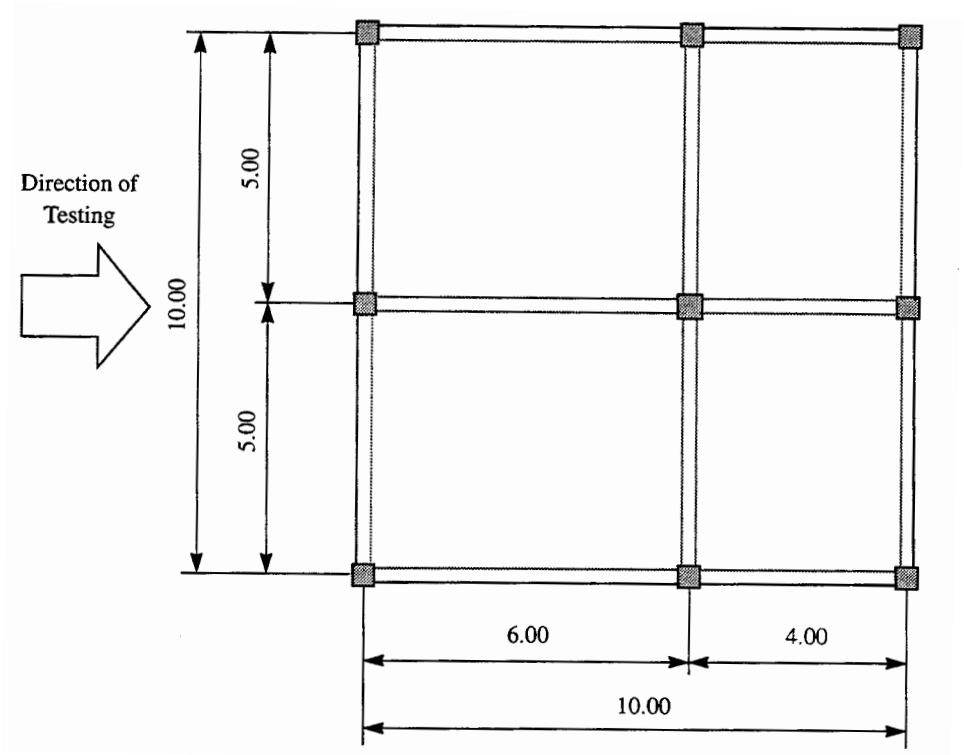

b)

Figure A3.1 *EC8-FRAME, layout of the specimen: a) side view; b) top view. Reproduced from JRC, (1994)*

Table A3.1 *EC8-FRAME, concrete characteristics (experimental). Adapted from JRC, (1994)*

Structure	R_C [Mpa]
Columns 1st story	49.8
Beams 1st story	56.4
Columns 2st story	47.6
Beams 2st story	53.2
Columns 3rd story	32.0
Beams 3rd story	47.2
Columns 4th story	46.3
Beams 4th story	42.1

Table A3.2 *EC8-FRAME, Steel rebars characteristics (experimental). Adapted from JRC, (1994)*

Diameter [mm]	Yielding stress [MPa]	Ultimate stress [MPa]	Ultimate strain [A %]
6	566.0	633.5	23.5
8	572.5	636.1	22.3
10	545.5	618.8	27.5
12	589.7	689.4	23.0
14	583.2	667.4	22.7
16	595.7	681.0	20.6
20	553.5	660.0	23.1
26	555.6	657.3	21.6

Table A3.3 *EC8-FRAME numerical model: material behavior laws, assigned parameters*

Characteristic	Concrete	Characteristic	Steel
Young Modulus	30 GPa	Young Modulus	190 GPa
Poisson ratio	0.21	Poisson ratio	0.3
Tension Strength	3.3 MPa	Yield stress	570 MPa
Compression Strength	-35 MPa	Rupture stress	655 MPa
Tension parameter A1	5.E-3	Yield strain	0.002
Tension parameter A2	3.8E-6	Rupture strain	0.23
Compr. parameter B1	1.	A1FA	18.5
Compr. parameter B2	1.1	A2FA	0.15
Crack closure stress	-3.3E6	ROFA	20
Tension energy threshold Y1	3.3E2	E_h/E	0.0033
Compr. energy threshold Y2	2.5E3		
Tension inelastic par. BETA1	1.075E6		
Compr. inelastic par. BETA2	-40.E6		

A4 SMART 2013

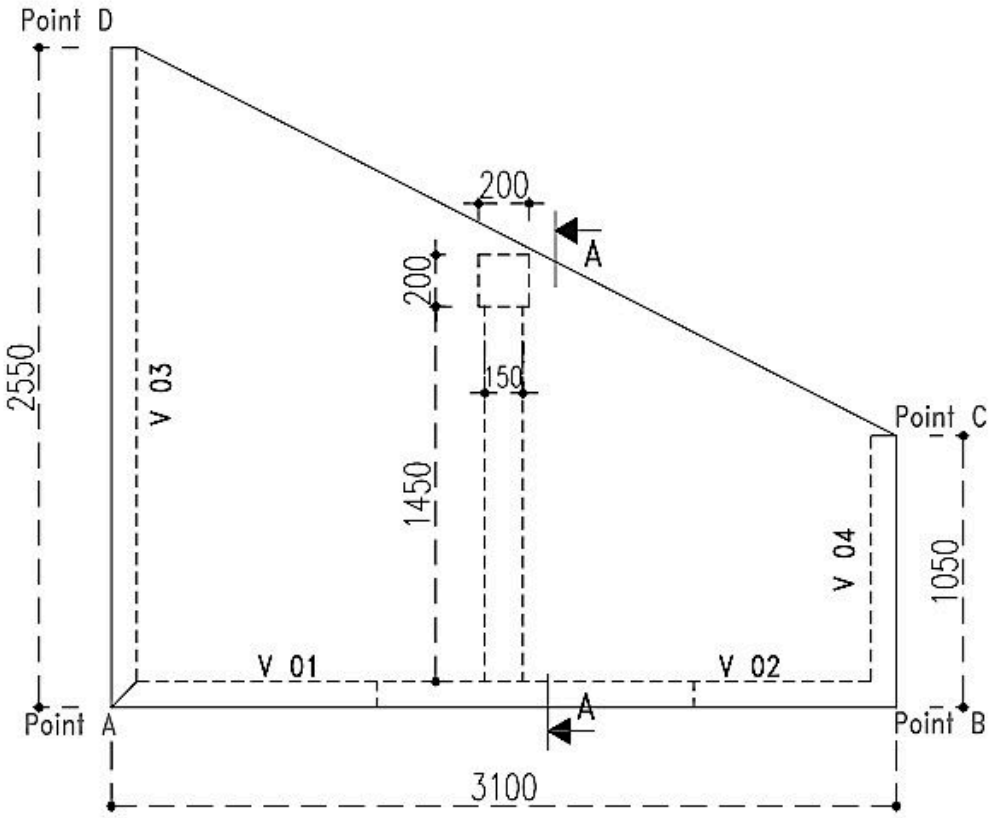

Figure A4.1 *SMART 2013 mock-up: layout, top view. Reproduced from CEA, (2013).*

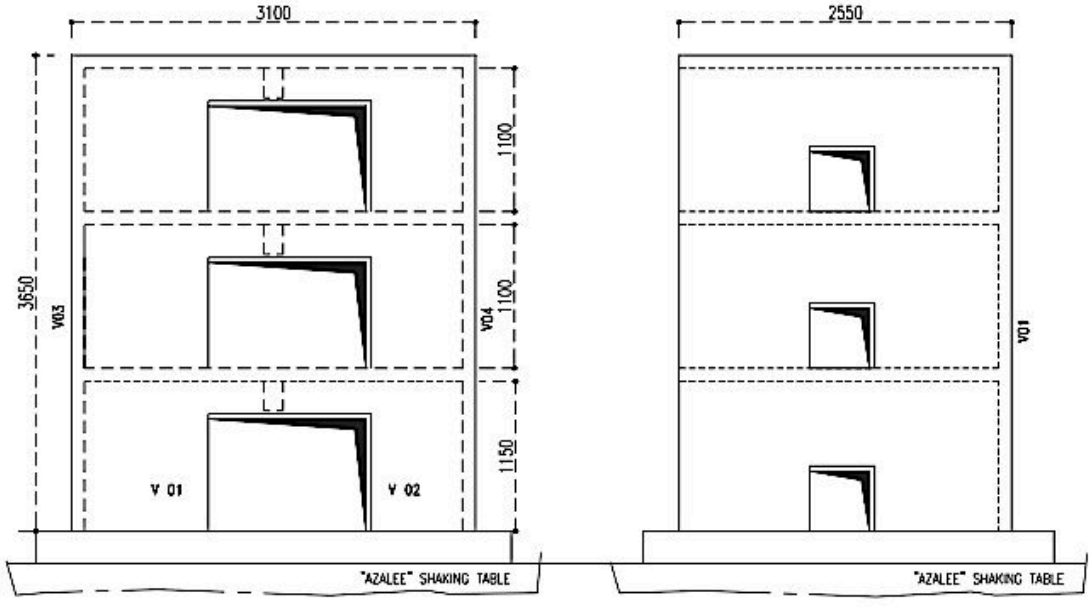

Figure A4.2 *SMART 2013 mock-up: layout, side view. Reproduced from CEA, (2013).*

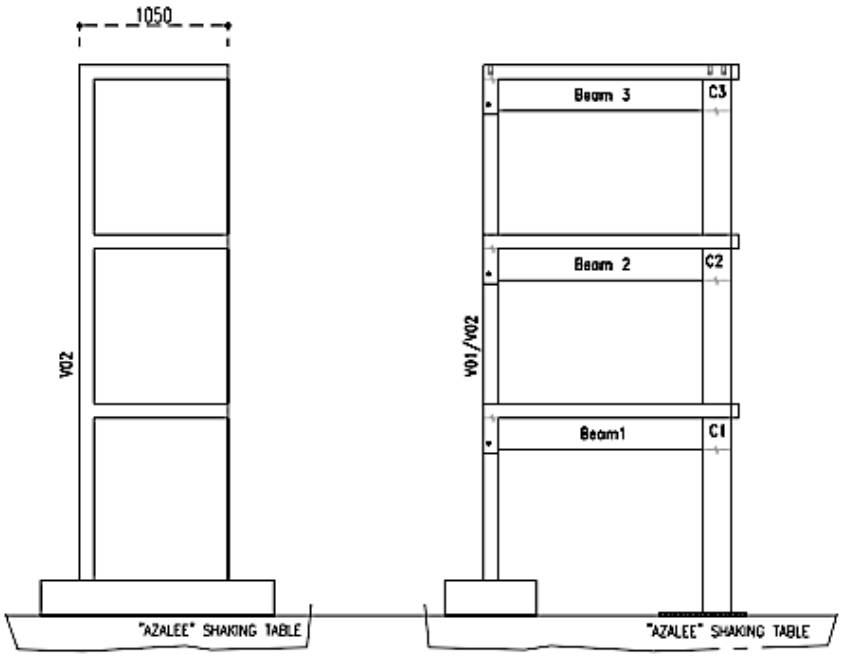

Figure A4.3 *SMART 2013 mock-up, layout, side view. Reproduced from CEA, (2013).*

Table A4.1 *SMART 2013 mock-up, steel characteristics. Reproduced from CEA, (2013).*

Nominal diameter (mm)	Steel type	Property	Young modulus (MPa)	Poisson ratio	Yield stress (MPa)	Ultimate stress (MPa)	Ultimate Strain (corresponding to the maximum stress)	Failure Strain	Mass density ($kg.m^{-3}$)
3	Smooth	Design value	210000	0,3	500	600	-	-	7800
		Mean measured value	314500	-	629	676	0.02	0.14	-
		Standard deviation	-	-	25.36	12.42	0	0	-
4	Smooth	Design value	210000	0.3	500	600	-	-	7800
		Mean measured value	332333	-	665	706	0.03	0.19	-
		Standard deviation	-	-	11,59	6,56	0	0.01	-
6	Ribbed	Design value	210000	0.3	500	600	-	-	7800
		Mean measured value	267333	-	528	581	0.11	0.20	-
		Standard deviation	-	-	3.06	3.21	0.03	0.04	-
8	Ribbed	Design value	210000	0.3	500	600	-	-	7800
		Mean measured value	252666	-	505	565	0.12	0.29	-
		Standard deviation	-	-	33,83	12,80	0.02	0.01	-
10	Ribbed	Design value	210000	0.3	500	600	-	-	7800
		Mean measured value	250166	-	500	571	0.09	0.26	-
		Standard deviation	-	-	2.52	6.03	0.04	0.04	-

Table A4.2 *SMART 2013 mock-up, concrete characteristics. Reproduced from CEA, (2013).*

Structural component	Property	Young modulus (MPa)	Poisson ratio	Compressive strength (MPa)	Tensile strength - splitting tests (MPa)	Tensile strength - bending tests (MPa)	Fracture energy ($J.m^{-2}$)	Mass density ($kg.m^{-3}$)
Foundation	Design value	32000	0.2	30	2.4	2.4	180	2300
	Mean measured value	25400	0.17	43.3	3.45	4.14	135.5	-
	Standard deviation	-	-	1.51	0.30	0.10	20.5	-
Floor #1	Design value	32000	0.2	30	2.4	2.4	180	2300
	Mean measured value	28200	0.18	41.1	3.25	3.74	136	-
	Standard deviation	-	-	0.92	0.4	0.30	6.53	-
Shear walls – cast #1	Design value	32000	0.2	30	2.4	2.4	180	2300
	Mean measured value	28700	0.19	41.7	3.15	3.89	133.6	-
	Standard deviation	-	-	0.07	0.15	0.24	26.16	-
Floor #2	Design value	32000	0.2	30	2.4	2.4	180	2300
	Mean measured value	24700	0.17	36.8	3.35	3.32	114	-
	Standard deviation	-	-	2.61	0.17	0.17	19.94	-
Shear walls – cast #2	Design value	32000	0.2	30	2.4	2.4	180	2300
	Mean measured value	25700	0.19	35.5	2.70	3.78	132	-
	Standard deviation	-	-	0.85	0.26	0.37	13.45	-
Floor #3	Design value	32000	0.2	30	2.4	2.4	180	2300
	Mean measured value	24400	0.18	37.8	3.40	3.80	135	-
	Standard deviation	-	-	1.45	0.05	0.17	5.4	-
Shear walls – cast #3	Design value	32000	0.2	30	2.4	2.4	180	2300
	Mean measured value	29500	0.18	46.6	4.00	3.57	123	-
	Standard deviation	-	-	4.24	0.30	0.04	12.05	-

Table A4.3 *SMART 2013 numerical model, assigned materials' characteristics.*

	Concrete	Steel
Young modulus	28 GPa	0.17
Poisson ratio	210 GPa	0.3

APPENDIX B

Relation between ASA_R/E-ASA_R and the Magnitude-Distance pair

In this appendix are reported three scatter plots showing, for the 2,045 ground motion records used in the study, the relationship between ASA_R and the M-R pair. The three plots differ for the value of frequency (i.e. f_1) at which the $ASA_R(f_1)$ is computed, i.e., 5.85 Hz (Figure B.1), 3.80 Hz (Figure B.2), and 1.57 Hz (Figure B.3). Due to the straight relation (i.e. Eq. 3.12) between ASA_R and $E\text{-}ASA_R$, it has not been considered necessary to give the analogous plots for this last.

From figures B1-B3, it is worth to note the ASA_R value evolves in consistent manner with respect to magnitude and distance, i.e. larger-magnitude/shorter-distance earthquakes produce higher ASA_R values. This observation highlights that the statistically proved sufficiency of ASA_R (and $E\text{-}ASA_R$) is related to the fact the information about magnitude and distance is actually "already caught" by ASA_R (and $E\text{-}ASA_R$).

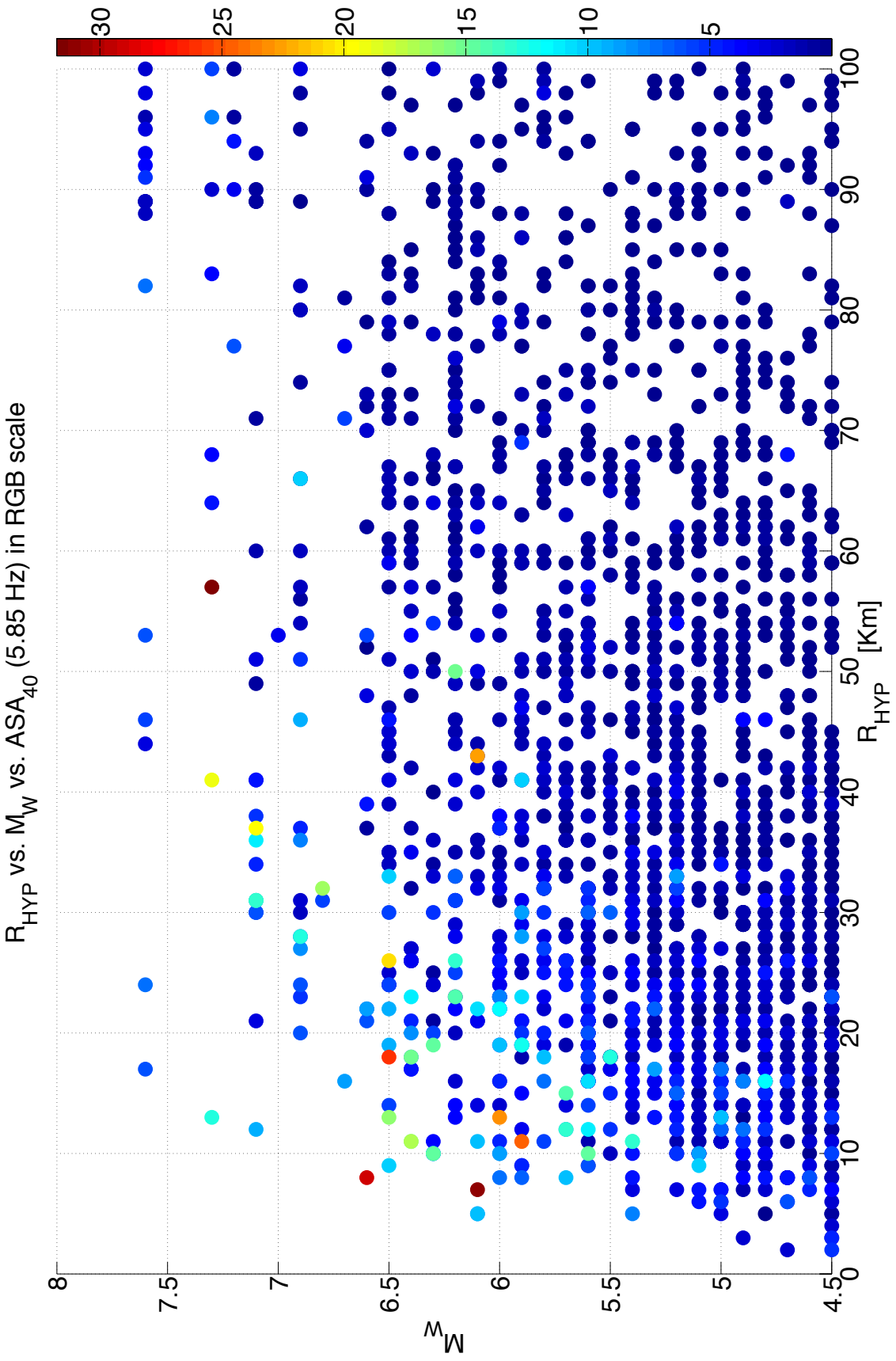

Figure B.1 *Hypocentral distance vs. moment Magnitude vs. ASA_{40} (5.85 Hz).*

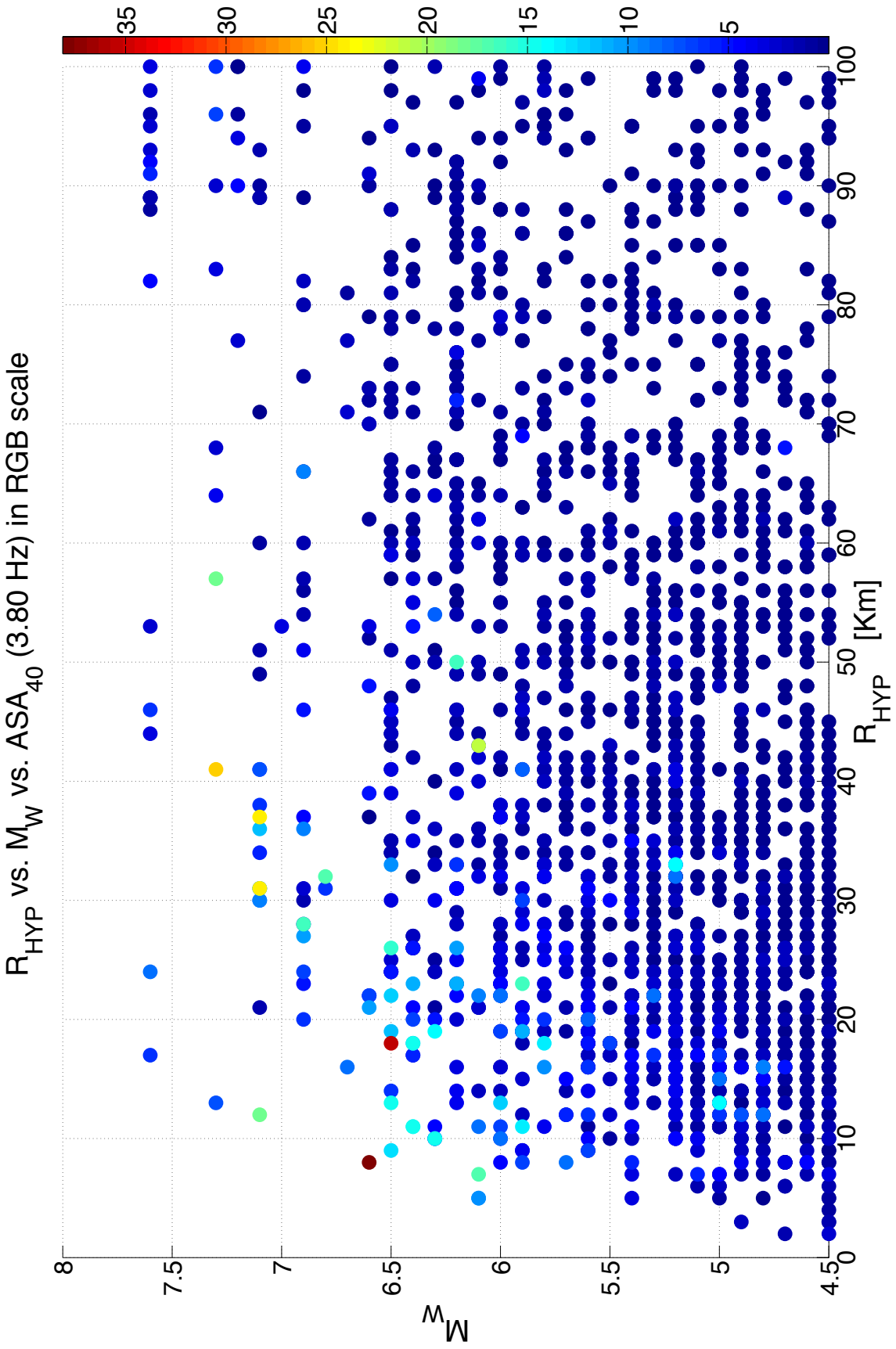

Figure B.2 *Hypocentral distance vs. moment Magnitude vs. ASA_{40} (3.80 Hz).*

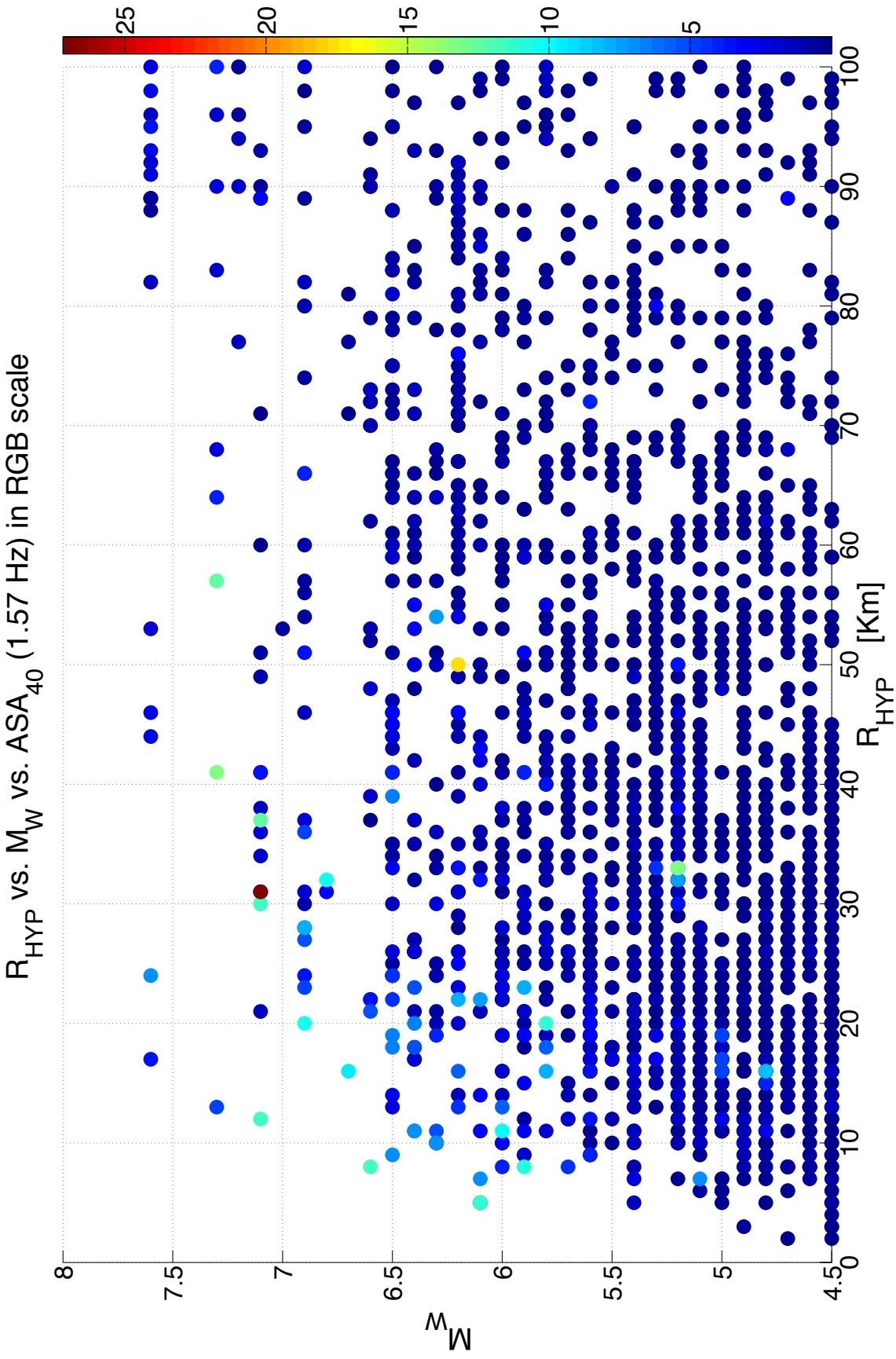

Figure B.3 *Hypocentral distance vs. moment Magnitude vs. ASA_{40} (1.57 Hz).*

APPENDIX C

Effect of damping on IMs computation

The ASA_R shows *robustness* with respect to the damping affecting the response spectra used for its computation. Indeed, with respect to the values of ASA_R computed on 5% damped response spectra, the values of ASA_R computed on 2% damped response spectra mainly differ of a scalar multiplicative factor (e.g., Fig. C.1). This implies that the ranking of the ground motion is nearly the same for both cases. Moreover, due to the relation (Eq. 3.12) the foregoing result is valid for both ASA_R and $E\text{-}ASA_R$.

The same argument can be used with respect to spectral acceleration values computed either on 2% or 5% damped response spectra (e.g., Fig. C.2).

In equivalent way, the analyses performed in paragraph 2.4 (through 2% damped response spectra) can be performed on 5 % damped response spectra in leading to the same conclusions (e.g., Fig. C.3).

Therefore, the choice among 2% or 5% damped response spectra does not affect the results and the conclusions of the present study.

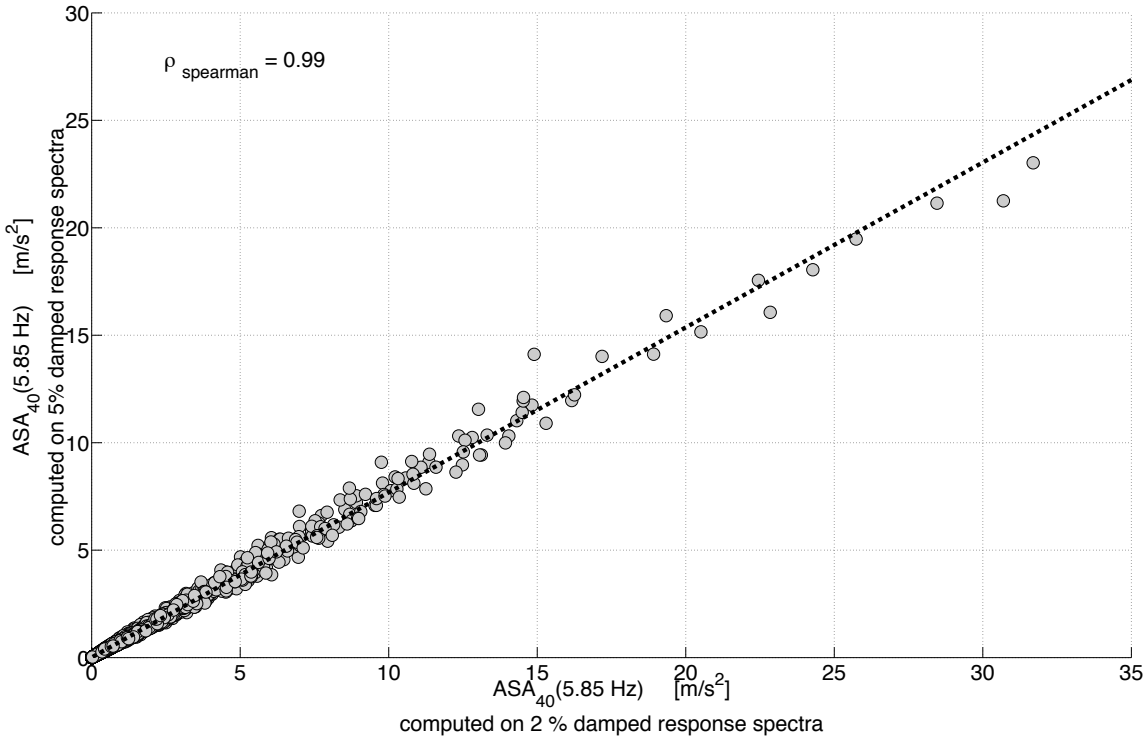

Figure C.1 *Scatter plot of ASA_{40} (5.85 Hz) computed on differently damped response spectra for the 2,045 ground motion records considered in this study*

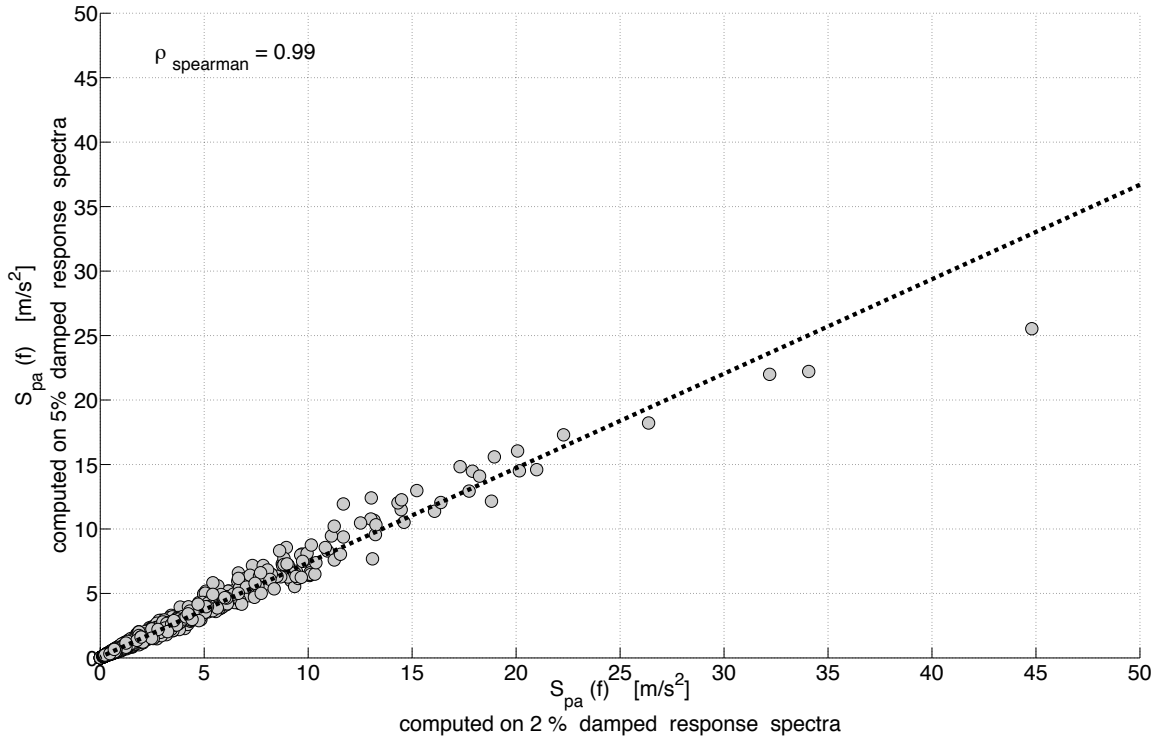

Figure C.3 *Scatter plot of S_{pa} (5.85 Hz) computed on differently damped response spectra for the 2,045 ground motion records considered in this study*

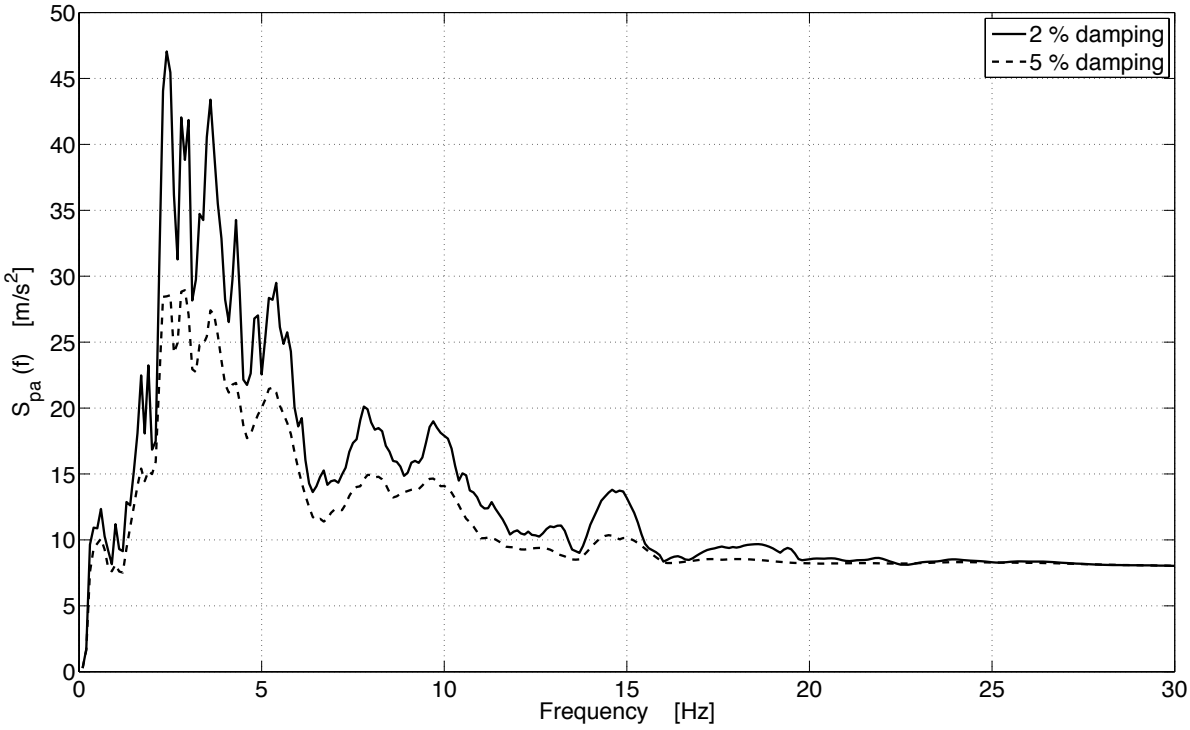

Figure C.3 *Differently damped response spectra of record 30.*

Ground Motion Intensity Measures for Seismic Probabilistic Risk Analysis
M. DE BIASIO - 2014

ABSTRACT

A fundamental issue that arises in the framework of Probabilistic Seismic Risk Analysis is the choice of ground motion Intensity Measures (IMs). In addition to reducing record-to-record variability, an improved IM (i.e. one able to better capture the damaging features of a record, as well as the site hazard) provides criteria for selecting input ground motions to loosen restrictions.

Two new structure-specific IMs are proposed in this study: the first, namely ASA_R (i.e. *Relative Average Spectral Acceleration*), is conceived for Structural demand prediction, the second namely, $E\text{-}ASA_R$ (i.e. *Equipment-Relative Average Spectral Acceleration*), aims to predict Non-Structural components acceleration demand. The performance of the proposed IMs are compared with the ones of current IMs, based on: a) a large dataset of thousands recorded earthquake ground motions; b) numerical analyses conducted with state-of-the-art FE models, representing actual load-bearing walls and frame structures, and validated against experimental tests; and c) systematic statistical analyses of the results. According to the comparative study, the introduced IMs prove to be considerably more "efficient" with respect to the IMs currently used. Likewise, both ASA_R and $E\text{-}ASA_R$ have shown to own the characteristic of "sufficiency" with respect to magnitude, source-to-site distance and soil-type (Vs_{30}). Furthermore, both the introduced IMs possess the valuable characteristics to need (in order to be computed) merely the knowledge of the building's fundamental frequency, exactly as it is for the wide-spread spectral acceleration $S_{pa}(f_1)$. This key characteristic makes both ASA_R and $E\text{-}ASA_R$ easily exploitable in Probabilistic Seismic Hazard Analysis.

Therefore, due to their proven efficiency, sufficiency, robustness and applicable formulation, both ASA_R and $E\text{-}ASA_R$ can be considered as worthy candidates for defining seismic hazard within the frameworks of both Probabilistic and Deterministic Seismic Risk Analysis.

RESUME

Une question fondamentale qui surgit dans le cadre de l'analyse probabiliste du risque sismique est le choix des indicateurs de nocivité des signaux sismiques. En plus de réduire la variabilité de la réponse structurelle (ou non-structurelle), un indicateur amélioré (i.e. capable de mieux capturer les caractéristiques de nocivité des mouvements sismiques, aussi bien que l'alea sismique) fournit des critères moins stricts pour la sélection des signaux sismiques.

Deux nouveaux indicateurs sont proposés dans cette étude: le premier, nommé ASA_R (i.e. *Relative Average Spectral Acceleration*), est conçu pour la prévision de la demande structurelle, le second, nommé $E\text{-}ASA_R$ (i.e. *Equipment Relative Average Spectral Acceleration*), vise à prévoir la demande des composants non structuraux. Les performances des indicateurs proposés sont comparées avec celles des indicateurs de la littérature, sur la base de: a) milliers d'enregistrements sismiques ; b) analyses numériques conduites avec des modèles représentants différents types de bâtiments; et c) analyses statistiques rigoureuses des résultats. Selon l'étude comparative, les indicateurs développés s'avèrent être plus "efficaces" que les indicateurs couramment utilisés. D'ailleurs, l'ASA_R et l'$E\text{-}ASA_R$ ont montré au propre la caractéristique de la "suffisance" en ce qui concerne la magnitude, la distance source-site, et le type de sol (V_{S30}). De plus, les deux indicateurs originaux peuvent être calculés simplement avec la connaissance de la fréquence fondamentale du bâtiment. Cette caractéristique rend l'ASA_R et l'$E\text{-}ASA_R$ facilement exploitables dans les études probabilistes d'alea sismique.

Par conséquent, en raison de leur efficacité, suffisance, robustesse et formulation simple, l'ASA_R et l'$E\text{-}ASA_R$ peuvent être considérés comme des candidats prometteurs pour la définition de l'alea sismique dans les cadres de l'analyse probabiliste et déterministe du risque sismique.